Exploration of Therapeutic Effects on the Hypoxic Pathway in Inflammatory Arthritis

Dr Shing Law

Thesis for Doctor of Philosophy in Molecular and Cellular Medicine

University College

Nuffield Department of Orthopaedics, Rheumatology and Musculoskeletal Sciences

University of Oxford

Trinity 2025

Acknowledgements

I thank my supervisors Duncan Richards, Eleanor Stride, Philippa Hulley and Jolet Mimpen for the advice, support and understanding. I acknowledge the raw data pre-processing of bulk RNA sequencing by Alina Kurjan, snRNA-seq data pre-processing into lane-demultiplexed FASTQ files by Carla Cohen, Alexandra Vasilyeva who provided nanobubbles, National Institute for Health and Care Research nurses who assisted with patient visits, Laura Coates who was Principal Investigator of the clinical study of nanobubbles, and teaching by Helen Knowles.

Disclosures

Eleanor Stride is a co-inventor on a patent "Beverage Composition Comprising Nanoencapsulated Oxygen" (Stride, E., Averre, R., Owen, J. 2016. UK Patent Publication No. EP3324929). Avrox Technologies Ltd. licensed this patent but did not fund this work or play any role in the study. The other investigators have no interests to declare.

Funding

This work is supported by the Climax Donation, University College Oxford Henni Mester Scholarship, UK SPINE, and National Institute for Health and Care Research.

Word count

Fewer than 50,000.

Table of Contents

Abstract

Synovial hypoxia is a feature of inflammatory arthritides such as rheumatoid arthritis (RA) and psoriatic arthritis (PsA). Whether joint hypoxia is a consequence or a cause of inflammatory arthritis is poorly understood. Targeting hypoxia in the inflamed joint directly would provide insight as to whether hypoxia is driving synovial inflammation. Lecithin encapsulated oxygen nanobubbles were purported to act as oxygen carriers that may relieve peripheral tissue hypoxia.

These nanobubbles were assumed to carry oxygen given that they downregulated hypoxia-inducible factor (HIF) 1α. I demonstrated that nanobubbles downregulated HIF-1α protein expression and hypoxia response element (HRE) transcription *in vitro* irrespective of gas loading. Animal and human *in vivo* studies by others confirmed that oxygen nanobubbles did not increase tissue oxygenation. Nanobubbles therefore would not be expected to relieve joint hypoxia and my proposed clinical study of nanobubbles was withdrawn.

Synovial hypoxia has been shown to be relieved in patients with inflammatory arthritis who responded to anti-inflammatory biologic therapies. Intra-articular methylprednisolone injection is a widely used anti-inflammatory treatment for inflammatory arthritis. I found that intra-articular methylprednisolone did not affect synovial fluid oxygen levels at 4 weeks follow-up, although interleukin-6 (IL-6) and tumour necrosis factor (TNF) cytokines were reduced at least in the PsA subgroup.

Single nucleus transcriptomic analysis of synovial tissue biopsies at baseline and 4 weeks after intra-articular methylprednisolone injection showed no change in hypoxia related genes. This *in vivo* therapeutic atlas found that tissue inhibitor of metalloproteinase 1

(*TIMP1*) was downregulated in lining fibroblasts and lipogenesis was upregulated in adipocytes after methylprednisolone treatment, consistent with previous studies. Exploratory analysis of lining fibroblasts showed upregulation of matrix Gla protein (*MGP*) in RA and bone morphogenetic protein-binding endothelial regulator (*BMPER*) in PsA, which may account for the preponderance of bony erosions in RA and bushy tortuous vasculature in PsA.

List of Figures

List of Tables

Abbreviations

6MWT	6 Minute Walk Test
Ab	Antibody
ACR	American College of Rheumatology
ACTH	Adrenocorticotropic Hormone
AHNAK	Neuroblast Differentiation-Associated Protein
AIA	Antigen-Induced Arthritis
ANGPTL	Angiopoietin-Like
AP-1	Activator Protein 1
APC	Antigen Presenting Cells
AKT	Ak Strain Transforming
AS	Ankylosing Spondylitis
ASIC	Acid-Sensing Ion Channel
ATP	Adenosine Triphosphate
AU	Absorbance Unit
BMP	Bone Morphogenetic Protein
BMPER	Bone Morphogenetic Protein-Binding Endothelial Cell Precursor-Derived Regulator
BSA	Bovine Serum Albumin
CASPAR	Classification Criteria for Psoriatic Arthritis
CCP	Cyclic Citrullinated Peptide
CHAPS	3-[(3-cholamidopropyl)dimethylammonio]-1-propanesulfonate
CI	Confidence Interval
CIA	Collagen-Induced Arthritis
COPD	Chronic Obstructive Pulmonary Disease

CPPD	Calcium Pyrophosphate Deposition Disease
CRF	Case Report Form
CRH	Corticotropin-Releasing Hormone
CRP	C-Reactive Protein
CST	CHAPS, salts and Tris
CXCL	CXC Chemokine Ligand
CXCR	CXC Chemokine Receptor
COVID-19	Coronavirus disease 2019
DAPSA	Disease Activity Index for Psoriatic Arthritis
DAS	Disease Activity Score
DIP	Distal Interphalangeal Joints
DLS	Dynamic Light Scattering
DMARDs	Disease Modifying Anti-Rheumatic Drugs
DUSP1	Dual Specificity Phosphatase 1
EGF	Epidermal Growth Factor
ELISA	Enzyme-Linked Immunosorbent Assay
EPAS1	Endothelial PAS Domain Protein 1
ERK	Extracellular Signal-Regulated Kinases
EULAR	European Alliance of Associations for Rheumatology
FBS	Foetal Bovine Serum
FDR	False Discovery Rate
FIH	Factor-Inhibiting HIF-1α
FLS	Fibroblast-Like Synoviocytes
FPR	Formyl Peptide Receptor
GAPDH	Glyceraldehyde-3-Phosphate Dehydrogenase

GEM	Gel bead-in-emulsion
GO	Gene Ontology
GP	General Practitioner
GRE	Glucocorticoid Response Elements
GWAS	Genome-Wide Association Study
H2AC6	H2A Clustered Histone 6
H_2DCFDA	2',7'-Dichlorodihydrofluorescein Diacetate
H_2O_2	Hydrogen Peroxide
HIF	Hypoxia Inducible Factor
HLA	Human Leukocyte Antigen
HRA	Health Research Authority
HRE	Hypoxia Response Element
HSP	Heat-Shock Proteins
HUVEC	Human Umbilical Vein Endothelial Cell
ICAM-1	Intracellular Adhesion Molecule 1
IL	Interleukin
IL2R	IL-2 Receptor
IL2RA	IL-2 Receptor Subunit Alpha
IL2RB	IL-2 Receptor Subunit Beta
ILC	Innate Lymphoid Cells
IMID	Immune-Mediated Inflammatory Disorder
IRAS	Integrated Research Application System
ISO	International Organization for Standardization
ITGB8	Integrin Subunit Beta 8
JAK	Janus Kinase

JIA	Juvenile Idiopathic Arthritis
JUND	JunD Proto-Oncogene
KIT	KIT Proto-Oncogene, Receptor Tyrosine Kinase
KLF6	Krueppel-Like Factor 6
KO	Knockout
LFC	Log2 Fold Change
LMNA	Lamin A/C
LPS	Lipopolysaccharide
LRP-1	Low-density Lipoprotein-Related Protein 1
MALDI-MSI	Matrix-Assisted Laser Desorption Ionization Mass Spectrometry Imaging
MCP	Metacarpophalangeal
ME-SIMS	Matrix-Enhanced Secondary Ion Mass Spectrometry
MERTK	MER Proto-Oncogene Tyrosine Kinase
MGP	Matrix Gla Protein
MIP	*Saccharomyces cerevisiae* mannan induced psoriatic arthritis
MMP	Matrix Metalloproteinase
MSD	Meso Scale Discovery
MSOT	Multi-Spectral Optoacoustic Tomography
MTP	Metatarsophalangeal
NA	Not Applicable
NALCN	Sodium Leak Channel Non-Selective
NALF1	Sodium Leak Channel (Non-Selective) Channel Auxiliary Factor 1
NCOA3	Nuclear Receptor Coactivator 3
NET	Neutrophil Extracellular Traps
NF-κB	Nuclear Factor Kappa-Light-Chain-Enhancer of Activated B Cells

NHS	National Health Service
NK	Natural Killer cells
NKT	NK T cells
NLGN4X	Neuroligin 4 X-Linked
OA	Osteoarthritis
OCT	Optimal Cutting Temperature
OUH	Oxford University Hospitals NHS Foundation Trust
padj	Adjusted P value
PAPS	3'-Phosphoadenosine-5'-Phosphosulfate
PBS	Phosphate-Buffered Saline
PC	Phosphatidylcholine
PCA	Principal Components Analysis
PE	Phosphatidylethanolamine
PHD	Prolyl-4-Hydroxylase Domain
PI3Ks	Phosphoinositide 3-Kinases
PIP	Proximal Interphalangeal
pO_2	Partial pressure of oxygen
PPAR	Peroxisome Proliferator-Activated Receptors
PRO	Patient Reported Outcomes
PsA	Psoriatic arthritis
PsO	Psoriasis
pVHL	von Hippel-Lindau protein
RA	Rheumatoid arthritis
RANK	Receptor Activator of Nuclear Factor-κB
RANKL	RANK Ligand

REC	Research Ethics Committee
RF	Rheumatoid factor
ROS	Reactive oxygen species
RUNX1	Runt-related Transcription Factor 1
SAE	Serious Adverse Event
SEM	Standard Error of Mean
siRNA	small interfering RNA
SIRS	Systemic Inflammatory Response Syndrome
SLAMF6	Self-Ligand Receptor of the Signalling Lymphocytic Activation Molecule Family 6
SLC24A3	Solute Carrier Family 24 Member 3
SLC35B3	Solute Carrier Family 35 Member B3
SLE	Systemic Lupus Erythematosus
snRNA-seq	Single Nucleus RNA Sequencing
SpA	Spondyloarthritis
SPOS	Single Particle Optical Sizing
SPP1	Secreted Phosphoprotein 1
SREBF	Sterol Regulatory Element-Binding Transcription Factor
SREBP	Sterol Regulatory Element-Binding Protein
STAT	Signal Transducer and Activator of Transcription
TCA	Tricarboxylic Acid
TGF-α	Transforming Growth Factor α
Th1	T helper 1 cells
TIMP	Tissue Inhibitor of Metalloproteinases
TLR	Toll-Like Receptor

TNF	Tumour Necrosis Factor
TNFi	TNF inhibitor
TNFAIP	TNF Alpha Induced Protein
Treg	Regulatory T cell
TST	Tween, salts, Tris
UMI	Unique Molecular Identifiers
VAS	Visual Analogue Scale
VCAM-1	Vascular Cell Adhesion Molecule 1
VCAN	Versican
VEGF	Vascular Endothelial Growth Factor
ZFP36L2	Zinc Finger Protein 36 C3H1 Type-Like 2

Preface

I embarked on a DPhil in Molecular and Cellular Medicine to develop as a clinician-scientist. This DPhil has equipped me with skills necessary to design and undertake clinical research studies, hands on experience with diverse wet lab techniques, and computational skills for analysing big data. During my time as a DPhil student, I attended courses including the European Alliance of Associations for Rheumatology (EULAR) course in Barcelona on ultrasound guided synovial biopsy, Oxford Biomedical Data Science courses at the Weatherall Institute of Molecular Medicine on "Genomics on the Linux command line", "Python programming and data science", "Python for single-cell RNA-seq", "R for data science and genomics", and "Single-cell RNA-seq data analysis using R". These training opportunities allowed me to complete my research and consequently my research abstract was accepted for publication and oral presentation at the European Congress of Rheumatology in Vienna (Law *et al*. OP0279-SINGLE NUCLEI TRANSCRIPTOMIC STUDY OF INTRA-ARTICULAR METHYLPREDNISOLONE EFFECTS ON INFLAMMATORY ARTHRITIS SYNOVIUM. *Annals of the Rheumatic Diseases* 2024, volume 83, supplement 1, year 2024, page 15).

I secured funding from the National Institute for Health and Care Research Biomedical Research Centre (Inflammation Across Tissues theme) to continue as a Clinical Research Fellow at University of Oxford until July 2026. This has allowed me to collaborate in national multicentre studies involving ultrasound guided synovial tissue biopsies. After the DPhil, I plan to publish my work, secure grants and fellowships, and transition into an independent clinician-scientist.

Introduction

The treatment of inflammatory arthritis has been revolutionised with advances in disease modifying antirheumatic drugs (DMARDs) such as TNF inhibitors (TNFi). However, many patients still do not reach disease remission and there remains an unmet clinical need for more efficacious therapies. Greater understanding of the pathogenesis underlying inflammatory arthritis would allow development of more effective therapies that targeted disease processes.

Synovial hypoxia is a well-recognised feature of inflammatory arthritis. Hypoxia may exacerbate inflammation in the arthritic joint and therefore may serve as a therapeutic target. Recently, novel orally delivered oxygen encapsulated nanobubbles patented by Professor Stride have been developed to relieve peripheral tissue hypoxia. These orally delivered oxygen nanobubbles may therefore relieve joint hypoxia in patients with inflammatory arthritis to provide therapeutic benefit.

It was my intention in this thesis to investigate the mechanism of action of nanobubbles *in vitro* and test whether nanobubbles relieve joint hypoxia *in vivo* in patients with inflammatory arthritis. To contextualise these clinical findings, I will also study the effects of intra-articular methylprednisolone injection, a widely used treatment, in a parallel cohort of patients with inflammatory arthritis. I will perform ultrasound guided synovial tissue biopsy to explore the therapeutic effects of nanobubbles and intra-articular methylprednisolone injection on synovial tissues in inflammatory arthritis.

1. Chapter 1: Scoping review of the role of hypoxia in rheumatoid and psoriatic arthritis

1.1 Introduction

1.1.1 Inflammatory arthritis

Rheumatoid arthritis (RA) and psoriatic arthritis (PsA) are inflammatory arthritides that have significant impacts on quality of life and may result in disabilities (1). Both are characterised by painful joint swellings and are associated with extra-articular manifestations (2). If left untreated, RA and PsA may lead to joint destruction with loss of function and reduced quality of life.

RA is a chronic, debilitating autoimmune disease characterized by synovial inflammation and joint destruction that affects about 1% of adults (3). The standard definition of RA is by classification criteria which provides benchmarks for disease definition. The 2010 American College of Rheumatology/European League Against Rheumatism criteria (ACR/EULAR) classification criteria for RA is designed to classify patients for clinical trials (4). The classification criteria for RA include synovitis, joint involvement, symptom duration, serological markers and elevated acute phase reactant (4).

PsA is a seronegative, chronic, inflammatory arthritis associated with psoriasis, with a prevalence of 0.25% (5). PsA may be defined by the Classification Criteria for Psoriatic Arthritis (CASPAR) which is designed to categorise patients for clinical trials (6). The classification criteria include evidence of psoriatic skin or scalp disease, personal or family history of psoriasis, psoriatic nail dystrophy, negative rheumatoid factor (RF), dactylitis and radiographic evidence of juxta-articular new bone formation. Skin psoriasis (PsO)

precedes PsA in 85% of patients and PsA typically develops a decade after the onset of PsO (2).

Joint involvement is typically symmetrical in RA and asymmetrical in PsA (2). The distribution of joint involvement varies in RA and PsA. RA can affect shoulder, elbow, wrist, metacarpophalangeal (MCP), proximal interphalangeal (PIP), hip, knee, ankle and metatarsophalangeal (MTP) joints (2). These joints may also be involved in PsA, but PsA may involve distal interphalangeal (DIP) joints of hands and feet not affected in RA. Unlike RA, PsA is a form of spondyloarthritis (SpA) that can affect the axial skeleton including spine and sacroiliac joints (2). Cervical atlantoaxial subluxation may be present in RA but typically not PsA (2). In both RA and PsA, innate and adaptive immune responses are involved in disease pathogenesis (Figure 1) (2, 7). The pathophysiology of both diseases is complex without a single aetiological factor. While there are similarities between RA and PsA, there are key differences distinguishing them (2).

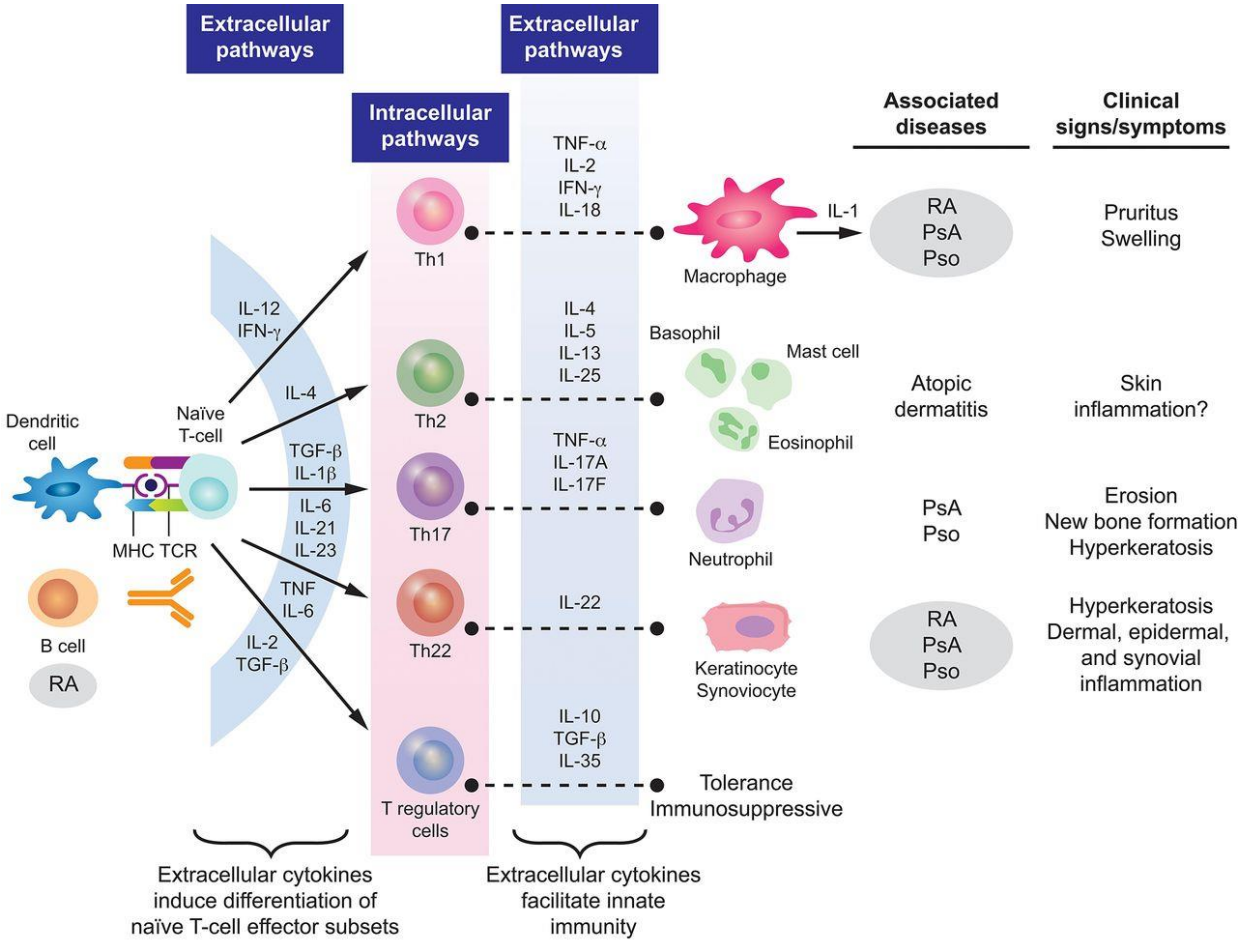

Figure 1 Pathogenesis of RA and PsA.

Reprinted in accordance with the Creative Commons Attribution Non-Commercial (CC BY-NC 4.0) license (https://creativecommons.org/licenses/by-nc/4.0/) from Coates et al. (7) and Merola et al. (2)

It is known that there are genetic factors that predispose to disease susceptibility in inflammatory arthritis. Human leukocyte antigens (*HLA*) alleles are associated with RA and PsA, implicating the adaptive immune system in their pathogenesis. *HLA-DRB1* alleles are associated with disease susceptibility and severity in seropositive RA patients (2). In PsA, *HLA-B27* is associated with enthesitis and sacroiliitis, whereas *HLA-B08* is associated with ankylosis, sacroiliitis and dactylitis (8).

Different immune system components have distinct roles in the pathogenesis of RA and PsA. For example, B cells and plasma cells produce RF and anti-cyclic citrullinated peptide (CCP) antibody which are features of RA (2). In PsA, T helper (Th) 17 cells are key in PsA as they produce pro-inflammatory IL-17A and IL-17F cytokines (2, 7).

DMARDs such as TNFi have revolutionised the treatment of patients with inflammatory arthritis. Although some DMARDs may be used for treating both RA and PsA, there are some differences in treatment strategies between RA and PsA as recommended by EULAR (Table 1) (2, 9, 10). The international experts convened by EULAR performed systematic literature reviews of evidence relating to therapeutics including safety, efficacy and cost-effectiveness. They then reached consensus by voting on the recommendations. The level of evidence varied depending on the individual context, but most recommendations had high level of evidence (9, 10).

Table 1 2022/2023 EULAR recommended DMARDs for treatment of RA and PsA.

Adapted in accordance with the Creative Commons Attribution Non-Commercial (CC BY-NC 4.0) license (https://creativecommons.org/licenses/by-nc/4.0/) from Merola et al. (2, 9, 10)

		Indication	
Class	Agent	RA	PsA
Conventional synthetic DMARDs			
	Methotrexate	+	+
	Leflunomide	+	+
	Sulfasalazine	+	+
	Hydroxychloroquine	+	-
Biological DMARDs			
TNF inhibitors	Adalimumab	+	+
	Certolizumab pegol	+	+
	Etanercept	+	+
	Golimumab	+	+
	Infliximab	+	+
IL-12/23 inhibitor	Ustekinumab	-	+
IL-17A inhibitor	Secukinumab	-	+
	Ixekizumab	-	+
IL-17A/F inhibitor	Bimekizumab	-	+
IL-23-p19	Gueselkumab	-	+
	Risankizumab	-	+
IL-6 receptor inhibitor	Tocilizumab	+	-
	Sarilumab	+	-
T-cell activation inhibitor	Abatacept	+	+
CD20 inhibitor	Rituximab	+	-
Targeted synthetic DMARDs			
PDE4 inhibitor	Apremilast	-	+
Janus kinase inhibitor	Baricitinib	+	-
	Filgotinib	+	-
	Tofacitinib	+	+
	Upadacitinib	+	+

Although some treatment regimens are shared between RA and PsA, distinguishing between RA and PsA is important to determine the optimal treatment regimen for patients. Differences in the pathogenesis of RA and PsA may underlie the difference in efficacy of their response to treatments. IL-17 and IL-12/23 play an important role in PsA whereas IL-

6 is a major contributor to disease in RA (2). It is therefore rational that IL-17A inhibitors (secukinumab, ixekizumab) and IL-12/23 inhibitor (ustekinumab) are efficacious for PsA whereas IL-6 receptor inhibitor (tocilizumab) is used for treating RA (2).

Although biologic DMARDs such as TNFi have revolutionised the treatment of RA and PsA, only two-thirds of patients have a good to moderate response to TNFi, whereas one-third have no or insufficient response (11, 12). Furthermore, up to half of patients who initially respond well to TNFi, subsequently lose their response within 12 months of starting therapy. DMARDs also have potential side effects such as an increased risk of serious infections. For example, treatment with TNFi and corticosteroid tripled the infection risk compared to conventional DMARD alone in patients with RA and spondyloarthropathy (13). Currently available treatments are not efficacious for all patients with inflammatory arthritis. Current therapeutic strategy involves trial and error until a treatment is found to be effective (9, 10). There is an unmet need for precision medicine to get the right medicine in the right patient at the right time (14, 15).

A greater understanding of the pathophysiology underpinning RA and PsA would help development of more effective and safer treatments for patients. The Advances in Targeted Therapies group identified unmet needs in rheumatology based on expert consensus (14). Across rheumatological conditions, there was a need for clinical trial design innovation with regards to therapeutics, endpoint and disease endotypes. In RA, unmet needs were identified in molecular classification of disease pathogenesis and activity, pre- and early RA strategies, pain profiling, and precision medicine strategies. For PsA, the unmet needs were markers that predict development of PsA, and evaluation of combination therapies for difficult-to-treat PsA. As synovial hypoxia has been implicated in the disease processes

underlying inflammatory arthritis, and recently oxygen nanobubbles (to be discussed later) have been developed to target peripheral tissue hypoxia, I therefore focussed on studying joint hypoxia.

1.1.2 Synovial hypoxia in inflammatory arthritis

Synovial joint hypoxia is a recognised feature of inflammatory arthritis (16). Hypoxia is a state in which oxygen is not available in sufficient amounts at the tissue level to meet demand. Joint hypoxia may be due to increased synovial tissue metabolic demand and diminished oxygen supply (17). HIFs are transcription factors that respond to hypoxia and orchestrate cellular responses to adapt to hypoxia.

Since the 1970s, joint hypoxia has long been recognised as a feature of inflammatory arthritis including RA and PsA (16). The seminal study on hypoxia in inflammatory arthritis was performed by Lund-Olesen *et al*. (16). They demonstrated synovial fluid oxygen levels were lower in RA (26.53 mmHg) than OA (42.92 mmHg) or haemarthrosis (63 mmHg) (16). This study was important because it was the first to suggest that joint oxygen level was lower in inflamed joints compared with non-inflamed joints in RA, although no clinical difference was found between the subgroups with high versus low joint oxygen levels (16). Joint hypoxia in inflammatory arthritis thus formed the foundation for investigation in this project.

Most of what is known about inflammatory arthritis synovial tissue response to hypoxia relates to studies involving RA. Less is known about synovial tissue response to hypoxia in PsA as studies have historically focused on RA rather than PsA. The mechanisms by which joint hypoxia influence synovial tissue inflammation may be shared across RA and

PsA. More studies are needed to determine whether synovial tissue response to hypoxia is the same or different in RA and PsA, as therapeutic targeting of joint hypoxia may be applicable to both diseases. The synovial tissue response to hypoxia is orchestrated by HIFs. HIF-1α is upregulated in RA fibroblasts (18), CD3+ T cells (19), and CD68+ synovial macrophages (20). RA synovial macrophages have also been shown to express hypoxia related genes including stromal cell-derived factor-1 (SDF-1), IL-8, VEGF, IL-1β and TNF (21). The mechanisms by which joint hypoxia influence synovial tissue inflammation may be shared across RA and PsA.

HIF-1 is a heterodimeric transcription factor composed of two subunits HIF-1α and HIF-1β (22, 23). The HIF pathway has been extensively reviewed previously so it is described briefly here. HIF-1α is regulated by post-translational modifications that are sensitive to oxygen levels. Under normoxic conditions, HIF-1α is hydroxylated by prolyl-4-hydroxylase domain protein (PHD) and asparagyl β-hydroxylases such as Factor-Inhibiting HIF-1α (FIH), followed by ubiquitination by the von Hippel-Lindau protein (pVHL) and proteasomal degradation (24). Although three isoforms of PHD have been identified, PHD1, PHD2, and PHD3, the most prominent hydroxylase regulating HIF-1α levels is PHD-2 (17, 24-26). In hypoxia, PHD and FIH are inactivated so HIF-1α is stabilised and translocates to the nucleus where it dimerises with HIF-1β. This heterodimeric transcription factor binds to hypoxia response element (HRE) enabling the transcription of HIF dependent genes such as *VEGF* (27).

The relevance of HIFs in the pathophysiology of inflammatory arthritis can be assessed by comparing HIF levels in inflamed synovial tissues with non-inflamed synovial tissues. HIF is regulated at the protein level through protein degradation, so HIF gene expression is a

poor reflection of HIF function. HIF-1α levels were characterised in synovial tissues from ten patients with RA, ten patients with OA, and six healthy controls (20). HIF-1α was found in higher levels in RA synovial tissues compared to OA and healthy controls. HIF-1α was also reported to be present at higher levels in RA synovium than OA synovium in another study (28).

HIF-1α has been shown to be involved in the pathogenesis of inflammatory arthritis (29). Cramer *et al*. used the K/BxN serum transfer model of inflammatory arthritis to study the effects of HIF-1α knockout (KO) (29, 30). This model involves injecting healthy mice twice with serum from K/BxN-TCR transgenic mice which results in inflammatory arthritis development over weeks (31). Cramer *et al*. used conditional gene targeting to delete *Hif1a* gene target in mice expressing cre recombinase in myeloid cells (29). Using the K/BxN serum transfer model, loss of HIF-1α in myeloid cells reduced ankle joint synovitis and cartilage destruction compared to wild-type mice demonstrating the importance of HIF-1α in inflammation (29).

HIF-1α is not the only HIF to be implicated in inflammatory arthritis. HIF-2α is a closely related isoform to HIF-1α as both HIF-1α and HIF-2α activate HRE-dependent gene expression. Both HIF-1α and HIF-2α were shown to be upregulated in RA and OA synovial tissues compared to non-arthritic synovial tissues from patients undergoing hip joint replacement following fracture (32). However, HIF-1α and HIF-2α have non-redundant roles due to "differences in tissue-specific and temporal patterns of induction" with distinct transcriptional targets (33). For example, HIF-1α coordinates the glycolytic pathway whereas HIF-2α does not appear to do so (33). In one study, HIF-2α was reported as the predominant isoform in RA synovium whereas HIF-1α expression was found to be

sparse in the RA synovium (34). HIF-2α has been shown to be expressed consistently in synovial and tenosynovial tissues in patients with RA, in co-localisation with VEGF in synovial lining and areas of inflammatory cell aggregates (35). HIF-1α and HIF-2α may have distinct roles and act via different mechanisms in pathogenesis of inflammatory arthritis (34). HIF-2α regulates receptor activator of nuclear factor-κB ligand (RANKL), IL-6 production, and Th17 cell differentiation (34). Indeed, Ryu *et al*. showed that HIF-2α deficiency inhibited the development of experimental RA (34).

In the study by Ryu *et al*., collagen-induced arthritis (CIA) in mice was used as an experimental model of inflammatory arthritis caused by an autoimmune response against cartilage type II collagen (29, 34, 36). As homozygous deletion of *Epas1* gene (which encodes HIF-2α) is lethal, Ryu *et al*. used heterozygous $Epas1^{+/-}$ mice to study the effects of systemic HIF-2α deficiency (29, 34, 37, 38). In contrast to wild-type mice, $Epas1^{+/-}$ mice showed significantly reduced incidence (89.4% ± 7.1% versus 33.2% ± 6.5%, p = 0.0004) and severity (2.85% ± 0.26% versus 1.10% ± 0.10%, p = 0.004) of CIA on day 60 after the first injection of type II collagen (29, 34). Ryu *et al*. further validated the role of HIF-2α in CIA by locally deleting *Epas1* in joint tissues using intra-articular injection of Ad-*Cre* (1 x 10^9 plaque-forming units) in mice (34). Local deletion of *Epas1* in joint tissues significantly inhibited synovitis, pannus formation, angiogenesis and cartilage destruction in CIA mouse models (34).

Furthermore, overexpression of HIF-2α in joint tissues was sufficient to cause experimental arthritis *in vivo* (34). Intra-articular injection of Ad-*Epas1* adenovirus in knee joint of mice upregulated HIF-2α in the synovium, cartilage and meniscus, as well as synovitis, angiogenesis and cartilage destruction (34). Together, these findings suggest that

HIF-2α plays a role in the pathogenesis of inflammatory arthritis (34). In contrast, overexpression of HIF-1α in joint tissues was insufficient to cause inflammatory arthritis *in vivo* highlighting the distinct roles of HIF-1α and HIF-2α in the pathogenesis of inflammatory arthritis (34).

1.1.3 Role of hypoxia and HIFs in inflammatory arthritis

Synovial hypoxia and associated HIF-1α activate transcription factors that promote synovitis, angiogenesis, cartilage destruction and bone erosion (Figure 2) (24, 39-41). Indeed, conditional knock-out of *HIF1α* in animal models of RA demonstrated significant reduction in synovial inflammation, pannus formation and cartilage destruction (29, 41). Similarly, endothelial PAS domain protein 1 (*EPAS1*) overexpression (which encodes HIF-2α) caused an RA-like phenotype and HIF-2α deficiency blunted the development of experimental RA (34).

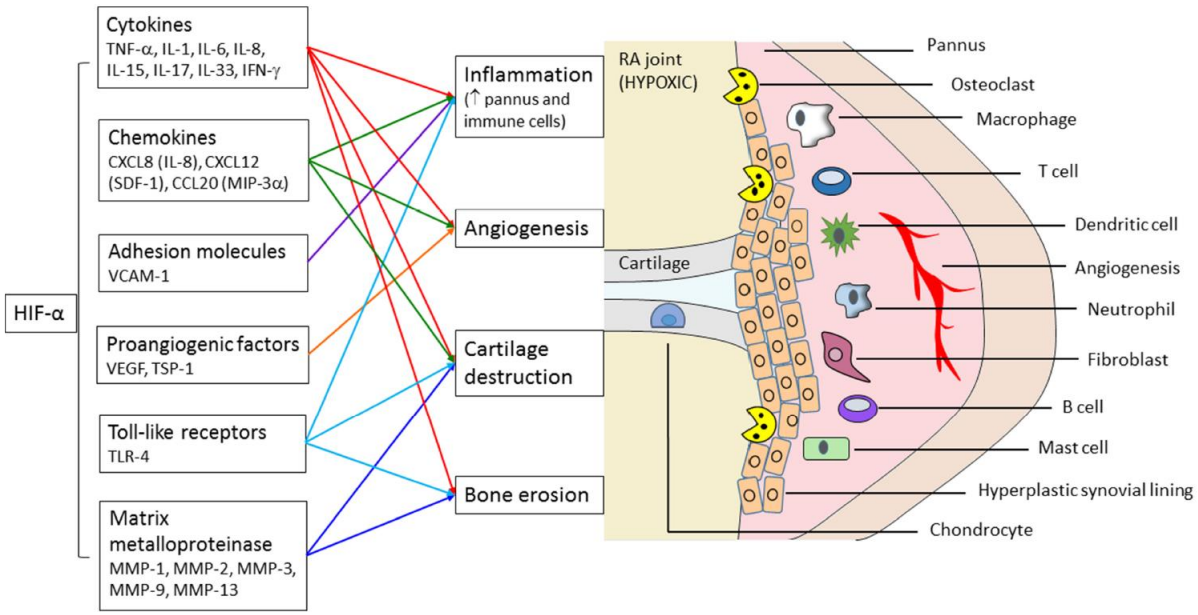

Figure 2 Role of HIF-α in inflammation and destruction of the RA joint.

Many downstream effects of HIF-1α are mediated by VEGF upregulation. The regulation of VEGF by HIF-1α through its HRE has been well characterised (39). Promotion of angiogenesis is an important role of HIFs in the pathogenesis of RA (42). In synovial tissues from patients with RA, the number of HIF-1α expressing cells correlated with the magnitude of the angiogenic response (43). HIFs induce pro-angiogenic factors including vascular endothelial growth factor (VEGF), VEGF receptor Flt-1, Tie-2, Tie-2 receptor Flk-1, angiopoietins, IL-8, CCL20 and CXCL12 (18, 28, 42, 44-47). These in turn promote endothelial cell migration and proliferation, and tissue remodelling leading to new blood vessel formation.

Angiogenesis would be expected to increase blood supply and therefore deliver more oxygen to ameliorate hypoxia. However, angiogenesis is also widely implicated in the pathogenesis of inflammatory arthritis (48-50). Blood vessel growth promotes recruitment of inflammatory cells to inflamed synovium (48). The role of angiogenesis in inflammatory arthritis is further supported by studies that inhibited VEGF pathway which attenuated arthritis severity in animal models of inflammatory arthritis (48, 50). Upregulation of VEGF promotes cartilage destruction and bone erosions through post-translational activation of MMP-9 (51-53). Responses to hypoxia may therefore be a double-edged sword with both beneficial and deleterious effects in the inflamed joint.

Chemokines such as CXC chemokine ligand (CXCL) 12 are upregulated by hypoxia and drive recruitment of monocytes and lymphocytes to the synovium in inflammatory arthritis

(24, 54, 55). The expression of CXCL12 is hypoxia dependent via HIF-1α and HIF-2α (18, 56). The CXCL12 receptor, CXCR4, is also HIF-1α regulated, as is β_2 integrin subunit CD18, which is known to recruit myeloid cells to inflamed tissues (57, 58). Conversely, passively induced arthritis mouse models with HIF-1α deficient macrophages exhibited reduced disease development, reduced paw swelling and decreased myeloid cell infiltration to the joint (29). These findings substantiate the role of HIF-1α in inflammatory arthritis.

In addition to recruiting inflammatory cells to synovial tissues, HIFs may promote arthritis by inducing cartilage damage (42). For example, hypoxia via HIF-1 promotes pannus invasion, cartilage destruction and bone erosion through Ets-1 (42). Hypoxia induces Ets-1 expression which co-localises with HIF-1α in the inflamed synovium (24, 59, 60). In turn, transcription factor Ets-1 induces matrix metalloproteinases (MMPs) leading to extracellular matrix remodelling and cartilage degradation (59, 61). Increased activity of MMPs is associated with articular cartilage destruction in RA (24). MMPs are regulated by tissue inhibitors of MMPs (TIMP). Hypoxia induces increased levels of MMP-1 and MMP-3, and decreased levels of TIMP-1, potentially contributing to cartilage degradation (24, 28, 62). Bone damage is also promoted by the hypoxic pathway. For example, HIF-1α induces overexpression of angiopoietin-like (ANGPTL) 4 in RA osteoclasts which drives bone resorption (24, 63).

Epidemiology studies into genetic polymorphisms may provide further insight as to whether certain genes contribute to pathogenesis of diseases. *HIF1A* polymorphisms may be associated with RA (27). In a case-control study of *HIF1A* gene polymorphisms in patients with RA, the polymorphic *HIF1A rs12434439 GG* genotype may protect from

development of RA. Although the functional role of this polymorphism is unknown, RA patients with *HIF1A rs12434439 GG* genotype were found to have higher Foxp3 expression in serum than other RA patients but this did not reach statistical significance (P = 0.06) (27). Given that no other *HIF1A* gene polymorphisms have been reported to be associated with RA, the contributions of *HIF1A* gene polymorphisms to the pathogenesis of RA may be limited.

The heritability of RA is approximately 65% and more than 100 genetic loci have been associated with susceptibility to RA (64). Genetic variants encoding the HLA molecules account for most of the known genetic heritability of RA (64). Genome-wide association studies (GWAS) identify genes in RA-risk loci that may encode proteins that are involved in pathogenesis of RA. However, GWAS studies have not found an association between *HIF1A rs12434439* gene polymorphisms with RA.

In 2010 a GWAS meta-analysis of 5,539 autoantibody-positive individuals with RA and 20,169 controls of European descent, HIF alleles including *HIF1A rs12434439* gene polymorphisms were not associated with RA (65). Similarly in 2013, GWAS meta-analysis of 29,880 RA cases and 73,758 controls of European and Asian ancestries identified RA risk loci but HIF alleles including *HIF1A rs12434439* gene polymorphisms were not associated with RA (66). In 2020, the largest ever trans-ancestral inverse-variance-weighted fixed-effects meta-analysis consisting of 311,292 individuals of Korean, Japanese and European populations identified RA susceptibility loci but no associations between HIF alleles and RA were found (67). More recently in 2022, a large-scale GWAS of RA involving 276,020 samples from five ancestral groups characterised

RA susceptibility loci but *HIF1A rs12434439* gene polymorphisms were not associated with RA (68). Therefore, genetic studies do not support HIF alleles as risk factors for RA.

1.1.4 Role of NF-κB in hypoxia

Nuclear factor kappa-light-chain-enhancer of activated B cells (NF-κB) mediates crosstalk between hypoxic and inflammatory pathways (24, 69-71). NF-κB is a master regulator of innate immunity, inflammation and apoptosis (17, 24). The NF-κB family is composed of five related proteins p65 (RelA, NF-κB3), p50 (NF-κB1), p52 (NF-κB2), c-Rel and RelB (70). Activation of toll-like receptors (TLRs) and cytokine receptors lead to NF-κB phosphorylation and activation through canonical and non-canonical pathways (70). The canonical pathway involves the heterotrimeric IκB kinase (IKK) complex comprising IKKα, IKKβ and NF-κB essential modulator (NEMO), which phosphorylates IκBα, targeting it for ubiquitylation-dependent degradation (70). Translocation of NF-κB dimers to the nucleus due to IκBα degradation results in gene transcription as canonical NF-κB signalling. By contrast, the non-canonical pathway is mediated by IKKα homodimers (72). Activation of lymphotoxin β receptor (LTβR), B cell activating factor receptor (BAFF-R) or receptor activator of nuclear factor-κB (RANK) induces NF-κB/RelB:p52 dimer in the nucleus (72).

Hypoxia can also activate NF-κB family members via oxygen-dependent hydroxylases or HIF-1α interactions (Figure 3) (24, 69, 70). HIF-1α synergises with TLR signalling such as NF-κB to upregulate inflammatory cytokines (IL-6, IL-8, TNF), MMPs and VEGF (17, 73). NF-κB is overexpressed in RA synovial tissues and regulate genes associated with inflammation, angiogenesis and tissue destruction (24, 74, 75). Low synovial pO_2 levels *in vivo* were associated with increased NF-κB activity in RA synovial biopsies (17, 76).

Synergistic interactions between NF-κB and HIF-1α maintain the inflammatory response (24, 77).

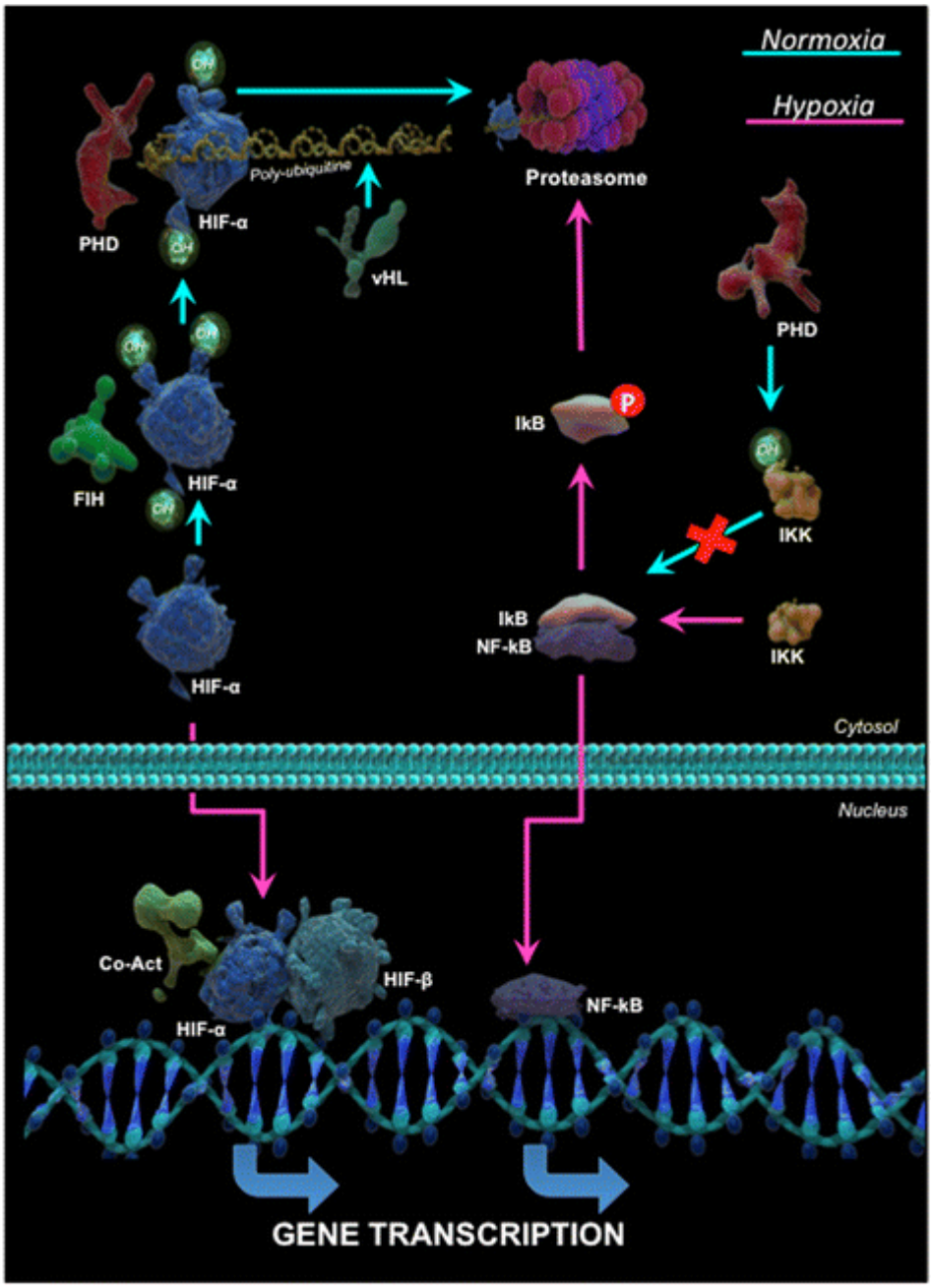

Figure 3 Hypoxia and signalling mediators.

Reprinted in accordance with the Creative Commons Attribution Non-Commercial (CC BY-NC 4.0) license (https://creativecommons.org/licenses/by-nc/4.0/) from Quinonez-Flores et al. (24)

NF-κB in turn affects the hypoxic response through interactions with HIF-1α and NF-κB overexpression increases HIF-1α protein levels (70, 78). Indeed, IKK-β deficient mice have reduced *HIF-1α* mRNA expression, HIF-1α protein levels and HIF-dependent gene expression (70, 71). Targeting the NF-κB pathway may therefore inhibit inflammation through hypoxia related pathways. High-mobility group box 1 (HMGB-1) protein is an endogenous TLR ligand present in RA synovial fibroblasts (79). NF-κB inhibition in a CIA model inhibited High-Mobility Group Box 1 (HMGB1) protein-dependent upregulation of HIF-1α, angiogenesis and synovial inflammation (17, 79).

1.1.5 Hypoxia in innate and adaptive immunity

The innate immune system responds to hypoxia (70). HIF-1α is essential for myeloid cell-mediated inflammation (29). Myeloid cells such as macrophages and neutrophils produce adenosine triphosphate (ATP) via glycolysis which is regulated by HIF-1α (29). Furthermore, HIF-1α regulates myeloid cell aggregation, motility, invasiveness and bacterial killing (29). Crosstalk between innate and adaptive immune systems is mediated by antigen presenting cells (APC) such as dendritic cells. Hypoxic exposure decreases dendritic cell presentation of co-stimulatory signals to T cells and induces cell death in immature dendritic cells (80-82).

The adaptive immune system is composed of lymphocytes including T cells and B cells. Hypoxia and HIF-1α play a role in T cell differentiation and function (83). For example, HIF-1α enhanced Th17 development through transcriptional activation of the IL-17 promoter and increased production of IFNγ and IL-17 (70, 84). Hypoxia and HIF-1α have pleiotropic functions in Treg differentiation (70). Treg cell development is inhibited by HIF-1α which binds Foxp3 and target it for proteasomal degradation (84). However,

FOXP3 expression and Treg differentiation are promoted by hypoxia. The role of hypoxia and HIF-1α in Treg cell differentiation and function may depend on other cytokine signalling in the microenvironment (70). Similarly for B cells, HIF-1α is essential for B cell development and function (70, 85, 86). Therefore, hypoxia and the HIF pathway have major roles in immune cell development and function which may influence inflammation in the setting of arthritis.

1.1.6 Joint hypoxia as inducer of inflammatory arthritis

It is unclear as to whether joint hypoxia is a consequence of inflammatory arthritis, or whether joint hypoxia has a role in the cause of inflammatory arthritis. It is likely that both may be true. Jeon *et al*. studied the reciprocal relationship between joint hypoxia and inflammation in collagen induced arthritis mice where synovial hypoxia was detected before the onset of arthritis (87). Hypoxic change as measured by the hydroxyprobe-1 stain was identified in synovium within one week after the collagen injection, prior to clinically evident arthritis (87). Moreover, markers of inflammation and hypoxia co-localised in the synovium and there was a positive correlation between the severity of hypoxia and the degree of synovitis (87). However, no difference in intra-articular oxygen tension was noted between naïve and pre-arthritic mice (88). This discrepancy may be due to the hydroxyprobe-1 stain which may be more sensitive to subtle hypoxic changes (87). The hydroxyprobe system uses pimonidazole hydrochloride as its hypoxia marker, which forms protein adducts in hypoxic cells *in vivo*, and may measure hypoxic changes not detectable with microelectrode (89, 90). Hypoxic changes preceding arthritis suggest that hypoxia may be involved in pathogenesis of inflammatory arthritis (17).

1.1.7 Adaptive and maladaptive responses to hypoxia

Physiological responses to hypoxia may be adaptive or maladaptive. For example, chronic intermittent hypobaric hypoxia pretreatment conferred a protective effect against collagen-induced arthritis in rat through downregulation of HIF-1α, NF-κB, TNF and IL-17 in synovial tissues (91). Conversely, HIF-1α has been shown to regulate IL-33 production by synovial fibroblasts, which in turn induced HIF-1α expression, thus forming a HIF-1α/IL-33 regulatory circuit that perpetuates inflammatory arthritis (92). Given that hypoxia and its downstream signalling are implicated in inflammatory arthritis, inhibiting the hypoxic pathway may be an effective anti-inflammatory strategy. However, HIF hydroxylase inhibitors which activate the HIF pathway were found to induce anti-inflammatory effects in animal models of inflammation (70). Relieving joint hypoxia therefore also has the potential to exacerbate inflammatory arthritis.

In addition to hypobaric hypoxia, environmental factors such as cigarette smoking can also lead to tissue hypoxia and activate HIF-1α (93, 94). Indeed, smoking is a risk factor for arthritis such as RA (95-100). Cohort studies have shown that people who smoke for more than 20 years have a twofold increased risk of developing seropositive RA (100). This association between smoking and RA may be due to multifactorial effects of smoking including hypoxia. Chronic cigarette smoking can result in chronic obstructive pulmonary disease (COPD) which impair pulmonary gas exchange resulting in systemic hypoxia (101). The binding of carbon monoxide in cigarette smoke to haemoglobin and mitochondrial cytochrome oxidase further exacerbate tissue hypoxia.

Animal models have been used to study the mechanistic basis by which cigarette smoking is linked to arthritis. In a CIA animal model, cigarette smoke exacerbated symptomatic

arthritis (102). This link between smoking and inflammatory arthritis was partially explained by citrullination of lung tissues, arthritic tissues and tracheal cartilage, as well as development of anti-CCP antibodies (102). To investigate whether cigarette smoke causes inflammatory arthritis through hypoxia in synovial tissues, future studies that monitor synovial tissue pO_2 with oxygen probes in mice exposed to cigarette smoke would clarify this relationship. In addition to inducing tissue hypoxia, cigarette smoking may activate hypoxic pathways independent of tissue pO_2. For example, cigarette smoke extract has been shown to activate HIF-1α *in vitro* and *in vivo* in non-hypoxic conditions (94).

Smoking may also contribute to the development of arthritis through mechanisms unrelated to hypoxia. Cigarette smoke contains thousands of toxic chemicals with cytotoxic, mutagenic and immunomodulatory properties (100). Smoking may result in genetic or epigenetic modifications, increased oxidative stress, hypoxia, and chemical toxicity (100). These multifactorial effects of smoking can increase the risk of inflammatory diseases by increasing immune cell proliferation, Treg inhibition, autoantibody generation and increasing inflammatory cytokines (100).

1.1.8 Tissue hypoxia as a therapeutic target

Targeting peripheral tissue hypoxia has long been of interest in wide ranging fields including cancer (103), aerospace medicine (104), sports (105-108), and warfare (109). As oxygen homeostasis is a fundamental physiological process, interventions that target hypoxia have profound effects on diverse biological pathways including cell survival, erythropoiesis, angiogenesis and metabolism (103). Different strategies to intervene in hypoxia are available.

“Oxygen is one of the most commonly used therapeutic agents” (110). Administering high flow oxygen is widely used to relieve hypoxia in patients with cardiopulmonary disease. This strategy has also been applied outside of healthcare settings. For example, closed-circuit rebreathers with 100% oxygen have been used for covert diving operations (111). However, breathing high partial pressure of oxygen culminates in harmful effects in a condition called oxygen toxicity (110). Consequences of oxygen toxicity include neurological effects such as convulsions and retinopathy of prematurity, as well as pulmonary toxicity such as inflammation and fibrosis of lung tissues (111).

The mechanisms underlying oxygen toxicity have previously been reviewed and are briefly described here (110, 112). Hyperoxia leads to generation of reactive oxygen species (ROS) which produce oxidative stress and damage proteins, enzymes, membrane lipids and nucleic acids (110). Products of oxidative stress such as the hydroxyl radical initiate lipid peroxidation in unsaturated lipids within cell membranes (110). Hyperoxia also elevate levels of free radicals including nitric oxide, peroxynitrite and trioxidane (112). Inadequate detoxification of free radicals by antioxidants such as glutathione underlie cell damage in oxygen toxicity (110).

The manifestations of oxygen toxicity in the form of retinopathy of prematurity resemble the tortuous vasculature seen in inflammatory arthritis such as PsA. Retinopathy of prematurity is characterised by disorganised growth of retinal blood vessels in premature babies treated with supplemental oxygen (113). Normally, blood vessels grow towards hypoxic areas of the retina. However, treatment with supplemental oxygen induces hyperoxia and VEGF suppression that leads to cessation of blood vessel growth in the retina (114). Removal of supplemental oxygen then results in hypoxia in the avascular

retina, increases VEGF expression, and rapid abnormal neovascularisation that extend into the vitreous humour from the retina (113, 114). Retinopathy of prematurity may be complicated by vascular dilation and tortuosity of the posterior retinal arterioles, vitreous haze and anterior chamber haze, iris vascular engorgement, and immature blood vessels overlying the lens which restrict pupil dilatation (115).

Peripheral retinal ablation is the main treatment for retinopathy of prematurity (114). Since VEGF has been implicated in the pathogenesis of retinopathy of prematurity, intravitreal injection of anti-VEGF drugs has also been reported as an adjunct treatment for retinopathy of prematurity (116). A Cochrane review found that combination treatment of retinopathy of prematurity with laser retinal ablation and intravitreal pegaptanib (a VEGF antagonist) reduced risk of retinal detachment compared to laser or cryotherapy alone (152 eyes; risk ratio 0.26, 95% CI 0.12 to 0.55; risk difference -0.29, 95% CI -0.42 to -0.16; low-quality evidence) (116). Retinopathy of prematurity highlights how abnormal tissue hypoxia can result in disease and the potential of the hypoxic pathway as a therapeutic target.

It has not been possible to relieve peripheral tissue hypoxia directly until recently. Formulation of oxygen encapsulated lecithin based nanobubbles in beverages have been proposed to increase oxygen delivery in blood by acting as oxygen carriers much like how perfluorocarbon nanodroplets function as blood substitutes (117-119). Indeed, oxygen nanobubble drinks demonstrated significant and meaningful performance improvements in elite cyclists (118). Moreover, orally administered oxygen nanobubbles have recently been shown to relieve peripheral tissue hypoxic markers in an animal cancer model (120). Measuring hypoxia in the arthritic joint however is poorly understood. Therefore, a

scoping literature review is warranted to provide insight into what is known about synovial oxygen measurements in humans, clinical benchmarks for hypoxia, how to measure pO_2 in human joints and entheses.

Systematic reviews and scoping reviews are types of literature reviews, but they differ in their purpose and analysis. The purpose of a systematic review is to answer a specific research question whereas the purpose of a scoping review is to provide an overview (121). If the results of the literature review will be used to answer a clinically meaningful question or to inform clinical practice, then a systematic review would be the valid approach (121). Conversely, a scoping review is more appropriate for a general discussion of characteristics and concepts in studies. As the purpose of this literature review is to explore concepts and gaps in our knowledge relating to hypoxia in inflammatory arthritis, a scoping review was selected for this purpose.

1.2 Methods

1.2.1 Information sources and search strategy

A scoping review was conducted to provide an overview of evidence from clinical studies relating to hypoxia and oxygen measurements in human joints and entheseal tissues. A scoping review is a rigorous but efficient approach to identify and synthesize the most relevant available evidence on a given topic. Due to the nature of the questions and the type of evidence sources available to address them, the Preferred Reporting items for Systematic Reviews and Meta-Analyses extension for scoping reviews was used to conduct the review (122). This study was not registered because PROSPERO does not accept scoping reviews. Evidence was sourced from EmBASE and PubMed. A broad

search strategy was applied to avoid missing relevant literature. The electronic search strategy was as follows: Title/Abstract: (arthritis* OR enthesitis*) AND Title/Abstract: (hypoxi* OR oxygen*) AND Title/Abstract: (synovi* OR joint OR tendon* OR ligament* OR enthes*). A systematic search of EmBASE and PubMed identified relevant studies for inclusion.

All citations retrieved from the databases were uploaded into Endnote with duplicates removed. All titles and abstracts were reviewed by one reviewer. Data processing method described in section 11. Appendix A: Scoping literature review data processing.

1.3 Results

816 references were imported from Pubmed on 17/03/21. 2047 references were imported from Embase on 17/03/21. References from Pubmed and Embase were pooled for total of 2863 references. 589 duplicates were automatically removed. All remaining references were manually reviewed for clinical relevance. 20 clinical studies were found to relate to hypoxia and oxygen measurements in human joints (Table 2). No studies relating to hypoxia and oxygen measurements were found in human entheses.

There was heterogeneity amongst the patient populations studied. Healthy participants were investigated in one study, whereas inflammatory arthritis such as RA and PsA were the most common populations studied. There was a range of sample size in the studies with the largest study involving 30 patients with RA and 42 patients with osteoarthritis (OA) (123).

A scoping review approach is indicated when examining how research is conducted on a particular topic (121). This scoping review surveyed the literature to determine how data pertinent to the measurement of pO_2 in synovial tissue and fluid were reported in studies, and whether the methods were similar enough to allow for comparison across studies. 12 studies measured synovial tissue pO_2, 7 studies measured synovial fluid pO_2, and one study did not specify whether the pO_2 measured was from synovial fluid or tissue (Table 2). There were variations in the methods used to measure pO_2 in the joint, if the method was reported at all. Generally, pO_2 was measured in synovial fluid using gas analysers and in synovial tissue using a Licox probe (124). There was disparity in the reporting of joint pO_2. All except 3 studies reported at least either the range, mean or median joint pO_2 (Table 2).

One study measured matched *in vivo* synovial and tenosynovial tissue pO_2 intra-operatively in patients with RA having elective hand surgery and in patients without RA having elective hand surgery for indications other than inflammatory arthritis as controls (35). Median tenosynovial tissue pO_2 was found to be 26 mmHg in invasive tenosynovium in patients with RA (interquartile range 18-33 mmHg) compared with 74 mmHg in patients without RA (interquartile range 69-89 mmHg, $P < 0.001$) (35). Invasive tenosynovium was significantly more hypoxic compared with both joint synovium and non-invasive tenosynovium in the same patients (35).

Table 2 Summary of clinical studies of synovial hypoxia in arthritis

Authors	Year	Disease	Sample size	Synovial sample	pO_2 range	Mean pO_2	Median pO_2	Method of pO_2 measurement
Lund-Olesen *et al.* (16)	1970	RA, osteoarthrosis, traumatic exudates, Reiter's syndrome	29 RA, 8 osteoarthrosis, 4 traumatic exudates, 1 Reiter's syndrome	Fluid	20-71 mmHg in osteoarthrosis, 42-87 mmHg in traumatic exudates	26.53 mmHg in RA, 42.92 mmHg in osteoarthrosis and 63 mmHg in traumatic exudates	Unspecified	Clark type microelectrode oxygen monitor
Falchuk *et al.* (125)	1970	RA, PsA, OA, torn menisci, ochronosis, Reiter's syndrome	22 RA, 2 PsA, 2 OA, 2 torn menisci, 1 ochronosis, 1 Reiter's syndrome	Fluid	9-53 mmHg	Unspecified	Unspecified	Blood gas analyser
Treuhaft *et al.* (126)	1971	Juvenile rheumatoid arthritis, granulomatous colitis, internal derangement, AS, RA, Reiter's, gout, PsA, unknown, trauma, OA, gonococcal arthritis, gout, vasculitis, SLE	44	Fluid	8-78 mmHg	Unspecified	Unspecified	Clark electrode
Goetzl *et al.* (127)	1974	Juvenile rheumatoid arthritis, adult RA	26 Juvenile rheumatoid arthritis and 32 adult RA	Fluid	Juvenile rheumatoid arthritis ranged from 1-49 mmHg. Adult RA ranged from 9-36 mmHg	21 mmHg in juvenile rheumatoid arthritis. 24 mmHg in adult RA.	Unspecified	Sealed heparinised synovial fluid was measured for pO_2

Authors	Year	Disease	Sample size	Synovial sample	pO_2 range	Mean pO_2	Median pO_2	Method of pO_2 measurement
Richman *et al*. (128)	1981	OA, hypertropic OA, CPPD, Reiter's syndrome, AS, RA	22	Fluid	0-78 mmHg	Unspecified	Unspecified	Blood gas analyser
Geborek *et al*. (129)	1988	RA, PsA, reactive arthritis, HLA-B27 associated arthropathy, unclassified chronic arthritis	9 RA, 2 PsA, 1 reactive arthritis, 1 HLA-B27 associated arthropathy, 1 unclassified chronic arthritis	Fluid	Unspecified	Unspecified	Unspecified	Blood gas analyser
Lee *et al*. (123)	2007	RA, OA	30 RA, 42 OA	Fluid	Unspecified	OA with synovial proliferation group (mean±SD, 79.2 ± 14.0). OA without synovial proliferation group (mean±SD 80.2 ± 14.0 mmHg). RA with synovial proliferation group (mean±SD 51.0 ± 16.5 mmHg)	Unspecified	Blood gas analyser

Authors	Year	Disease	Sample size	Synovial sample	pO_2 range	Mean pO_2	Median pO_2	Method of pO_2 measurement
Sivakumar *et al*. (35)	2008	Patients having elective hand surgery for RA and indications other than inflammatory synovitis	21 RA patients, 10 patients without RA	Tissue	14-35 mmHg in encapsulating tenosynovium. 65-102 mmHg in tenosynovium of individuals without RA.	Unspecified	46 mmHg in synovium, 40 mmHg in encapsulating tenosynovium, 26 mmHg in invasive tenosynovium	Microelectrode
Bosco *et al*. (130)	2009	Healthy	Unspecified	Unspecified	Physiologic O_2 concentration in healthy joints range between 7-10%. Rheumatic joint pO_2 ranges between 0.8-7%.	Unspecified	Unspecified	Unspecified
Biniecka *et al*. (131)	2010	Inflammatory arthritis	16 RA, 7 PsA	Tissue	Unspecified	Unspecified	19.35 mmHg (2.5%)	Licox probe
Ng *et al*. (132)	2010	Unspecified	Unspecified	Tissue	3.2–54.1 mmHg	22.5 mmHg	Unspecified	Unspecified
Biniecka *et al*. (133)	2011	RA, PsA	14 RA, 4 PsA	Tissue	Unspecified	Unspecified	23.5 mmHg for RA and 14.5 mmHg for PsA	Licox probe
Kennedy *et al*. (134)	2011	RA, PsA	20	Tissue	Unspecified	Unspecified	22.78 mmHg	Licox probe
Balogh *et al*. (135)	2012	RA, PsA	30 RA, 14 PsA	Tissue	Unspecified	25.9 mmHg	Unspecified	Licox probe
Biniecka *et al*. (136)	2012	Inflammatory arthritis	48	Tissue	3.2-63 mmHg	Unspecified	26.3 mmHg	Unspecified

Authors	Year	Disease	Sample size	Synovial sample	pO_2 range	Mean pO_2	Median pO_2	Method of pO_2 measurement
Harty *et al*. (137)	2012	RA, PsA	9 RA, 12 PsA	Tissue	Unspecified	Unspecified	Unspecified	Unspecified
Balogh *et al*. (138)	2013	RA, PsA	18 RA, 5 PsA	Tissue	Unspecified	25.94 mmHg.	Unspecified	Licox probe
Hardy *et al*. (139)	2014	RA	Unspecified	Tissue	Unspecified	Unspecified	Unspecified	An oxygen/temperature probe
Fisher *et al*. (140)	2016	RA	23 RA	Tissue	Unspecified	Unspecified	31.1 mmHg	Microelectrode
Biniecka *et al*. (141)	2019	RA	Unspecified	Tissue	3.2-63 mmHg	Unspecified	25.4 mmHg	Unspecified

1.4 Discussion

1.4.1 Quality of evidence

As demonstrated in the clinical evidence map (Table 2), these studies were heterogeneous in disease populations of interest and sample size. The methods used to measure joint oxygen were highly variable. Some measured synovial fluid oxygen using gas analysers whereas others measured synovial tissue oxygen using oxygen probes *in situ*. None of the studies outlined in the evidence map measured both joint fluid and tissue oxygen to validate their joint oxygen measurements. The quality of evidence available was limited in terms of small sample size and joint pO_2 measurements for the purpose of this scoping review. Finally, there were marked evidence gaps relating to the effects of therapeutics on joint hypoxia other than TNFi, as well as hypoxia in enthesitis.

1.4.2 Clinical evidence for joint hypoxia in RA and PsA

It is important to note that pO_2 benchmarks for synovial fluid and tissues in normoxia and hypoxia are unknown. The scoping literature review showed no consensus on the reference range for synovial tissue or fluid pO_2 (Table 2). The scoping review therefore provided insight into the evidence vacuum by which hypoxia is defined in the literature. Without widely accepted pO_2 benchmarks for normoxia and hypoxia in synovial fluid and tissues, there is inconsistency by which researchers report hypoxia in inflammatory arthritis. Bosco *et al*. presented a poster which referred to physiologic O_2 concentrations in healthy joints as between 7-10% but provided no data or citations to substantiate this (130). Future studies on normal synovial tissue or fluid pO_2 in healthy individuals would define such reference range but such studies may be limited by ethical concerns. It would be

challenging to justify an invasive arthroscopic procedure in a healthy subject given the risk of serious harm and no potential for benefit to the participants.

Increased metabolic demand in synovial cells increases oxygen requirements which may result in joint hypoxia. Synovial oxygen uptake and lactate production *in vivo* were shown to be higher in patients with RA than patients with degenerative joint disease (142). These measurements were based on the rate of fall of pO_2 and the rate of rise in lactate concentration in an intra-articular saline pool after an interruption of the circulation to the joint with an arterial tourniquet (142). *In vitro* studies also showed that synovial tissues from patients with RA have greater oxygen consumption rate and greater lactate production rate than control synovial tissues (143-145). Increased oxygen consumption by synovial tissue would be expected to result in hypoxia especially if oxygen supply is insufficient to meet demand.

Inadequate perfusion, which is affected by intra-articular pressure, may result in synovial hypoxia. Joint movement and synovial fluid effusion within the rigid joint capsule may lead to increased intra-articular pressure and tamponade effects which collapse the capillary network and reduces perfusion to synovial tissues (146). During exercise of the knee for example, the intra-articular pressure rises above the synovial capillary perfusion pressure, causing intra-articular hypoxia which resolves with cessation of exercise (146). Furthermore, synovial fluid pO_2 was shown to be inversely correlated with synovial fluid volume ($r = -0.54$, $P < 0.01$) (128). These studies suggest that the synovial effusion volume and intra-articular pressure may affect the articular blood supply. Dysregulated vasculature may also inhibit blood flow to the synovium causing hypoxia.

Metabolites in the joint provide further evidence for joint hypoxia. This topic has been extensively reviewed previously so it is described briefly here (17). Hypoxia in the inflamed joint drives glycolysis and generation of metabolic intermediates including lactate, succinate and itaconate (17). The increased levels of glycolytic metabolites confirm hypoxia in the inflamed joint. These in turn can activate synovial cells further perpetuating disease (17). Lactic acid increases the production of pro-inflammatory cytokines IL-23 and IL-6 from monocytes, IL-17 by T cells, and promotes RA fibroblast-like synoviocytes (FLS) invasiveness (17, 147-149). Succinate enhances macrophage production of IL-1β via HIF-1α (150, 151). Succinate also interacts with Nod-like receptor family pyrin domain containing 3 (NLRP3) inflammasome to activate RA FLS in a HIF-1α dependent manner (152). Moreover, succinate induces synovial angiogenesis in RA through metabolic remodelling and HIF-1α/VEGF axis (153). Itaconate is one of the most highly induced metabolites in macrophages and is a biomarker of inflammatory arthritis in an animal model (154). Itaconate exerts anti-inflammatory effects by regulating succinate levels and macrophage secretion of inflammatory cytokines (17, 155).

There is no consensus as to whether joint hypoxia should be measured according to the pO_2 in the synovial fluid or synovial tissue. pO_2 in synovial tissue can be measured using a Licox probe which requires an arthroscopic port placement with associated risks of infection and bleeding (124). The technology for measuring tissue pO_2 is based on the Clark polarographic electrode, first described in the 1950s, which is the basis for measurement of pO_2 by blood gas analysers (124). The Clark electrode measures the electrical current generated when a cathode and anode immersed in an electrolyte solution come into contact with oxygen (124). In the Licox probe, the polarographic cathode and anode are immersed in an electrolyte solution separated from the tissue by an 80 μm thick

polyethylene membrane which prevents a liquid junction with tissue. The measured current is correlated with pO_2, but this relationship varies with temperature. The Licox probe has a tendency to underestimate oxygen tension (mean error, -3.8 ± 3.5%) between 33 – 39 ºC (124). The Licox probe also has a tendency to underestimate temperature when compared with a resistance thermometer (mean error, -0.67 ± 0.22 ºC) (124). There is therefore variability in the calibration of O_2 and temperature readings by the Licox probe.

The synovial tissue pO_2 reading would also be highly variable depending on probe placement in the synovial tissue, as there is no established standard operating protocol for Licox probe use in synovial tissues. On the other hand, measuring pO_2 in synovial fluid is more straightforward with use of a blood gas analyser which is widely available and without the need for arthroscopic access. In this case, the objective was to look for a change in joint pO_2 with treatment rather than an absolute value. As the synovial fluid pO_2 is representative of joint hypoxia and capable of demonstrating differences, then synovial fluid pO_2 was a reasonable choice to measure joint hypoxia in the absence of clear benefit of measuring synovial tissue pO_2. Some studies investigated the correlation of joint hypoxia with clinical and tissue biomarkers.

Joint hypoxia is correlated with inflammatory arthritis. Ng *et al*. showed that synovial tissue pO_2 correlated inversely with the severity of synovial tissue macroscopic synovitis ($r = -0.421$, $P = 0.02$), sublining CD3 cells ($r = -0.611$, $P < 0.01$) and sublining CD68 cells ($r = -0.615$, $P < 0.001$) (132). This finding strengthened the association between joint inflammatory disease with joint hypoxia in RA, but unfortunately these cross-sectional observations did not answer whether hypoxia is primary or secondary to inflammation. To address the question of whether joint hypoxia is causative of inflammation, longitudinal

studies to investigate whether joint hypoxia preceded the onset of arthritis would be invaluable. Such studies would be challenging as it may be difficult to justify measuring joint pO_2, with its associated risks, in otherwise healthy individuals and then follow them up to see if they develop inflammatory arthritis.

An alternative approach would be to target hypoxia specifically in the inflamed joints and assess whether joint inflammation is ameliorated. An intervention proposed to target peripheral tissue hypoxia specifically emerged recently (to be discussed below) but has not yet been investigated in inflammatory arthritis. However, previous studies of how joint hypoxia responded to anti-inflammatory treatments such as TNFi, provided insight into the biological relevance of joint hypoxia in inflammatory arthritis.

RA and PsA patients who had clinical improvements with TNFi treatment had statistically significant increase in synovial tissue pO_2 (134). Kennedy *et al*. showed that successful biologic therapy improved *in vivo* synovial hypoxia which was associated with significant reduction in DAS28, macroscopic synovitis and macroscopic vascularity (134). The synovial tissue pO_2 median value of approximately 18 mmHg at baseline increased to approximately 39 mmHg after treatment (134). Similarly in another study, a trend towards an increase in synovial tissue pO_2 was noted in patients with RA who responded well to TNFi although this was not statistically significant (140).Whether this constituted restoring synovial tissue pO_2 to normal was unknown as the reference range for physiological synovial tissue pO_2 is unknown. Conversely, no change in synovial tissue pO_2 was seen in non-responders (134). Therefore, resolution of inflammation in inflamed joints may involve reversing the hypoxic state in synovium. This supported the notion that joint hypoxia exacerbated joint inflammation but did not provide insight as to whether joint

hypoxia was primary or secondary to joint inflammation. The authors suggested that "as inflammation is reduced, *in vivo* synovial tissue oxygen levels are increased and thus the tissue becomes less hypoxic" (134). However, it may be that joint hypoxia was relieved through other means such as vascular remodelling during the 3 month follow-up period leading to increased oxygen delivery.

1.4.3 *In vivo* targeting of joint hypoxia

Cross-sectional associations of biomarkers relating to hypoxia and inflammation provide circumstantial evidence linking these processes, but *in vivo* perturbation of hypoxia would provide more direct evidence of its role in inflammatory arthritis. The effects of intra-articular oxygenotherapy on joint hypoxia have been studied in animals. Intra-articular oxygen infusion into rabbit knee joints reduced tissue lactic acid and inhibited glycolysis, compared to control rabbits that were not infused with oxygen (the method of oxygen infusion was not described) (156). Unfortunately, the effects of intra-articular oxygenotherapy on synovial tissue inflammation were not characterised so this study did not address how relieving joint hypoxia may impact on joint inflammation. Other studies of interventions that target the hypoxic pathway are reviewed below. Nonetheless, given that RA and PsA often have polyarticular presentations involving small joints, intra-articular interventions that target single joints are unlikely to have significant therapeutic use. Furthermore, oxygen therapy such as hyperbaric oxygen therapy is limited by practical concerns such as resource availability and adverse effects such as oxygen toxicity.

Oxygen availability may be increased diffusely in the body by hyperbaric oxygen therapy (157). Increased pressure leads to increased amounts of oxygen dissolved in blood

unrelated to haemoglobin binding. In antigen and collagen induced inflammatory arthritis mouse models, hyperbaric oxygen therapy reduced paw swelling, clinical arthritis scores, reduced HIF-1α and Th17 levels, and increased IL-2 receptor subunit beta (IL2RB) expression by regulatory T (Treg) cells (158, 159). This demonstrated proof-of-concept that synovial tissue HIF-1α can be altered through increased oxygen delivery.

Hyperbaric oxygen therapy has also been used to treat inflammatory disorders such as systemic inflammatory response syndrome (SIRS) (160, 161). The manifestations of SIRS include systemic inflammation, organ dysfunction and organ failure. In adults, the presence of at least two SIRS criteria (fever, tachycardia, tachypnoea, leukocytosis) are needed to fulfil diagnosis of SIRS (162). SIRS may be due to infectious causes such as sepsis and non-infectious causes such as trauma, burns and pancreatitis. Complications of SIRS include shock and multiple organ dysfunction syndrome related to ischaemia-reperfusion injury (160).

Hyperbaric oxygen therapy can be used as an adjunct treatment of SIRS by increasing endothelial nitric oxide synthase (which regulates vasoconstriction and vasodilation in setting of SIRS), promoting neovascularisation and post-ischaemia tissue oxygenation (160, 161, 163). Hyperbaric oxygen therapy has been shown to be safe and tolerable in dogs with SIRS (160). In a prospective cohort study involving 49 dogs with SIRS, all dogs were treated with hyperbaric oxygen therapy resulting in improvement in 73.5% of dogs (160). None of the dogs showed major side effects, supporting its safety and tolerability in dogs with SIRS.

In case reports, patients with SIRS due to ischaemia-reperfusion injury improved with hyperbaric oxygen therapy (161). Two patients with avulsions of the hand severed by machetes at the wrist joint and forearm underwent hand replantation. Post-surgical recovery was complicated by ischaemia-reperfusion injury related SIRS. The patients received 90 minutes sessions of hyperbaric therapy on 3 consecutive days. In these two patients with post-hand replantation SIRS, hyperbaric oxygen therapy resulted in favourable hand function and improvements in laboratory markers such as leukocyte count, renal and liver profiles (161).

However, there have been no clinical trials into the effects of hyperbaric oxygen therapy on inflammatory arthritis. Although it may be feasible to perform short term physiological studies of hyperbaric oxygen therapy in patients with inflammatory arthritis, long term treatment with hyperbaric oxygen may be impractical given its risks such as ear barotrauma, pneumothorax, pulmonary barotrauma, decompression sickness and oxygen toxicity (164). Alternative interventions that increase the oxygen carrying capacity of blood may have therapeutic potential for inflammatory arthritis.

The oxygen carrying capacity of blood is reduced in anaemia because of reduced haemoglobin containing red blood cells which bind oxygen. The oxygen carrying capacity of blood can be increased with higher levels of haemoglobin containing red blood cells. Erythropoietin is used to treat chronic anaemia by stimulating red blood cell production to increase the oxygen carrying capacity of blood. Subcutaneous treatment with erythropoietin in CIA mouse models at the onset of arthritis improved clinical signs and histologic status in the joints (165). However, it is unknown as to whether erythropoietin improved arthritis through increased oxygen delivery. Moreover, erythropoietin induced

cell growth, invasion and angiogenesis risk exacerbating inflammation (166). Other strategies to target joint hypoxia therapeutically need to be considered.

1.4.4 Joint hypoxia as a clinical therapeutic target

Current therapeutic strategies for inflammatory arthritis involve anti-inflammatory agents but there are no approved treatments that directly target the hypoxic pathway to treat RA and PsA. The contributions of hypoxia and HIFs to inflammation suggest that these may be therapeutic targets in the treatment of RA and PsA. Indeed, hypoxia and HIFs as therapeutic targets in inflammatory arthritis have been extensively reviewed (41, 42). The strategies reviewed included HIF inhibitors and targeting HIF downstream pathways.

Although HIF inhibitors show promise in preclinical studies, the complexity of the HIF pathway pose a challenge for HIF inhibitors in clinical trials for inflammatory arthritis (41). HIF-2α inhibitor Belzutifan was approved by the FDA for treatment of von Hippel-Lindau disease associated tumours but no HIF inhibitors are currently approved for treatment of inflammatory arthritis (167). This may be because systemic inhibition of HIF-1α can harm physiologically hypoxic tissues such as cartilage (41, 42). Moreover, pharmacokinetic issues such as premature systemic degradation may make it challenging for HIF inhibitors to reach multiple joints. Targeting downstream effects of HIF may be another therapeutic approach.

Many downstream effects of HIF are mediated by VEGF upregulation. In animal models of inflammatory arthritis, inhibition of VEGF ameliorated arthritis (41, 168, 169). The timing of VEGF inhibition may be important in its efficacy. Lu *et al*. reported that anti-VEGF Ab administration prior to onset of experimental arthritis ameliorated arthritis in the

CIA model, but administration post-onset of disease was ineffective (169). This suggested that joint hypoxia may be less attractive as a therapeutic target in late stages of inflammatory arthritis, and conversely may be more attractive as a target prior to onset of arthritis, for example in RF or anti-CCP Ab seropositive individuals without arthritis (170). In humans, anti-VEGF therapies are approved for cancer and age-related macular degeneration (171, 172). Clinical trials are needed to test whether anti-VEGF therapies may be efficacious for different stages of inflammatory arthritis.

Joint hypoxia is associated with inflammatory arthritis, but it is unknown as to whether hypoxia is causative or secondary to inflammatory arthritis. Recently, Professor Stride has developed novel oxygen sparged nanobubbles that deliver oxygen to tissues with low oxygen tension (117, 118). Oxygen nanobubbles given orally in mouse xenograft tumour models significantly reduced hypoxia markers in peripheral tumours, whereas oxygen saturated water and argon nanobubbles did not (120). Specifically, oral oxygen nanobubbles reduced tumour tissue HIF-1α protein levels by 25% (120). This provided proof-of-concept that oral oxygen nanobubbles can relieve peripheral tissue hypoxia. These surfactant-stabilised nanobubbles are so small that they are thought to be absorbed into the bloodstream when administered as a drink (120). However, the assumption that "nanobubbles pass into the blood intact" requires investigation because the disintegrated constituents may be absorbed leading to physiological effects too (120). Nanobubbles also have clinical relevance as demonstrated by human data in elite cyclists which showed improved exercise performance following oral administration of oxygen nanobubbles (118). These nanobubbles are a novel intervention that specifically relieve hypoxia with therapeutic potential for inflammatory arthritis, but their mechanisms of action are poorly understood. Therefore, *in vitro* characterisation of the physiological effects of nanobubbles

is warranted to guide clinical investigation into their therapeutic potential for relieving joint hypoxia in inflammatory arthritis.

1.5 Thesis Structure

In Chapter 1, I undertook a scoping review of the pO_2 measurements in joints and discussed joint hypoxia as a potential therapeutic target in inflammatory arthritis. Professor Stride has developed orally delivered surfactant-stabilised oxygen nanobubbles to treat hypoxia. The aim of Chapter 2 is to characterise the physiological effects of oxygen nanobubbles *in vitro* using cell culture and *in vivo* in a clinical study. A double-blinded placebo controlled clinical study of orally delivered nanobubbles was set up, as well as a parallel study of intra-articular methylprednisolone injection effects on joint hypoxia. As *in vitro* investigations showed no oxygen gas related effects of oxygen nanobubbles, the effects of oxygen nanobubbles on downstream hypoxic pathway may be due to biochemical effects of its constituents independent of oxygen gas. This led to the discontinuation of the clinical study of whether orally delivered nanobubbles can relieve joint hypoxia.

Therefore, the direction of the DPhil pivoted to the investigation of intra-articular methylprednisolone injection effects in the joints of patients with inflammatory arthritis. Intra-articular methylprednisolone injection is widely used as a treatment for inflammatory arthritis. Synovial tissue hypoxia has been shown to be relieved in patients who respond to TNFi but whether joint hypoxia is relieved by other anti-inflammatory agents such as intra-articular methylprednisolone injection is not well understood. In a single arm study of intra-articular methylprednisolone injection in patients with RA and PsA, I found no changes in synovial fluid pO_2 4 weeks after intra-articular methylprednisolone injection.

Next, I went onto explore the effects of intra-articular methylprednisolone injection on synovial tissue single nucleus RNA sequencing (snRNA-seq) profiles in inflammatory arthritis in Chapter 4. Single cell transcriptomic analysis has advanced our understanding of the cells and molecules underpinning health and disease. The effects of intra-articular methylprednisolone injection on inflammatory arthritis synovial tissues at single cell level is poorly understood. This chapter provides a single cell therapeutic atlas of intra-articular methylprednisolone injection on inflammatory arthritis synovial tissues. Although no effects were seen on biomarkers with direct links to hypoxia, perturbation in established and potentially novel biomarkers were found after intra-articular methylprednisolone injection.

2. Chapter 2: Do nanobubbles relieve joint hypoxia?

2.1 Introduction

2.1.1 Oxygen nanobubbles

"Increased metabolic demand of activated immune and stromal cells within the synovial compartment leads to a hypoxic joint microenvironment" (173). In patients with inflammatory arthritis, synovial tissue pO_2 correlated inversely with macroscopic synovitis and increased in those who responded to biologic therapies (132, 134). These findings suggest that joint hypoxia may be a therapeutic target in the treatment of inflammatory arthritis. Targeting hypoxia in the arthritic joint may be a potential therapeutic approach but conventional strategies for treating hypoxia such as breathing high partial pressure of oxygen increases oxygenation but risks oxygen toxicity (110). Similarly, erythropoietin stimulates erythropoiesis to ameliorate hypoxia with performance enhancing effects, but risks adverse effects including myocardial infarction, stroke and venous thromboembolism (174-176). Alternative approaches to directly target hypoxia would allow us to understand whether joint hypoxia is a consequence of inflammatory arthritis, or a primary phenomenon driving development of inflammatory arthritis.

A novel strategy to treat hypoxia was developed by Professor Stride who developed novel orally delivered surfactant-stabilised oxygen nanobubbles which improved cyclist performance in a placebo-controlled study (118, 120). Bubbles are defined as gas in a medium enclosed by an interface as defined by the International Organization for Standardization (ISO) (177). Bubbles may be categorised into bubbles, microbubbles or ultrafine bubbles (nanobubbles) depending on their size (177-179). Ordinary bubbles float in water and burst at the air-water interface (180). Microbubbles are spherical bubbles with

a diameter of ≤ 50 µm (178). Microbubbles have low rising velocity in water, and gradually decrease in size and collapse due to dissolution of interior gases into the surrounding water (178, 179). Nanobubbles are bubbles with a diameter of less than 1000 nm that can remain stable for months (178, 179, 181).

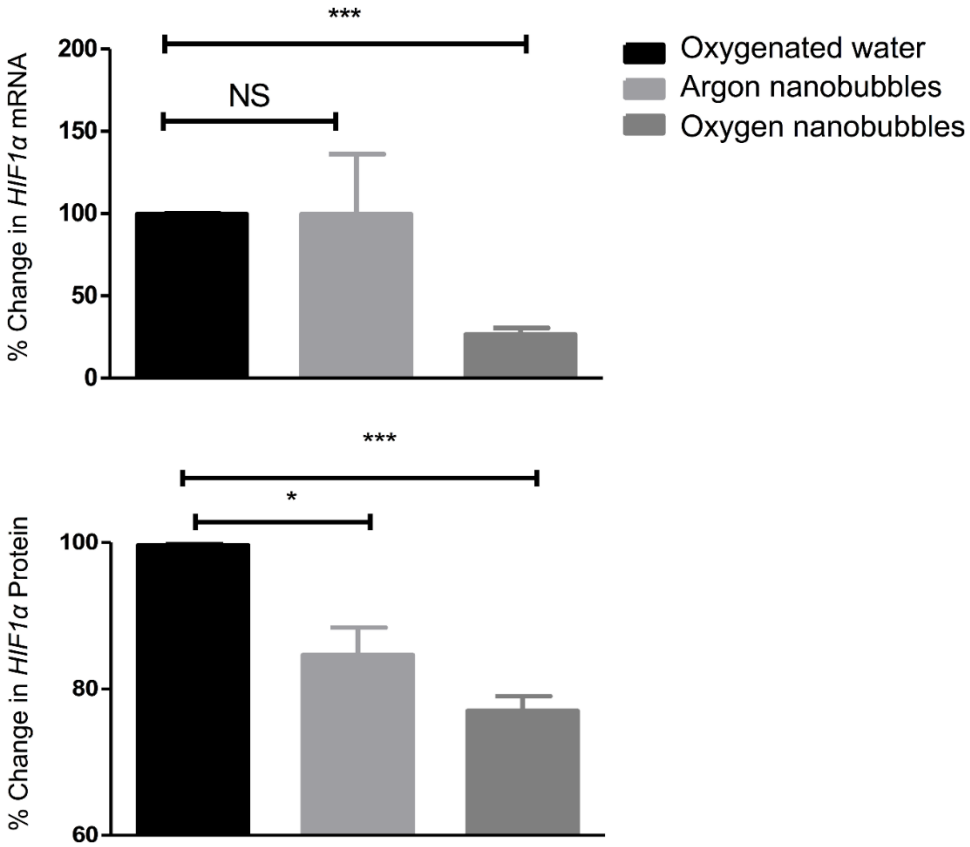

Figure 4 Expression of HIF-1α at (a) a transcriptional level and (b) a translational level in a mouse xenograft tumour model for human pancreatic cancer following administration of oxygen nanobubbles (dark grey), argon nanobubbles (light grey) and oxygenated water (black).

*n = 3 per group, * denotes P < 0.05, ** denotes P < 0.01, *** denotes P < 0.001, NS = not significant. Reprinted in accordance with the Creative Commons Attribution Non-*

Commercial (CC BY-NC 4.0) license (https://creativecommons.org/licenses/by-nc/4.0/) from Owen et al. (120)

By encapsulating oxygen in sub-micrometre sized nanobubbles, Professor Stride's group showed that oxygen nanobubbles have beneficial effects in animal and human studies (Figure 4) (117, 118, 120). Nanobubble suspensions were prepared using a mixture of glycyrrhizin (3 mg/mL), lecithin (3 mg/mL), citric acid (5 mg/mL) and glycerol (0.0125 mL/mL) in untreated tap water (120). This mixture was then heated, mechanically agitated and loaded with oxygen to generate oxygen nanobubbles (120). Oral administration of these oxygen nanobubbles suspensions in mouse xenograft tumour *in vivo* models significantly reduced hypoxic markers in peripheral tumours (Figure 4), although there was no statistically significant difference in tumour tissue pO_2 at up to 30 min follow-up (120). A follow-up experiment by the same group using an implanted oxygen probe with a longer follow-up of 60 min again found no statistically significant difference in tissue pO_2 following administration of either oxygen nanobubbles or air sparged nanobubbles (117).

The authors pointed out that orally administered oxygen nanobubbles downregulated *HIF1A* mRNA in excised tumour tissue, but argon nanobubbles did not, as evidence of a gas mediated effect (Figure 4) (120). However, direct pO_2 measurements in tumour tissues showed no statistically significant difference with oxygen nanobubbles (120). Moreover, hypoxia regulates HIF-1α through post-translational changes as discussed in the previous chapter. The absence of transcriptional change in *HIF1A* mRNA in the argon nanobubble group may be due to opposing effects of downregulation by the biochemical constituents of nanobubbles and upregulation by argon. Although noble gases such as argon and xenon are generally thought to be inert, they have been shown to increase *HIF1A* expression and

induce angiogenesis (182, 183). Indeed, argon and xenon were added to the World Anti-Doping Code International Standard prohibited list in 2014 as erythropoietins. Therefore, nitrogen nanobubbles would be preferred over argon nanobubbles as controls for comparison with oxygen nanobubbles (120).

Further questions regarding the gas related effects oxygen nanobubbles were raised when HIF-1α protein levels were assessed in the mouse xenograft tumour models (Figure 4) (120). HIF-1α protein levels were reduced by nanobubbles, regardless of whether it was sparged with oxygen or argon (Figure 4) (120). These findings implied that the nanobubble effects may be mediated by biochemical properties of nanobubble constituents rather than by oxygen gas mediated mechanisms. This warranted *in vitro* investigations to ascertain whether the oxygen nanobubbles mediate effects through oxygen gaseous mechanism or gas independent biochemical effects.

Although the authors assumed the reduced hypoxia markers in tissues as evidence for increased oxygen delivery by nanobubbles (Figure 4), the existence of nanobubbles and their effects are controversial (184). The nanobubble nomenclature varies in the literature. In this thesis, the term nanobubble is used to describe gas-filled spherical bubbles that have a diameter of less than 1000 nm (181). Nanobubbles are thermodynamically never stable due to the effects of Laplace pressure (181). The Laplace pressure, ΔP, for a spherical object of radius r is given by $\Delta P = 2\gamma/r$ where γ is the interfacial tension of the bubble interface and ΔP describes the increase in pressure within the bubble with respect to the immediate surroundings (181). Therefore, the smaller the bubble, the less stable they are. However, the nanobubble surface may be stabilised to reduce surface tension and provide a diffusion barrier for gas molecules crossing the bubble interface (181). “The stability of

nanobubbles remains unexplained and reports of nanobubbles are generally treated with scepticism" (181). Circumstantial evidence was published by Professor Stride's group demonstrating that these nanobubbles contained gas (117, 120).

Owen *et al*. measured single particle optical sizing (SPOS) and dynamic light scattering (DLS) of these lecithin surfactant-stabilised nanobubbles (Figure 5, Table 3) (120). The nanobubble suspensions had greater amounts of nanoscopic particles than oxygenated water (Figure 5, Table 3). Although the transmission electron micrographs showed spherical particles, this did not prove that they were hollow and contained gas (Figure 5C and D).

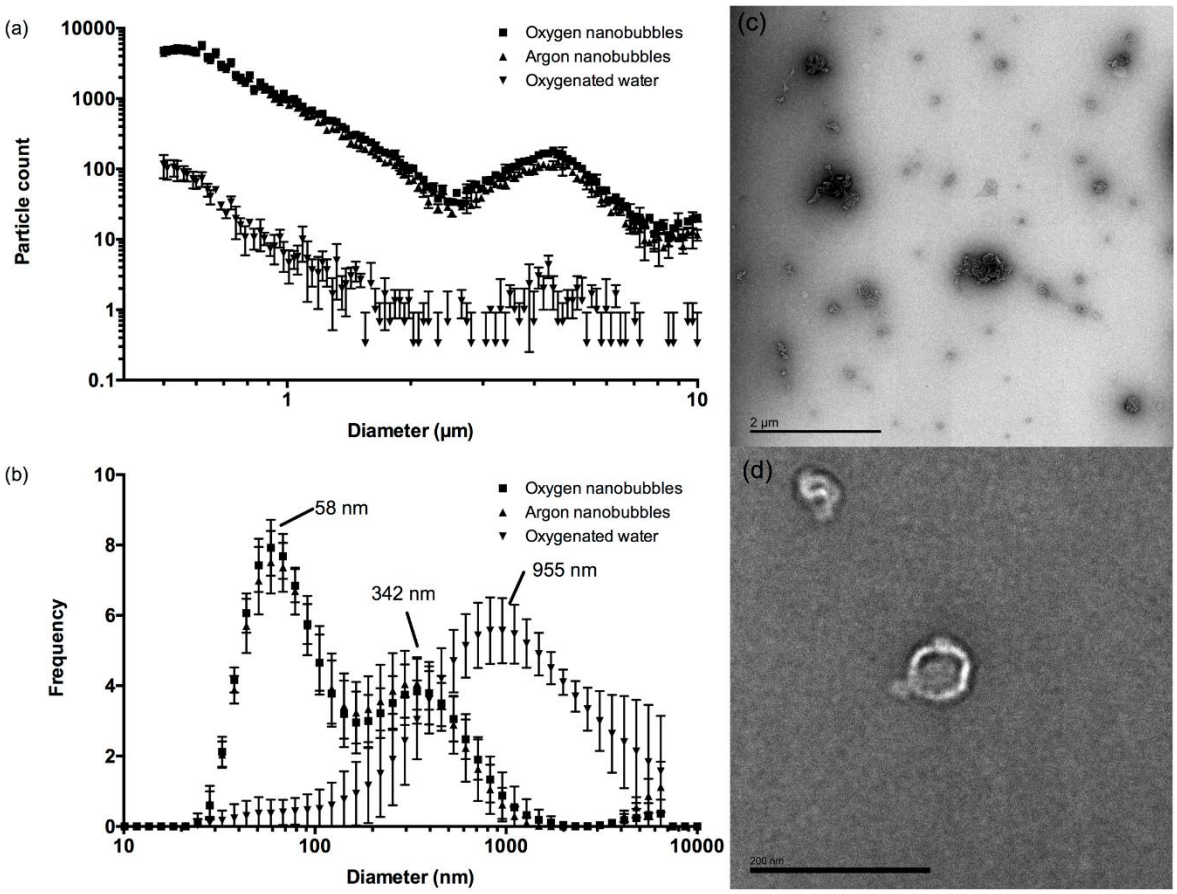

Figure 5 Mean particle size distributions measured for oxygen nanobubbles, argon nanobubbles and oxygenated water by (a) SPOS and (b) DLS. Panels (c) and (d) show

transmission electron micrographs of a sample from the oxygen nanobubble suspension indicating the presence of nanoscale particles (scale bar in (c) is 2 µm, in (d) 200 nm).

Error bars indicate the standard deviation in each measurement (n = 9). Reprinted in accordance with the Creative Commons Attribution Non-Commercial (CC BY-NC 4.0) license (https://creativecommons.org/licenses/by-nc/4.0/) from Owen et al. (120)

Table 3 Population statistics for oxygen nanobubbles, argon nanobubbles and oxygenated water as measured by SPOS.

Reprinted in accordance with the Creative Commons Attribution Non-Commercial (CC BY-NC 4.0) license (https://creativecommons.org/licenses/by-nc/4.0/) from Owen et al. (120)

Suspension	Particle size (µm)				Concentration (ml)
	Mean	*Standard deviation*	*Mode*	*Median*	
Oxygen nanobubbles	0.86	0.70	0.63	0.66	3×10^7
Argon nanobubbles	0.85	0.69	0.63	0.66	3×10^7
Water	0.76	0.61	0.55	0.61	3×10^6

Having established that the nanobubble suspensions contained nanoscopic sized particles, Owen *et al*. went on to demonstrate their oxygen carrying properties (117, 120). The oxygen nanobubble suspension had sustained elevation of pO_2 whereas oxygen-sparged water demonstrated elevated pO_2 which gradually declined (Figure 6, Figure 7) (117, 120). Although these findings showed that oxygen nanobubble suspensions carried more oxygen than either argon nanobubbles or oxygenated water, it did not provide evidence as to whether oxygen was held in gaseous form within nanobubbles as opposed to in a dissolved state. After all, oxygen is known to be highly soluble in lecithin (117, 185-189).

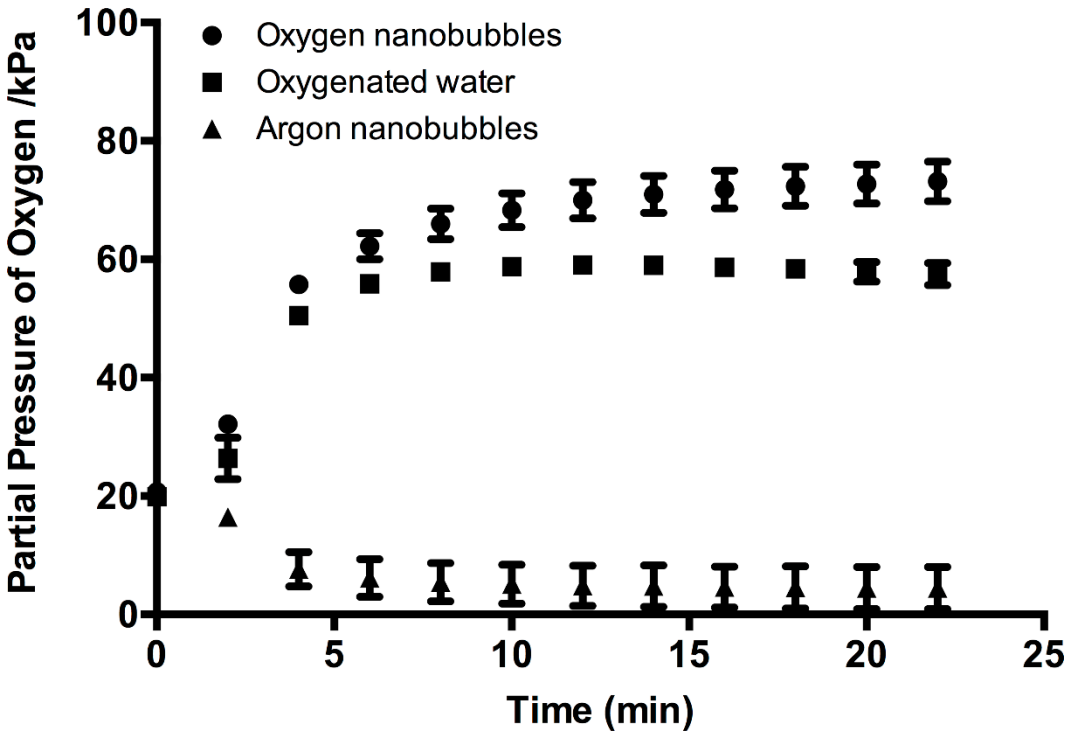

Figure 6 pO_2 in water following introduction of oxygen nanobubbles (circles), argon nanobubbles (triangles) and oxygenated water (squares).

Initial readings represented air-saturated water. Reprinted in accordance with the Creative Commons Attribution Non-Commercial (CC BY-NC 4.0) license (https://creativecommons.org/licenses/by-nc/4.0/) from Owen et al. (120)

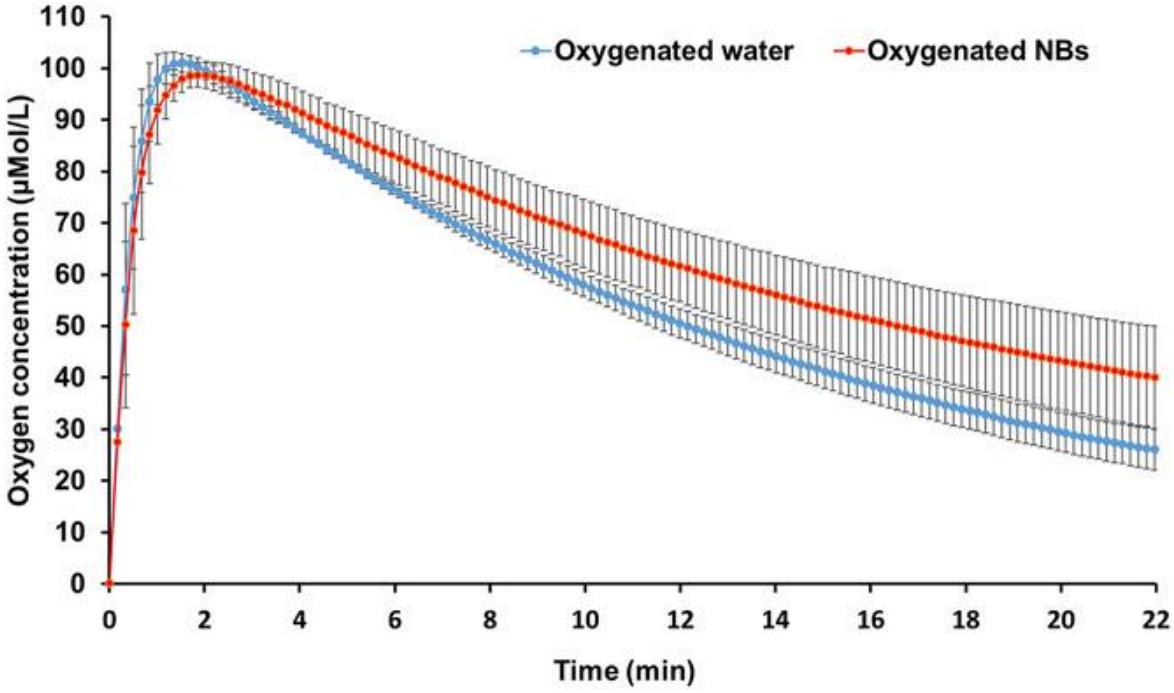

Figure 7 Measurements of oxygen concentration after addition of 1 mL of oxygenated sample (nanobubble solution or Milli-Q water) to 10 mL of deoxygenated (nitrogen-saturated) water under constant mixing of solution and nitrogen flow in vial headspace (n = 3; measurement every 10 seconds; error bars indicate standard deviation).

Reprinted in accordance with the Creative Commons Attribution Non-Commercial (CC BY-NC 4.0) license (https://creativecommons.org/licenses/by-nc/4.0/) from Owen et al. (117)

Evidence to show that nanobubbles are indeed gas-filled include demonstrating that they are less dense than surrounding aqueous solution, have a lower refractive index, provide strong reflection of sound waves, have surface charges consistent with the air-water interface, and imaging using cryogenic techniques (181). Biophysical validation of nanobubbles was beyond the scope of this DPhil and instead I sought to characterise the physiological effects of nanobubbles developed by Professor Stride (118, 120, 190). Clinical investigation of nanobubbles would investigate whether nanobubbles relieve joint

hypoxia and *in vitro* investigations of nanobubbles would provide insight into whether their effects were mediated by gas or biochemical mediated mechanisms of action.

2.1.2 *In vitro* investigations of oxygen nanobubbles

All novel therapeutics require *in vitro* toxicity testing for preliminary safety assessment. The physiological effects of nanobubbles on cell number and metabolism were investigated using crystal violet and alamarBlue respectively. Crystal violet is a dye that binds to proteins and DNA (191). Crystal violet is used to stain adherent cells, allowing cytotoxicity and cell viability to be determined (191). It relies on the detachment of adherent cells from cell culture plates during cell death. After dead detached cells are washed away, live adherent cells are stained with crystal violet. After a wash step, the crystal violet dye is solubilised and measured by absorbance. The amount of crystal violet staining is directly proportional to the cell biomass that is attached to the plate.

alamarBlue is another assay to quantitatively measure cell viability (192). Resazurin, the active ingredient in alamarBlue, is a non-toxic, cell-permeable compound that is blue and non-fluorescent. Upon entering cells, resazurin is reduced to resorufin which is red and fluorescent. The oxidised alamarBlue is reduced in the cytosol by mitochondrial enzyme activity. Changes in cell viability can therefore be detected by fluorescence after incubating with alamarBlue.

To further explore their effects at cellular levels, the effects of nanobubbles on cell migration were measured in musculoskeletal relevant cell types as cell migration is key to the pathogenesis of inflammatory arthritis (193). Cell migration involves cellular polarisation and reorganisation of actin filaments and microtubules. Cell membrane

protrusion and dynamic substrate adhesion, followed by membrane retraction at the lagging cell edge, results in cell migration. The IncuCyte scratch assay is established for measuring cell migration into a wound region (194). It facilitates reproducible and quantitative analysis of migration of adherent cell lines in the presence of experimental agents. The spatial cell density in the wound area relative to the spatial cell density outside of the wound is the relative wound density. This metric has the advantage of self-normalising for changes in cell density which may occur outside the wound because of cell proliferation and pharmacological effects. This is relevant as the incubation of cell cultures with nanobubbles (which comprise of foodstuff ingredients including lecithin, glycerol, glycyrrhizin, and citric acid) may induce diverse effects other than cell migration. In addition to characterising the nanobubble effects at cellular levels, I also characterised the nanobubble effects at molecular levels.

At a molecular level, the HIF-1α proteins were measured using Western blots to assess the impacts of nanobubbles on downstream pathways of hypoxia. As HIF-1α protein degrades rapidly, the transcriptional activity of HRE may be a more sensitive marker of hypoxia changes by nanobubbles. Therefore, transcriptional activity of HRE was also measured. Genetic reporter systems are widely used to study gene expression. Dual reporters improve experimental accuracy by allowing simultaneous measurement of two individual reporter enzymes within a single system. One reporter is correlated with the effect of specific experimental condition, while the activity of the co-transfected control reporter allows normalisation to control for differences in cell viability or transfection efficiency. The Dual-Luciferase Reporter Assay System provides an efficient means of performing dual-reporter assays (195). Using this system, the activities of firefly (*Photinus pyralis*) and *Renilla* (*Renilla reniformis* or sea pansy) luciferases are measured sequentially from a

single sample. In addition to investigating the transcriptional response to hypoxia, I also evaluated translational response to hypoxia *in vitro*.

Hypoxia upregulates VEGF and transforming growth factor α (TGF-α) expression in a physiological response to induce angiogenesis and reverse hypoxia (42, 196, 197). TGF-α is a member of the epidermal growth factor family of cytokines that are synthesised as transmembrane precursors with soluble forms released by proteolytic cleavage. TGF-α is relevant to inflammatory arthritis as it induces fibroblast proliferation and angiogenesis (197-199). I applied enzyme-linked immunosorbent assays to cell culture supernatants to investigate whether hypoxia-induced VEGF and TGF-α protein expression were affected by nanobubbles. The resolution of hypoxia also has important physiological consequences.

Hypoxia followed by normoxia causes ischaemia-reperfusion injury through generation of free radicals. Indeed, oxidative damage by free radicals in synovial tissue has been shown to be associated with the *in vivo* hypoxic status in the arthritic joint (131). Therefore, therapeutics that abrogate the damage mediated by ischaemia-reperfusion injury may be beneficial in inflammatory arthritis. The impact of nanobubbles on ROS production was measured using CM-H_2DCFDA (200, 201). This chloromethyl derivative of H_2DCFDA is widely used as an indicator for ROS in cells. CM-H_2DCFDA passively diffuses into cells where its acetate groups are cleaved by intracellular esterases and its thiol-reactive chloromethyl group reacts with intracellular glutathione and other thiols. Subsequent oxidation yields a fluorescent adduct that is trapped inside the cell, allowing CM-H_2DCFDA to act as a fluorescent dye-based sensor of free radicals.

To perform these *in vitro* experiments, immortal human MG-63 osteosarcoma cells and primary human umbilical vein endothelial cells (HUVECs) were selected for their ease for cell culture investigations. MG-63 is an osteoblast cell line originating from the bone of a 14-year-old male Caucasian osteosarcoma patient (202). The immortal MG-63 cell line has the advantage of being easy to culture and transfect, as well as having fibroblast properties relevant to studying musculoskeletal tissues (202, 203). Another advantage of MG-63 cell line is its amenability for transfection hence they are extensively used in transfection studies to investigate gene expression and function. However, MG-63 cell line may not recapitulate synovial tissue cells due to their osteoblast-like features and as a cancer cell line may not represent normal cell physiology.

I also used HUVECs as a non-cancerous *in vitro* model to study oxygen nanobubbles. HUVECs are isolated from the vein of normal umbilical cords and exhibit characteristics of endothelial cells (204). HUVECs are a widely used source of primary endothelial cells for studying angiogenesis and provide a convenient *in vitro* model for endothelium in synovial tissues. Although HUVECs are the most well characterised type of endothelial cells for research, HUVECs also may not reflect true endothelial states in the synovium due to their origin from umbilical cord veins. The umbilical vein carries blood rich in oxygen (pO_2 ranging from 22 to 53 mmHg) from the placenta to the foetus, in contrast to the pO_2 in joints which may be as low as 0 mmHg (128, 205).

To induce hypoxia in these cell cultures, 0.1% O_2 was used to induce maximal hypoxic states. Although this extreme setting may usually be more hypoxic than that of the arthritic joint, at least it would provide early signal as to the mechanism of actions of oxygen nanobubbles. If gas related effects of oxygen nanobubbles were found, I would have

repeated the experiments at different O_2 settings to see whether such findings were reproducible at more physiological levels of hypoxia.

2.1.3 Clinical study of nanobubbles effects on joint hypoxia

We had set up a double-blind, single-centre, randomised, controlled study to investigate the physiological effects of nanobubbles in RA and PsA patients (https://www.hra.nhs.uk/planning-and-improving-research/application-summaries/research-summaries/do-nanobubbles-improve-joint-hypoxia/) (Figure 8). Participants were to be randomized to drink 200 mL of either unsparged Avrox nanobubbles (N = 10) or citrus flavoured Dioralyte drinks (N = 10) twice daily for 28 days. The randomized study was designed to balance interventional arms diagnosis (RA or PsA) by stratification using a web-based commercially available registration system (Sealed Envelope).

This was an exploratory hypothesis generating study of the biological effects of nanobubbles (12. Appendix B: Clinical study to investigate whether nanobubbles improve joint hypoxia). A sample size of 20 (10 in each arm) was selected pragmatically for this pilot study based on clinical prevalence. The primary objective was to compare the effects on joint hypoxia (synovial fluid pO_2) of orally delivered nanobubbles versus Dioralyte in patients with RA and PsA. The secondary objectives were to compare the effects of orally delivered nanobubbles versus Dioralyte on hypoxic and inflammatory biomarkers. This study would have provided an understanding of the biological effects of orally delivered nanobubbles versus Dioralyte.

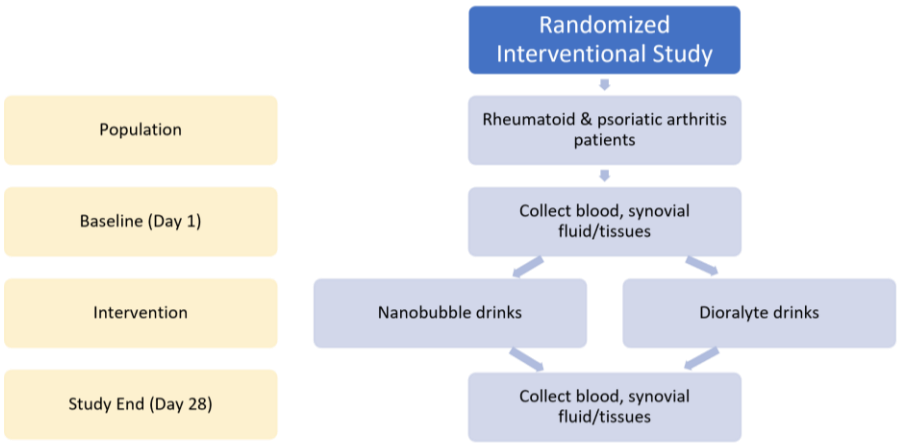

Figure 8 Schematic outline of nanobubble clinical study

2.2 Materials and methods

2.2.1 Cell culture

The human MG-63 osteosarcoma cell line was purchased from European Collection of Authenticated Cell Cultures. Cells were cultured in DMEM containing 10% foetal bovine serum (FBS), 2 mM L-glutamine, 50 IU/mL penicillin and 50 µg/mL streptomycin sulphate. MG63 cell cultures were tested for mycoplasma infection using MycoAlert™ per manufacturer protocol (Lonza). HUVECs were certified mycoplasma free by supplier.

Pooled human umbilical vein endothelial cells (HUVECs) were obtained from Invitrogen (Cat. No. C-015-5C). Cells were cultured in endothelial cell growth base media (R&D Systems Cat No. 390598) containing endothelial cell growth supplement (R&D Systems Cat No. 390599) and penicillin-streptomycin per manufacturer instructions.

2.2.2 Hypoxic exposure

Hypoxic exposure of 0.1% O_2 was conducted with 5% CO_2, balance N_2 in a MiniGalaxy incubator (RS Biotech).

2.2.3 Nanobubble production

300 mg lecithin (ThermoFisher, catalogue number J61675.30), 500 mg citric acid (Sigma-Aldrich, catalogue number 251275), 50 mg glycyrrhizin (Sigma-Aldrich, catalogue number 50531), 1.25 mL glycerol (1.26 g/cm^3) (Sigma-Aldrich, catalogue number G2025) were mixed in 100 mL purified water (milliQ) at 40 ^oC for 30-60 min using magnetic stirring hot plate until mixture is fully dissolved. 10 mL of dissolved lecithin mixture was then placed into a 50 mL vial where oxygen or nitrogen was sparged through a blunt needle at the bottom (Figure 9), or left unsparged. The vial headspace is filled with either oxygen or nitrogen or room air, and then sealed for immediate use. Oxygen nanobubbles are just under 1 μm in diameter with a concentration of 3 x 10^7/mL (120). The oxygen content of nanobubbles and the concentrations of nanobubbles were not measured directly in this study as these were previously characterised (120).

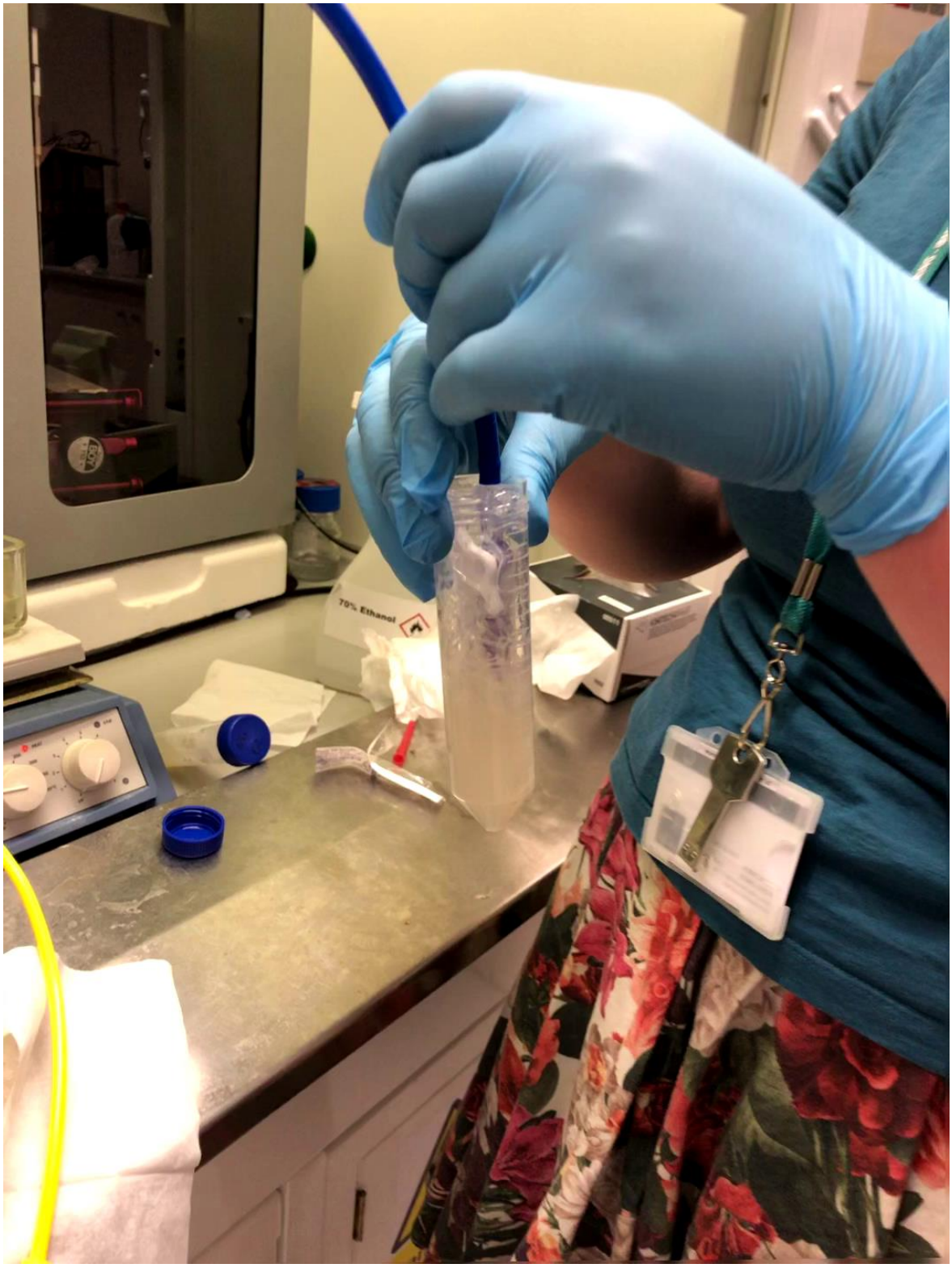

Figure 9 Photo of gas sparging through nanobubbles

2.2.4 Cell metabolism and viability

Cell metabolism and viability were determined by using alamarBlue (Invitrogen). AlamarBlue in an amount equal to 10% of the culture volume was added then cell cultures were returned to incubator for 3 h. Fluorescence was measured with excitation wavelength at 530-560 nm and emission wavelength at 590 nm using FLUOstar Omega. Cell viability was also assessed by crystal violet (Sigma). Cells were washed with phosphate-buffered saline (PBS) and fixed with 4% formalin for 10 min at room temperature. Then cells were incubated with 1% crystal violet for 60 min at 37 ºC. Cells were washed thoroughly to remove excess dye. Crystal violet stain was extracted from cells by incubating with 0.2% Triton X-100 overnight. Crystal violet absorbance at 550 nm was read using FLUOstar Omega.

2.2.5 Cell migration assay

IncuCyte (S3 Live-Cell Analysis System) ZOOM® 96-Well Scratch Wound Cell Migration Assay was performed using WoundMaker™ per manufacturer instructions (Essen BioScience). The WoundMaker™ is a 96-pin mechanical device designed to create homogeneous, 700-800 μm wide wounds in cell monolayers on 96-well ImageLock™ microplates. Scratch wounds were made at T0h when cell monolayers were at 100% confluence. Cells were incubated in either normoxia or 0.1% O_2. IncuCyte was used to take images of cells at T0h and T6h post wounding. The first image from each well is used to generate an initial scratch wound mask which defines the initial wound region. IncuCyte was used to measure relative wound density which is a measure of the density of the wound region relative to the density of the cell region, i.e. rapid increase in relative wound

density demonstrates rapid closure of the wound due to rapid cell migration into the wound.

2.2.6 Western blots

Cells were homogenized in HIF lysis buffer (6.2 M urea, 10% glycerol, 5 mM dithiothreitol, 1% sodium dodecyl sulphate, protease inhibitors). Gels were evenly loaded with cell lysates and compared against the Precision Plus Protein All Blue Standards molecular weight marker (Bio-Rad). Primary antibodies were mouse monoclonal anti-HIF-1α IgG1 (BD Biosciences), mouse monoclonal anti-β-tubulin IgG1 (Sigma-Aldrich), rabbit polyclonal anti-Glucose Transporter GLUT1 IgG (Abcam), rabbit monoclonal anti-Glyceraldehyde-3-Phosphate Dehydrogenase (GAPDH) IgG (Epitomics). Densitometric quantification of Western blots was performed in ImageJ, normalizing experimental bands to the corresponding β-tubulin control.

2.2.7 Reactive oxygen species assay

The protocol was optimised by determining the concentration of H_2O_2 required to induce ROS production. 96-well plates were seeded with HUVECs in 100 µL medium in each well 24 h prior to T0h for target confluence 70-90% at T0h. Cells were cultured in normoxia. ROS were detected using a fluorescent dye-based free radical sensor CM-H2DCFDA (Invitrogen Cat No. C6827) per manufacturer protocol. Cells were washed with PBS and incubated with CM-H2DCFDA in the dark for 45 min. Washed cells were then incubated with 200 µM H_2O_2 and intervention at 37 ^oC for 1 h. 200 µM was selected as the concentration for H_2O_2 as this dose has been shown previously to reliably induce ROS production in MG63 cells (206). ROS was measured by fluorescence with excitation

wavelength 495 nm and emission wavelength 529 nm using FLUOstar Omega. ROS formation was also profiled by fluorescence microscopy using IncuCyte.

2.2.8 Luciferase assay

Phosphoglycerate kinase is a transcriptional target of HIF-1α, induced by binding of the transcription factor to its HRE. As a measure of HIF-1α transcriptional activation, MG-63 cells were transfected with PGK HRE-firefly luciferase plasmids (gifted by Professor AL Harris, University of Oxford, UK) and pHRG-TK *Renilla* luciferase control reporter vector (Promega) using Lipofectamine® 2000 reagent (Invitrogen). Luminescence was assayed after 4 and 24 h using the Dual-Luciferase® Reporter Assay System (Promega), with firefly luciferase normalized to the *Renilla* transfection control.

2.2.9 ELISA

VEGF and TGF-α ELISA were performed using DuoSet kits per manufacturer's protocols (catalog number DY293B and DY239). The capture antibody was diluted to the working concentration in PBS without carrier protein. A 96-well microplate was coated with 100 µL per well of the diluted capture antibody. The plate was sealed and incubated overnight at room temperature. Each well was aspirated and washed with wash buffer, repeating the process two times for a total of three washes. Each well was washed by filling with 400 µL wash buffer using a squirt bottle. After the last wash, the plate was inverted and blotted against clean paper towels to remove any remaining wash buffer. Each plate was blocked by adding 300 µL of reagent diluent to each well. The plate was incubated at room temperature for a minimum of 1 h. The plate was washed again as previously described. 100 µL of sample or standard in reagent diluent was added to each well. The plate was

covered with an adhesive strip and incubated for two h at room temperature. The plate was washed as previously described. 100 µL of detection antibody, diluted in reagent diluent, was added to each well. The plate was covered with a new adhesive strip and incubated for two h at room temperature. The plate was washed as previously described. 100 µL of working dilution of Streptavidin-HRP was added to each well. The plate was covered and incubated for 20 min at room temperature away from direct light. The plate was washed as previously described. 100 µL of substrate solution was added to each well and incubated for 20 min at room temperature away from direct light. 50 µL of stop solution was added to each well. The optical density of each well was determined immediately using a microplate reader set to 450 nm. Wavelength correction was set to 540 nm to correct for optical imperfections in the plate.

2.2.10 Statistical analysis

Experiments were performed with triplicates of complete experimental repeats unless otherwise specified. Data were presented as mean ± standard error of mean (SEM) unless otherwise specified. Data were analysed using Prism (Graphpad Software). For analysis of crystal violet, alamarBlue and HIF-1α assays, statistical analysis comprised grouped analysis with ordinary two-way ANOVA and corrected for multiple comparisons using Dunnett's multiple comparisons test, with individual variances computed for each comparison. For other experiments including relative wound density, HRE luciferase, VEGF and ROS assays, analyses involved one-way ANOVA corrected for multiple comparisons using Dunnett's multiple comparison as a post-hoc test. Results were considered significant at $P < 0.05$.

2.3 Results

2.3.1 Nanobubble effects on cell viability by crystal violet

Oxygen sparged, nitrogen sparged and unsparged nanobubbles at doses less than 50 µL had no significant effects on MG63 cell viability in normoxia or 0.1% O_2 hypoxia at T24-72h. MG63 cell number was significantly reduced at 72 h after incubation with 50 µL oxygen sparged, nitrogen sparged or unsparged nanobubbles in 0.1% O_2 or normoxia (Figure 10) ($N = 3$, $P < 0.05$ in normoxia, $P < 0.001$ in 0.1% O_2). Subsequent experiments therefore used 20 µL nanobubbles as the maximum *in vitro* dose. Oxygen sparged, nitrogen sparged and unsparged nanobubbles were found to have pH of 3 which may relate to their effects on cell viability.

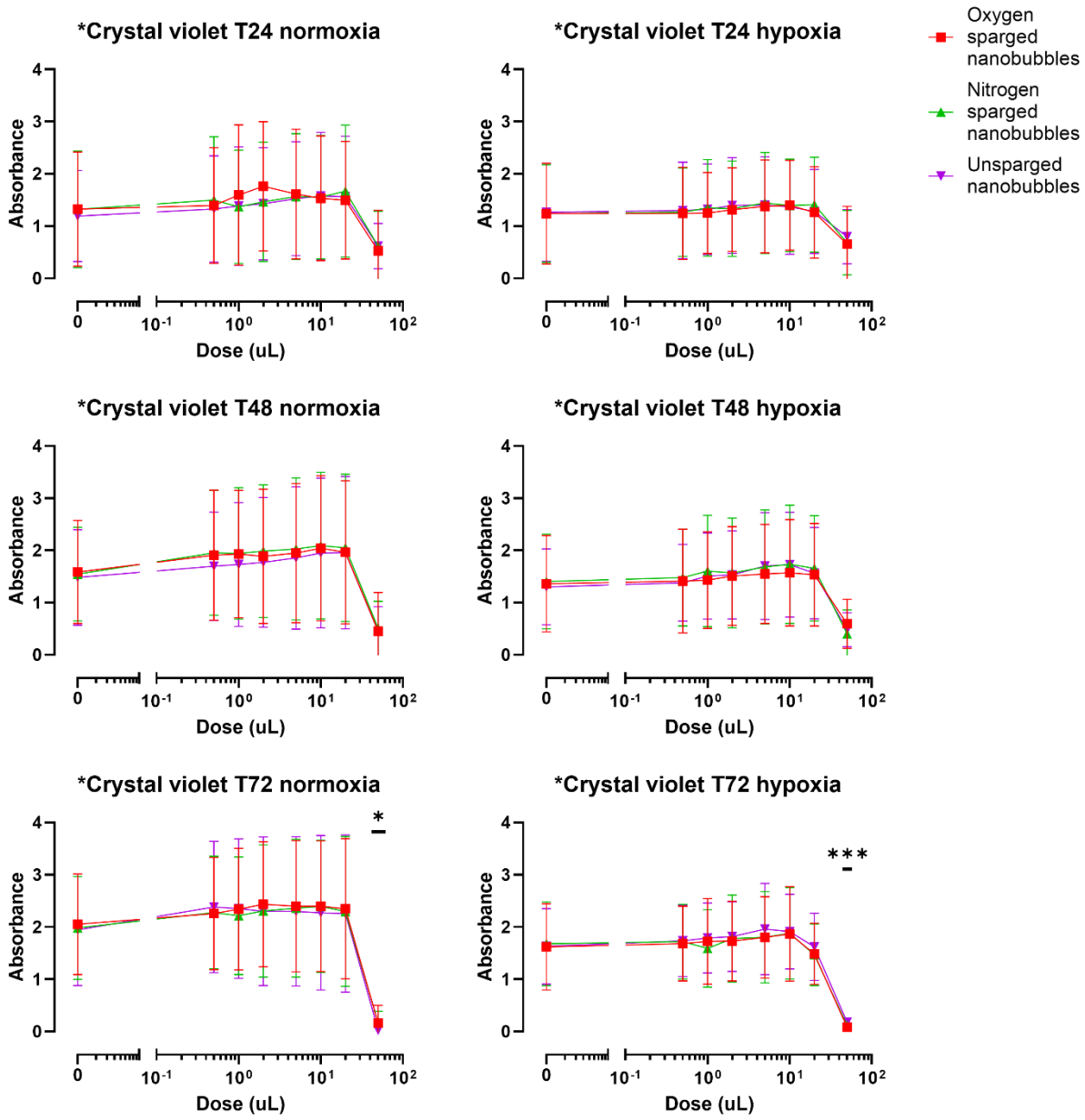

Figure 10 Nanobubble effects on MG63 cell viability in either normoxic or 0.1% O_2 hypoxic incubator at T24h, T48h and T72h as assessed by absorbance of crystal violet after treatment at T0h with either oxygen sparged, nitrogen sparged, or unsparged nanobubbles (N = 3).

Data plotted as mean ± SEM. Grouped analysis with ordinary two-way ANOVA and Dunnett's multiple comparisons test, with individual variances computed for each comparison, showed no significant differences between oxygen sparged nanobubbles,

nitrogen sparged nanobubbles or unsparged nanobubbles (P > 0.05). Using zero dose as control for comparison, absorbance of crystal violet was significantly reduced at the highest dose of 50 µL at T72h timepoint across all treatment groups (denotes P < 0.05, *** denotes P < 0.001).*

2.3.2 Nanobubble effects on cell metabolism and viability by alamarBlue

MG63 cell metabolism in either normoxic or 0.1% O_2 hypoxic incubator at T24h, T48h and T72h was assessed by fluorescence of alamarBlue, after treatment at T0h with up to 20 µL of either oxygen sparged, nitrogen sparged or unsparged nanobubbles (N = 3). There was a trend towards reduced metabolism in MG63 cells after incubation in either normoxia or 0.1% O_2 for 72 h with either oxygen sparged, nitrogen sparged, or unsparged nanobubbles but this did not reach statistical significance (Figure 11) (N = 3, P > 0.05). Grouped analysis with ordinary two-way ANOVA and Dunnett's multiple comparisons test, with individual variances computed for each comparison, using zero dose as control for comparison, showed no significant differences (P > 0.05).

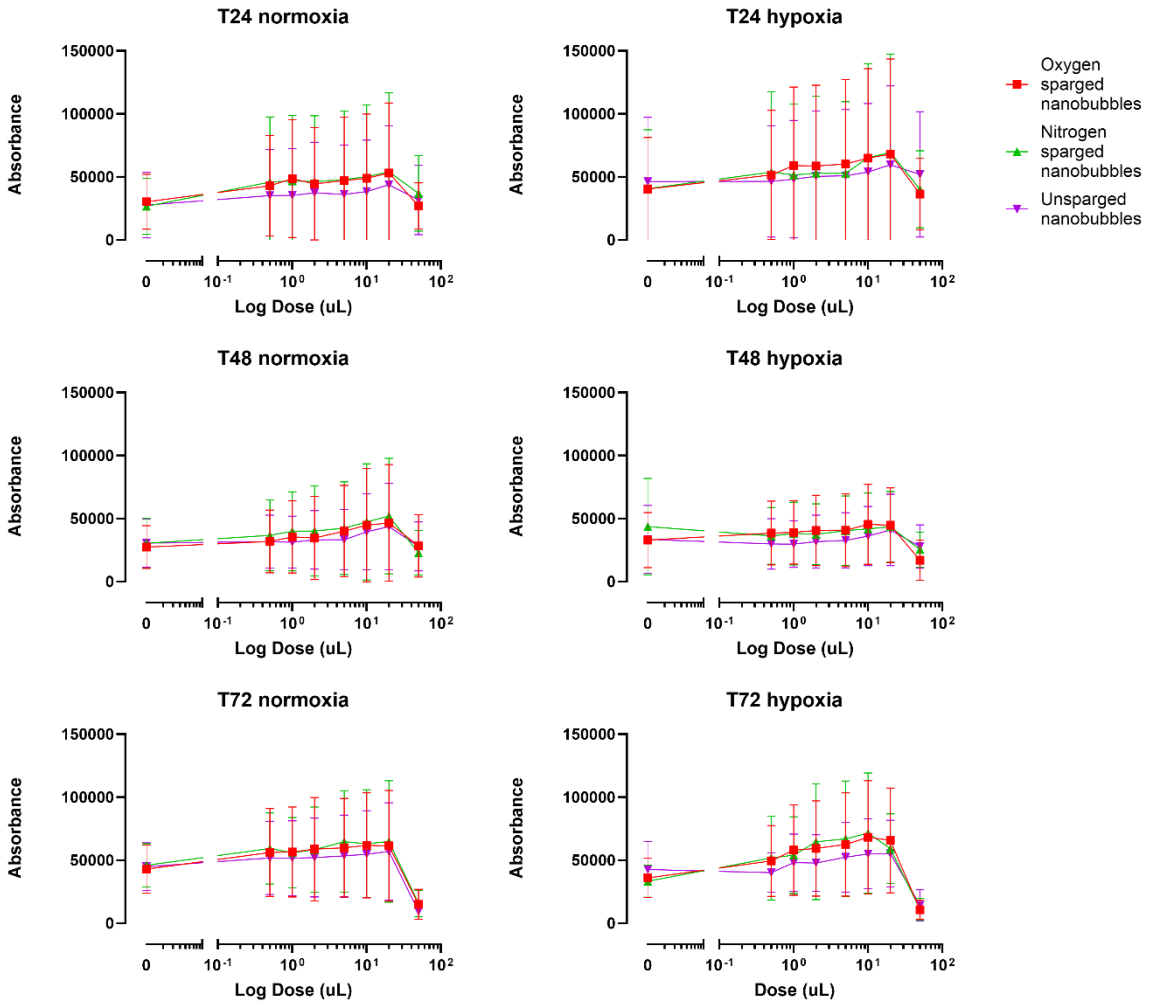

Figure 11 MG63 cell metabolism and viability in either normoxic or 0.1% O_2 hypoxic incubator at T24h, T48h and T72h was assessed by fluorescence of alamarBlue, after treatment at T0h with up to 20 µL of either oxygen sparged, nitrogen sparged or unsparged nanobubbles (N = 3).

Data plotted as mean ± SEM. Grouped analysis with ordinary two-way ANOVA and Dunnett's multiple comparisons test, with individual variances computed for each comparison, using zero dose as control for comparison, showed no significant differences across treatment groups and doses at all timepoints (P > 0.05).

2.3.3 Nanobubble effects on cell migration

Using the scratch wound assay, there was no difference in the relative wound density of MG63 cells after being cultured in hypoxia for 6 h and incubated with either PBS, oxygen sparged, nitrogen sparged or unsparged nanobubbles (Figure 12).

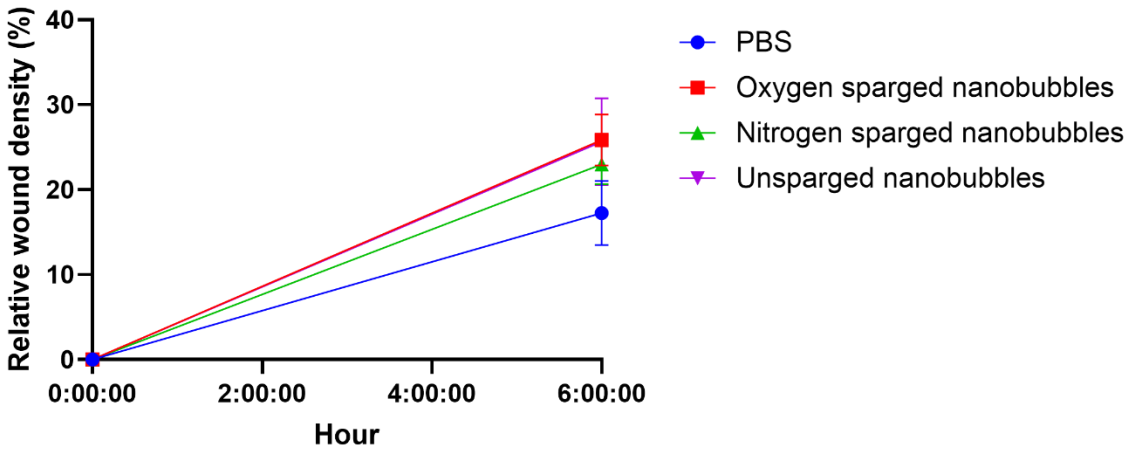

Figure 12 Relative wound density of MG63 cells 6 h after incubation in 0.1% O_2 with either PBS, oxygen sparged, nitrogen sparged or unsparged nanobubbles.

Ordinary one-way ANOVA with Dunnett's multiple comparison test, using PBS treatment group as control for comparison, showed no difference in relative wound density with nanobubbles (N = 3, not statistically significant).

2.3.4 Nanobubble effects on HIF-1α protein, HRE transcription and VEGF protein levels

Western blots were performed to assess expression of hypoxia-related proteins with β-tubulin as a loading control. HIF-1α protein levels increased after 2 h of incubation in 0.1% O_2 (N = 1) (Figure 13). No difference in GADPH or GLUT-1 protein expression was

seen after adding either oxygen sparged, nitrogen sparged or unsparged nanobubbles (data not shown) (N = 1).

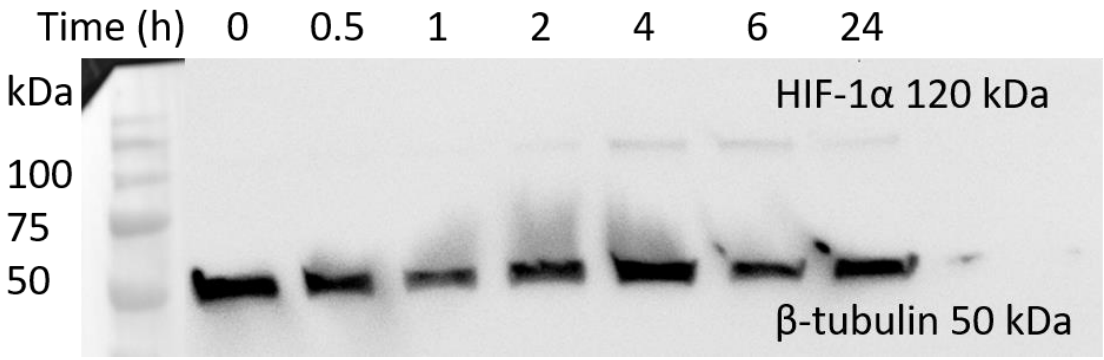

Figure 13 Western blot analysis of HIF-1α and β-tubulin (housekeeper) expression in MG63 human osteosarcoma cells after incubation in hypoxia 0.1% O_2 for up to 24 h

HIF-1α and β-tubulin expression in MG63 cells were analysed using Western blot analysis after incubation in hypoxia 0.1% O_2 for up to 24 h (Figure 14A). Cells were treated at T0 with 250 µL of PBS, oxygen sparged nanobubbles, nitrogen sparged nanobubbles, or unsparged nanobubbles (N = 3). Using quantitative analysis on Western blots with densitometry, grouped analysis with ordinary two-way ANOVA and Dunnett's multiple comparisons test, with individual variances computed for each comparison, using unsparged PBS group as control for comparison, nanobubbles reduced HIF-1α to β-tubulin ratio at 24 h only (Figure 14A) ($P < 0.05$).

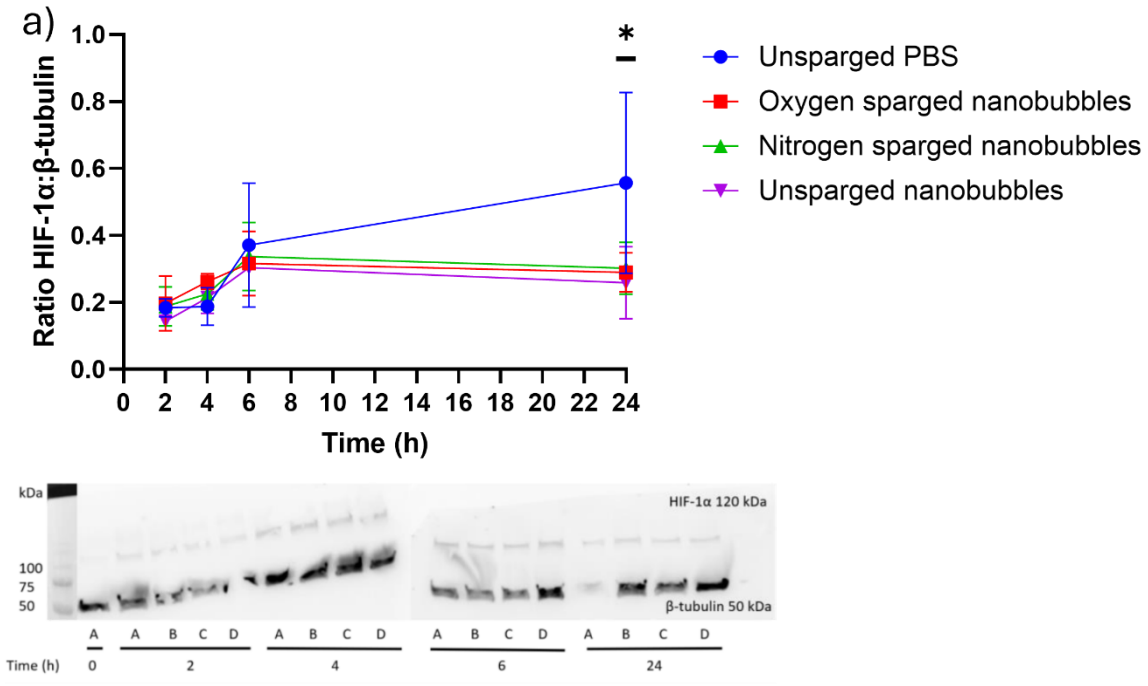
a)
Ratio HIF-1α:β-tubulin
Time (h)
*
Unsparged PBS
Oxygen sparged nanobubbles
Nitrogen sparged nanobubbles
Unsparged nanobubbles
kDa
100
75
50
HIF-1α 120 kDa
β-tubulin 50 kDa
A B C D
Time (h)
0
2
4
6
24

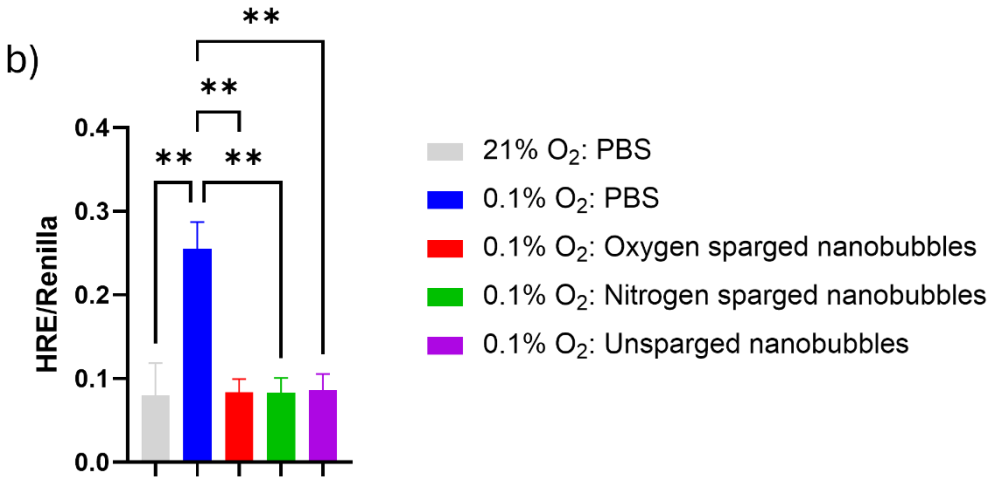
b)
HRE/Renilla
**
21% O2: PBS
0.1% O2: PBS
0.1% O2: Oxygen sparged nanobubbles
0.1% O2: Nitrogen sparged nanobubbles
0.1% O2: Unsparged nanobubbles

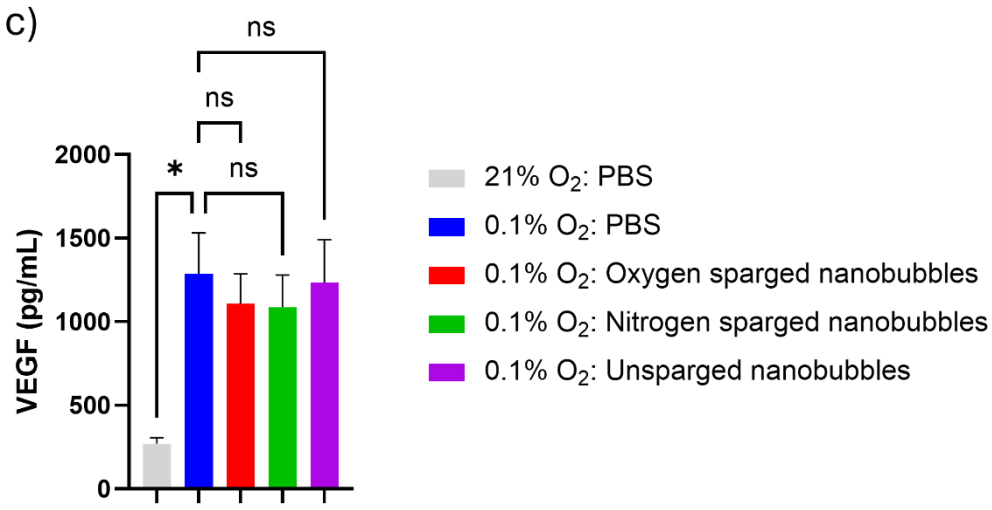
c)
VEGF (pg/mL)
ns
*
21% O2: PBS
0.1% O2: PBS
0.1% O2: Oxygen sparged nanobubbles
0.1% O2: Nitrogen sparged nanobubbles
0.1% O2: Unsparged nanobubbles

Figure 14 (a) Western blot analysis of HIF-1α and β-tubulin in MG63 cells incubated in 0.1% O_2 and treated with either unsparged PBS, oxygen sparged nanobubbles, nitrogen sparged nanobubbles or unsparged nanobubbles. Grouped analysis with ordinary two-way ANOVA and Dunnett's multiple comparisons test, with individual variances computed for each comparison, using zero dose as control for comparison, showed significant increase in HIF-1α:β-tubulin ratio in unsparged PBS group compared to either oxygen sparged nanobubbles, nitrogen sparged nanobubbles or unsparged nanobubbles at T24h timepoint ($P < 0.05$). (b) HRE-luciferase activity normalized to Renilla luciferase gene for MG63 cells incubated in either normoxia or 0.1% O_2 and treated with either PBS, oxygen sparged nanobubbles, nitrogen sparged nanobubbles or unsparged nanobubbles. One-way ANOVA using Dunnett's multiple comparison showed increased HRE-luciferase activity in 0.1% O_2 treated with PBS, compared to in 21% O_2 treated with PBS, or in 0.1% O_2 treated with either oxygen sparged, nitrogen sparged, or unsparged nanobubbles ($P < 0.01$). (c) VEGF levels in culture medium of MG63 cells, after incubation in normoxia or 0.1% O_2 for 24 h and treated with either PBS, oxygen sparged nanobubbles, nitrogen sparged nanobubbles or unsparged nanobubbles. One-way ANOVA using Dunnett's multiple comparison showed increased VEGF levels 0.1% O_2 treated with PBS, compared to in 21% O_2 treated with PBS ($P < 0.05$). No difference in VEGF was seen with treatment with either oxygen sparged, nitrogen sparged, or unsparged nanobubbles in 0.1% O_2 ($P > 0.05$).

*ns denotes not statistically significant, * denotes $P < 0.05$, ** denotes $P < 0.01$*

HRE-luciferase activity normalized to *Renilla* luciferase gene was measured for MG63 cells in normoxic or 0.1% O_2 hypoxic incubator at T24h (N = 3). 48h prior to T0h, each well in 96-well plate was seeded with MG63 cells in 200 µL medium for target confluence

of 70-90% at T0h. 24 h prior to T0h, each well was transfected with HRE luciferase plasmid and *Renilla* luciferase control reporter vector using Lipofectamine 2000 reagent. At T0h, each well was treated with either 50 µL PBS, or either 20 µL oxygen sparged, nitrogen sparged or unsparged nanobubbles, made up to 50 µL with PBS. Nanobubbles significantly reduced HRE transcription in MG63 human osteosarcoma cells after incubation in 0.1% O_2 for 24 h (Figure 14B, data plotted as mean ± SEM. ** denotes $P < 0.01$). This effect was irrespective of whether the nanobubbles were unsparged or sparged with either oxygen or nitrogen.

Having shown that nanobubbles reduced HIF-1α proteins and HRE transcription, I expected nanobubbles to inhibit HIF-1α mediated responses including VEGF and TGF-α (207). VEGF levels were measured in culture medium of MG63 cells after incubation in normoxia or 0.1% O_2 for 24 h (N = 3). Cells were untreated or treated at T0 with 10% well volume of PBS, or nanobubbles sparged with oxygen, nitrogen or unsparged. Using ELISA, I found that 0.1% O_2 increased VEGF protein levels in culture medium of MG63 cells but that treatment of cells with nanobubbles had no significant effects, irrespective of gas sparging (Figure 14C, data plotted as mean ± SEM. Ordinary one way ANOVA with multiple comparison test comparing means with mean of 0.1% O_2 + PBS as control. * denotes $P < 0.05$. ns denotes not statistically significant). TGF-α was undetectable in culture medium in both normoxic and hypoxic conditions (data not shown).

In my *in vitro* experiments, the physiological effects of nanobubbles were unrelated to gas sparging. Instead, the biochemical constituents of nanobubbles may be mediating its effects. The next logical question was which components were responsible for the effects of nanobubbles on hypoxia related signalling? Through systematic elimination of

individual ingredients from nanobubbles, I demonstrated that lecithin was a necessary ingredient in nanobubbles for suppression of HRE transcription in hypoxia (N = 3, P < 0.05) (Figure 15).

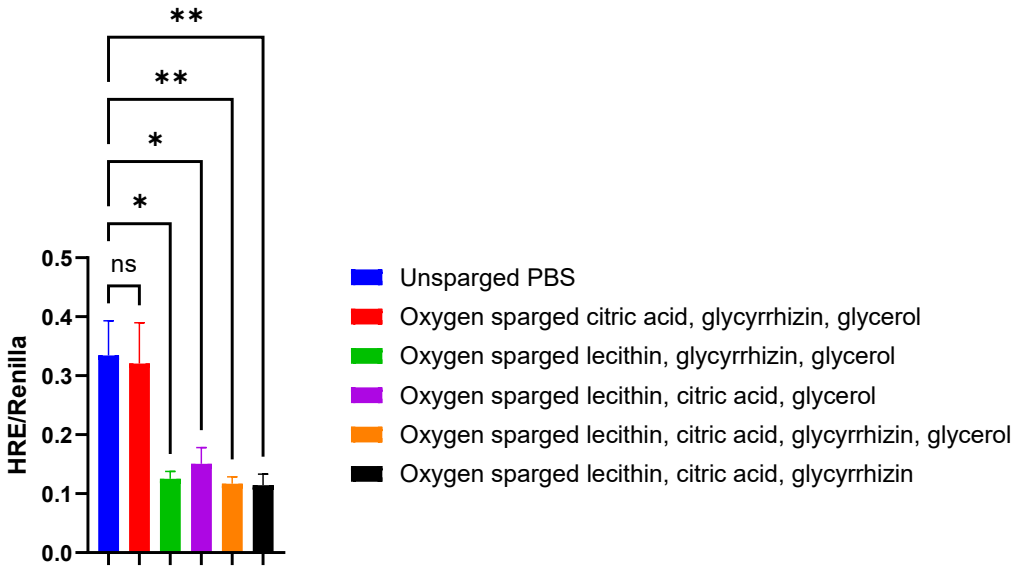

Figure 15 HRE-luciferase activity normalized to Renilla luciferase gene for MG63 cells in 0.1% O_2 hypoxic incubator at T24h treated with either unsparged PBS as control or oxygen nanobubbles without individual ingredients (N = 3).

*Data plotted as mean ± SEM. Ordinary one-way ANOVA with Dunnett's multiple comparison test comparing means with mean of unsparged PBS as control. * denotes P < 0.05, ** denotes P < 0.005.*

A downward trend in HRE transcription was seen with lecithin alone and unsparged nanobubbles although this was not statistically significant (Figure 16) (N = 8). Although lecithin was necessary, lecithin alone may not be sufficient for suppression of HRE transcription.

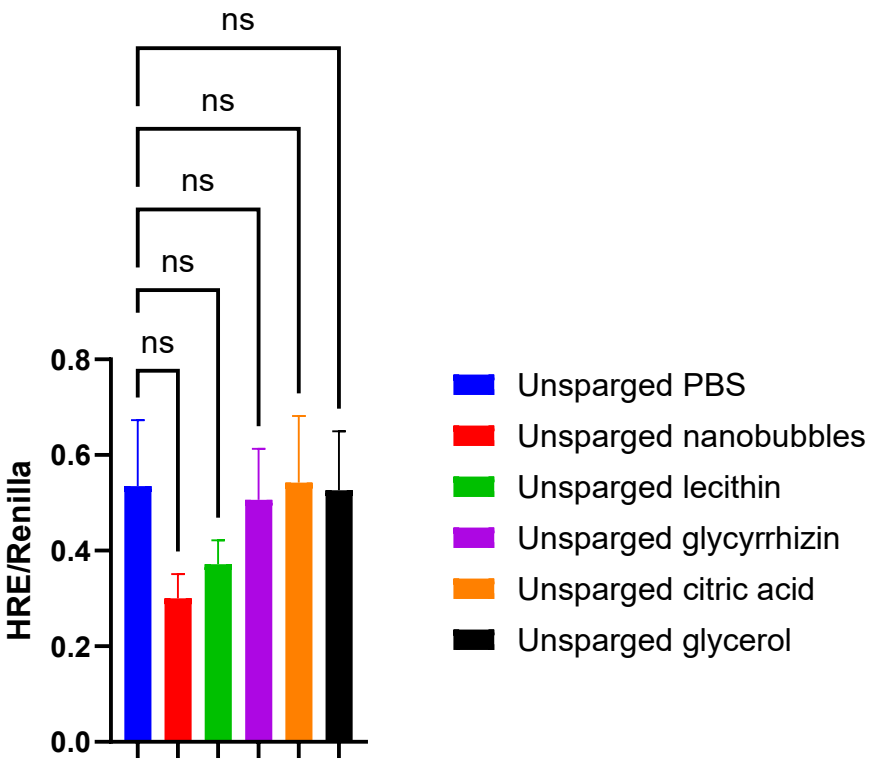

Figure 16 HRE-luciferase activity normalized to Renilla luciferase gene for MG63 cells in 0.1% O_2 hypoxic incubator at T24h treated with either unsparged PBS as control or individual ingredients that comprise nanobubbles (N = 8).

At T0h, each well was treated with either 50 µL unsparged PBS, or 20 µL of either unsparged nanobubbles, lecithin, citric acid, glycyrrhizin, or glycerol, made up to 50 µL with PBS. Data normalized with PBS group as 1. Data plotted as mean ± SEM. Ordinary one-way ANOVA with Dunnett's multiple comparison test comparing means with mean of unsparged PBS as control showed no statistically significant differences (ns denotes P > 0.05).

Confirmation of these findings were attempted with HUVECs. However, HUVECs being primary cells proved challenging to transfect due to toxicity despite trying different

transfection times, different lipid to DNA ratios, culturing in normoxia, or replacement of culture medium after transfection (data not shown). Transfection involves insertion of foreign nucleic acids into eukaryotic cells. Primary cells including HUVECs are notoriously difficult to transfect because they degrade exogenous nucleic acids in the cytoplasm and are susceptible to the toxic effects of transfection reagents (208). In contrast, immortalised cell lines such as MG63 can easily be transfected as they are rapidly dividing and resistant to cytotoxicity. Transfection efficiency below 40% has been reported for primary cells including HUVECs regardless of the transfection reagents used, confirming primary cells as being difficult to transfect (209). Transfection experiments involving primary synovial fibroblasts were also not taken forward due to this issue.

Alternative transfection strategies to chemical methods include viral or physical methods. Viral transduction is widely recognised as a highly effective method to transfect primary cells (209). However, viral transduction risks immunogenic reactions and would require stringent laboratory safety measures for use of viral vectors due to infection risks (208). Physical methods of transduction include electroporation but such methods may damage cells, and usually require cell suspensions *in vitro* as well as specialised equipment (210).

2.3.5 Nanobubble effects on hydrogen peroxide induced ROS production

Free radicals such as ROS may exacerbate inflammation in the arthritic joint and are known to elevate HIF levels (17). Reduction of ROS levels by antioxidant may be beneficial for inflammatory arthritis. Hydrogen peroxide (H_2O_2) is a widely used inducer of ROS, but it can be toxic at high doses. In a pilot experiment of HUVECs to optimise ROS detection assay, 10^{-4} M H_2O_2 was found to be optimal to produce a ROS signal that was at least double the background reading, and ROS signal dropped for H_2O_2 above 10^{-3}

M likely due to cytotoxicity (Figure 17, Figure 18) (N = 1). This was consistent with the literature which showed that the optimal H_2O_2 concentration for ROS induction is approximately 400 µM for HUVECs and 200-400 µM for MG63 (206, 211).

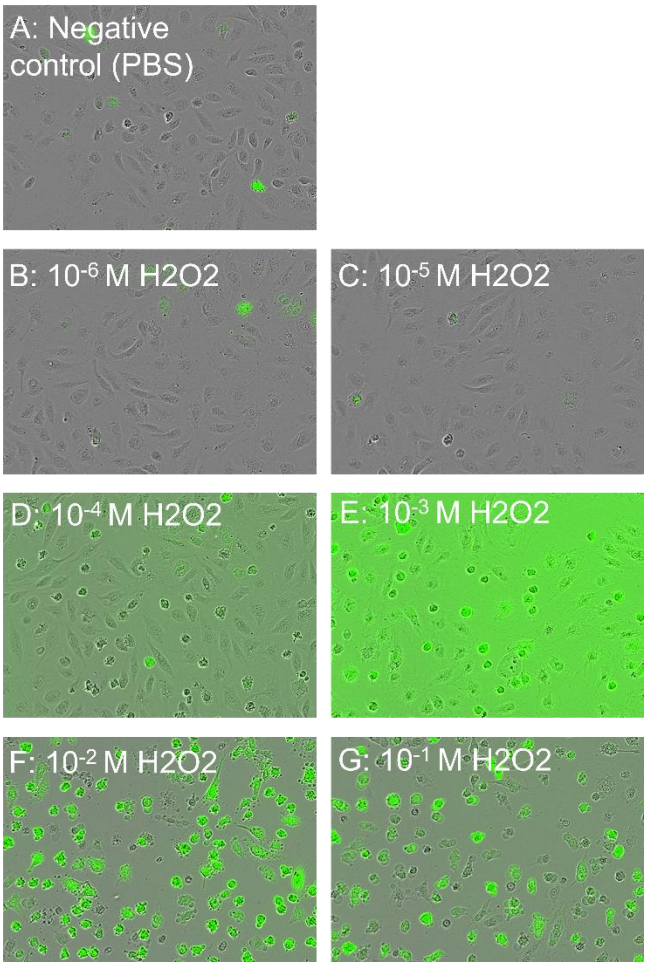

Figure 17 Photos from IncuCyte (10x objective) of ROS as measured by fluorescence after HUVECs cells (P5) were treated in normoxia for 1 h with (A) PBS as negative control, (B-G) H_2O_2 at 10^{-6} M, 10^{-5} M, 10^{-4} M, 10^{-3} M, 10^{-2} M, or 10^{-1} M (N = 1).

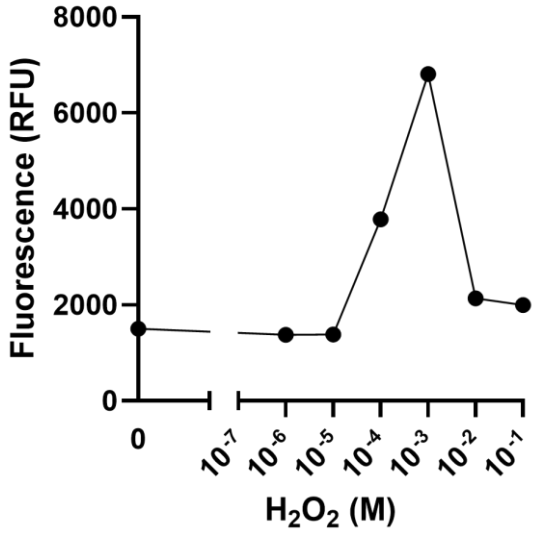

Figure 18 *ROS as measured by fluorescence after HUVECs cells (P5) were treated in normoxia for 1 h with (A) PBS as negative control, (B-G) H_2O_2 at 10^{-6} M, 10^{-5} M, 10^{-4} M, 10^{-3} M, 10^{-2} M, or 10^{-1} M (N = 1)*

Nanobubbles reduced H_2O_2 induced ROS production (Figure 19) (N = 3, P < 0.0005). This effect was irrespective of whether the nanobubbles were unsparged, or sparged with either oxygen or nitrogen.

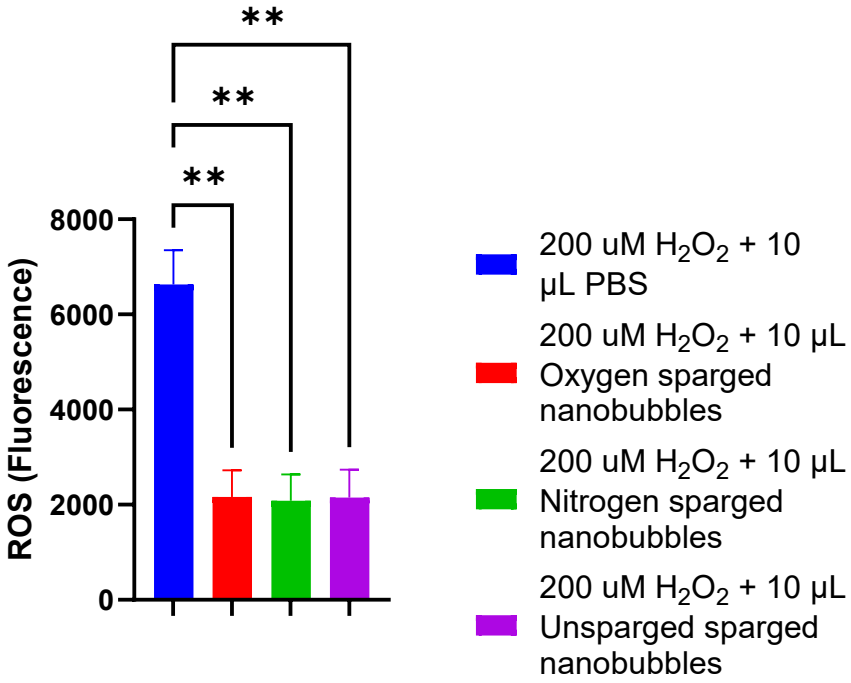

Figure 19 H_2O_2 induced ROS production in MG63 cultured in normoxia after incubation with either PBS, oxygen sparged nanobubbles, nitrogen sparged nanobubbles, or unsparged nanobubbles.

*Grouped analysis with ordinary one-way ANOVA corrected for multiple comparisons using Dunnett's multiple comparison, with PBS as control for comparison, showed significant downregulation in H_2O_2 induced ROS production with nanobubbles (N = 3, ** denotes P < 0.005).*

I then tested whether individual ingredients of nanobubbles affected H_2O_2 induced ROS production (Figure 20). In the negative control, absence of green signal represents absence of ROS (Figure 20a). Using H_2O_2 as the positive control, there was marked green fluorescence consistent with H_2O_2 induced ROS production (Figure 20b). H_2O_2 induced ROS production was abrogated by either unsparged nanobubbles or citric acid alone

(Figure 20c, Figure 20d). H_2O_2 induced ROS production was unaffected by either glycerol, glycyrrhizin, or lecithin (Figure 20e, Figure 20f, Figure 20g).

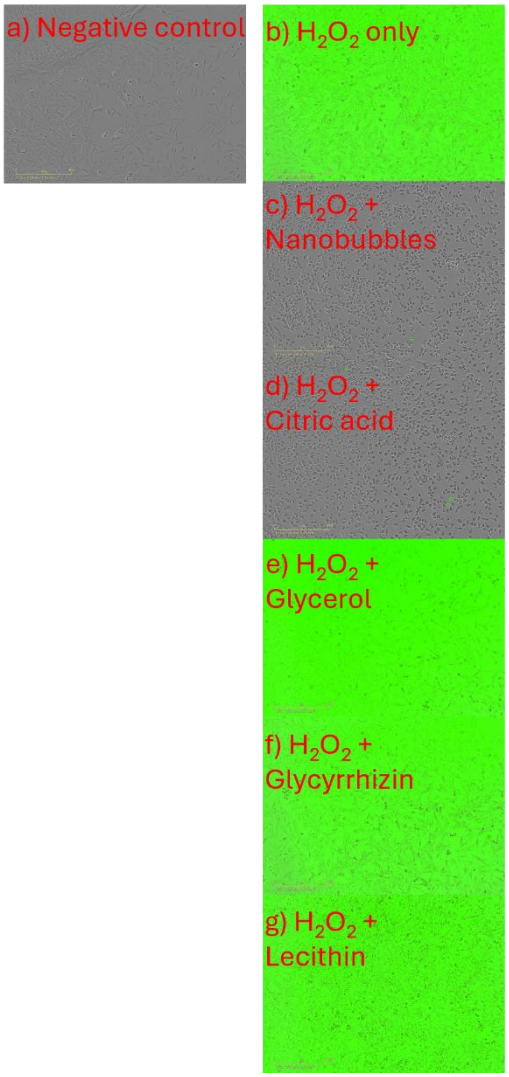

Figure 20 ROS production in normoxic MG63 after incubation with either a) negative control (PBS only), b) positive control (H_2O_2 only), c) H_2O_2 + unsparged nanobubbles, d) H_2O_2 + citric acid, e) H_2O_2 + glycerol, f) H_2O_2 + glycyrrhizin, or g) H_2O_2 + lecithin (10x objective).

Green signal represents fluorescence related to ROS presence.

Citric acid alone reduced the H_2O_2 induced ROS production to a similar degree as unsparged nanobubbles ($N = 3$, $P < 0.00005$) (Figure 21). Therefore, the antioxidant effect of nanobubbles may primarily be accounted for by citric acid alone, which is known to scavenge ROS (212, 213). A limitation is that the strong ROS signal induced by H_2O_2 may have exceeded the detection limit which may limit the detection of an effect by weaker antioxidants. For example, glycyrrhizin is a known antioxidant but only demonstrated a statistically non-significant downward trend in ROS signal in both MG63 and HUVEC cells (214).

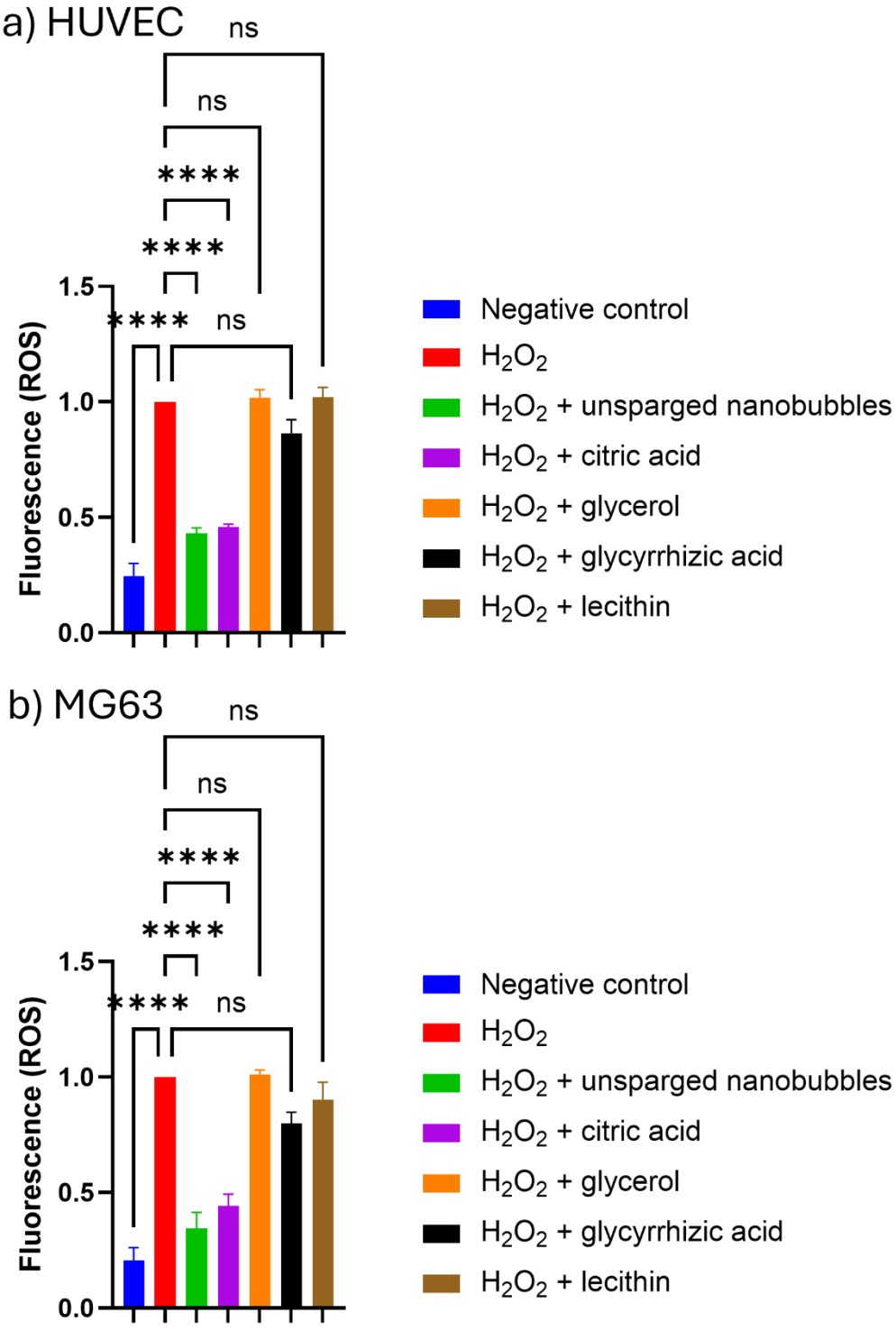

Figure 21 H_2O_2 induced ROS production in a) HUVEC and b) MG63 cells cultured in normoxia after incubation with either PBS, unsparged nanobubbles, citric acid, glycerol, glycyrrhizin, or lecithin.

*Grouped analysis with ordinary one-way ANOVA was corrected for multiple comparisons using Dunnett's multiple comparison, with H_2O_2 positive control group as control for comparison (N = 3. ns denotes not statistically significant, **** denotes P < 0.0001).*

2.4 Discussion

2.4.1 *In vitro* properties of oxygen nanobubbles

Owen *et al*. demonstrated that oxygen nanobubbles administered orally relieved hypoxic markers in peripheral tissues *in vivo* (120). However, there were outstanding questions as to their mechanisms of action, specifically whether nanobubble effects were mediated by gaseous properties of oxygen carried by nanobubbles or biochemical effects of nanobubble constituents (184). I therefore undertook an *in vitro* investigation using nanobubbles to treat cells.

I found that the nanobubbles were not cytotoxic over most of the range of doses tested *in vitro* (Figure 10, Figure 11). Of note, the cellular toxicity of nanobubbles was not altered by sparging with either oxygen or nitrogen. The toxicity of high dose nanobubbles to cells may be related to non-gaseous properties such as their pH of 3. My findings relating to high dose nanobubble related cytotoxicity were consistent with published findings by my supervisors who also found nanobubbles had dose related cytotoxicity in bone relevant cells *in vitro* (190).

HIF-1α protein levels were reduced by nanobubbles *in vitro* which was consistent with the *in vivo* study of nanobubbles (Figure 14A) (120). Furthermore, HIF-1α protein reduction by nanobubbles *in vitro* was shown to be independent of oxygen sparging. This finding

was also consistent with the *in vivo* study of oxygen nanobubbles which showed tissue HIF-1α protein reduction without changes in tissue pO_2 (120). As HIF-1α is the most well-known HIF, I focused on HIF-1α in the preliminary experiments, and I would have sought to confirm nanobubble effects on other HIFs if HIF-1α reduction was oxygen dependent.

Having demonstrated that nanobubbles reduced HIF-1α protein levels independently of oxygen sparging, I then investigated whether nanobubbles had gas dependent effects on HIF-1α downstream signalling through HRE transcription. HIF-1α activity as measured by HRE-luciferase was also reduced by nanobubbles. Moreover, HRE-luciferase reduction by nanobubbles *in vitro* was also independent of oxygen. This result was consistent with the findings that nanobubbles reduced HIF-1α proteins independently of oxygen sparging *in vitro* (Figure 14A) and *in vivo (120)*.

After demonstrating that nanobubbles reduced HIF-1α expression at transcriptional and translational levels, independently of oxygen sparging, I went on to investigate whether nanobubbles affected VEGF expression through gas related mechanisms. I found nanobubbles had no effects on VEGF protein levels after 24 h incubation in hypoxia (Figure 14C). Although I could have investigated this further using different nanobubble doses, cell lines, hypoxic levels, or follow-up timepoints, I opted not to pursue this further. This was because there was sufficient evidence to show that nanobubbles did not mediate effects through gas related mechanisms *in vitro*, which was consistent with previous animal *in vivo* experiments (120).

For example, a limitation of this study is that only 0.1% O_2 was used to induce hypoxia. 0.1% O_2 is more hypoxic than would be expected in an arthritic joint whereas 1% O_2

would more accurately reflect the physiology in an arthritic joint. As the body of evidence thus far from the *in vitro* experiments described in this thesis, as well as *in vitro* and *in vivo* experiments by others were consistent in showing that oxygen nanobubbles would not be expected to relieve hypoxia in peripheral tissues, it was unnecessary to repeat the experiments at different O_2 levels (117, 120, 190).

In hindsight, the lack of change in peripheral oxygen levels in animal *in vivo* experiments was further supported by a double-blind, randomised, placebo-controlled pilot study which examined oxygen nanobubble beverage in elite cyclists (118, 184). The manufacturer Avrox commissioned and funded this study which found "oxygen-nanobubble beverage" improved exercise physiology and performance in cyclists, but this study was not without controversy (118, 184). Some of the strengths of this study were that it was double-blinded and placebo-controlled. Compared to placebo drinks, oxygen nanobubble drinks did not increase capillary blood pO_2 or SpO_2 by pulse oximetry, which would be expected to support the hypothesis that oxygen nanobubbles increase oxygen delivery. It may be that no difference was seen in capillary blood pO_2 due to its insensitivity and poor association with arterial pO_2 (118). Similarly, it may be that no difference was seen in oxygen saturation by pulse oximetry in the treatment groups because haemoglobin saturation is high and may not reflect total oxygen carrying capacity (118).

Moreover, there were also no differences between oxygen nanobubble drinks and placebo drinks in blood lactate levels, pH, pCO_2, HCO_3, and total CO_2 (118). King *et al*. pointed out that measurements of skeletal muscle oxygenation using near-infrared spectroscopy would have helped clarify whether oxygen nanobubbles increased oxygen delivery to peripheral tissues (118). Their study design would have been more transparent if the

research team clarified how they selected which bottles to load with oxygen, given these bottles contained the same beverage supplied by Avrox (118). In my opinion, their study would have been more rigorous if the research team had randomised the bottles from Avrox into oxygen-nanobubble beverage and placebo beverage, rather than using the manufacturer's assignments (118). Indeed, the study design was criticised and its findings were attributed to placebo effects by Tiller *et al*. (184).

The surprising improvement in exercise physiology and performance in cyclists by oxygenated nanobubbles provoked controversy. The study by King *et al*. contradicted previous studies which found no effects of oxygen-enriched beverages on exercise performance or exercise O_2 uptake (118, 184, 215-217). Tiller *et al*. commented that the "oxygenated beverages allegedly improve performance via a mechanism which is physiologically implausible" (184). To which the authors of the original study conceded, "the surprising nature of the results reported in the paper" may be due to nanobubbles being "of a novel design" (118). The dispute related to the amount of oxygen purported to be delivered by nanobubbles (118, 184).

Given that the nanobubble drinks were estimated to contain approximately 15 mL of oxygen, such a small amount of oxygen would be expected to yield only 0.073 – 0.075 calories (304-315 joules), which the authors recognised were unlikely to account for the increase in exercise performance (118, 184). It was speculated that recirculation of nanobubbles could potentially deliver more oxygen to peripheral tissues than initially encapsulated in the consumed dose (117, 118). However, there is no evidence to support the speculation that these nanobubbles act as circulating "oxygen carriers" that "absorb oxygen during their passage through the lung capillary bed and subsequently release it in

areas of hypoxia" (117). In the absence of evidence showing that nanobubbles mediate effects through gas mediated mechanisms, the evidence thus far point to their effects as mediated by established biochemical means. My *in vitro* investigations suggested that nanobubbles may mediate effects through its biochemical constituents, rather than gaseous mechanisms, providing an alternative rationale for findings reported in previous studies of these nanobubbles (117, 118, 120, 184).

Recent *in vitro* characterisation of oxygen nanobubbles on bone related cells by my supervisors also did not show definitive gas dependent effects of nanobubbles on HIF-1α (190). Knowles *et al*. found that osteoclast formation was suppressed by oxygen nanobubbles compared to nitrogen nanobubbles, and that osteoclastogenesis was promoted by oxygen nanobubbles compared to nitrogen nanobubbles (190). However, without an oxygen sparged nanobubble-free control for comparison, it was not clear whether these gas-dependent effects are due to dissolved oxygen in liquid or gaseous oxygen encapsulated in nanobubbles. For example, by omitting lecithin from the mixture, oxygen sparged mixture of glycyrrhizin, citric acid and glycerol could have been used as a comparator group without the lecithin surfactant-stabilised nanobubbles.

2.4.2 Potential mechanisms of action of oxygen nanobubbles

If HIF-1α protein and activity were reduced by nanobubbles independently of oxygen, then could the biochemical properties of nanobubbles be driving this reduction? After all, Knowles *et al*. also showed that individual biochemical constituent in nanobubbles may be the predominant driver of nanobubble effects (190). In my *in vitro* characterisation, individual ingredients were systematically eliminated from the nanobubbles to see whether any single ingredient was responsible. Lecithin turned out to be necessary but insufficient

for the reduction of HIF-1α activity (Figure 15, Figure 16). The role of lecithin in HIF pathway needs to be considered.

Lecithin is a generic colloquial term to describe the yellowish fatty substance in foodstuff such as eggs, soy and sunflower. It is widely used in industry for emulsifying food mixtures. Lecithin comprises of glycerophospholipids including phosphatidylcholine, phosphatidylethanolamine, phosphatidylinositol, phosphatidylserine and phosphatidic acid. To be consistent with the method by which Professor Stride's group generated nanobubbles, I used the same lecithin that their group used with a molecular formula of C42H80NO8P (ThermoScientific, catalogue number J61675.30). In aqueous solutions, the phospholipids in lecithin form nanoscopic liposomes and micelles, spherical structures which resemble the shape of nanobubbles (218).

In fact, the biochemical composition of lecithin may account for the nanobubble effects on hypoxic markers, even if not hypoxia itself. Lipid metabolism is well known to affect the hypoxic pathway (219-221). For example, Shao *et al*. demonstrated that decreasing extracellular lipid supply inhibited HIF prolyl hydroxylation, which was suppressed by addition of fatty acids (219). In the absence of lipoproteins, depletion of fatty acid oleate led to the generation of mitochondrial ROS that inhibited PHD enzymes resulting in HIF stabilisation (219). Their model by which lipid metabolism modulates the hypoxic pathway offers a useful insight into the potential mechanisms by which nanobubbles may affect the hypoxic pathway without affecting hypoxia (219). As ROS may mediate between the lipid metabolism pathway and hypoxic pathway, I went on to investigate whether nanobubbles may also affect HIF signalling through ROS.

Inflammatory arthritis is known to be related to ischaemia-reperfusion and free radicals. Reversing hypoxia may lead to generation of free radicals which in turn may exacerbate inflammation. Therapeutic agents that target hypoxia may therefore also benefit from having antioxidant properties to prevent free radical induced damage. In my *in vitro* experiments, nanobubbles inhibited H_2O_2 induced ROS (Figure 20). This antioxidant effect was unrelated to gas sparging and may have been accounted for by citric acid alone which is a known antioxidant. Knowles *et al*. also showed that citric acid was the primary mechanism mediating the nanobubble effects on cytotoxicity and osteoclastogenesis (190). The antioxidant effects of citric acid in nanobubbles may therefore account for the reduction in HIF-1α *in vitro* and *in vivo* (Figure 14, Figure 20) (120). As the model by Shao *et al*. suggests, lipoproteins in nanobubbles and antioxidant effect of citric acid may reduce ROS leading to activated PHD and HIF-1α degradation (219).

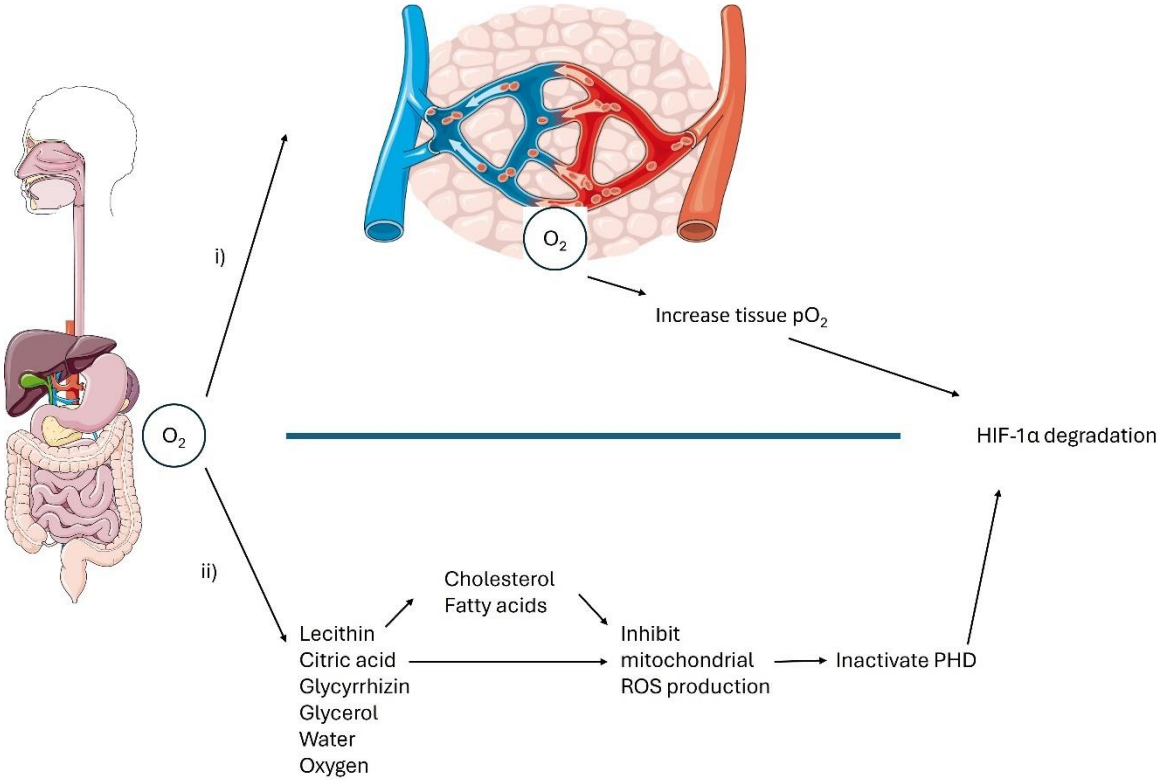

Figure 22 Graphical abstract of potential mechanisms of action of oxygen nanobubbles

Oxygen nanobubbles are consumed orally. i) Oxygen nanobubbles may be absorbed intact into the bloodstream. Oxygen nanobubbles may deliver oxygen to peripheral tissues where it relieves hypoxia resulting in HIF-1α degradation. ii) Oxygen nanobubbles may be broken down into its constituents in the gastrointestinal tracts. Lecithin may be metabolised into cholesterol and fatty acids. Absorption of cholesterol, fatty acids and citric acid may inhibit mitochondrial ROS production, leading to PHD inactivation and HIF-1α degradation. Adapted in accordance with the Creative Commons Attribution Non-Commercial (CC BY-NC 4.0) license (https://creativecommons.org/licenses/by-nc/4.0/) from Servier Medical Art.

In summary, my experimental work provides insight into the mechanisms by which oxygen nanobubbles may affect HIF-1α (Figure 22). It was previously thought that oxygen nanobubbles reduce HIF-1α through oxygen gas mediated mechanisms (Figure 22i).

However, there remains a degree of uncertainty as to whether nanobubbles carry oxygen in gaseous form on a nanoscopic scale, whether oxygen nanobubbles are absorbed in its intact form into the bloodstream through the gastrointestinal tract, whether nanobubbles can replenish its oxygen content when passing through the respiratory system, and whether oxygen nanobubbles can increase peripheral tissue pO_2 (Figure 22i) (117, 118, 120, 184, 190). Furthermore, nanobubbles have never been reported to be present in the blood despite the assumption that nanobubbles are absorbed into the bloodstream after oral ingestion.

The reason for the lack of pharmacokinetic study of nanobubbles is that the cells and molecules present in bodily fluids such as blood would impair the detection of nanobubbles. For example, Owen *et al*. demonstrated the nanoscopic size and shape of nanobubbles *in vitro* using techniques such as single particle optical sizing system, dynamic light scattering and electron microscopy (120). However, the cells and vesicles in blood would confound these techniques because they resemble nanobubbles in size and shape. For example, chylomicrons are approximately 200 – 600 nm in diameter and exosomes are approximately 30 – 150 nm in diameter (222, 223).

In the absence of pharmacokinetic analysis because the concentration of nanobubbles in bodily fluids or tissues cannot be measured directly, the assumption that orally delivered oxygen nanobubbles relieve peripheral tissue hypoxia rests on pharmacodynamic studies. However, given that *in vitro* and *in vivo* studies of oxygen nanobubbles suggest nanobubbles affect HIF-1α through non oxygen gas mediated mechanisms without altering pO_2, the chemical constituents of nanobubbles may be wholly responsible for the effects of

oxygen nanobubbles (Figure 14, Figure 15, Figure 19, Figure 20, Figure 21, Figure 22ii) (117, 118, 120, 184, 190).

My findings demonstrated that nanobubbles may alter hypoxic pathways through non-gaseous mechanisms. On the basis that my *in vitro* findings suggested that nanobubbles may mediate effects through biochemical effects rather than oxygen gas delivery, the clinical study of whether joint hypoxia may be alleviated by nanobubbles was abandoned. On a related note, a negative clinical study of oxygen nanobubbles by my supervisors in patients with pulmonary fibrosis was recently reported (224).

Hypoxia may contribute to decreased exercise performance and shortness of breath in patients with pulmonary fibrosis. In the abstract by Sheth *et al*., an *in vivo*, randomised, cross-over, double-blind, placebo-controlled study was conducted to investigate whether drinking oxygen nanobubbles would increase the exercise capacity of patients with pulmonary fibrosis during a 6 Minute Walk Test (6MWT) (224). Each participant performed two 6MWTs, each 6MWT was 10 minutes after drinking oxygen nanobubbles or placebo, with a 2-hour washout period between the 6MWTs. 27 patients with pulmonary fibrosis completed the study. Compared to placebo, drinking oxygen nanobubbles significantly worsened the primary outcome. The 6 Minute Walk Distance was the primary outcome and this was 9.3 m (0.8 – 17.8 m; $p < 0.05$) less in participants drinking oxygen nanobubbles compared to drinking placebo (224). Drinking oxygen nanobubbles also did not improve secondary outcomes including changes in oxygen saturation, heart rate and breathlessness. The full publication of this clinical study is eagerly awaited for critical analysis of how the oxygen nanobubbles were formulated, whether the nanobubble gas levels were measured directly, how the dose of nanobubbles

was standardised, and how oxygen nanobubbles may have contributed to deterioration in clinical outcomes.

Even though nanobubbles may not mediate its effects through oxygen delivery as intended, they may nonetheless have value as HIF modulators (118, 120, 190). The combination of lipids, lecithin, antioxidants, pH regulator, was also used to generate nanoscopic liposomes for targeted drug delivery and HIF modulation (225). For example, lipid liposomes were investigated in a mouse model of liver cancer where HIF-1α expression was known to be increased in liver cancer tissues. In turn, HIF-1α was directly linked to the resistance of 10-hydroxycamptothecin, a treatment for liver cancer (225). Berberine chloride was known to reduce HIF-1α levels (225). Qi *et al*. found that intravenous administration of lipid lipospheres loaded with berberine chloride and 10-hydroxycamptothecin reduced tissue HIF-1α concentration and inhibited tumour growth in a mouse model of liver cancer (225). These liposomes share strikingly similar biochemical composition, size and effects on HIF-1α as Professor Stride's oxygen nanobubbles. Unfortunately, they did not have a comparator group to show whether administration of lipid microsphere without drug loading affected tissue HIF-1α levels (225).

Although oxygen nanobubbles are unlikely to impact peripheral tissue oxygen levels, joint hypoxia remains a potential therapeutic target as discussed in Chapter 1. Glucocorticoids have been shown to have protective effects in hypoxic settings such as high-altitude mountain sickness and perinatal hypoxia (226). A clinical study of how current therapies such as intra-articular glucocorticoid injection affect hypoxia and hypoxic pathways in joints is warranted.

3. Chapter 3: Exploration of intra-articular methylprednisolone effects on joint hypoxia in inflammatory arthritis

3.1 Introduction

3.1.1 Glucocorticoids

As discussed in Chapter 1, joint hypoxia may be involved in the pathogenesis of inflammatory arthritis and was shown to be relieved in patients who responded to TNFi (149, 227). The original plan was to undertake an interventional study to investigate whether orally delivered nanobubbles can relieve joint hypoxia in patients with inflammatory arthritis, as discussed in Chapter 2. In view of the *in vitro* data, the clinical study of nanobubbles was no longer justified.

It is unknown as to how other therapies affect hypoxia and hypoxic pathway in arthritic joints. Glucocorticoids have been widely used to treat inflammatory arthritis since the Nobel Prize was awarded for the discovery of glucocorticoid effects in patients with RA in 1950 (228). The direction of the DPhil pivoted to investigate how an established treatment in the form of intra-articular methylprednisolone injection joint hypoxia in patients with inflammatory arthritis.

Glucocorticoids are important in regulating homeostasis, metabolism, inflammation, and mediating response to stress (229). They are endogenously produced in the adrenal cortex. Stress induces corticotropin-releasing hormone (CRH) release from the hypothalamus. CRH in turn stimulates the release of adrenocorticotropic hormone (ACTH) from the anterior pituitary gland. ACTH induces the synthesis and release of glucocorticoids such as cortisol in the adrenal cortex. Cortisol is inactivated to inactive form cortisone by 11β-

hydrosteroid dehydrogenase type 2 (11β-HSD2) expressed in tissues such as kidneys, which is reversed by 11β-hydrosteroid dehydrogenase type 1 (11β-HSD1) expressed in tissues such as adipose tissues. Negative feedback mediated by cortisol inhibits further release of CRH and ACTH to prevent overproduction of and prolonged exposure to glucocorticoids. Although glucocorticoids have many uses, they are associated with diverse adverse effects such as hypertension, obesity, diabetes mellitus, infection, osteoporosis and Cushing's syndrome (229, 230).

Intra-articular glucocorticoid injection is a commonly used therapy for the treatment of inflammatory arthritis (231, 232). Intra-articular glucocorticoid injection into the affected joint has the advantage of treating inflammatory arthritis while limiting adverse effects of systemic glucocorticoid therapy (233). Depot glucocorticoids formulated for joint injections release glucocorticoid at a much slower rate for sustained effects (230). Intra-articular glucocorticoids such as triamcinolone acetonide and methylprednisolone acetate have similar efficacy in treating inflammatory arthritis (234, 235). To avoid confounding in the choice of glucocorticoid injected, this study investigated the effects of intra-articular methylprednisolone acetate. Although there are other methylprednisolone esters such as methylprednisolone aceponate and methylprednisolone succinate, methylprednisolone acetate is hereafter referred to simply as methylprednisolone.

Much is known about the effects of glucocorticoids but the exact molecular mechanisms of action underlying their effects remain incompletely understood (230). More precise targeting of anti-inflammatory pathways mediated by glucocorticoids would deliver the beneficial effects of glucocorticoids without associated adverse effects. The binding of glucocorticoid such as methylprednisolone with intracellular glucocorticoid receptors

induces a conformational change and ligand-receptor dimerisation which mediate many physiological effects (Figure 23) (236).

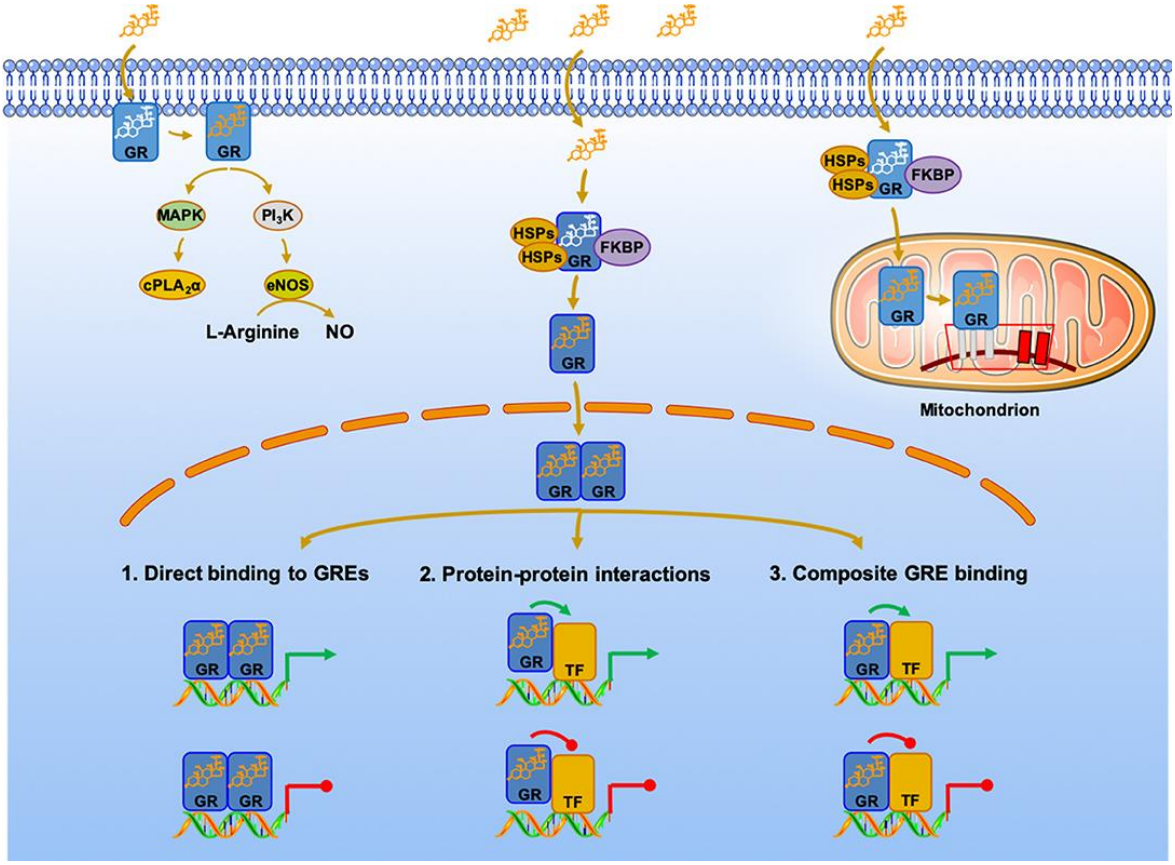

Figure 23 Genomic, non-genomic, and mitochondrial glucocorticoid signalling pathways

Reprinted in accordance with the Creative Commons Attribution Non-Commercial (CC BY-NC 4.0) license (https://creativecommons.org/licenses/by-nc/4.0/) from Meduri et al. (237)

In the cytoplasm, glucocorticoid receptors are bound to co-chaperones such as heat-shock proteins (HSP) and immunophilins FK506 binding proteins (237). Binding of glucocorticoid to glucocorticoid receptors displaces the chaperone and the activated receptor translocates into the nucleus where it interacts with glucocorticoid response

elements (GRE) leading to transactivation. Activated glucocorticoid receptors also interact with transcription factors such as NF-κB and activator protein 1 (AP-1) (237). Transrepression of NF-κB and AP-1 signalling are important mechanisms of the anti-inflammatory effects of glucocorticoids. Translocation of activated glucocorticoid receptors into the mitochondria also results in interaction with mitochondrial DNA glucocorticoid responsive elements (237). These genomic signalling pathways mediated by glucocorticoids have slow onset and slow dissipation (238). Conversely, non-genomic signalling pathways mediated by glucocorticoids have a fast onset (238). For example, activated glucocorticoid receptors activate mitogen-activate protein kinase (MAPK) and phosphoinositide 3-kinases (PI3Ks) (Figure 23) (237). Non-genomic effects on metabolism such as increased itaconate levels are important mediators of glucocorticoids effects on resolution of inflammation (239). Activated glucocorticoid receptors interact with the pyruvate dehydrogenase complex to potentiate tricarboxylic acid (TCA)-cycle dependent production of anti-inflammatory metabolite itaconate (239).

3.1.2 Glucocorticoids in hypoxic settings

Previous studies suggest glucocorticoids such as methylprednisolone may protect from hypoxia induced damage (226, 240). Inflammation is a metabolically active process that consumes oxygen through aerobic respiration. The anti-inflammatory effects of glucocorticoids may reduce oxygen consumption thereby relieving hypoxia. Glucocorticoids may also be beneficial in hypoxic settings such as altitude sickness and neonatal hypoxia through biochemical means independent of oxygen.

People are exposed to hypobaric hypoxia when they travel to regions of altitudes higher than 2500 m (226). For non-acclimatised individuals, rapid high-altitude ascent may result

in acute mountain sickness which is characterised by headache, nausea, loss of appetite, fatigue and dizziness. This phenomenon is due to systemic hypoxia, vascular leakage and increased levels of circulating pro-inflammatory cytokines (226). In the setting of high-altitude related hypoxia, prophylactic treatment with glucocorticoids such as dexamethasone and prednisolone reduced symptoms of acute mountain sickness, suppressed inflammatory pathways, reduced vascular permeability and vasoconstriction, and improved arterial oxygenation (226).

Glucocorticoids have also been shown to be beneficial in the setting of neonatal hypoxia. For example, hypoxic-ischaemic damage in the brain has been shown to be improved with glucocorticoids (240, 241). Indeed, glucocorticoid administration reduced cerebral infarction in neonatal rat model of hypoxic-ischaemic induced brain damage (240-242). The protective effect was thought to be mediated by glucocorticoid receptors, as opposed to mineralocorticoid receptors, since this effect was inhibited by glucocorticoid receptor antagonism (240, 243). Although joint hypoxia was associated with inflammatory arthritis, whether hypoxic pathway in arthritic joints may be targeted with glucocorticoid is unclear (16). Given that successful TNFi treatment has been shown to relieve joint hypoxia, I sought to understand whether another common treatment, intra-articular glucocorticoid injection, relieves hypoxia and hypoxic pathways in arthritic joints in patients with RA and PsA.

3.1.3 Prospective Longitudinal Effects of Intra-articular Methylprednisolone Injection on Synovial Fluid Oxygen

I undertook a prospective clinical study to investigate the effects of intra-articular methylprednisolone injection on synovial fluid oxygen. To avoid confounding by other

medications such as DMARDs, the dose of DMARD regimen must be stable for at least 4 weeks prior to baseline visit. Other than the intra-articular methylprednisolone injection, none of the participants had changes in their medications such as DMARDs during the study.

To measure therapeutic effect on pO_2 in the arthritic joint, the options included measuring pO_2 in the synovial fluid or synovial tissue as discussed in Chapter 1. Measuring synovial tissue pO_2 would be substantially more complex as it would require insertion of a port to allow a rigid oxygen probe to reach the synovial tissue. As the synovial fluid pO_2 would be expected to reflect the synovial tissue pO_2 as it is a closed system, and measuring synovial fluid pO_2 was substantially more convenient with less risk to the patient, synovial fluid pO_2 was the assay of choice for measuring joint hypoxia. I also undertook ultrasound guided synovial tissue biopsies to interrogate biomarkers of hypoxia and inflammation.

To determine whether biomarkers were associated with clinical disease activity, composite disease activity scores were collected. Disease Activity Score 28 (DAS28) and Disease Activity Index for Psoriatic Arthritis (DAPSA) were used to assess disease activity in patients with RA and PsA, respectively (244, 245). The DAS28 is a composite disease activity score based on a count of 28 swollen and tender joints, a measure of general health, and the acute phase response. The disease activity states in patients with RA may be defined using the DAS28 score as being high (> 5.1), moderate (3.2 - 5.1), low (2.6 - 3.2) and in remission (≤ 2.6) (244). The DAS28 score at baseline along with the change in DAS28 at follow-up can be used to define response to treatment (244, 246). For patients with RA, DAS28 has been validated against radiographic progression and physical function (244).

DAS28 is not appropriate for assessing patients with PsA because it does not capture joints commonly affected in PsA such as the DIP, ankle and foot joints (245). For patients with PsA, the DAPSA is a disease specific tool validated for assessing disease activity states and treatment response (245). The DAPSA integrates five key components: swollen joint counts, tender joint counts, patient's assessment of pain severity, patient's assessment of rheumatic disease activity, and CRP levels. It is endorsed by the EULAR recommendations on treat-to-target management of PsA (247). These composite disease activity scores provide clinical context for the evaluation of therapeutic effects on joint hypoxia.

There was scant data available to guide as to the optimal follow-up timepoint for assessment in my study. Biniecka *et al*. showed that successful TNFi treatment increased synovial tissue pO_2 levels at 3 months (149). However, TNFi treatment is administered by the patient repeatedly with peak effects expected at 3 months. Conversely, an intra-articular methylprednisolone is injected once into the patient and its effects may have waned after 3 months (248). Indeed, EULAR states a general accepted rule in clinical practice is to wait at least 3 months before repeating an intra-articular glucocorticoid injection, although this was not evidence based (231). A follow-up timepoint earlier than 3 months would therefore be needed to study the effects of intra-articular methylprednisolone injection.

The concentration of methylprednisolone in synovial fluid following an intra-articular injection was previously studied in thoroughbred racehorses, which provided insight when determining the follow-up timepoint in this clinical study (249, 250). After an intra-articular methylprednisolone acetate injection in horses, the half-life of

methylprednisolone in synovial fluid was approximately 4 days (249, 250). Methylprednisolone was detected in synovial fluid in the majority of horses up to 42 days after an intra-articular injection (249).

Although these repeated arthrocentesis in animal studies were helpful in demonstrating pharmacokinetics of methylprednisolone in synovial fluid, recurrent joint aspirations would have to be more limited in human clinical studies to ensure acceptability to patients and with ethical concerns of repeated procedural risks. As the early effects of intra-articular methylprednisolone within 2 weeks of injection have been studied previously, I opted to study the effects at follow-up timepoint of 4 weeks where the late effects are less well known and yet there is evidence for methylprednisolone to still be present in synovial fluid (249). I characterised the change in synovial fluid cytokine profiles as biomarkers for the therapeutic effects of intra-articular methylprednisolone injection (Table 4).

Table 4 Summary of cytokines tested in synovial fluid

Cytokine	Source	Targets	Role	Therapeutic implication	References
IFN-γ	CD4+ T helper 1 (Th1) cells, natural killer (NK) cells, CD8+ cytotoxic T cells, innate lymphoid cells (ILC), dendritic cells, macrophages, B cells	Activates Janus kinase /signal transducer and activator of transcription (JAK/STAT) signalling pathway. Activates macrophages. Induces CD8+ cytotoxic T cell differentiation and activation. Induces IgG isotype switching in B cells.	Innate and adaptive immunity. Promote inflammation, cell proliferation and differentiation.	IFN-γ levels in synovium correlate with arthritis disease severity and therapy evaluation. Glucocorticoids downregulate IFN-γ expression.	(251-254)
IL-1β	Monocytes, macrophages, dendritic cells	Activates osteoclasts. Drives Th17 differentiation. Promotes endothelial vasodilation.	Contribute to joint inflammation.	IL-1RA (anakinra), anti-IL-1β (canakinumab)	(255-257)
IL-2	CD4+ T cells, CD8+ T cells, NK cells, dendritic cells	Activates regulatory T (Treg) cells and inhibits differentiation of Th17 cells to maintain immune tolerance. Activates T cells and NK cells.	Pleiotropic functions including promotion of inflammation and maintaining immune tolerance.	IL-2 under investigation as a treatment for inflammatory arthritis	(258, 259)
IL-4	Th2 cells, NK cells, Th1 cells, CD8+ T cells, ILCs, B cells, mast cells, macrophages, basophils, eosinophils	Activates STAT6 signalling. Induce macrophage polarisation into the anti-inflammatory M2 phenotype. Switching immunoglobulin class of IgE and IgG4. Stimulate B cells proliferation. Activates eosinophils, basophils, mast cells, endothelial cells. Promotes Th2 differentiation.	Suppresses production of pro-inflammatory cytokines (IL-1β, IL-6, IL-8, TNF), VEGF and metalloproteinases. Role in allergic inflammation and parasite infection.	Subcutaneous administration of IL-4 reduced inflammatory cytokines in patients with skin psoriasis. Induction of IL-4/IL-13 signalling pathway may be beneficial in treating inflammatory arthritis.	(260, 261)

Cytokine	Source	Targets	Role	Therapeutic implication	References
IL-6	Monocytes, macrophages, synovial fibroblasts	Induce synovial fibroblast activation and proliferation. Induced osteoclast differentiation. Induce Th17 differentiation and proliferation. Induce B cell survival and antibody production. Induce hepatocyte production of acute phase reactants.	Drives inflammation, atherosclerosis, impaired lipid metabolism, and anaemia.	Anti-IL-6R (tocilizumab, sarilumab), anti-IL-6 (sirukumab)	(262, 263)
IL-8	Macrophages, endothelial cells, osteoclasts	Promotes chemotaxis of neutrophils and leukocytes. Activates osteoclasts.	Drives leukocyte chemotaxis. Activate immune and stromal cells to promote inflammation.	Synovial tissue IL-8 expression in higher in involved joints compared to uninvolved joints in patients with RA. However, an anti-IL-8/CXCL8 agent was tested in RA but the trial results were not published and the compound was not developed further.	(264)
IL-10	Monocytes, Th2 cells, mast cells, Tregs	Inhibits inflammatory cytokines, downregulates antigen-presenting cell function, inhibits NF-κB activity, suppresses T cells and macrophages.	Pleiotropic effects in immunoregulation and inflammation	Recombinant IL-10 failed to improve disease in RA, skin psoriasis or Crohn's disease.	(265-268)
IL-12p70	Macrophages, dendritic cells	Induce Th1 and Th17 cell differentiation. Stimulates Th1 cells to produce IFNγ and GM-CSF (granulocyte-macrophage colony-stimulating factor)	Promotes Th1 and Th17 phenotype	Anti-p40 (common subunit of IL-12/23; ustekinumab)	

Cytokine	Source	Targets	Role	Therapeutic implication	References
IL-13	Th2 cells, NK cells, Th1 cells, CD8+ T cells, ILCs, B cells, mast cells, macrophages, basophils, eosinophils	Binds receptor which comprises the IL-4R chain and IL-13RA1 chain. Activates STAT6 signalling. Induce macrophage polarisation into the anti-inflammatory M2 phenotype. Switching immunoglobulin class of IgE and IgG4. Stimulate B cells proliferation. Activates eosinophils, basophils, mast cells, endothelial cells.	Suppresses production of pro-inflammatory cytokines (IL-1β, IL-6, IL-8, TNF), VEGF and metalloproteinases. Role in allergic inflammation and parasite infection.	Induction of IL-4/IL-13 signalling pathway may be beneficial in treating inflammatory arthritis.	(260)
TNF	Monocytes, macrophages	Induce synovial fibroblast pro-inflammatory cytokine production. Induce osteoclasts differentiation and activation. Induce neovascularisation. Inhibit Tregs.	Drives inflammation and bone erosion	Anti-TNF (infliximab, adalimumab, golimumab, certolizumab), anti-TNFR (etanercept)	(7)

3.2 Materials and methods

3.2.1 Clinical study design

This was a prospective, longitudinal, single arm, pilot study to investigate the physiological effects of intra-articular corticosteroid injection on markers of joint hypoxia and inflammation in patients with RA and PsA who were due to receive intra-articular corticosteroid injection as part of their routine care. I was the Chief Investigator and Principal Investigator. I designed and wrote the study protocol in collaboration with co-investigators Professor Duncan Richards, Professor Laura Coates, Professor Philippa Hulley, and Dr Helen Knowles.

University of Oxford was the study sponsor and the Climax Donation at University of Oxford funded this study. This study was registered on clinicaltrials.gov (https://clinicaltrials.gov/ct2/show/NCT04804449). The main research question was to investigate the effects of intra-articular methylprednisolone injection on joint oxygen tension in patients with RA and PsA. The primary outcome measure was change in synovial fluid pO_2 at Day 28 (study end) compared to Day 1 (baseline). The other aim of the study was to understand the biological effects of intra-articular methylprednisolone injection by identifying the biomarkers related to the intervention and disease activity.

The study aimed to recruit 10 patients to study completion. Participants were recruited from Nuffield Orthopaedic Centre, Oxford University Hospitals NHS Foundation Trust (OUH). Biological samples (blood, synovial fluid, synovial tissues) and questionnaire information were collected at Day 1 and Day 28 to investigate the biological effects of intra-articular corticosteroid injection (Figure 24). To allow for scheduling of

investigations the day 28 assessments may take place between 26 and 30 days. Study visits were conducted in compliance with Oxford University and OUH guidance for prevention of transmission of COVID19 at the time of the visit.

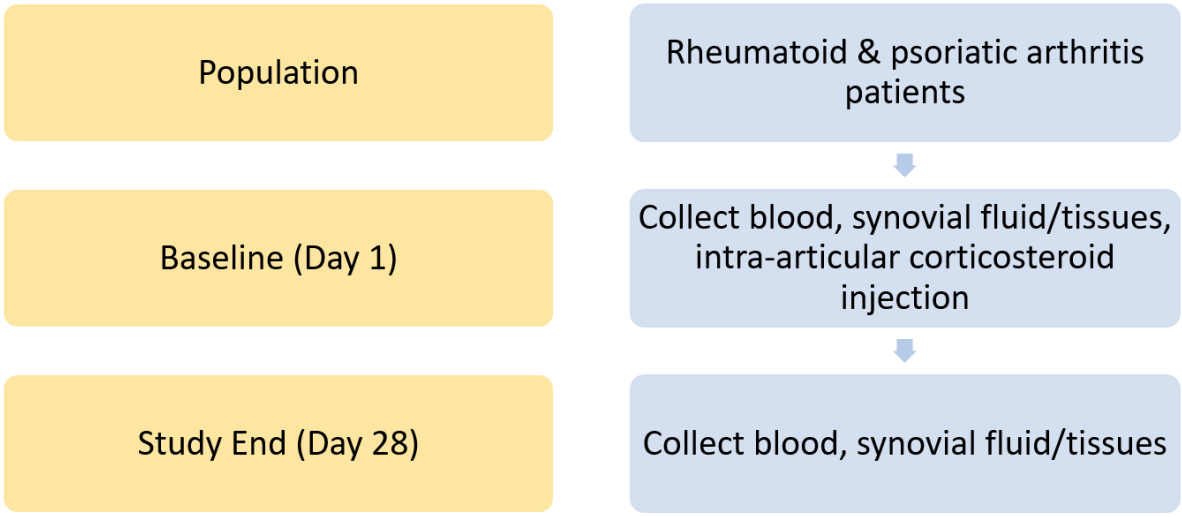

Figure 24 Clinical study flow chart

3.2.2 Patient recruitment

Adult patients with RA or PsA who require intra-articular corticosteroid injection at Nuffield Orthopaedic Centre were invited for eligibility screening. I assessed patients' eligibility by review of their medical notes. Potentially eligible subjects were provided with an invitation letter and Participant Information Sheet prior to attending clinic. The inclusion and exclusion criteria are shown in Table 5.

Table 5 Eligibility criteria for intra-articular corticosteroid injection study

Inclusion criteria
Participant is willing and able to give informed consent for participation in the study.
Male or Female, aged 18 years or above.
Fulfil ACR/EULAR 2010 Rheumatoid Arthritis Classification Criteria or fulfil Classification Criteria for Psoriatic Arthritis 2006 (CASPAR).
Participant has been selected for intra-articular corticosteroid injection as part of their routine clinical care.
Selected joint for biopsy must be minimum Grade 2 synovial thickening for large joint (knee)
Exclusion criteria
Current enrolment in any other clinical study involving an investigational study treatment.
Intramuscular, intravenous or intra-articular administration of corticosteroid within 4 weeks prior to baseline visit.
Oral corticosteroid > 10 mg/day prednisolone or equivalent within 4 weeks prior to baseline visit.
Oral corticosteroid dose not stable for at least 4 weeks prior to baseline visit.
Oral non-steroidal anti-inflammatory drugs (including aspirin > 75 mg/ day and selective-cyclooxygenase inhibitors) dose not stable for at least 4 weeks prior to baseline visit.
Disease modifying anti-rheumatic drugs (DMARDs) dose not stable for at least 4 weeks prior to baseline visit.
History of septic arthritis.
Participants on warfarin, heparin, low molecular weight heparin, direct oral anticoagulants. Oral anti-platelet agents are permitted.
History of haemophilia.

3.2.3 Informed consent

The participant signed the approved version of the Informed Consent form before any study specific procedures were performed. Written and verbal versions of the Participant Information and Informed Consent were presented to the participants detailing no less than: the exact nature of the study; what it involved for the participant; the implications and constraints of the protocol; the known side effects and any risks involved in taking part.

It was clearly stated that the participant is free to withdraw from the study at any time for any reason without prejudice to future care, without affecting their legal rights, and with no obligation to give the reason for withdrawal.

The participant was allowed as much time as wished to consider the information, and the opportunity to question the Investigator, their GP or other independent parties to decide whether they would like to participate in the study. Written Informed Consent was obtained by means of participant-dated signature and dated signature of the person who presented and obtained the Informed Consent.

3.2.4 Screening and eligibility assessment

After informed consent was given, all screening assessments were completed within 42 days prior to baseline. Each participant must satisfy all the approved inclusion and exclusion criteria of the protocol. Re-screening was permitted.

3.2.5 Study procedures

Participants received intra-articular methylprednisolone 80 mg injection into the knee as part of their routine clinical care. The selection of treatment was not affected by study participation.

Patient reported outcomes (PROs):

All PROs were collected before any laboratory assessments and other procedures or consultations to avoid influencing the participant's perception of their disease. The following PROs were completed:

Patient's Assessment of Arthritis Pain. Participants assessed the severity of their arthritis pain over the past week, using a 100 unit visual analogue scale (VAS), with anchors "0" (no pain) and "100" (most severe pain).

Patient's Global Assessment of Arthritis. Participants completed a global assessment of disease activity using the patient global assessment (PtGA) item, a VAS with anchors "0" (very well) to "100" (very poor).

Joint Assessment:

An evaluation of all 68 joints for tenderness and 66 joints for swelling was performed (Figure 25). Joint swelling and joint tenderness were classified as either present or absent. Replaced or fused joints were considered non-evaluable and were not included in joint evaluations.

	Swollen joints	Tender joints
Temporomandibular joint	_____(0-2)	_____ (0-2)
Sternoclavicular joints	_____ (0-2)	_____ (0-2)
Acromioclavicular joints	_____ (0-2)	_____ (0-2)
Glenohumeral(s)	_____ (0-2)	_____ (0-2)
Elbow(s)	_____ (0-2)	_____ (0-2)
Wrist(s)	_____ (0-2)	_____ (0-2)
Metacarpal phalangeal joints	_____ (0-10)	_____ (0-10)
Finger Proximal interphalangeal joints	_____ (0-10)	_____ (0-10)
Finger Distal interphalangeal joints	_____ (0-8)	_____ (0-8)
Hip(s)	NA	_____ (0-2)
Knee(s)	_____ (0-2)	_____ (0-2)
Ankle(s)	_____ (0-2)	_____ (0-2)
Tarsus/Midfoot(feet)	_____ (0-2)	_____ (0-2)
Metatarsal phalangeal joints	_____ (0-10)	_____ (0-10)
Toe PIP(s)	_____ (0-10)	_____ (0-10)
Total joint counts	_____ (0-66)	_____ (0-68)

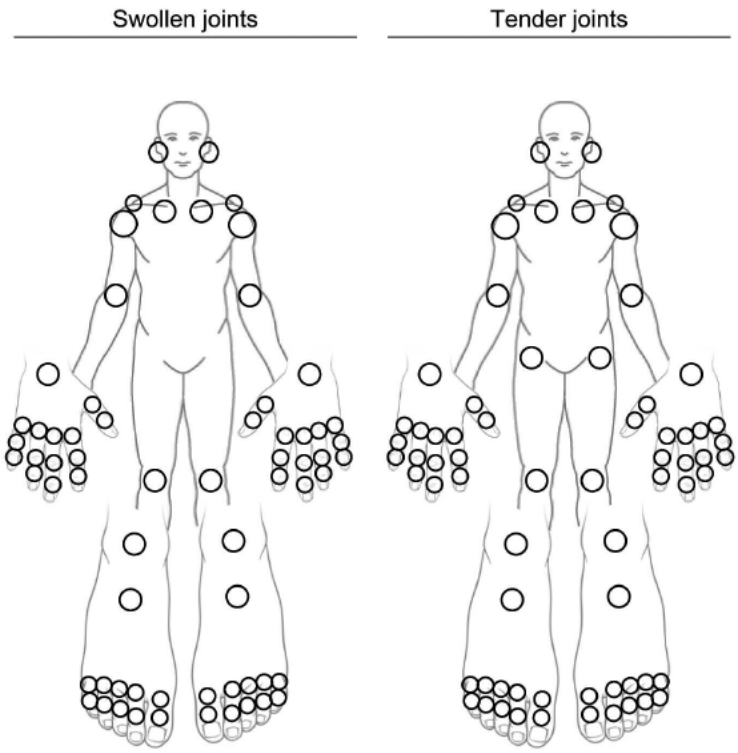

Figure 25 Joint assessment

Blood samples:

Blood samples for research were collected from all participants at Day 1 and Day 28.

Rheumatoid Arthritis Disease Activity Score:

DAS28 assessment is a derived measurement with differential weighting given to each component. The components of the DAS 28 arthritis assessment include:

Tender/Painful Joint Count (28).

Swollen Joint Count (28).

High sensitivity C-reactive protein (CRP)

Patient's Global Assessment of arthritis

Psoriatic Arthritis Disease Activity Score:

DAPSA is a validated tool for psoriatic arthritis assessment. The components of DAPSA include:

Tender/Painful Joint Count (68).

Swollen Joint Count (66).

High sensitivity CRP

Patient's Assessment of Arthritis Pain

Patient's Global Assessment of arthritis

Musculoskeletal Ultrasound:

Musculoskeletal ultrasound was necessary to assess whether there was sufficient synovial fluid and tissue for sampling. Ultrasound is widely used in the routine assessment of disease. Ultrasound of the knee joint took no more than 15 min to complete and assess eligibility for biopsy.

Ultrasound guided synovial tissue needle biopsy:

I attended Queen Mary University of London to train in ultrasound guided synovial tissue needle biopsy. At Oxford University Hospitals NHS Foundation Trust, I performed ultrasound guided synovial tissue needle biopsy under direct supervision of a competent trainer from Queen Mary University of London. My tissue biopsy was confirmed to be synovial tissue as quality control by an accredited NHS histopathology department at The Royal London Hospital. I attended the EULAR course on ultrasound guided synovial biopsy. Prior to this DPhil, I performed 15 ultrasound guided synovial tissue needle biopsies at Oxford University Hospitals NHS Foundation Trust. An example of an ultrasound guided knee synovial tissue needle biopsy I performed is shown in Figure 26.

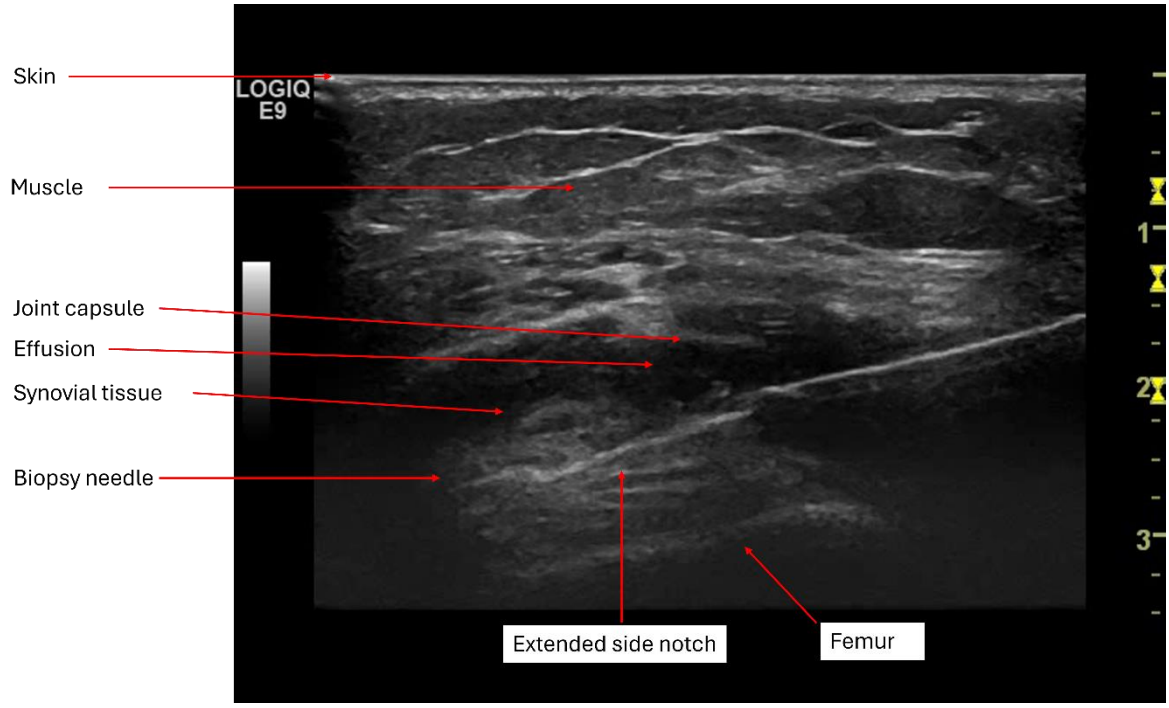

Figure 26 Ultrasound image of knee synovial tissue needle biopsy in suprapatellar transverse view

Synovial fluid and 20 small synovial tissue samples were collected under ultrasound guidance to investigate biological effects of the study interventions (13. Appendix C: Ultrasound guided synovial tissue needle biopsy). This procedure was conducted under local anaesthesia. Each biopsy procedure took approximately 1 h to complete.

3.2.6 Sample size determination

This was a hypothesis driven study of the physiological effects of intra-articular methylprednisolone injection. The primary outcome of the effects on synovial fluid oxygen level determined the sample size needed. The primary outcome was reported at both time points and analysed using paired t-test and reported as mean difference between baseline and Day 28, together with a 95% confidence interval.

The mean difference between baseline and Day 28 in the primary outcome was postulated to be 20 mmHg based on a study which showed that successful TNFi treatment increased synovial pO_2 levels from 11 mmHg at baseline to 31 mmHg at 3 months (149). The follow up timepoint in my study is 28 days but it is unknown what is the effect of intra-articular methylprednisolone injection on synovial fluid oxygen tension at 28 days so I postulated this to be 20 based on the study by Biniecka *et al*. (149).

To estimate sample size, the standard difference between means was postulated to be 19.29 based on study which showed that standard deviation in synovial fluid oxygen measurement is 19.29 from a sample of 85 patients with RA (Lund-Olesen *et al*. 1970). Using sample size calculator http://www.biomath.info/power/prt.htm, for a paired t-test with alpha value (probability of type I error) of 0.05, power value (1–β, where β is the risk of a type II error) of 0.8, mean difference of 20, standard deviation of the mean difference

as 19.29, the number of subjects needed was 10. These were replaced if participants were lost to follow up.

3.2.7 Safety reporting

Intra-articular corticosteroid injection is an established practice in clinical care. Consistent with good clinical practice, participants were monitored for any adverse effects that might be due to study interventions or procedures. Safety reporting window started from time of consent until the participant completed the study.

A serious adverse event (SAE) is any untoward medical occurrence that:

- Results in death
- Is life-threatening
- Requires inpatient hospitalisation or prolongation of existing hospitalisation
- Results in persistent or significant disability/incapacity
- Consists of a congenital anomaly or birth defect.

Other 'important medical events' may also be considered a serious adverse event when, based upon appropriate medical judgement, the event may jeopardise the participant and may require medical or surgical intervention to prevent one of the outcomes listed above.

A SAE occurring to a participant would be reported to the REC that gave a favourable opinion of the study where in the opinion of the Chief Investigator the event was 'related' (resulted from administration of any of the research procedures) and 'unexpected' in relation to those procedures. Reports of related and unexpected SAEs would be submitted within 15 working days of the Chief Investigator becoming aware of the event.

3.2.8 Early Discontinuation/Withdrawal of Participants

During the study, a participant may choose to withdraw early from the study at any time. This may happen for several reasons, including but not limited to inability to comply with study procedures or participant decision. Participants may also withdraw their consent, meaning that they wish to withdraw from the study completely. Data and samples obtained up until the point of withdrawal will be retained for use in the study analysis. No further data or samples would be collected after withdrawal.

In addition, the Investigator may discontinue a participant from the study if the Investigator considers it necessary for any reason including, but not limited to:

- Pregnancy
- Ineligibility (either arising during the study or retrospectively having been overlooked at screening)
- Significant protocol deviation
- Significant non-compliance with treatment regimen or study requirements
- Clinical decision

Participants that have withdrawn from study would be seen by the clinical rheumatology care team without further research follow up. Withdrawn participants would be replaced.

3.2.9 Data management

Data Storage and Confidentiality

Source documents were where data were first recorded, and from which participants' Case Report Form (CRF) data were obtained. These included, but were not limited to, hospital

records from which medical history and previous and concurrent medication may be summarised into the CRF. Entries in CRF were considered as source data. On all study-specific documents and database, other than the signed consent, the participants were referred to by the study participant number, not by name.

The study complied with the General Data Protection Regulation and Data Protection Act 2018, which require data to be de-identified as soon as it is practical to do so. All documents were stored securely in a locked cabinet and all study data were entered in study database stored on password-firewall protected servers maintained by the University of Oxford. Only the study staff and authorised personnel could access study documents and database.

3.2.10 Risk assessment

A risk assessment and mitigation strategy for the research protocol was in place (not shown).

3.2.11 Ethical and regulatory considerations

As the Principal Investigator and Chief Investigator, I conducted this study in accordance with the principles of the Declaration of Helsinki and Good Clinical Practice.

Approvals

As the Principal Investigator and Chief Investigator, I obtained written approvals from the Sponsor (IRAS project ID 288760), North of Scotland Research Ethics Committee (REC reference 21/NS/0002), HRA, and the host institution OUH.

3.2.12 Sample processing

Blood:

Blood RNA processing tubes were stored at -80 ºC. Blood in EDTA tubes were spun at room temperature at a speed of 1,500 *g* for 10 min in centrifuge. The upper supernatants were removed with a sterile pipette and then centrifuged at 2,000 *g* for 15 min at 4 ºC to remove all remaining cells. The plasma supernatants were aliquoted in 1.5 mL cryovials and stored at -80 ºC.

Synovial fluid:

The volume of synovial fluid aspirated was recorded. 1 mL of synovial fluid was tested using a i-STAT CG4+ cartridge (Abbott, code 03P85-51) at bedside immediately after arthrocentesis. The i-STAT system measures pO_2 amperometrically. The oxygen sensor was like a conventional Clark electrode. The hub of the syringe was directed into the sample well of the i-STAT CG4 cartridge to slowly dispense synovial fluid into the sample well until it reached the fill mark indicated on the cartridge. The snap closure of the cartridge was folded over the sample well. The cartridge was processed using an i-STAT1 analyser (Abbott, code 04P75-03) per manufacturer's instructions.

Remaining synovial fluid was cooled in ice, spun at 4 ºC at a speed of 2,000 *g* for 10 min in centrifuge. Synovial fluid supernatants were aliquoted (200 µL) in 1.5 mL cryovials and stored at -80 ºC.

Synovial tissue:

Synovial tissues were snapfrozen in cryovials and embedded in OCT compound by snap freezing.

3.2.13 Meso Scale Discovery (MSD) analysis of proteins in synovial fluid

The MSD methodology uses a sandwich ELISA method to quantify the target protein via light emitted upon electrochemical stimulation initiated at the electrode surface of the MSD microplates. This generates raw signals that are converted to concentrations by the operation application software called MSD Discovery Workbench. Synovial fluids were tested using the MSD U-PLEX Biomarker Group 1 (Human) multiplex assay (Lot# Z00U0202) per manufacturer's instructions.

In brief for U-PLEX assays, U-PLEX linkers are joined to biotinylated capture reagents and allowed to bind to spots on the U-PLEX plate. Synovial fluid is incubated in the plate so synovial fluid proteins are bound to the capture reagents and detected using electrochemiluminescent labelled antibodies (MSD GOLD SULFO-TAG). 200 µL of each biotinylated antibody was added to 300 µL of the unique assigned Linker. Each U-PLEX Linker-coupled antibody solution was mixed by vortexing and incubated at room temperature for 30 min. 200 µL of Stop solution was added, mixed by vortexing, and incubated at room temperature for 30 min. 600 µL of each U-PLEX Linker-coupled antibody solution was combined into a single tube and mixed by vortexing to make the multiplex coating solution. The U-PLEX 96-well plate was coated with 50 µL of the multiplex coating solution. The plate was sealed with an adhesive plate seal and shaken for 1 h at room temperature. The U-PLEX 96-well plate was washed three times with at least 150 µL/well of 1x wash buffer.

25 µL of assay diluent was added to each well along with 25 µL of the prepared calibrator standard or sample. The plate was sealed with an adhesive plate seal and incubated at room temperature with shaking for 1 h. The plate was washed three times with at least 150

µL/well of wash buffer. 50 µL of detection antibody solution was added to each well. The plate was sealed with an adhesive plate seal and incubated at room temperature with shaking for 1 h. The plate was washed three times with at least 150 µL/well of wash buffer. 150 µL of MSD GOLD Read Buffer B was added to each well. The plate was analysed on a MSD Discovery Sector Imager SQ 120 plate reader per manufacturer's instructions.

3.2.14 Blood bulk RNA sequencing

RNA was extracted from blood samples using Tempus™ Blood RNA Tube and Tempus™ Spin RNA Isolation Kit (ThermoFisher Scientific: catalogue number 4342792 and 4380204) following the manufacturer's instructions. RNA concentration was measured using a NanoDrop spectrophotometer and RNA quality assessed using High Sensitivity RNA ScreenTapes (Agilent, Santa Clara, CA, United States) on an Agilent 4200 TapeStation. Libraries were created using a NEBNext Ultra II Directional RNA Library Prep Kit for Illumina (New England Biolabs, Ipswich, MA, USA) and a NextSeq High Output Kit (Illumina, San Diego, CA, USA) as per the manufacturers' instructions. Libraries were quantified for RNA content with High Sensitivity DNA ScreenTapes (Agilent). Libraries with unique identifiers were pooled and run on an Illumina NextSeq 500 using the 75 cycles NextSeq High Output kit (Illumina).

Raw FASTQ files containing reads were generated by the Illumina software CASAVA v1.8. The raw FASTQ files were kindly processed by Alina Kurjan using CGAT-flow readqc and mapping workflows (https://github.com/cgat-developers/cgat-flow) (269). The quality of the reads was kindly processed by Alina Kurjan using FASTQC. Raw reads were kindly aligned by Alina Kurjan to the GRCh38 reference genome using HiSat2

version 2.0.5. All downstream analyses and figures were generated by me unless otherwise specified. Downstream analyses were performed using R version 4.4.1 (R Foundation, Vienna, Austria) and RStudio (Boston, MA, United States). Differential expression analysis was performed with the DESeq2 package (270). The design was set as the treatment status of the participant, pre- or post-treatment with intra-articular methylprednisolone injection, to measure the effect of treatment on blood bulk RNA sequencing. The apeglm method to apply the shrinkage of logarithmic fold change (271). The adjusted P value (padj) and significance of changes in gene expression were determined using DESeq2 by applying the Benjamini-Hochberg correction of 5% false discovery rate (FDR) (270, 272). PCA plots were generated using the package ggplot2, heatmaps were generated using the package pheatmap, and EnhancedVolcano was used to create volcano plots.

3.2.15 Statistical analysis

Statistical analysis for bulk RNA-seq were performed by me using R and RStudio. All other statistical analyses were performed by me using GraphPad Prism version 10.2.3 for Windows, GraphPad Software, Boston, Massachusetts, USA, www.graphpad.com. P values were not corrected for multiple comparisons unless otherwise specified. Statistical analysis with DESeq2 was corrected for multiple testing using the Benjamini and Hochberg method by default (270, 272).

3.3 Results

3.3.1 Clinical study details

The clinical study started on 01/10/2021 and closed on 24/02/2023. Study set-up and patient recruitment were profoundly delayed due to COVID-19. 17 patients were screened for study eligibility (Figure 27). 3 participants were lost to study follow up so these were replaced so that 10 participants completed the study. Out of the participants who completed follow-up, 4 have RA and 6 have PsA. The clinical characteristics of the patients who completed the study were reported (Table 6).

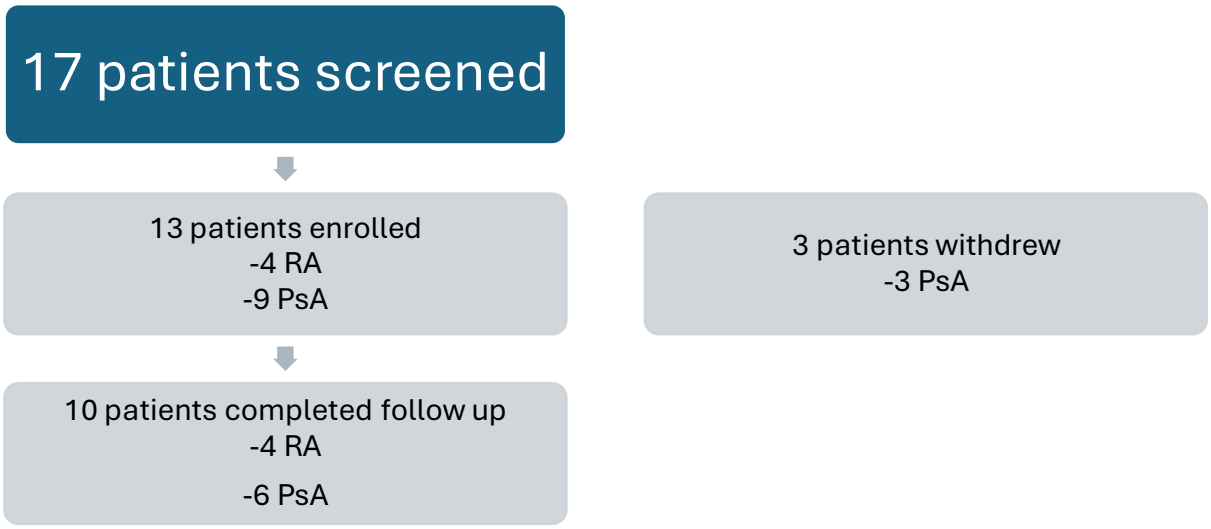

Figure 27. Study recruitment

Table 6 Clinical characteristics of study participants

Clinical data		RA	PsA
Sample size		4	6
Gender		3 men and 7 women	
Age mean (range)		62.5 (48 - 74)	39 (28 - 49)
Disease duration in years (mean ± SD)		13.7 ± 13.7	8.7 ± 5.6
Treatment history		1 participant not on DMARD, 2 participants on csDMARDs and bDMARD naïve, 1 participant on TNFi	2 participants on csDMARDs and bDMARD naïve, 4 participants on TNFi
CRP (mean ± SD)	Baseline	5.15 ± 5.39	8.6 ± 8.40
	Follow up	2.6 ± 1.83	5.43 ± 4.57
SJC66 (mean ± SD)	Baseline	1.25 ± 1.26	2 ± 1.10
	Follow up	0.75 ± 1.5	1.67 ± 0.82
TJC68 (mean ± SD)	Baseline	1.5 ± 0.58	2.33 ± 2.07
	Follow up	2.25 ± 3.86	1.83 ± 1.60
Composite disease activity scores (mean ± SD)	Baseline	3.16 ± 0.48	16.81 ± 4.80
	Follow up	2.53 ± 1.14	11.33 ± 4.79

DAS28 and DAPSA disease activity scores were measured for patients with RA and PsA respectively at baseline and follow-up (Figure 28). After intra-articular methylprednisolone injection, DAPSA was significantly reduced in patients with PsA ($P < 0.05$, mean of differences -5.48, 95% CI -10.15 to -0.82), but DAS28 was unchanged in patients with RA ($P > 0.05$, mean of differences -0.63, 95% CI -2.77 to 1.52).

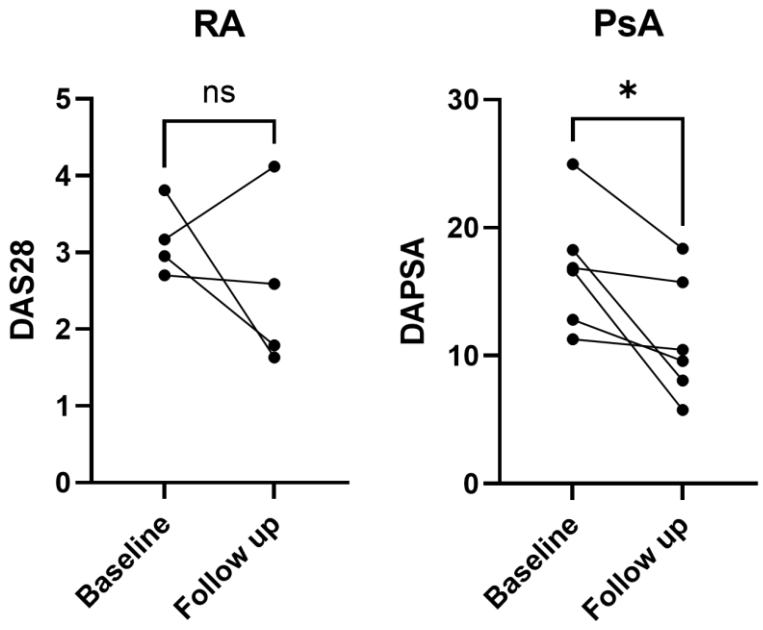

Figure 28 Disease activity of patients with RA (DAS28) and PsA (DAPSA) at baseline and follow-up after intra-articular glucocorticoid injection.

*Baseline and follow-up values were compared using paired parametric t test. ns denotes P > 0.05, * denotes P < 0.05.*

There was no statistically significant difference in the volume of synovial fluid aspirated at baseline and follow up in the RA group (P > 0.05, mean of differences -4.98, 95% CI -25.58 to 15.63) or the PsA group (P > 0.05, mean of differences -27.67, 95% CI -78.87 to 23.53) (Figure 29). A limitation of this study is the small sample size which may have led to underpowering to detect a difference in synovial fluid volume aspirated. Patients with the synovial effusion greater than 50 mL at baseline were patients with PsA (Figure 29).

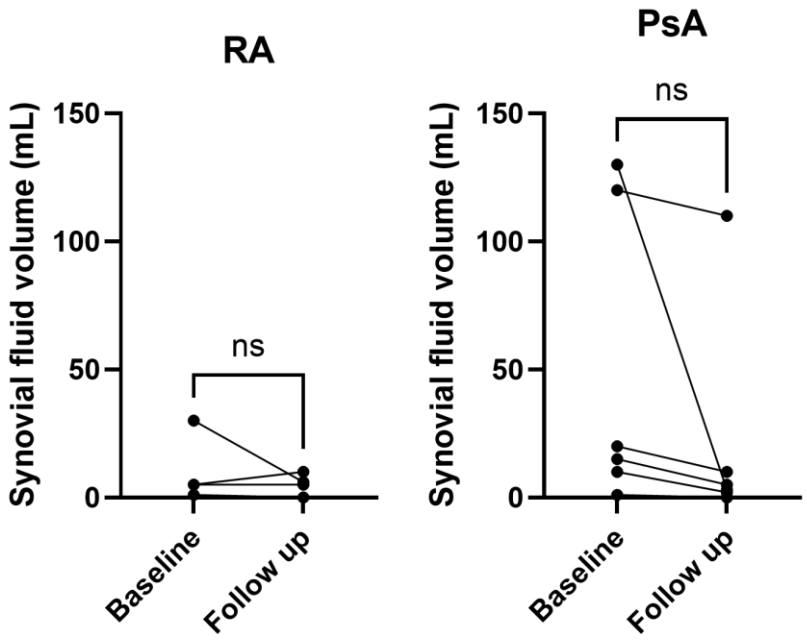

Figure 29 Synovial fluid volume aspirated in patients with RA and PsA at baseline and follow-up after intra-articular glucocorticoid injection

Baseline and follow-up values were compared using paired parametric t test. ns denotes P > 0.05.

3.3.2 Effects of intra-articular methylprednisolone injection on hypoxia in synovial fluid

Synovial fluid was aspirated and tested for pO_2 and lactate using a blood gas analyser. There was no difference in synovial fluid pO_2 after intra-articular methylprednisolone injection in participants with RA and PsA ($P > 0.05$, mean of differences 0.33, 95% CI -2.50 to 3.15) (Figure 30). Subgroup analysis showed no difference in synovial fluid pO_2 before and 4 weeks after intra-articular glucocorticoid injection in either the RA subgroup ($P > 0.05$, mean of differences 0.10, 95% CI -4.43 to 4.63) or PsA subgroup ($P > 0.05$, mean of differences 0.46, 95% CI -4.84 to 5.76) (Figure 31).

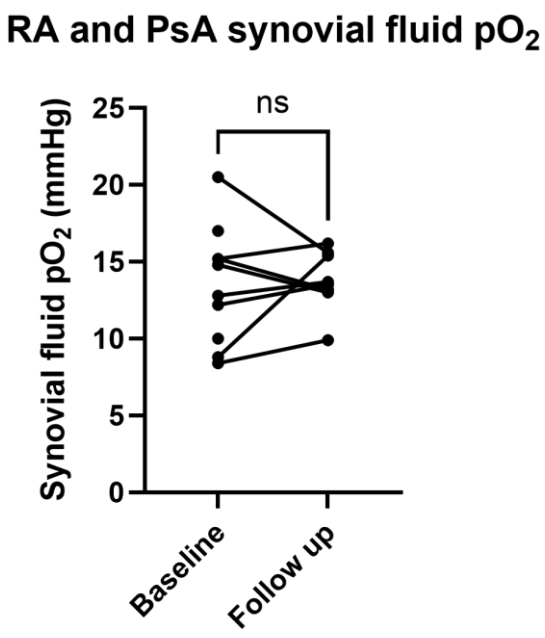

Figure 30 Synovial fluid pO_2 in patients with RA and PsA at baseline and follow-up after intra-articular methylprednisolone injection

Baseline and follow-up values were compared using paired parametric t test. ns denotes P > 0.05.

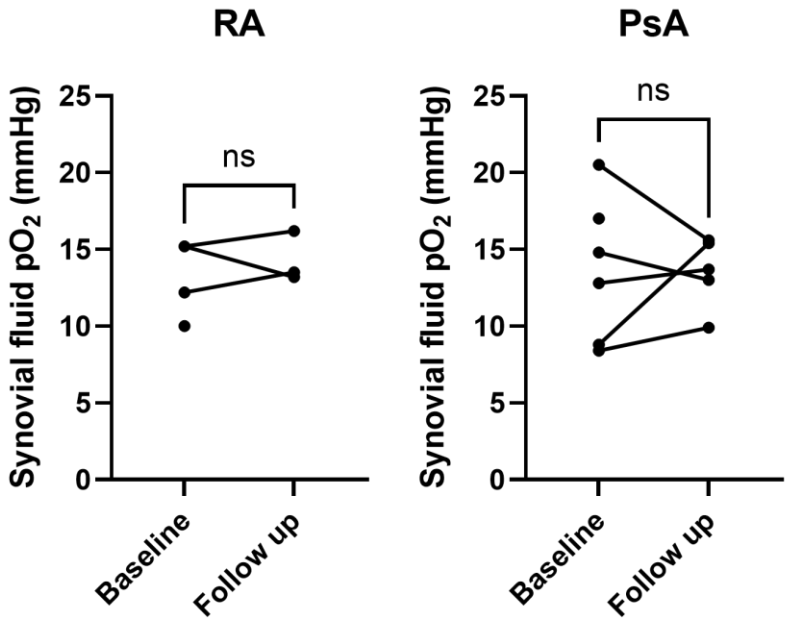

Figure 31. Subgroup analysis of synovial fluid pO_2 in RA subgroup and PsA subgroup at baseline and follow-up after intra-articular methylprednisolone injection

Baseline and follow-up values were compared using paired parametric t test. ns denotes P > 0.05.

There was also no difference in synovial fluid lactate before and 4 weeks after intra-articular glucocorticoid injection in patients with RA and PsA (P > 0.05, mean of differences -0.07, 95% CI -0.69 to 0.55) (Figure 32). Subgroup analysis showed no difference in synovial fluid lactate before and 4 weeks after intra-articular glucocorticoid injection in either the RA (P > 0.05, mean of differences -0.56, 95% CI -2.19 to 1.07) or PsA subgroups (P > 0.05, mean of differences 0.22, 95% CI -0.63 to 1.07) (Figure 33).

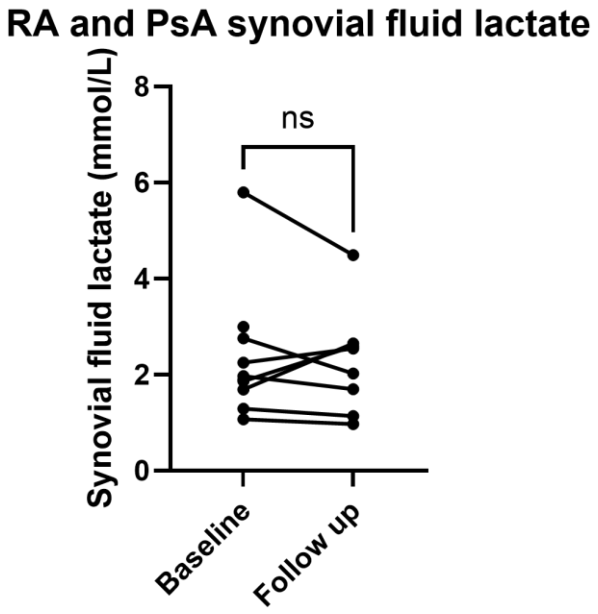

Figure 32 Synovial fluid lactate in patients with RA and PsA at baseline and follow-up after intra-articular glucocorticoid injection.

Baseline and follow-up values were compared using paired parametric t test. ns denotes P > 0.05.

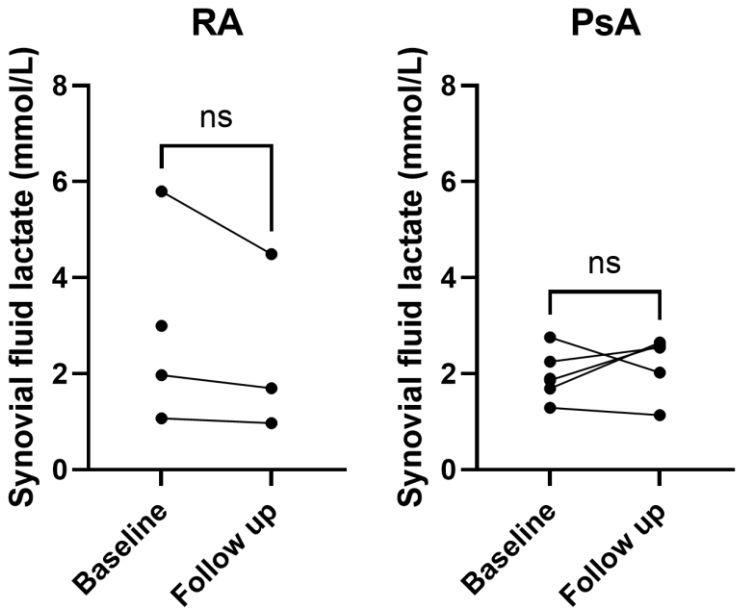

Figure 33 Subgroup analysis of synovial fluid lactate in RA subgroup and PsA subgroup at baseline and follow-up after intra-articular glucocorticoid injection

Baseline and follow-up values were compared using paired parametric t test. ns denotes P > 0.05.

3.3.3 Effects of intra-articular methylprednisolone injection on cytokines in synovial fluid

After intra-articular methylprednisolone injection, synovial fluid IL-6 levels were significantly reduced in patients with inflammatory arthritis ($P < 0.05$, mean of differences -2277, 95% CI -4369 to -185.6) (Figure 34).

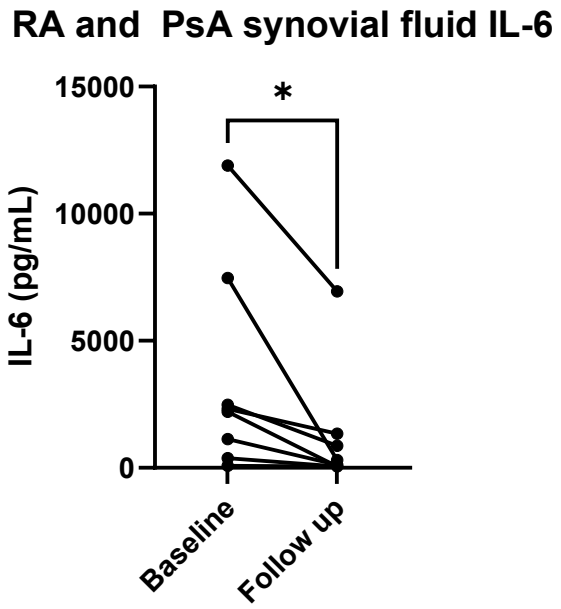

Figure 34 Paired pre- and post-treatment synovial fluid IL-6 levels

*Baseline and follow-up values were compared using paired parametric t test. * denotes P < 0.05.*

In subgroup analysis, synovial fluid IL-6 levels were significantly reduced after intra-articular methylprednisolone injection in the PsA subgroup ($P < 0.05$, mean of differences

-2142, 95% CI -4184 to -100.6) but not in the RA subgroup (P > 0.05, mean of differences -2502, 95% CI -12555 to 7551) (Figure 35).

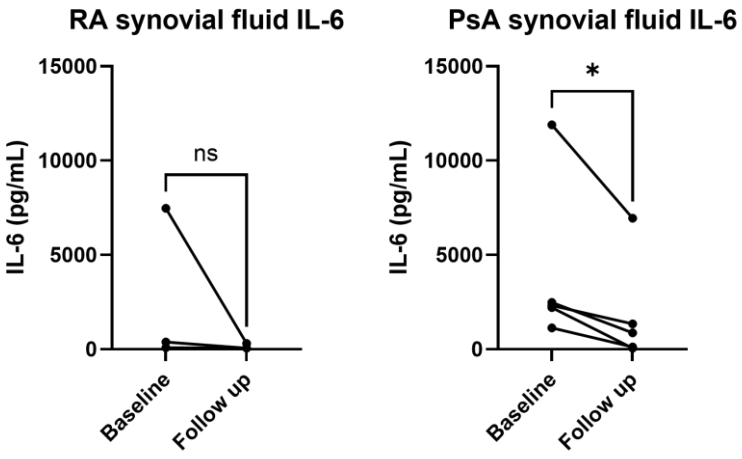

Figure 35 Subgroup analysis of paired pre- and post-treatment synovial fluid IL-6 levels.

*Baseline and follow-up values were compared using paired parametric t test. ns denotes P > 0.05, * denotes P < 0.05.*

After intra-articular methylprednisolone injection, synovial fluid TNF levels were significantly reduced in patients with inflammatory arthritis (P < 0.01, mean of differences -0.49, 95% CI -0.82 to -0.16) (Figure 36).

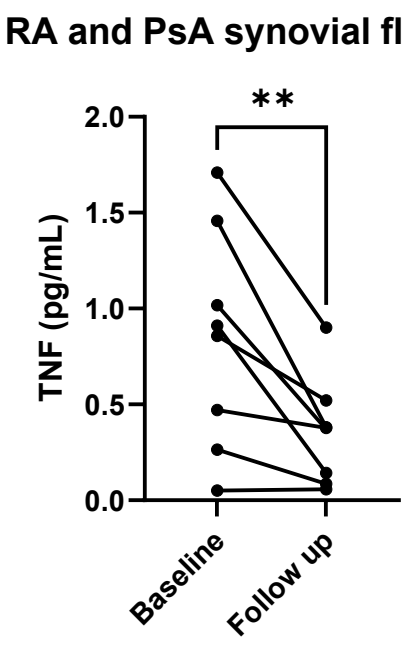

Figure 36 Paired pre- and post-treatment synovial fluid TNF levels

*Baseline and follow-up values were compared using paired parametric t test. ** denotes P < 0.01.*

Subgroup analysis showed after intra-articular methylprednisolone injection, synovial fluid TNF levels were significantly reduced in the PsA subgroup ($P < 0.05$, mean of differences -0.58, 95% CI -1.06 to -0.11) but not the RA subgroup ($P > 0.05$, mean of differences -0.33, 95% CI -1.39 to 0.74) (Figure 37).

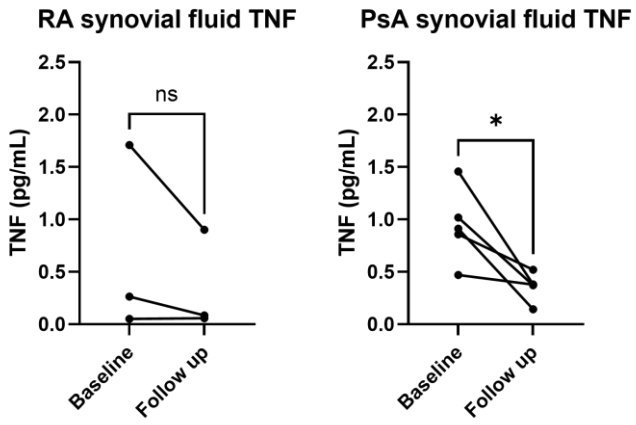

Figure 37 Subgroup analysis of paired pre- and post-treatment synovial fluid TNF levels

*Baseline and follow-up values were compared using paired parametric t test. ns denotes P > 0.05, * denotes P < 0.05.*

There were no differences in synovial fluid levels of IL-12p70 (P > 0.05, mean of differences -0.50, 95% CI -1.11 to 0.11), IL-1β (P > 0.05, mean of differences -0.57, 95% CI -1.54 to 0.40), IL-10 (P > 0.05, mean of differences -1.71, 95% CI -4.20 to 0.79), IL-8 (P > 0.05, mean of differences -36.06, 95% CI -144.5 to 72.44), or IFN-γ (P > 0.05, mean of differences -77.19, 95% CI -170.6 to 16.18) with intra-articular methylprednisolone injection in patients with inflammatory arthritis (P > 0.05) (Figure 38). Subgroup analysis of the RA group showed there were no differences in synovial fluid levels of IL-12p70 (P > 0.05, mean of differences -0.52, 95% CI -2.40 to 1.35), IL-1β (P > 0.05, mean of differences -0.57, 95% CI -1.54 to 0.40), IL-10 (P > 0.05, mean of differences -3.00, 95% CI -15.56 to 9.56), IL-8 (P > 0.05, mean of differences -110.1, 95% CI -538.0 to 317.8), IFN-γ (P > 0.05, mean of differences -93.25, 95% CI -455.9 to 269.4) with intra-articular methylprednisolone injection (Figure 39). Subgroup analysis of the PsA group showed there were no differences in synovial fluid levels of IL-12p70 (P > 0.05, mean of differences -0.49, 95% CI -1.50 to 0.52), IL-1β (P > 0.05, mean of differences -0.24, 95%

CI -0.79 to 0.31), IL-10 (P > 0.05, mean of differences -0.93, 95% CI -2.04 to 0.18), IL-8 (P > 0.05, mean of differences 8.36, 95% CI -103.1 to 119.8), IFN-γ (P > 0.05, mean of differences -67.55, 95% CI -196.9 to 61.85) with intra-articular methylprednisolone injection (Figure 39). IL-2, IL-4, and IL-13 were undetectable in most synovial fluid samples (data not shown).

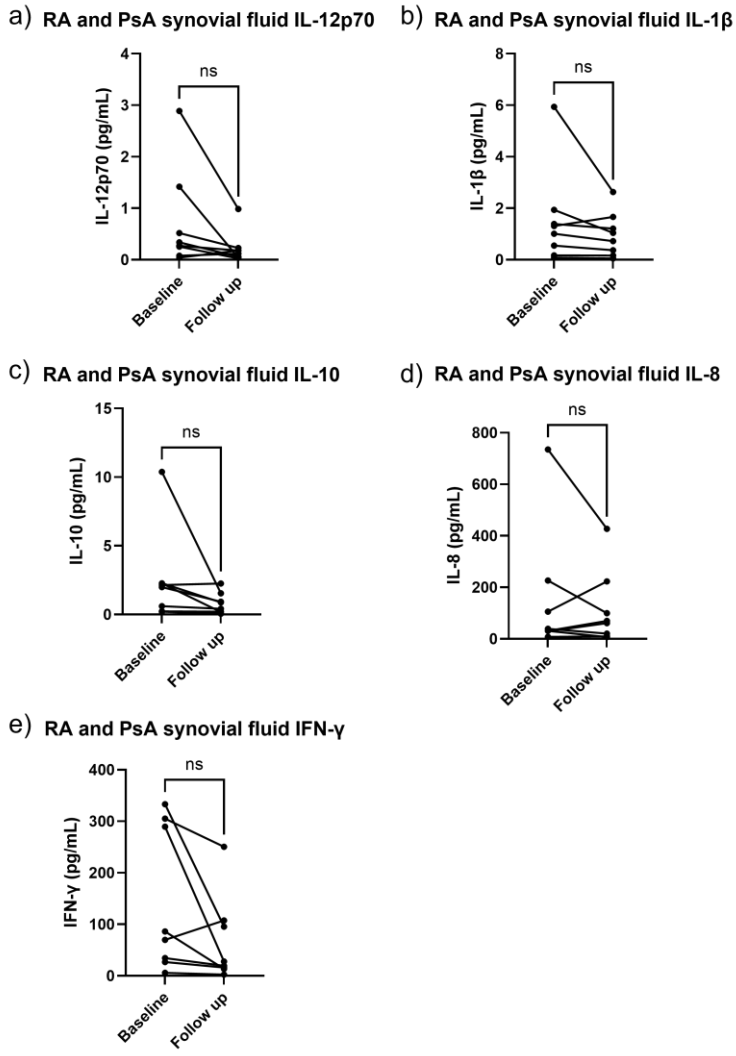

Figure 38 Paired pre- and post-treatment synovial fluid a) IL-12p70, b) IL-1β, c) IL-10, d) IL-8, and e) IFN-γ levels

Baseline and follow-up values were compared using paired parametric t test. ns denotes P > 0.05

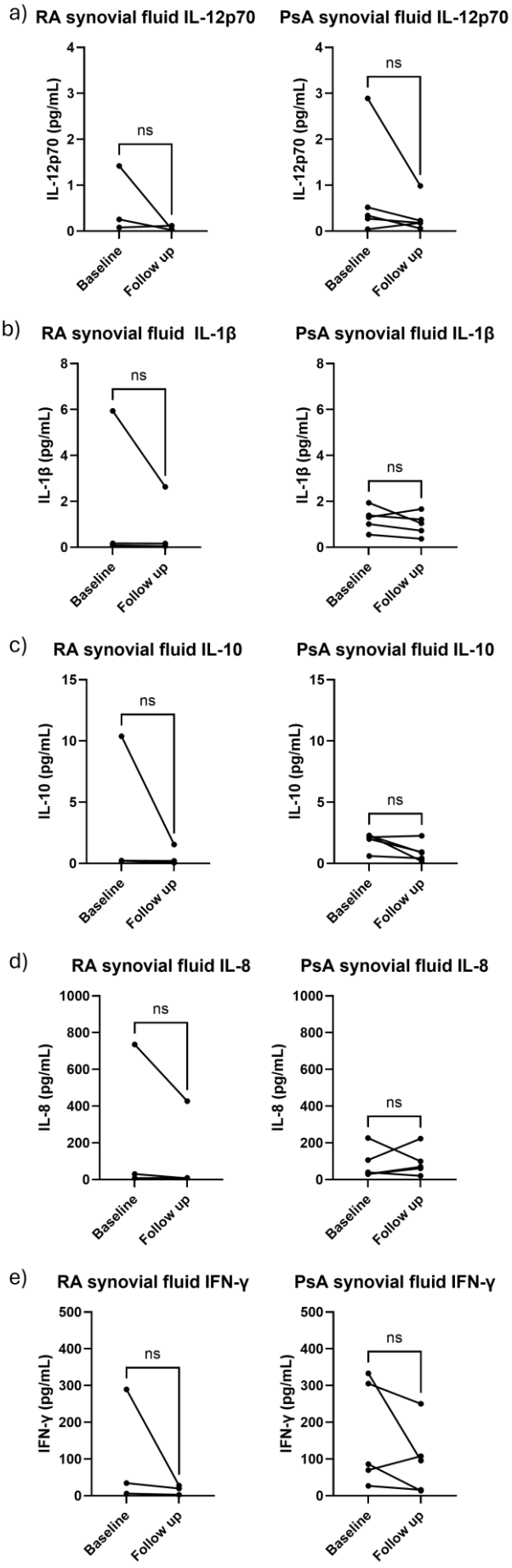
a)
RA synovial fluid IL-12p70
PsA synovial fluid IL-12p70
IL-12p70 (pg/mL)
ns
Baseline
Follow up
b)
RA synovial fluid IL-1β
PsA synovial fluid IL-1β
IL-1β (pg/mL)
c)
RA synovial fluid IL-10
PsA synovial fluid IL-10
IL-10 (pg/mL)
d)
RA synovial fluid IL-8
PsA synovial fluid IL-8
IL-8 (pg/mL)
e)
RA synovial fluid IFN-γ
PsA synovial fluid IFN-γ
IFN-γ (pg/mL)

Figure 39 Subgroup analysis of paired pre- and post-treatment synovial fluid a) IL-12p70, b) IL-1β, c) IL-10, d) IL-8, and e) IFN-γ levels

Baseline and follow-up values were compared using paired parametric t test. ns denotes P > 0.05

3.3.4 Effects of intra-articular methylprednisolone injection on blood bulk RNA sequencing

Where available, blood from each visit was analysed for bulk RNA sequencing. Blood samples were categorised as either pre-treatment or post-treatment with intra-articular methylprednisolone injection. To undertake principal component analysis, the object was transformed using rlog function and the plotPCA function was applied with the default setting of using the top 500 most variable genes for analysis (270). Principal component analysis showed no overall effects of intra-articular methylprednisolone injection on blood bulk RNA sequencing at 4 weeks follow up (Figure 40).

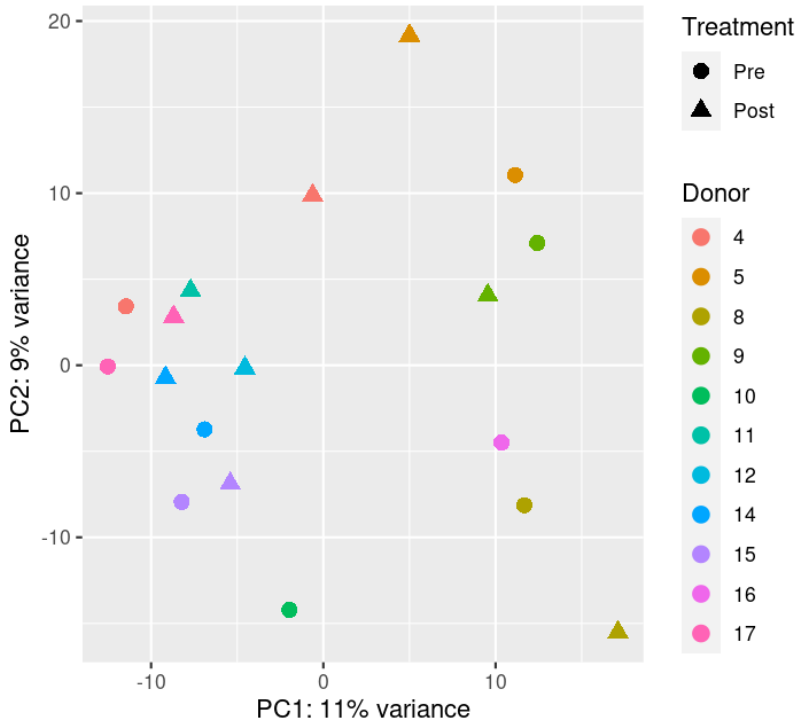

Figure 40 Principal components analysis (PCA) of blood bulk RNA sequencing

A PCA is an unsupervised analysis to look for sources of variation from factors such as treatment groups or donors.

Differential gene expression analysis analysed perturbation effect of intra-articular methylprednisolone injection on blood bulk RNA sequencing, with the pre-treatment sample as the control and the adjusted p value cutoff set to 0.05. The log fold change was shrunk using the apeglm method (271). There were two differentially expressed genes in the blood by bulk transcriptomic analysis at 4 weeks after intra-articular methylprednisolone injection (log2foldchange > 1, adjusted P value < 0.05) (Figure 41). Self-ligand receptor of the signalling lymphocytic activation molecule family 6 (*SLAMF6*) was upregulated and solute carrier family 35 member B3 (*SLC35B3*) was downregulated in bulk transcriptomic analysis of blood after intra-articular methylprednisolone injection (log2foldchange > 1, adjusted P value < 0.05) (Figure 41).

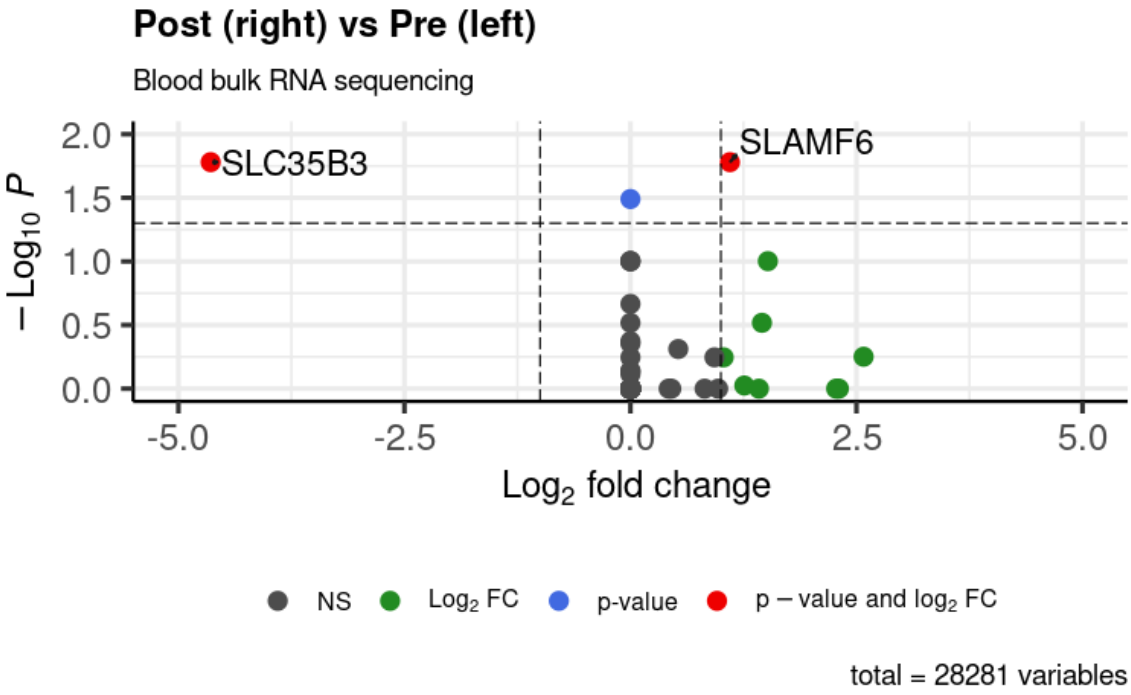

Figure 41 Volcano plot of differential gene expression in blood bulk RNA sequencing

Volcano plots are a type of scatterplot that shows statistical significance versus magnitude of change, enabling quick visual identification of genes with large fold changes that are also statistically significant. P values were corrected for multiple testing using the Benjamini and Hochberg method in DESeq2 by default (270, 272)

3.4 Discussion

3.4.1 Intra-articular methylprednisolone injection effects on disease activity scores

After intra-articular methylprednisolone injection, DAPSA was statistically significantly reduced in patients with PsA but the DAS28 reduction in patients with RA was not statistically significant (Table 6, Figure 28). Given that intra-articular methylprednisolone

injection is known to be efficacious at reducing joint swelling, joint tenderness and pain, this treatment would be expected to reduce disease activity scores in both patients with RA and PsA. In particular, Salem *et al*. showed that intra-articular methylprednisolone injections have been shown to reduce DAS28 at 4 weeks follow up in patients with RA (n = 25) (273). This surprising discrepancy between the efficacy of intra-articular methylprednisolone in previous studies compared to this study for patients with RA may be due to the limitation of small sample size of the RA group in this study (RA: n = 4). However, this study was not designed to assess efficacy of intra-articular methylprednisolone injection. Instead, this study was designed to assess effects on synovial fluid oxygen.

3.4.2 Intra-articular methylprednisolone injection did not change synovial fluid oxygen

Biniecka *et al*. showed that successful TNFi treatment increased synovial tissue pO_2 levels (149). By contrast, I observed no consistent difference in synovial fluid oxygen concentration 4 weeks after intra-articular methylprednisolone injection. This negative finding may be due to my study being underpowered. The sample size calculation in my study was based on the change in synovial tissue pO_2 with successful TNFi treatment whereas the intervention used in my study was an intra-articular methylprednisolone injection. Given that there was no change in disease activity with treatment in the RA group of my study, the sample size calculation based on the study by Biniecka *et al*. may not be applicable to my study population. After all, patients who did not respond to TNFi also exhibited no change in synovial tissue pO_2 (149).

The discrepancy between my results and that of Biniecka *et al*. may also be because of differences in oxygen measurement methods (149). Biniecka *et al*. measured synovial tissue pO_2 by inserting an oxygen probe *in vivo* whereas I measured the pO_2 of synovial fluid *ex vivo*. Synovial tissue pO_2 may vary widely with synovial fluid pO_2 depending on the position of the oxygen probe, such as its proximity to vasculature. Of note, my synovial fluid pO_2 readings were at similar levels to that seen with their synovial tissue pO_2, albeit without change before and after treatment.

The lack of consistent change in synovial fluid pO_2 with intra-articular methylprednisolone injection in my study conflicted with a previous study which showed increase in synovial fluid pO_2 levels albeit unchanged synovial oxygen uptake *in vivo* after intra-articular corticosteroid injection (142). *In vivo* oxygen consumption and lactate production were based on the rate of fall of synovial fluid pO_2 and rise in lactate concentration in an intra-articular saline pool after interruption of the circulation to the joint with an arterial tourniquet (142). In a previous study, of 8 patients who underwent intra-articular corticosteroid injection with follow-up at 7-10 days, there was increased synovial fluid pO_2, decreased lactate production, and reduced circulatory flow as assessed by ^{133}Xe washout rate but no difference in synovial oxygen uptake (142). The difference in the change in synovial fluid pO_2 after intra-articular glucocorticoid injection between these studies may be due to the follow-up of 7-10 days in the study by Goetzl *et al*. and follow-up of 4 weeks in my study (142). Due to the short half-life of methylprednisolone in synovial fluid of approximately 4 days, the pharmacodynamic effect of intra-articular methylprednisolone on synovial fluid pO_2 at 7-10 days may have resolved at 4 weeks follow up (249, 250).

Imaging at the level of the joint may provide better characterisation of synovial tissue oxygenation than synovial fluid pO_2. Optoacoustic imaging, also known as photoacoustic imaging, utilises the optoacoustic effect phenomenon to allow non-invasive evaluation of tissue molecules *in vivo* (274). Ultrashort light pulses are absorbed by tissue molecules resulting in transient rise in local temperature. The photo-absorbing molecules undergo thermoelastic expansion which generate acoustic waves detectable by ultrasound. Multispectral optoacoustic tomography (MSOT) incorporates ultrasound with photoacoustic imaging. MSOT illuminates tissues at multiple wavelengths to quantify chromophores such as deoxyhaemoglobin, oxyhaemoglobin, lipids and collagen. MSOT has demonstrated impaired oxygen saturation in inflamed synovial structures in PsA, compared with healthy individuals, by demonstrating higher signal intensities of oxyhaemoglobin and deoxyhaemoglobin (275). MSOT has also shown that enthesitis was associated with increased total haemoglobin levels, oxygen saturation and collagen content, reflecting increased vascularisation, whereas synovitis was associated with increased haemoglobin levels but reduced oxygen saturation and collagen content (276). Future clinical studies of synovial tissue hypoxia using MSOT may allow more accurate characterisation of response to therapies such as intra-articular methylprednisolone injection or orally administered oxygen nanobubbles.

Another imaging modality that may be useful to characterise microcirculatory changes is fluorescence optical imaging (274). This technique uses near-infrared light to measure accumulation of a fluorescent dye administered intravenously. This dye accumulates in inflamed tissues due to impaired microcirculation and angiogenic activity. However, fluorescence optical imaging is limited to microcirculation imaging in the joints of hands and wrists, and therefore unsuitable for studying knee synovitis as in this study (277).

Doppler ultrasound can visualise blood flow but imaging of blood flow in small vessels is limited due to low resolution and movement artefact. Contrast-enhanced ultrasonography involves intravenous administration of microbubble contrast agents, lipid shells filled with inert gas agents (278). This technique successfully enhanced vascularisation signal of synovitis in RA (279). Future studies using contrast-enhanced ultrasonography may provide insight into whether intra-articular methylprednisolone injections affect blood flow and hypoxia in inflammatory arthritis.

Many factors can affect the synovial fluid pO_2 readings leading to discrepancy with synovial tissue pO_2. The i-STAT1 system is intended for use with blood but has also been used for other bodily fluids. Exposure of synovial fluid to air would cause an increase in pO_2 when values are below 150 mmHg (approximate pO_2 of room air). However, the exposure of synovial fluid to air was minimised by measuring the synovial fluid pO_2 immediately after aspiration. This was facilitated by having the i-STAT1 system at bedside at the time of ultrasound guided synovial tissue biopsy, instead of having to transport samples to the Intensive Care Unit where blood gas analysers are conventionally located. The presence of haemoglobin in synovial fluid samples may confound the synovial fluid pO_2 reading but haemarthrosis was not noted in any of the synovial fluid samples. pO_2 results may be falsely elevated in cold samples but the synovial fluid samples were not chilled before testing. pO_2 results may be falsely decreased if the cartridge was cold but the cartridges were at room temperature when used. Although I found that intra-articular methylprednisolone injection had no impact on synovial fluid pO_2, a pharmacodynamic effect was noted in synovial fluid inflammatory cytokines.

3.4.3 Intra-articular methylprednisolone injection reduced synovial fluid levels of IL-6 and TNF

Although my findings demonstrated no effects of intra-articular methylprednisolone injection on synovial fluid pO_2 at 4 weeks follow up, there may nonetheless be therapeutic effects on downstream hypoxic pathways. Hypoxia related mitochondrial dysfunction is known to be a feature of inflammatory arthritis and methylprednisolone has been shown to affect hypoxia induced mitochondrial dysfunction (141). For example, in isolated perfused rat livers, methylprednisolone protected against mitochondrial membrane depolarisation under hypoxic conditions (280). However, there is a knowledge gap relating to the impact of methylprednisolone on downstream hypoxic pathways in synovial tissues. Before studying the synovial tissues, I investigated the synovial fluid cytokine profiles to confirm that the intra-articular methylprednisolone injection effects persist at four weeks follow-up.

The U-PLEX pro-inflammatory panel kit from MSD offers convenient analysis of biomarkers associated with inflammatory response and immune system regulation. IL-6 and TNF levels are known to be elevated in synovial fluids from patients with inflammatory arthritis (281-290). Compared to OA, synovial fluid IL-6 and TNF levels were increased in RA and PsA (281, 288-291). The expression levels of TNF and IL-6 in synovial tissues were as high in PsA as in RA (292). Moreover, synovial fluid IL-6 and TNF levels have been shown to correlate with disease activity in patients with RA and PsA (286, 293-295). My findings showed synovial fluid IL-6 and TNF levels were significantly reduced with intra-articular methylprednisolone injection (Figure 34, Figure 36). These findings are consistent with previous studies where intra-articular glucocorticoid injections reduced synovial protein expression of TNF as well as serum levels of IL-6 and TNF (296, 297). In a study of 31 patients treated with intra-articular glucocorticoid, af Klint *et al*.

found reduced synovial protein expression of TNF, IL-1β, VEGF and ICAM-1 (296). Further subgroup analysis showed that IL-6 and TNF levels were reduced in the PsA subgroup but not the RA subgroup (Figure 35, Figure 37). This may reflect the limitation of the very small sample size, as well as differences in joint inflammation in participants at baseline between the two disease groups.

IL-12 is a heterodimeric cytokine encoded by genes IL12A (p35) and IL12B (p40). The active heterodimer (p70) and homodimer of p40 are formed after protein synthesis. Some studies showed direct correlation between RA disease activity and synovial fluid IL-12 levels, whereas others did not (298, 299). The effects of intra-articular glucocorticoid injection on synovial fluid IL-12p70 levels have not been assessed previously. My results showed no statistically significant difference in synovial fluid IL-12p70 with intra-articular methylprednisolone injection in patients with RA and PsA (Figure 38, Figure 39). A limitation is that the small sample size may not be sufficiently powered to detect perturbation in synovial fluid IL-12p70 levels. Perhaps this finding was not too surprising as *IL12A* and *IL12B* genes were previously shown in GCgx to be unaffected by methylprednisolone *in vitro* (300). GCgx is a tool shared by the National Institute of Arthritis and Musculoskeletal and Skin Diseases which allows easy review of how methylprednisolone affects gene expression in different cell types *in vitro* (300).

The presence of neutrophils in the synovial joints of patients with inflammatory arthritis was thought to be due to the chemotactic factors such as IL-8. Synovial fluid IL-8 was previously found to be abundant in patients with inflammatory arthritis such as RA (301). However, another study found only 32% (27/83) of synovial fluids from patients with RA had detectable levels of IL-8 (302). My findings showed no statistically significant change

in synovial fluid IL-8 with intra-articular methylprednisolone injection in patients with RA or PsA (Figure 38, Figure 39). *CXCL8* which encodes IL-8 was known to be downregulated in response to methylprednisolone (300). It may be that no difference in synovial fluid IL-8 levels was seen due to the late follow-up timepoint (4 weeks) in the clinical study, whereas the *in vitro* study looked at early glucocorticoid effects within 6 h (300). The disparity may also be due to differences in glucocorticoid effects on IL-8 at protein and RNA levels. In a rabbit model of post-traumatic osteoarthritis, intra-articular glucocorticoid injection reduced synovial tissue IL-8 mRNA expression but not IL-8 protein levels (303). The small sample size in my study also limits evaluation of therapeutic effects on synovial fluid IL-8.

My study showed IL-4 and IL-13 levels were mostly undetectable in synovial fluids which contradicted with some previous studies showing elevation in patients with RA and PsA. Synovial fluid IL-4 levels were previously found to be elevated in patients with RA and seronegative spondyloarthropathy compared to OA (304). IL-13 was also found to be present in synovial fluid from patients with RA and PsA (305-307). For example, Isomäki *et al*. reported synovial fluid from patients with RA were found to have IL-4 levels of 240 ± 98 pg/mL (mean ± SEM) and IL-13 levels of 1,081 ± 257 pg/mL (mean ± SEM) (305). These levels far exceed the lower limit of detection in my U-PLEX assay of 0.08 pg/mL for IL-4 and 3.1 pg/mL provided by the manufacturer. It is worth noting that in the study by Isomäki *et al*., IL-4 was also undetectable in 10/28 (36%) of synovial fluids from patients with RA (305).

On the other hand, Woods *et al*. showed IL-13 was undetectable in synovial fluids from 69% of patients with RA, and 82% of patients with OA (308). Moreover, Woods *et al*.

found that IL-13 protein was also undetectable by immunohistochemistry within joints from patients with RA, OA and normal joints (308). The discrepancy in the synovial fluid findings between my study and some previous studies may be due to underlying duration of disease. Indeed, Raza *et al*. found that synovial fluid cytokine levels including IL-2, IL-4, IL-13, IL-17, IL-15, fibroblast growth factor and epidermal growth factor were elevated within 3 months after symptoms onset, but these were no longer present in established RA (285). The participants in my study have established disease with mean disease duration of 13.7 years in the RA group and 8.7 years in the PsA group (Table 6). Therefore, it may be that some synovial fluid cytokines were lower in my study compared to previous studies due to differences in disease duration of study participants.

3.4.4 Intra-articular methylprednisolone injection had no effects on hypoxia related genes in blood bulk RNA sequencing

Examination of blood bulk RNA transcriptomics showed only *SLC35B3* and *SLAMF6* were differentially expressed genes at 4 weeks after intra-articular methylprednisolone injection, neither of which are known to be related to hypoxia (Figure 41). This finding was to be expected given that the systemic effects of intra-articular glucocorticoid injection on blood bulk RNA profiles would likely have resolved after four weeks. After all, methylprednisolone was undetectable in the blood one week after intra-articular methylprednisolone injection (249). The only genes that were significantly different by blood bulk transcriptomic analysis were upregulation in *SLAMF6* and downregulation in *SLC35B3*, four weeks after an intra-articular glucocorticoid injection (Figure 41).

SLAMF6 encodes a protein belonging to the CD2 subfamily of the immunoglobulin superfamily. This protein is expressed on NK, T and B cells. SLAMF6 is involved in both

innate and adaptive immune response. Its functions include NK cell activation, Th17 cell differentiation and activation, maintaining B cell tolerance in germinal centres by inhibiting adhesion between T cells and B cells (309, 310). *SLAMF6* is known to be glucocorticoid responsive. For example, Cao *et al*. showed that *SLAMF6* was upregulated in CD4+ T cells and downregulated in B cells by methylprednisolone *in vitro* (300). A limitation of bulk transcriptomic analysis is that it is not known whether the upregulation seen in *SLAMF6* was due to increased transcription of *SLAMF6* in cells or differences in cell composition, i.e. more cells that expressed *SLAMF6*. This finding could have been confirmed at protein level using flow cytometry of blood. Alternatively, single nucleus transcriptomic analysis of synovial tissues (to be discussed later) would provide insight as to whether *SLAMF6* transcription in individual cell population was affected by intra-articular methylprednisolone injection.

The other gene that was significantly affected at 4 weeks follow-up by intra-articular methylprednisolone injection by bulk blood transcriptomic analysis was *SLC35B3* (Figure 41). This gene is a member of the solute carrier family and encodes a protein involved in the transport of 3'-phosphoadenosine-5'-phosphosulfate (PAPS) from the nucleus or the cytosol to the Golgi lumen (311). PAPS is a cofactor for sulfation reactions (312). *SLC35B3* was not known to be glucocorticoid responsive (300). Single nucleus transcriptomic analysis of synovial tissues would delineate if *SLC35B3* was perturbed by glucocorticoid in individual cell types.

In this chapter, I demonstrated that intra-articular methylprednisolone injection downregulated synovial fluid levels of IL-6 and TNF but had no effects on synovial fluid pO_2 at 4 weeks follow up. Nonetheless, investigation of the synovial tissue biopsies from

this cohort may reveal hypoxia related and anti-inflammatory effects of glucocorticoids. Systemic and intra-articular glucocorticoids are widely used for treatment of inflammatory arthritis but their effects on synovial tissue using modern deep phenotyping methods are incompletely described. In the next chapter, I will investigate how intra-articular glucocorticoid injection affects synovial tissues, from the same cohort, using snRNA-seq to characterise perturbation in cellular proportion of tissues and differential gene expression.

4. Chapter 4: Effects of intra-articular glucocorticoid injection on synovial tissue snRNA-seq expression in inflammatory arthritis

4.1 Introduction

4.1.1 Synovial tissue biopsy to study disease processes and therapeutic effects in inflammatory arthritis

Inflammatory arthritis such as RA and PsA have articular and extra-articular manifestations. Blood is commonly analysed in the investigation of inflammatory arthritis, but blood may not present an accurate picture of disease mechanisms predominant in synovial tissues. An understanding of the molecular and cellular basis of disease in the synovium would help provide insights as to the pathogenesis and therapeutic targets. The articular manifestations may be studied through synovial tissue biopsies. Synovial tissues may be sampled through arthroscopic or ultrasound guided synovial biopsies (313).

Synovium lines diarthrodial joints and is comprised of lining and sublining tissues (314). Healthy synovial lining consists of macrophages and fibroblasts while the sublining includes blood vessels, lymphatic vessels, adipocytes, lymphocytes and macrophages (314, 315). The microscopic anatomy of normal synovial tissue may be classified based on the structure and content of the subintimal layer: fibrous, areolar and adipose (315). Adipose synovium is found mainly in fat pads but is also seen within villi (315). The lining may lie directly on adipocytes but is often separated by a band of collagen-rich substratum, while the deeper tissue is fat (315). Ultrasound guided synovial biopsy is a minimally invasive procedure that allows sequential biopsies before and after interventions to study the longitudinal effects of treatments on tissue at the site of disease (313).

4.1.2 Glucocorticoid effects on inflammatory arthritis synovium

Glucocorticoids are widely used for the treatment of arthritis. Intra-articular glucocorticoid injections help with local joint inflammation, swelling and pain, whereas systemic glucocorticoids are used for polyarticular flare of inflammatory arthritis. Despite widespread use for many decades, the therapeutic mechanisms of glucocorticoids in rheumatic diseases remain poorly understood (230). The nuclear receptor subfamily 3, group C, member 1 (*NR3C1*) gene encodes two main transcriptional variants of the glucocorticoid receptor, GRα and GRβ. GRα contains all the domains required for glucocorticoid receptor signalling and is thought to mediate most of the classical effects of glucocorticoids (230). GRβ can form GRα-GRβ heterodimers or GRβ-GRβ homodimers that may mediate glucocorticoid resistance through negative effects on GRα (316).

Additional diversity in glucocorticoid receptors arises from variation in isoforms such as splice variants and isoforms with different translational start sites (317). Translational variants from the GRα transcript include GRA, GRB, GRC, GRC1, GRC2, GRD1, GRD2 and GRD3 (318). GRA is the classical glucocorticoid receptor isoform that has been extensively characterised and is most well-known compared to other isoforms.

Much is known about the effects of glucocorticoids but the effects of glucocorticoids on synovium in patients with inflammatory arthritis have not been characterised at single cell transcriptomic level. I undertook a systematic literature review on the glucocorticoid effects on synovial tissues. Unlike the previous scoping literature review (Table 2), the purpose here is to answer the specific question relating to glucocorticoid effects on synovial tissue. A systematic literature review, rather than a scoping review, is therefore performed to synthesise evidence from studies to provide a definitive answer relating to

glucocorticoid effects on synovial tissues (121). Using Web of Science, I used search terms: All Fields (methylprednis* OR dexamethasone* OR triamcinolone OR steroid* OR predniso*) And All Fields (synovi*) And All Fields (biops*). Of the 134 results generated, 17 were deemed to be relevant as having synovial tissue data comparing before and after glucocorticoid treatment (Table 7) (296, 319-334).

The studies were highly variable as to the glucocorticoid drug used, route of administration, disease of interest, follow-up timeline, joint biopsied, and sample size (Table 7). The physiological effects of glucocorticoid on synovium as classified by follow-up timepoints and assay used were summarised in Table 8. Most studies looked at early glucocorticoid effects with little described beyond 14 days after glucocorticoid treatment. Intra-articular methylprednisolone injections may have sustained effects for up to 3 months so there is a knowledge gap relating to late effects of intra-articular glucocorticoid in synovial tissues (248). There were some discrepancies among the study findings. For example, synovial tissue expression of tissue inhibitor of metalloproteinases (TIMP) was noted to be reduced at RNA (334) and protein levels (329) after glucocorticoid treatment in some studies, but not others (328). Such discrepancies may be due to differences in the study design including patient populations, glucocorticoid choice, route of glucocorticoid administration, follow-up timepoint, and TIMP assay readouts.

Table 7 Systematic literature review of glucocorticoid effects on synovial tissues

Authors	Year	Observational/Intervention	Sample size	Disease	Joint biopsied	Follow-up
Makrygiannakis *et al*. (319)	2012	Intra-articular 40 mg triamcinolone hexacetonide injection	15	RA	Unspecified	2 weeks
van der Goes *et al*. (320)	2012	Intra-articular glucocorticoid injection	14	Persistent knee arthritis	Knee	12 weeks
Gheorghe *et al*. (321)	2009	Intra-articular 40 mg triamcinolone hexacetonide injection	11	RA	Knee	10 days
Makrygiannakis *et al*. (322)	2008	Intra-articular triamcinolone injection	12	RA	Knee	11 days
Vandooren *et al*. (323)	2008	Oral prednisolone 60 mg/day the first week and 40 mg/day the second week	10	SpA	Knee	12 weeks
Makrygiannakis *et al*. (324)	2006	Intra-articular triamcinolone hexacetonide injection	13	Inflammatory arthritis	Knee	2 weeks
af Klint *et al*. (296)	2005	Intra-articular triamcinolone hexacetonide injection	31	Chronic arthritides	Knee	9-15 days
Korotkova *et al*. (325)	2005	TNFi or intra-articular glucocorticoid injection	18 TNFi, 16 intra-articular glucocorticoid injection	RA	Unspecified	10 weeks after TNF inhibitor. 9-12 days after intra-articular injection
Gerlag *et al*. (326)	2004	Oral prednisolone or placebo	Oral prednisolone (n=10) or placebo (n=11)	RA	Knee, ankle, wrist	14 days
Wong *et al*. (327)	2001	Intravenous pulse methylprednisolone	7	RA	Unspecified	24 h
Young *et al*. (328)	2001	Intra-articular 120 mg methylprednisolone acetate or placebo	Methylprednisolone (n=21). Placebo (20).	OA	Knee	1 month
Wong *et al*. (329)	2000	Intravenous pulse methylprednisolone	11	RA	Knee	24 h

Youssef *et al*. (330)	1997	Intravenous pulse methylprednisolone	10	RA	Knee	24 h
Youssef *et al*. (331)	1996	Intravenous pulse methylprednisolone	10	RA	Knee	24 h
Debois *et al*. (332)	1993	Intra-articular 20 mg triamcinolone hexacetonide injection	7	RA	Knee	14 days
Corkill *et al*. (333)	1991	Parenteral gold therapy alone or combined with 120 mg intramuscular methylprednisolone acetate	11	RA	Unspecified	2 and 12 weeks
Firestein *et al*. (334)	1991	Intra-articular triamcinolone injection	3	RA	Knee	1-2 weeks

Table 8 Summary of physiological effects of glucocorticoid on synovial tissues

Follow-up (days)	Assay	Synovial tissue glucocorticoid effects		
		Cell	Cytokine	Other
1	Immunohistochemistry		↓MCP1, ↓MIP-1α (327). ↓IL-8, ↓TNF (330)	↓MMP-1, ↓TIMP-1 (329). ↓E-selectin, ↓ICAM-1 (331)
7-14	Immunohistochemistry	↓Macrophage infiltration (326)	↓TNF, ↓IL-1β (323). ↓VEGF (296)	↓Citrullinated proteins and peptidylarginine deiminases (319). ↓cadherin 11 (323). ↓HMGB-1, ↓ICAM-1 (296). ↓mPGES-1, ↓COX-2 (325)
	Immunofluorescence	↓T cells (322)	↓RANKL (324)	↓ 5-lipoxygenase (321)
	in situ hybridization			↓collagenase, ↓TIMP, ↓HLA-DR, ↓complements (334)
28	Immunohistochemistry	↓Macrophage infiltration (328)		
84	Immunohistochemistry	↓ Steroid hormone receptor positive cells (320)		

Ultrasound guided synovial tissue biopsy has been applied to investigate the effects of therapeutics such as biologics, but not glucocorticoids, on synovial tissues at single cell transcriptomic level (335-338). Longitudinal single cell transcriptomic studies of synovial tissues are limited. A prospective longitudinal study was needed to study the effects of glucocorticoid on synovial single cell transcriptomic profiles. Ideally, all synovial tissue

biopsy samples from the POLO cohort would be taken forward for snRNA-seq analysis but due to financial limitations, only 8 pairs of pre- and post-treatment synovial tissue samples were able to be analysed. To allow for even sample size between RA and PsA subgroups, 4 pairs of RA and 4 pairs of PsA synovial tissue biopsy samples were analysed with snRNA-seq. As only 4 pairs of RA synovial tissue biopsy samples were available, all of these were analysed. As there were 6 pairs of PsA synovial tissue biopsy samples were available, 4 pairs were randomly selected for analysis to avoid selection bias. The patient demographics and clinical data for the snRNA-seq study is therefore slightly different from those presented in the previous chapter as 2 patients with PsA were omitted. This was the first reported longitudinal snRNA-seq of inflammatory arthritis synovium to provide insight into mechanisms of action of intra-articular methylprednisolone injection at single cell transcriptomic level. This study also established the approach by which novel therapeutics may be studied using synovial tissue snRNA-seq in future.

4.1.3 Inflammatory arthritis synovial tissue adipocytes transcriptomic analysis at single cell level

Adipocytes are absent from previous single cell atlases because mature adipocytes are buoyant and therefore lost in the tissue disaggregation process in traditional single cell approaches (339). There is therefore a knowledge gap about synovial tissue adipocytes at single cell transcriptomic level in inflammatory arthritis. The advantage of using single nucleus transcriptomics in this study is that single nucleus sequencing can capture and describe adipocytes (339, 340). Single nucleus transcriptomic atlas of adipocytes from subcutaneous adipose tissues, visceral adipose tissues and infrapatellar fat pad have previously been described, but not in inflammatory arthritis synovial tissues (339, 340). Single nucleus transcriptomic analysis of adipocytes in inflammatory arthritis synovial

tissues could shed light on their roles in pathogenesis and resolution of inflammatory arthritis. Adipocytes used to be regarded as morphologically and functionally bland, but are now recognized as dynamic, plastic, heterogeneous, and involved in diverse biological processes (340). There is emerging evidence of roles of synovial tissue adipocytes in inflammation and signalling beyond energy storage (341, 342).

4.1.4 Comparison of RA and PsA synovial tissues

Both RA and PsA are inflammatory arthritides, but they are distinct diagnoses with different clinical manifestations. Differential diagnosis of inflammatory arthritis may be diagnostically challenging due to similarities in clinical presentations. Radiologically, bone erosions without new bone growth are characteristic of RA (2, 343). On the other hand, juxta-articular bony proliferations, ankylosis, pencil-in-cup deformities and arthritis mutilans are characteristic of PsA (343). In arthroscopic views of knee synovitis, straight branching vessels are observed in RA, whereas tortuous bushy vessels are observed in PsA (2, 344). The aetiology of tortuous vessels in synovial tissues that distinguish PsA from RA has long eluded rheumatologists (345). This physiological difference was previously thought to be due to differences in interleukins, but remains poorly understood (2). Understanding the molecular endotypes underpinning the differences in synovial tissue vasculature in RA and PsA may identify novel therapeutic targets.

Characterisation of synovial tissues from patients with RA and PsA at single cell transcriptomic level has so far been limited (346). Exploratory cell-cell communication analysis of RA and PsA synovial tissues may provide insight into the role of synovial tissue immune-stromal cell crosstalk in inflammatory arthritis. Pre-treatment samples were prioritised for this exploratory analysis of inter-disease differences to limit confounding by

intra-articular methylprednisolone injection. Nonetheless, a caveat with this exploratory analysis of RA versus PsA is that there may be other confounders such as differences in age, gender, disease stage, disease severity, comorbidities and medications.

4.2 Materials and methods

4.2.1 Patient cohort and ethics

8 paired synovial tissue biopsies before and 4 weeks after 80 mg intra-articular methylprednisolone injection from patients with RA (n = 4) and PsA (n = 4) from the POLO observational study (REC 21/NS/0002) were used for snRNA-seq (Figure 42). No statistical method was used to predetermine sample size.

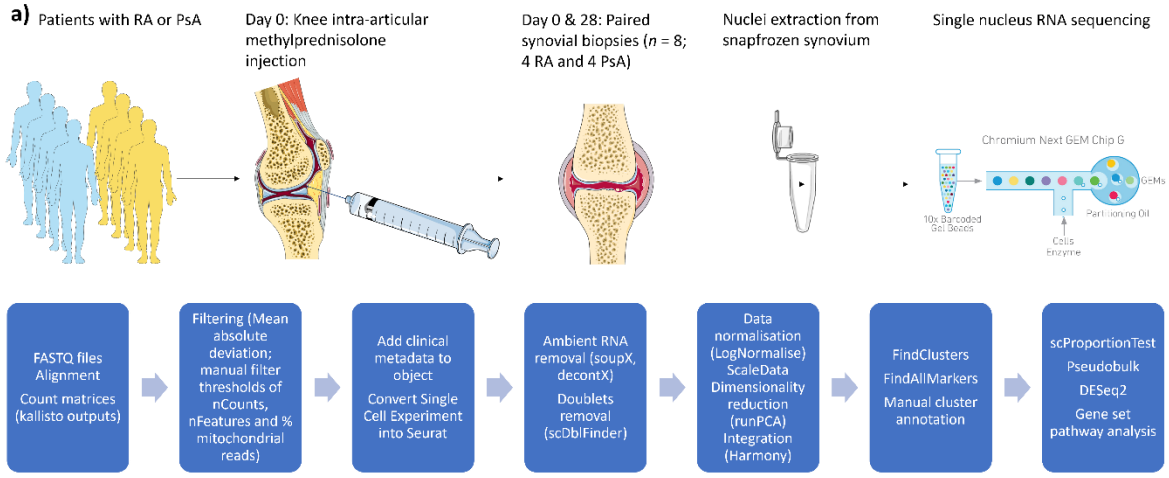

Figure 42 Overview of (a) synovial tissue single nucleus transcriptomic sequencing pipeline and (b) computational analysis strategy

4.2.2 Sample preparation

All synovial tissue samples were collected into cold DMEM-F12 media supplemented with 10% FBS and 1% Penicillin/Streptomycin in 1.5 mL Eppendorf tubes and kept on ice. All samples were processed within 2 h of the procedure. Sample processing was performed under sterile conditions. Samples to be used for single nucleus transcriptomic analysis were gently washed with 1x PBS, snapfrozen in 1.5 mL cryogenic vials using liquid nitrogen. Tissues were stored at -80 ºC until use.

4.2.3 Nuclei isolation

Nuclei were isolated based on previously published protocol involving musculoskeletal tissues (347). Briefly, forceps, scalpels and petri dishes were pre-cooled on dry ice. Ultrasound guided synovial tissue biopsies were minced using scalpels to ensure fragments were < 1 mm in diameter. Tissue fragments were stored in a pre-cooled 50 mL Falcon tube. The tubes containing the minced tissues were thawed and 4 mL of cold 1x CST buffer (salts and Tris buffer, including NaCl, Tris-HCL pH 7.5, $CaCl_2$, $MgCl_2$, CHAPS hydrate (Sigma), BSA (Sigma), Rnase inhibitors (RnaseIn Plus (Promega) and SUPERase In (Invitrogen)), and protease inhibitor (cOmplete tablet, Roche) was added. After 10 min of incubation on a rotor at 4 ºC, the tissue/buffer mixture was poured through a 40 µm strainer and the tube used for tissue lysis was washed twice with 2 mL PBS with 1% BSA. The nuclei solution was then transferred to a 15 mL Falcon tube, and the previous 50 mL tube was washed once with 4 mL PBS with 1% BSA. The solution was centrifuged at 500 g at 4 ºC for 5 min. After pouring off the supernatant, the tubes were briefly spun down. The nuclei were then re-suspended in the remaining supernatant, and remaining volume

was determined. The concentration of nuclei was determined by staining the nuclei with DAPI and counting using a Neubauer Improved haemocytometer (NanoEnTek).

4.2.4 Library preparation and sequencing

Nuclei suspensions were diluted (PBS with 1% BSA) to 200-1000 nuclei/µL and loaded on the Chromium Next Gel bead-in-emulsion (GEM) Chip G (10x Genomics) with a targeted nuclei recovery of 5,000-10,000 nuclei per sample. Samples were then loaded to the Chromium Controller (10x Genomics) and libraries were prepared using the Chromium Next GEM Single Cell 3' Reagent Kits v3.1 (10x Genomics) following the manufacturer's instructions and indexed with the single-index kit T set A (10x Genomics). Quality control of cDNA and final libraries was analysed using High Sensitivity ScreenTape assays on a 4150 TapeStation System (Agilent). Final libraries were pooled and sequenced on a NovaSeq 6000 (Illumina) by Genewiz at a minimum depth of ~20,000 read pairs per expected nuclei. Sequencing by Genewiz was performed at their headquarter in Leipzig, Germany.

4.2.5 snRNA-seq quality control

Raw Fastq files were mapped by kind courtesy of Dr Carla Cohen to the human genome hg38 using kallisto bustools kb count (release 99) with kmer size = 31 (https://www.kallistobus.tools/kb_usage/kb_count/). Spliced and unspliced matrices were merged by Dr Carla Cohen to create the count matrix for downstream analysis. All downstream analyses were performed by me unless otherwise specified. Analysis training and pipelines were provided by my supervisors and collaborators including Dr Carla Cohen and Dr Jolet Mimpen. All figures were generated by me unless otherwise specified.

Droplets more than 3 median absolute deviations from the median were discarded to remove outliers. Nuclei with greater than 300 unique genes expressed, greater than 500 UMIs, of which less than 5% are mitochondrial genes, were taken forward for snRNA-seq analysis which was performed using R v3.6.1 and Seurat v4.0 (348).

Ambient RNA removal was performed with soupX using automated method to determine cell specific contamination fraction (349). All Seurat objects were merged. Ambient RNA above decontX threshold 0.2 was removed (350). Doublets were removed using scDblFinder (351).

4.2.6 Normalisation, dimensionality reduction, clustering and annotation

Log normalisation (NormalizeData), selection of 5000 variable genes (FindVariableFeatures), scaling (ScaleData), dimensionality reduction (RunPCA), clustering (FindNeighbors with 40 dimensions and FindClusters with 0.3 resolution), and RunUMAP were performed on the merged object. The merged object was integrated with Harmony v1.2.1 (reduction.use = pca_name, group.by.vars = “orig.ident”, dims.use = 1:40, kmeans_init_nstart = 20, kmeans_init_inter_max = 100) to minimise technical variation from batch effects. I manually annotated cell clusters by identifying genes that are differentially expressed between clusters and by comparing them with literature-based marker genes (352-355).

4.2.7 Compositional analysis, differential gene expression and gene set enrichment analysis

The difference between the proportion of cells in clusters was analysed using scProportionTest (permutation_test(prop_test, cluster_identity = “cluster_id”, sample_1 = “Pre”, sample_2 = “Post”, sample_identity = “treatment_status”)) (356). I set the FDR threshold at 5% using scProportionTest to correct for multiple testing (356). Pseudobulked profiles were generated at the compartment level to account for pseudoreplication for differential expression analysis. Counts were aggregated with AggregateExpression (group.by = c(“cluster_id”, “sample”), assays = ‘SoupXcounts’, slot = “counts”). Counts less than 10 were discarded. Differential gene expression required cell types to contain at least 10 cells from at least 3 participants for analysis.

Using an interaction term consisting of treatment status and adjusting for patient, paired analysis of differential gene expression was performed using DESeq2 (270). I shrunk the Log2FoldChange values using the apelgm method to facilitate visualisation (270). Statistical analysis with DESeq2 was corrected for multiple testing using the Benjamini and Hochberg method by default (270, 272). Absolute Log2FoldChange greater than 1 and adjusted p value of less than 0.05 were considered statistically significant. Gene set enrichment analysis was performed with g:GOSt (organism = “hsapiens”, ordered_query = FALSE, multi_query = FALSE, significant = TRUE, exclude_iea = FALSE, measure_underrepresentation = FALSE, evcodes = FALSE, user_threshold = 0.05, correction_method = “g_SCS”, domain_scope = “annotated”, custom_bg = all_gene_ids, numeric_ns = “”, sources = NULL) and fgsea (pathways = hallmark_list, stats = ranks, nperm = 10000, maxSize = 500).

4.2.8 Exploratory subgroup analysis of RA and PsA synovial tissue snRNA-seq profiles

Exploratory analysis comparing RA and PsA was performed on the snRNA-seq dataset. I used scProportionTest to compare synovial tissue cell proportions between RA and PsA. DESeq2 was performed on pseudobulked data for differential gene expression analysis between RA and PsA. Gene set enrichment analysis comparing RA and PsA was performed. CellChat was used to compare cell-cell communication in RA and PsA synovial tissues before treatment (mergeCellChat(object.list, add.names = NULL, merge.data = FALSE, cell.prefix = FALSE)).

To facilitate the interpretation of the complex intercellular communication networks, I applied CellChat to quantitatively measure networks through methods abstracted from graph theory, pattern recognition and manifold learning. CellChat readily identifies dominant senders, receivers, mediators and influencers in the intercellular communication network by computing several network centrality measures for each cell group (357).

4.3 Results

4.3.1 Synovial tissue snRNA-seq therapeutic atlas of intra-articular methylprednisolone in RA and PsA

8 paired synovial tissue biopsies (4 patients with RA and 4 patients with PsA) before and 4 weeks after treatment with intra-articular methylprednisolone were processed for single nucleus RNA sequencing. The clinical data for these 8 patients are described in Table 9. The gender of the participants is not shown to avoid inadvertent identification due to $n < 5$ (Table 9). There was a trend towards reduced composite disease activity scores at follow-

up, but this was not statistically significant for either the RA (P = 0.42) or PsA subgroups (P = 0.11).

Table 9 Clinical data of the snRNA-seq study

Clinical data		RA	PsA
Sample size		4	4
Gender		3 men and 5 women	
Age mean (range)		62.5 (48 - 74)	43.8 (36 - 49)
Disease duration in years (mean ± SD)		13.7 + 13.7	8.7 ± 6.5
Treatment history		1 participant not on DMARD, 2 participants on csDMARDs and bDMARD naïve, 1 participant on TNFi	2 participants on csDMARDs and bDMARD naïve, 2 participants on TNFi
CRP (mean ± SD)	Baseline	5.15 ± 5.39	5.08 ± 3.64
	Follow up	2.6 ± 1.83	5.13 ± 3.72
SJC66 (mean ± SD)	Baseline	1.25 ± 1.26	2.25 ± 1.26
	Follow up	0.75 ± 1.5	1.75 ± 0.96
TJC68 (mean ± SD)	Baseline	1.5 ± 0.58	3 ± 2.16
	Follow up	2.25 ± 3.86	1.75 ± 2.06
Composite disease activity scores (mean ± SD; DAS28 for RA and DAPSA for PsA)	Baseline	3.16 ± 0.48	16.48 ± 6.13
	Follow up	2.53 ± 1.14	13.54 ± 4.21

4.3.2 Library preparation

Sample clogs impacted several samples as evidenced by reduced GEM recovery particularly in the pre-treatment sample of participant 12 (labelled 12-1) and post-treatment sample of participant 14 (labelled 14-2) (Figure 43). The post-treatment sample of participant 8 was also affected by clogging although this was not photographed (Figure 44). Due to the preciousness of the samples, processing continued with cDNA generation albeit at lower levels.

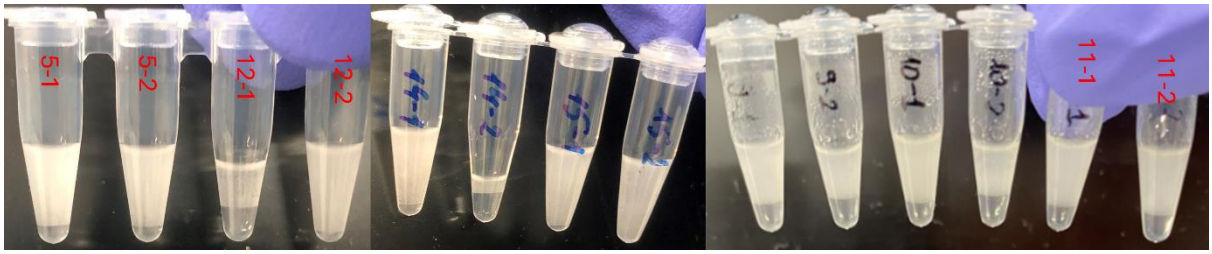

Figure 43 GEM recovery (samples 8-1 and 8-2 not shown)

4.3.3 Quality control

For quality control, commonly used filtering thresholds of nFeatures > 300, nCounts > 500, mitochondrial RNA < 5%, decontX score < 0.2 and doublet removal using scDblFinder default settings were applied to all samples by me. A total of 26,453 nuclei passed quality control with mean of 1,653 nuclei per sample (Figure 44, Supplementary Figure 1). The clogged samples had lower nuclei recovery, e.g. the clogged post-treatment sample of participant 14 had the lowest nuclei count of 247 (Figure 44).

Figure 44 Clinical data and final nuclei count in snRNA-seq study

Sample identifier	Patient identifier	Disease	Sex	Age (years)	Treatment status	CRP	SJC66	TJC68	Composite disease activity score	Nuclei
POLO-008-1	008	RA	M	74	Pre	2.8	0	2	2.7	1759
POLO-008-2	008	RA	M	74	Post	1.8	0	1	2.59	585
POLO-011-1	011	RA	F	48	Pre	2.9	1	2	2.95	2306
POLO-011-2	011	RA	F	48	Post	2.9	0	0	1.79	1853
POLO-012-1	012	RA	F	63	Pre	13	1	1	3.81	912
POLO-012-2	012	RA	F	63	Post	5	0	0	1.63	956
POLO-014-1	014	RA	F	65	Pre	1.7	3	1	3.17	2110
POLO-014-2	014	RA	F	65	Post	0.7	3	8	4.12	247
POLO-005-1	005	PsA	M	47	Pre	4.2	1	1	12.82	2519
POLO-005-2	005	PsA	M	47	Post	1.9	0	1	9.59	3753
POLO-009-1	009	PsA	M	36	Pre	0.9	2	2	11.29	1601
POLO-009-2	009	PsA	M	36	Post	6.6	1	3	10.46	1214
POLO-010-1	010	PsA	F	49	Pre	9.7	6	4	24.97	679
POLO-010-2	010	PsA	F	49	Post		3	4	18.37	1634
POLO-015-1	015	PsA	F	43	Pre	5.5	2	3	16.85	2889
POLO-015-2	015	PsA	F	43	Post	2.3	2	0	15.73	1436

4.3.4 Integration, clustering and annotation

The merged object was integrated with Harmony (Supplementary Figure 2, Supplementary Figure 3). I applied FindClusters to identify clusters of cells using a shared nearest neighbour modularity optimisation based clustering algorithm (358). Differentially expressed cluster markers were used to annotate clusters as fibroblasts, macrophages, T cells, adipocytes, NK cells/NKT cells, B cells, myocytes, vascular endothelial cells, plasma cells, proliferating cells, granulocytes, mural cells, dendritic cells, lymphatic endothelial cells, and plasmacytoid dendritic cells (Figure 45, Figure 46).

There was agreement in broad cell-type composition between this study and previously published scRNA-seq and snRNA-seq studies of synovium and musculoskeletal tissues (354, 359). The presence of skeletal myocytes was likely due to accidental uptake of adjacent tissues outside of the joint capsule. Skeletal myocytes were present in synovial tissue biopsy samples from 2 participants with RA and 1 participant with PsA. A limitation in the analysis of samples containing skeletal myocytes is that the other cell types in these biopsies may also arise from extra-articular tissues, such as adipocytes from fat tissues as well as vascular endothelial cells and immune cells from blood vessels outside the joint capsule. Initial analyses therefore excluded all samples from these 3 participants to limit confounding by extra-articular cells. However, exclusion of these patients may constrain the statistical power so exploratory analyses of samples from all 8 participants was also performed.

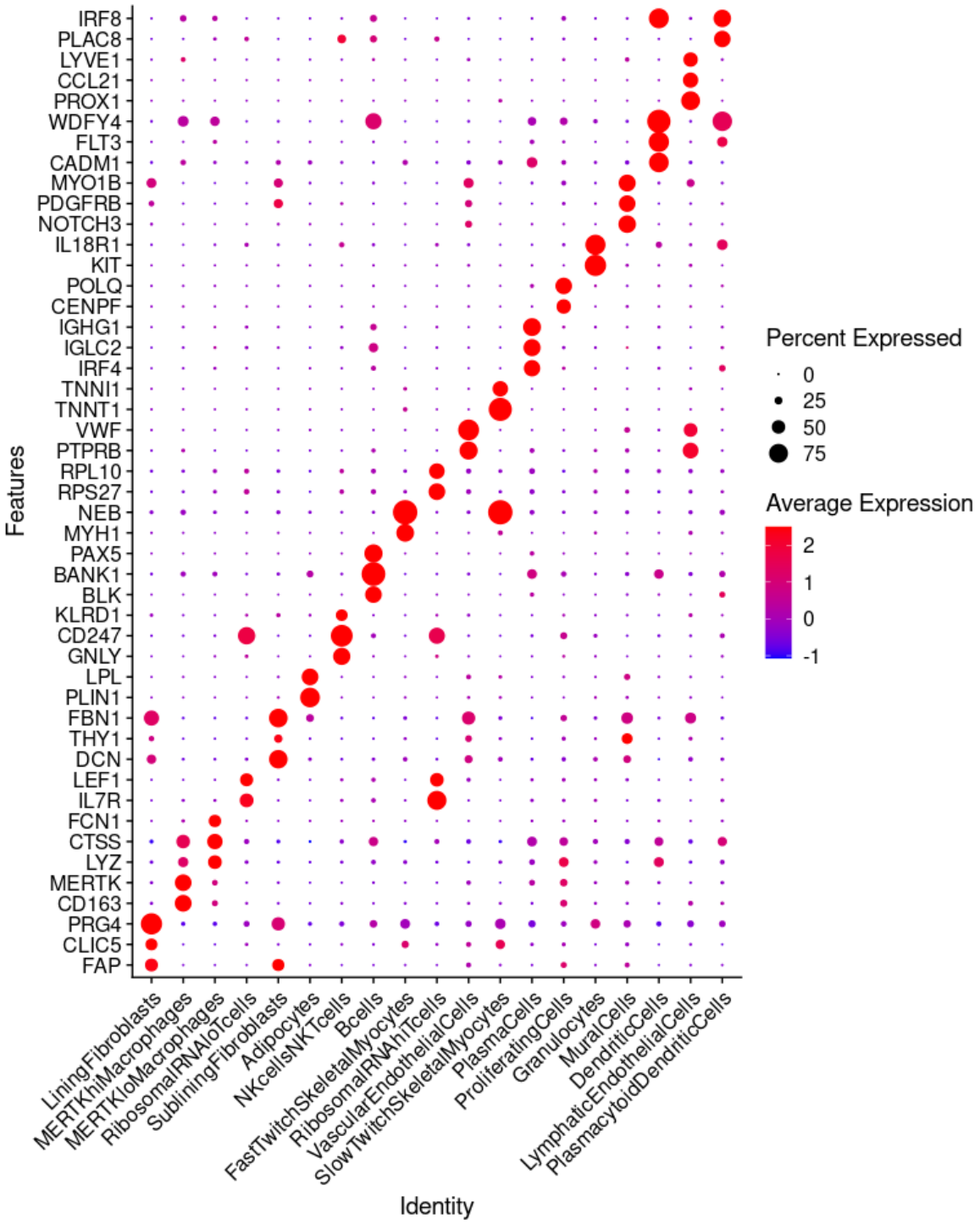

Figure 45 Dotplot of select differentially expressed cluster markers

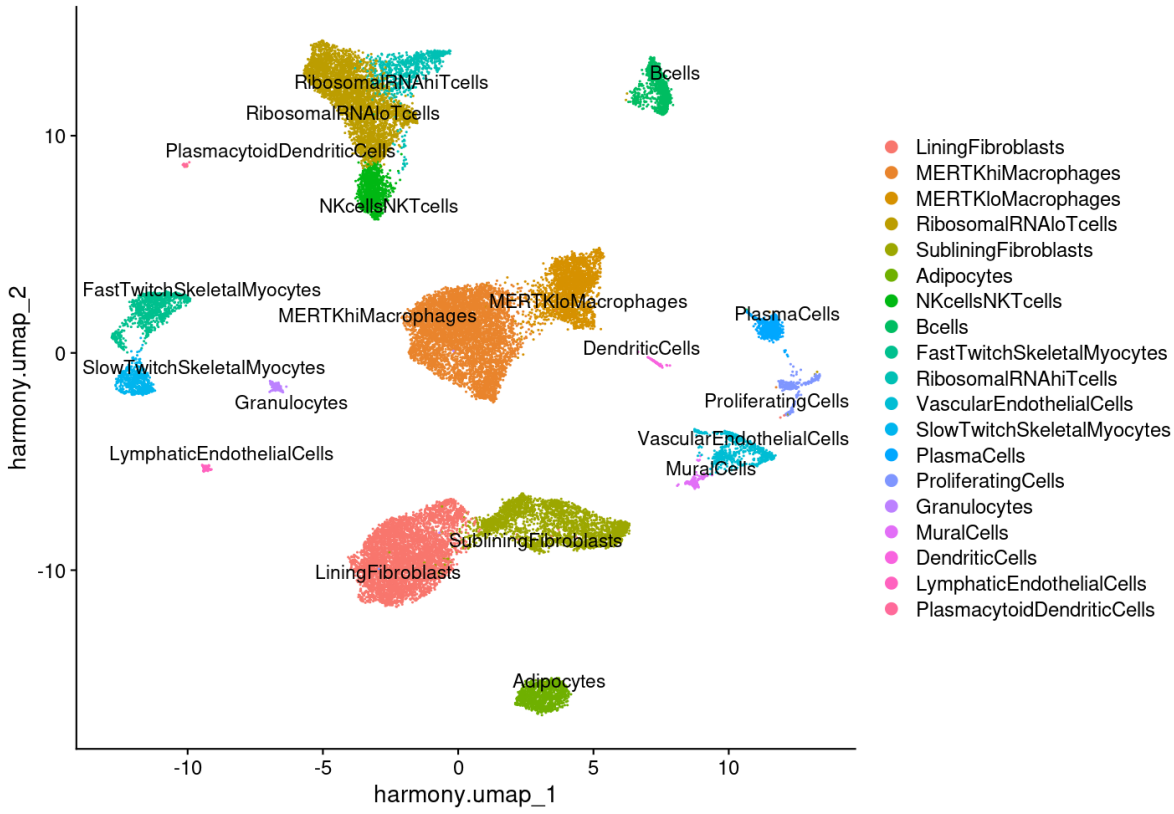

Figure 46 UMAP of integrated cell cluster annotations

4.3.5 Effects of intra-articular methylprednisolone injection on synovial tissue cellular composition

Cellular composition analysis excluded samples from patients containing skeletal myocytes to ensure analysis is not confounded by extra-articular cells. There were fewer adipocytes, and more NK/NKT cells and ribosomal RNA high T cells in synovial tissues after intra-articular methylprednisolone injection (Figure 47). Having evaluated the effects of intra-articular methylprednisolone on synovial tissue cellular composition, I then evaluated its effects on differential gene expression.

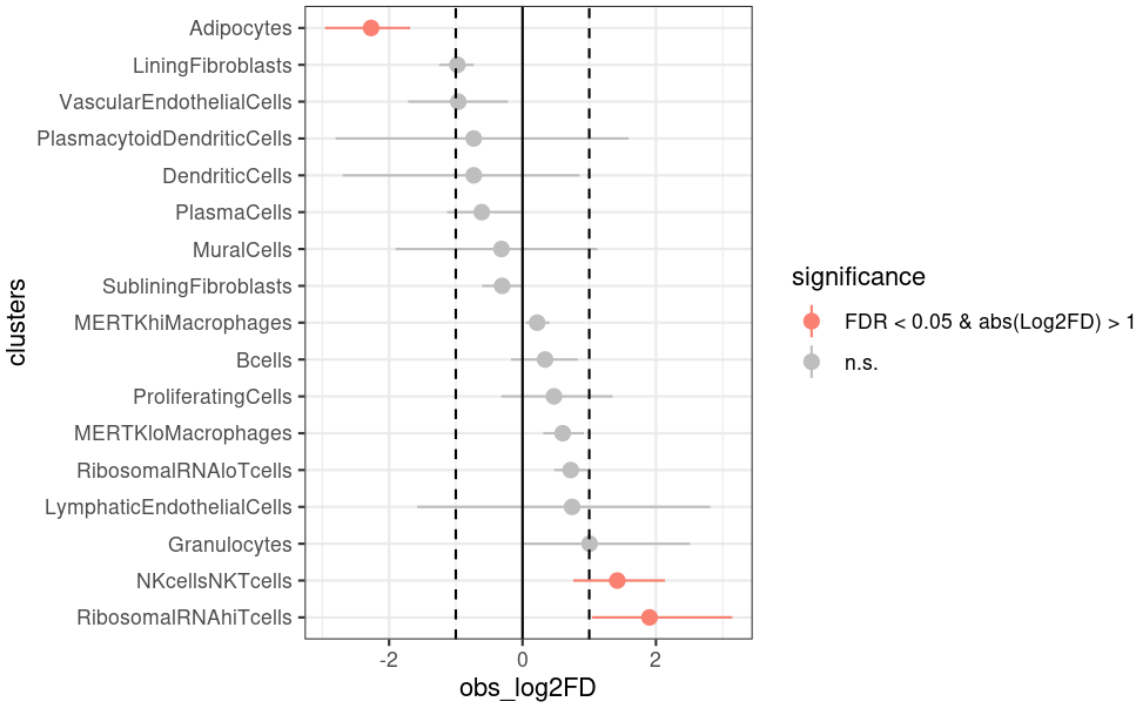

Figure 47 Paired differential cellular proportions before and after intra-articular methylprednisolone injection (n = 5; 2 RA and 3 PsA)

FDR was set at < 0.05 to account for multiple testing (272)

4.3.6 Effects of intra-articular methylprednisolone injection on differential gene expression across cell types, excluding samples from patients containing skeletal myocytes

Initial analysis of intra-articular methylprednisolone effects on differential gene expression excluded samples from patients containing skeletal myocytes to avoid misinterpretation due to the presence of extra-articular cells. Using an interaction term consisting of treatment status and adjusting for patient, I examined gene expression changes in each cell cluster following intra-articular methylprednisolone injection. The only differentially expressed genes were sodium leak channel (non-selective) channel auxiliary factor 1 (*NALF1*) and integrin subunit beta 8 (*ITGB8*) which were downregulated in sublining

fibroblasts after intra-articular methylprednisolone injection, neither of which are currently known to be directly related to hypoxia (Table 10, Figure 48). Unlike the blood bulk RNA sequencing, there was no differential gene expression of *SLAMF6* or *SLC35B3* in synovial tissue cell types with intra-articular methylprednisolone injection (Figure 41, Table 10, Supplementary Figure 4, Supplementary Figure 5).

Table 10 Differentially expressed genes (Log2FoldChange < -1 or >1 and adjusted P value < 0.05) in synovial tissues with intra-articular methylprednisolone injection, excluding samples from patients containing skeletal myocytes (n = 5; 2 RA and 3 PsA. - denotes no differentially expressed genes. Not applicable denotes analysis was not possible as there were not at least 10 cells of that cell type from at least 3 participants.)

P values were corrected for multiple testing using the Benjamini and Hochberg method in DESeq2 by default (270, 272)

	Downregulated genes post-treatment	Upregulated genes post-treatment
Adipocytes	-	-
B cells	-	-
Dendritic cells	-	-
Granulocytes	-	-
Lining fibroblasts	-	-
Lymphatic endothelial cells	Not applicable	Not applicable
MERTKhi macrophages	-	-
MERTKlo macrophages	-	-
Mural cells	Not applicable	Not applicable
NK cells/NKT cells	-	-
Plasma cells	-	-
Plasmacytoid dendritic cells	-	-
Proliferating cells	-	-
Ribosomal RNA hi T cells	-	-
Ribosomal RNA lo T cells	-	-
Sublining fibroblasts	*NALF1, ITGB8*	-
Vascular endothelial cells	-	-

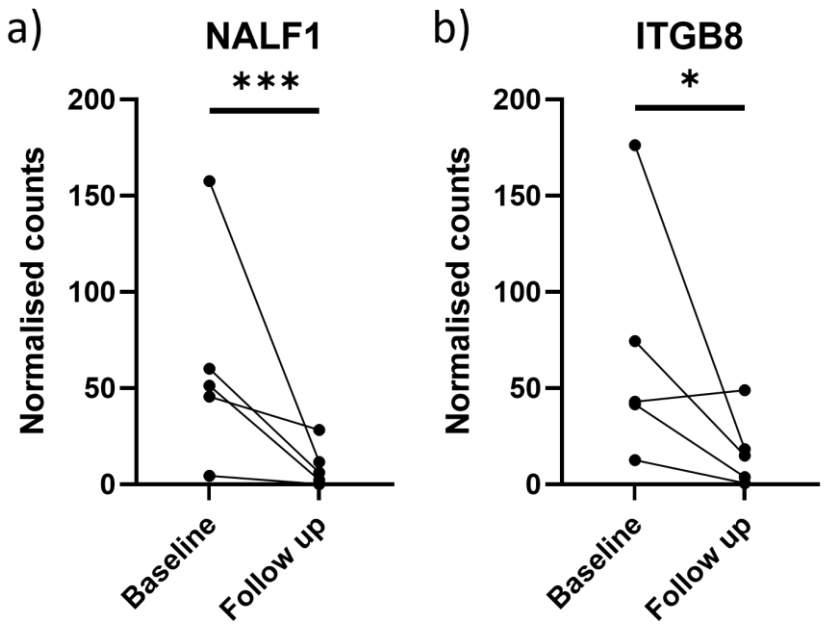

Figure 48 a) NALF1 and b) ITGB8 expression in sublining fibroblasts at baseline and follow-up after intra-articular methylprednisolone injection, excluding samples from patients containing skeletal myocytes (N = 5; 2 RA and 3 PsA)

** denotes padj < 0.05 and *** denotes padj < 0.001 by DESeq2 analysis of pseudobulked data. P values were corrected for multiple testing using the Benjamini and Hochberg method in DESeq2 by default (270, 272)*

4.3.7 Exploratory analysis of intra-articular methylprednisolone effects on differential gene expression, including samples from patients containing skeletal myocytes

Initial analysis excluded samples from 3 patients that contained skeletal myocytes to ensure that the cells were of articular origin rather than from extra-articular tissues. However, the reduction in sample size limits the statistical power for differential gene expression. I proceeded to undertake exploratory analysis utilising samples from all 8

participants to increase statistical power to detect treatment effects, with the caveat that some samples may include cells from extra-articular tissues (n = 8; 4 RA and 4 PsA) (Table 11).

Table 11 Differentially expressed genes (Log2FoldChange < -1 or >1 and adjusted P value < 0.05) in synovial tissues with intra-articular methylprednisolone injection in patients with RA and PsA, including samples from patients containing skeletal myocytes (n = 8; 4 RA and 4 PsA. - denotes no differentially expressed genes. Not applicable denotes analysis was not possible as there were not at least 10 cells of that cell type from at least 3 participants)

P values were corrected for multiple testing using the Benjamini and Hochberg method in DESeq2 by default (270, 272)

	Downregulated genes post-treatment	Upregulated genes post-treatment
Adipocytes	*PENK-AS1, ENSG00000254865, ENSG00000287720, PRKCH-AS1, FAM151B-DT*	*INSIG1, FADS2, ACLY, GPAM, PNPLA3, SCD, ACACA, ME1*
B cells	*ENSG00000286221, VCAN, IL2RA*	-
Dendritic cells	-	-
Fast twitch skeletal myocytes	-	-
Granulocytes	-	-
Lining fibroblasts	*TIMP1, NLGN4X, NALF1*	-
Lymphatic endothelial cells	-	-
MERTK high macrophages	-	-
MERTK low macrophages	*FPR3*	-
Mural cells	-	-
NK cells/NKT cells	-	-
Plasma cells	-	-
Plasmacytoid dendritic cells	-	-
Proliferating cells	-	-
Ribosomal RNA high T cells	-	-
Ribosomal RNA low T cells	-	-
Slow twitch skeletal myocytes	Not applicable	Not applicable
Sublining fibroblasts	*ENSG00000254303*	-
Vascular endothelial cells	-	-

Adipocytes

Adipocytes were found to have the most differentially expressed genes after intra-articular methylprednisolone injection, although this result may be confounded by extra-articular adipocytes that may have been included (Table 11). In adipocytes following treatment with intra-articular methylprednisolone, there was significant upregulation in markers of steroid metabolism and lipid metabolism such as stearoyl-CoA desaturase (*SCD*), glycerol-3-phosphate acyltransferase, mitochondrial (*GPAM*), fatty acid desaturase 2 (*FADS2*), acetyl-CoA carboxylase alpha (*ACACA*), ATP citrate lyase (*ACLY*), patatin like domain 3, 1-acylglycerol-3-phosphate O-acyltransferase (*PNPLA3*), malic enzyme 1 (*ME1*), insulin induced gene 1 (*INSIG1*) (Figure 49).

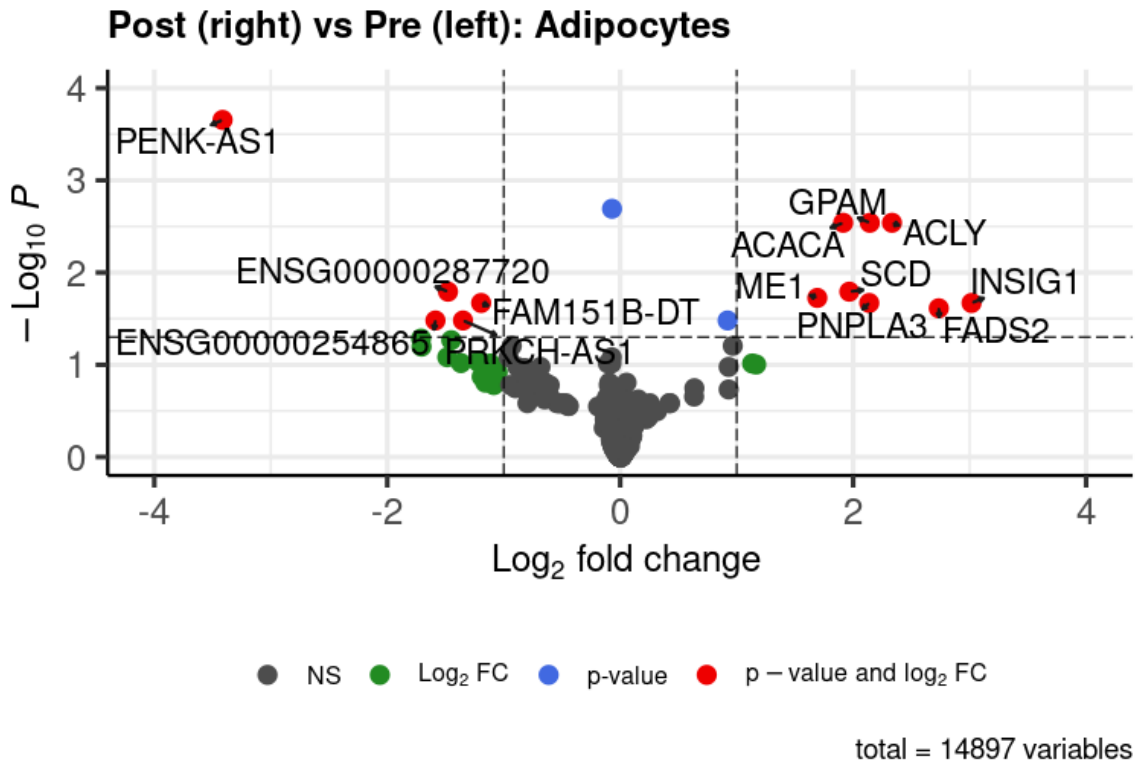

Figure 49 Volcano plot of differentially expressed genes in adipocytes pre- and post-intra-articular methylprednisolone injection, including samples from patients containing skeletal myocytes (n = 8; 4 RA and 4 PsA)

P values were corrected for multiple testing using the Benjamini and Hochberg method in DESeq2 by default (270, 272)

Glucocorticoids are metabolised into sterols which are known to regulate sterol regulatory element-binding transcription factors (SREBFs), such as SREBF1 and SREBF2, and are master regulators of lipid homeostasis (360). Since lipogenesis was upregulated in adipocytes, I analysed the effects of intra-articular methylprednisolone injection on *SREBF1* and *SREBF2* expression in adipocytes to see whether these mediated methylprednisolone induced lipogenesis. There was a trend towards increase in *SREBF1* and *SREBF2* expression in adipocytes but these were not statistically significant (Figure 50).

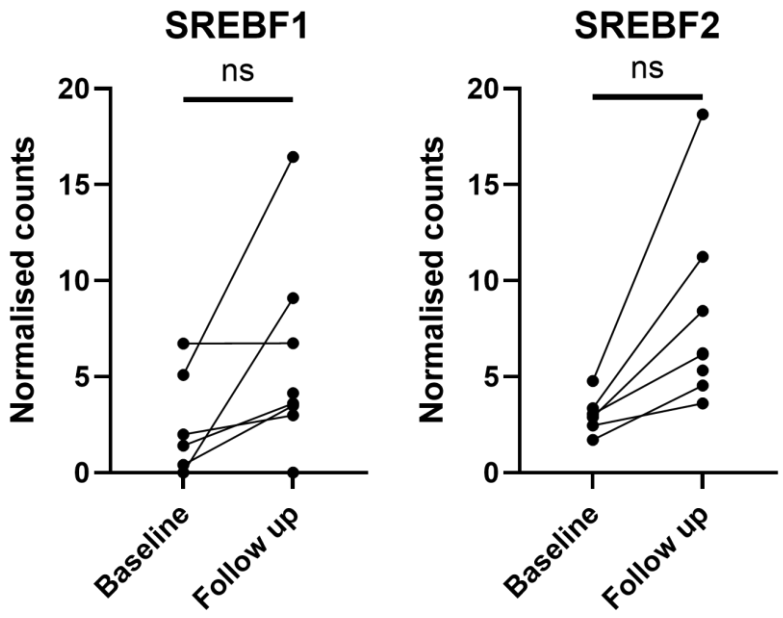

Figure 50 SREBF1 and SREBF2 expression in adipocytes at baseline and follow-up after intra-articular methylprednisolone injection, including samples from patients containing skeletal myocytes (n = 8; 4 RA and 4 PsA)

ns denotes non-statistically significant by DESeq2 analysis of pseudobulked data. P values were corrected for multiple testing using the Benjamini and Hochberg method in DESeq2 by default (270, 272).

Over-representation analysis of gene pathways showed intra-articular methylprednisolone upregulated metabolic and biosynthetic processes in adipocytes (Table 12). Gene set enrichment analysis of Hallmark pathways in adipocytes showed statistically significant upregulation of cholesterol homeostasis pathway (Figure 51).

Table 12 Over-representation analysis of gene pathways affected by intra-articular methylprednisolone in adipocytes, including samples from patients containing skeletal myocytes

id	term_id	term_name		p_value
1	GO:0032787	monocarboxylic acid metabolic process		2.0e-07
2	GO:0019752	carboxylic acid metabolic process		2.0e-06
3	GO:0006631	fatty acid metabolic process		2.6e-06
4	GO:0043436	oxoacid metabolic process		2.9e-06
5	GO:0006082	organic acid metabolic process		3.4e-06
6	GO:0008610	lipid biosynthetic process		1.3e-04
7	GO:0044281	small molecule metabolic process		2.4e-04
8	GO:0006633	fatty acid biosynthetic process		2.9e-04
9	GO:0072330	monocarboxylic acid biosynthetic process		7.2e-04
10	GO:0044255	cellular lipid metabolic process		1.0e-03

g:Profiler (biit.cs.ut.ee/gprofiler)

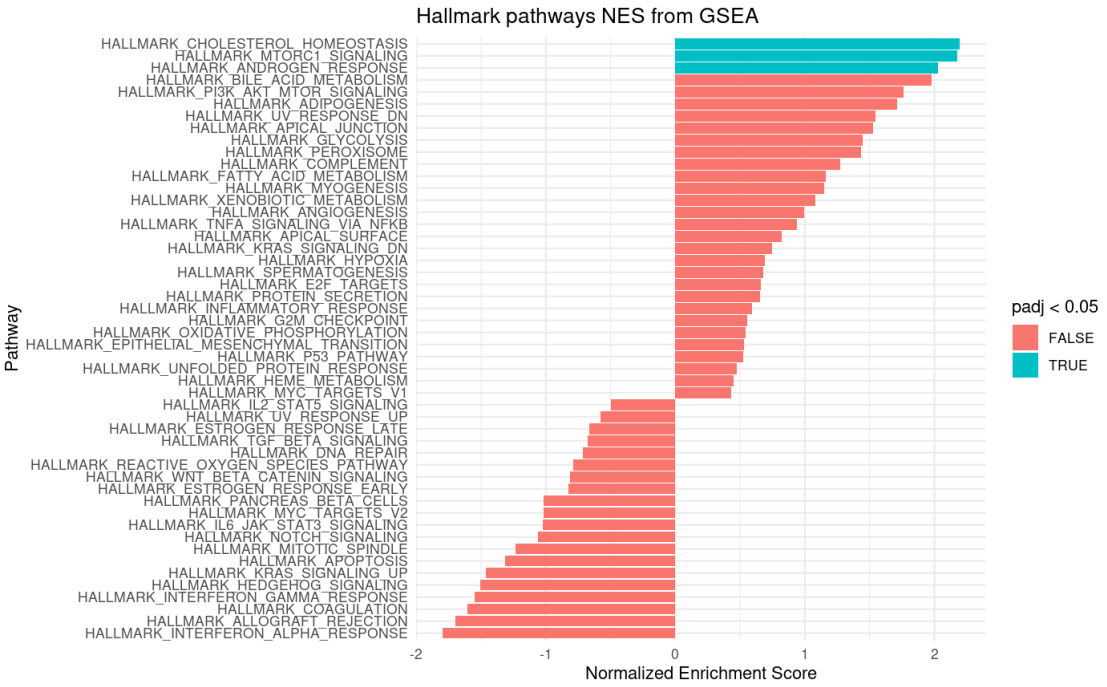

Figure 51 Gene set enrichment analysis of Hallmark pathways in adipocytes, including samples from patients containing skeletal myocytes

P values were corrected for multiple testing using gprofiler2 by default (361)

Lining fibroblasts

Tissue inhibitor of metalloproteinases 1 (*TIMP1*), *NALF1* and neuroligin 4 X-Linked (*NLGN4X*) were significantly downregulated in lining fibroblasts (Figure 52, Figure 53).

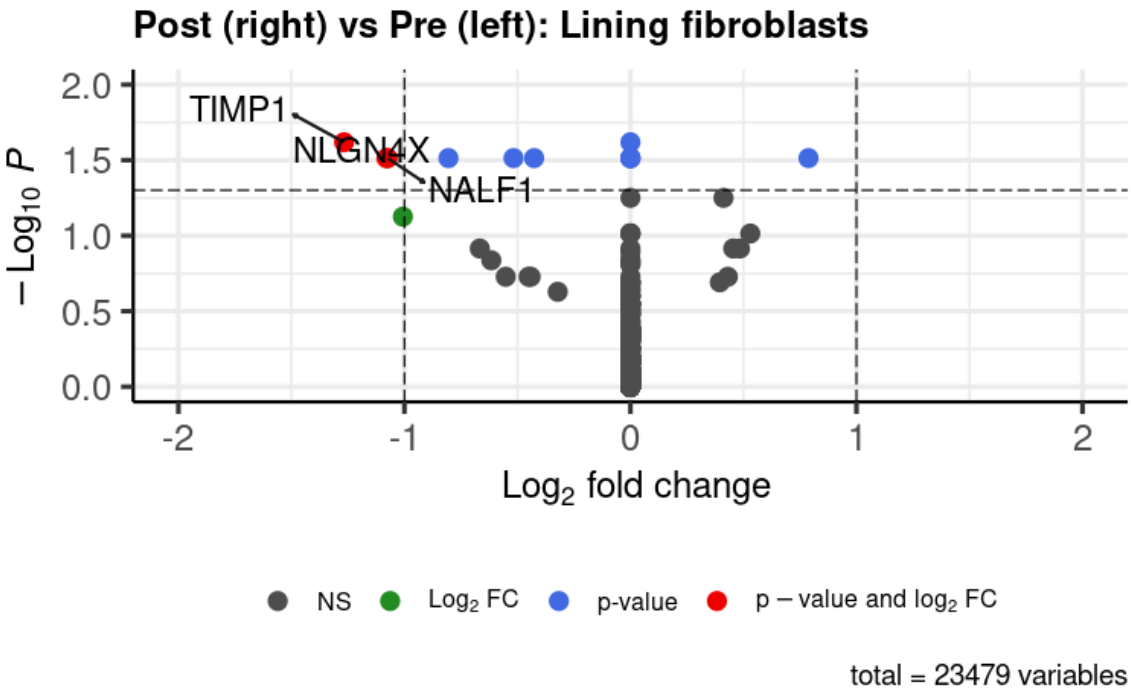

Figure 52 Volcano plot of differentially expressed genes in lining fibroblasts pre- and post- intra-articular methylprednisolone injection, including samples from patients containing skeletal myocytes (n = 8; 4 RA and 4 PsA)

P values were corrected for multiple testing using the Benjamini and Hochberg method in DESeq2 by default (270, 272).

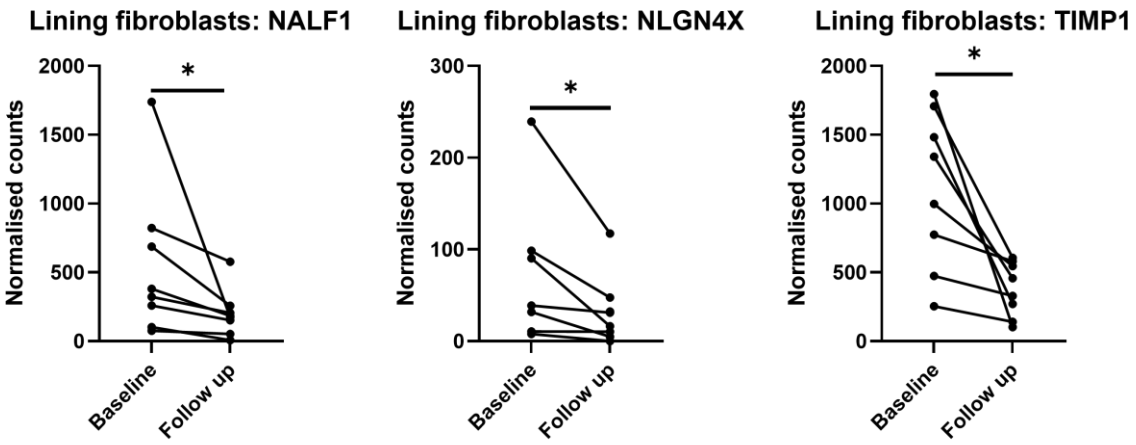

Figure 53 NALF1, NLGN4X and TIMP1 gene expression in lining fibroblasts at baseline and follow-up after intra-articular methylprednisolone injection, including samples from patients containing skeletal myocytes (n = 8; 4 RA and 4 PsA)

** denotes padj < 0.05 by DESeq2 analysis of pseudobulked data. P values were corrected for multiple testing using the Benjamini and Hochberg method in DESeq2 by default (270, 272).*

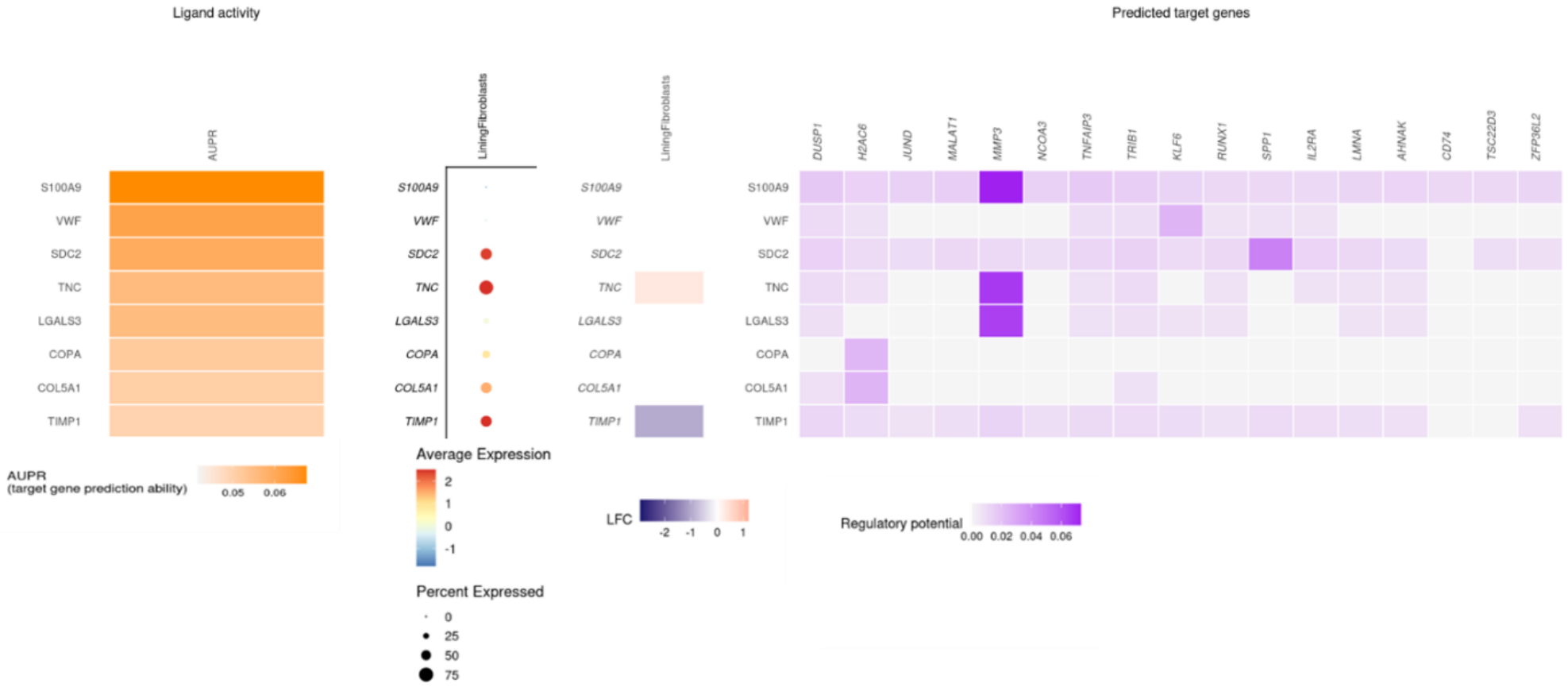

Figure 54 Plot of ligand activities, expression, differential expression and predicted target genes of ligands in lining fibroblasts by nichenet analysis

I applied nichenet to model how cell-cell communication in synovial tissues is perturbed by intra-articular methylprednisolone injection (362). This analysis included samples from patients containing skeletal myocytes because the differential gene expression was supported by ground truth, i.e. independent studies also found downregulation of *TIMP1* with intra-articular methylprednisolone injection (329, 334). Although there were diverse cell-cell communication changes predicted by nichenet, only the predicted *TIMP1* perturbation in lining fibroblasts was supported by statistically significant differential gene expression (padj < 0.05, absolute log fold change > 1) (Figure 52, Figure 53, Figure 54). This perturbation in *TIMP1* expression synovial lining fibroblasts was predicted to target genes including Dual Specificity Phosphatase 1 (*DUSP1*), H2A Clustered Histone 6 (*H2AC6*), JunD proto-oncogene (*JUND*), matrix metalloproteinase 3 (*MMP3*), Nuclear receptor Coactivator 3 (*NCOA3*), TNF induced protein 3 (*TNFAIP3*), Krueppel-like factor 6 (*KLF6*), Runt-related transcription factor 1 (*RUNX1*), secreted phosphoprotein 1 (*SPP1*), IL-2 receptor subunit alpha (*IL2RA*), lamin A/C (*LMNA*), neuroblast differentiation-associated protein (*AHNAK*) and zinc finger protein 36 C3H1 Type-Like 2 (*ZFP36L2*) (Figure 54). These predicted target genes of TIMP-1 were found to be expressed in synovial tissues, except for *ZFP36L2* (Figure *55*).

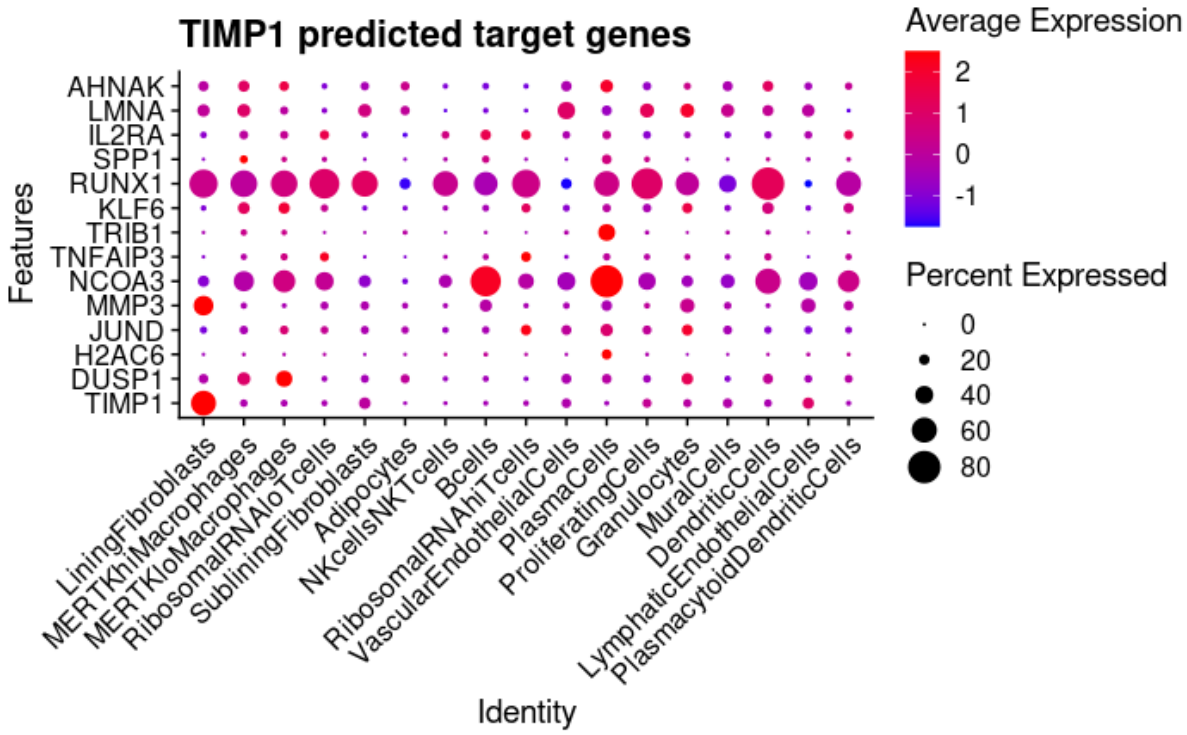

Figure 55 Dotplot of expression of TIMP-1 predicted target genes

Sublining fibroblasts

In the analysis including samples containing skeletal myocytes, there was a trend towards reduction in sublining fibroblasts expression of *NALF1* and *ITGB8* after intra-articular methylprednisolone injection but this was not statistically significant, in contrast to the analysis excluding samples containing skeletal myocytes (Supplementary Figure 6, Supplementary Figure 7).

4.3.8 Intra-articular methylprednisolone injection effects in RA and PsA subgroups

Having reviewed the perturbation effects across both disease groups, I went on to analyse perturbation effects in individual disease subgroups. As biopsy samples from two of the

participants with RA contained skeletal myocytes, exclusion of samples from participants with skeletal myocytes would mean there would not be samples from at least 3 participants with RA for subgroup analysis. This exploratory analysis of intra-articular methylprednisolone injection effects in RA and PsA subgroups therefore included all samples from participants including those that contained skeletal myocytes. There were scant differentially expressed genes in RA and PsA subgroups in cell types other than lining fibroblasts (*Supplementary Table 2*). Subgroup analysis of RA group showed no differentially expressed genes in lining fibroblasts with treatment (*Figure 56*), but there were differentially expressed genes in PsA lining fibroblasts with intra-articular methylprednisolone injection (*Figure 57*).

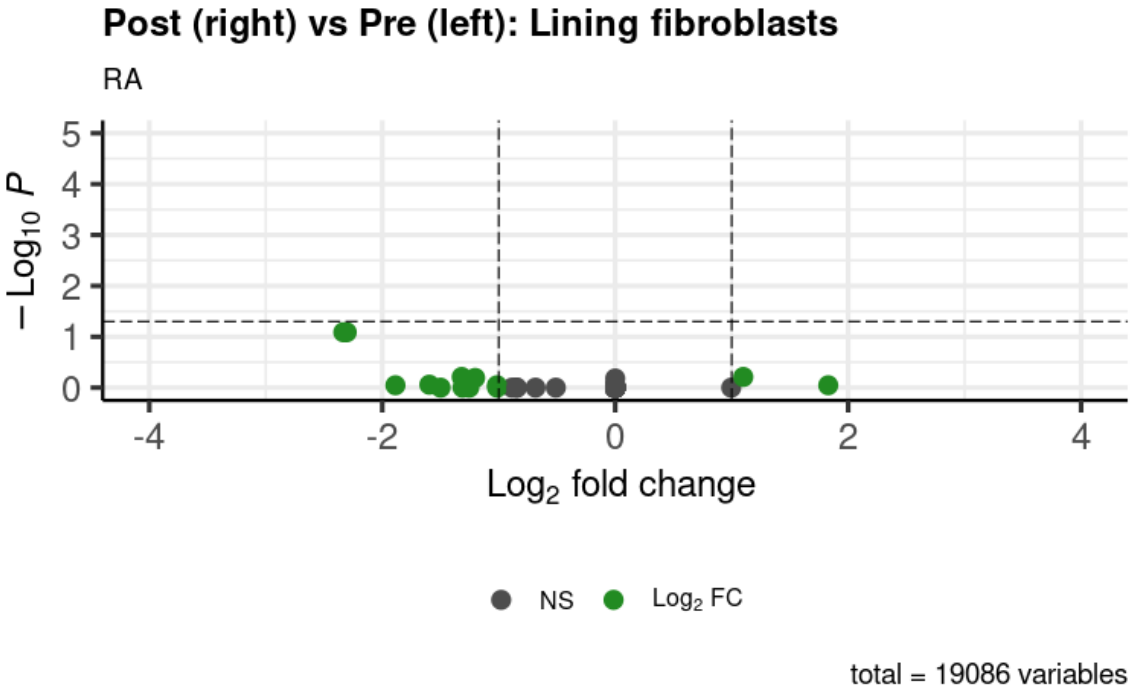

Figure 56 Volcano plot of differentially expressed genes in RA patients in lining fibroblasts after vs before intra-articular methylprednisolone injection (n = 4)

P values were corrected for multiple testing using the Benjamini and Hochberg method in DESeq2 by default (270, 272).

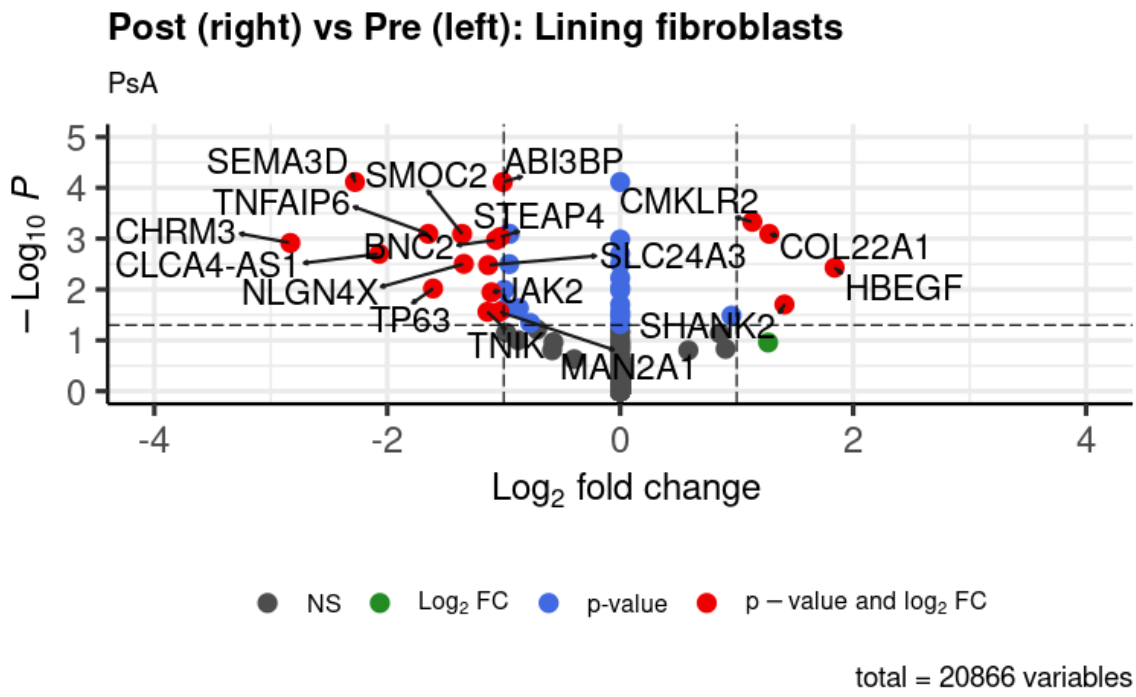

Figure 57 Volcano plot of differentially expressed genes in PsA patients in lining fibroblasts after vs before intra-articular methylprednisolone injection (n = 4)

P values were corrected for multiple testing using the Benjamini and Hochberg method in DESeq2 by default (270, 272).

4.3.9 Exploratory subgroup comparison of RA and PsA synovial tissue snRNA-seq profiles

Exploratory subgroup comparison of RA versus PsA was performed with the caveat that results may be confounded by other factors such as disease type, disease stage, age, gender, comorbidities and medications. Synovial tissue biopsy samples including those containing skeletal myocytes were included in the analysis, but skeletal myocytes were excluded because they originate from outside the joint capsule and their multinucleated nature is unsuitable for analysis with scProportionTest. In the pre-treatment samples, there were more adipocytes, ribosomal RNA high T cells, NK/NKT cells, B cells and mural

cells in RA, whereas PsA synovium had more lymphatic endothelial cells and plasmacytoid dendritic cells (Figure 58). The increased abundance of lymphatic endothelial cells in PsA synovium persisted even in the post-injection analysis (Figure 59).

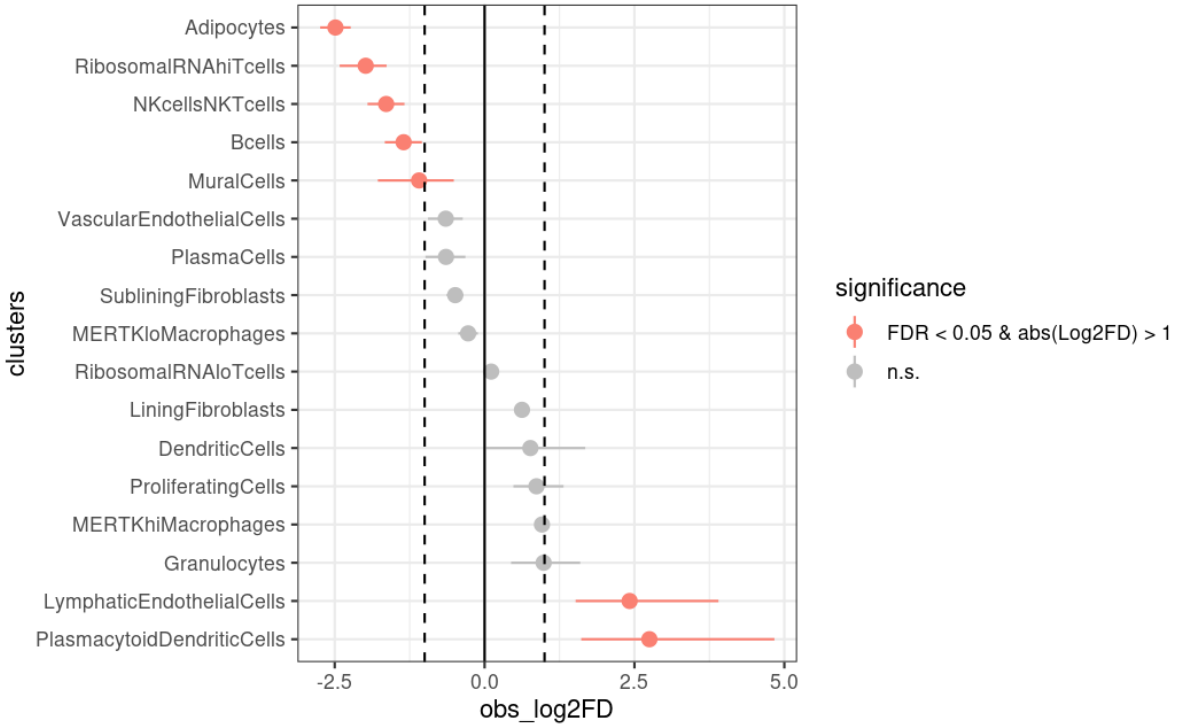

Figure 58 Differential cellular proportions in pre-treatment RA (left) and PsA (right) synovial tissues

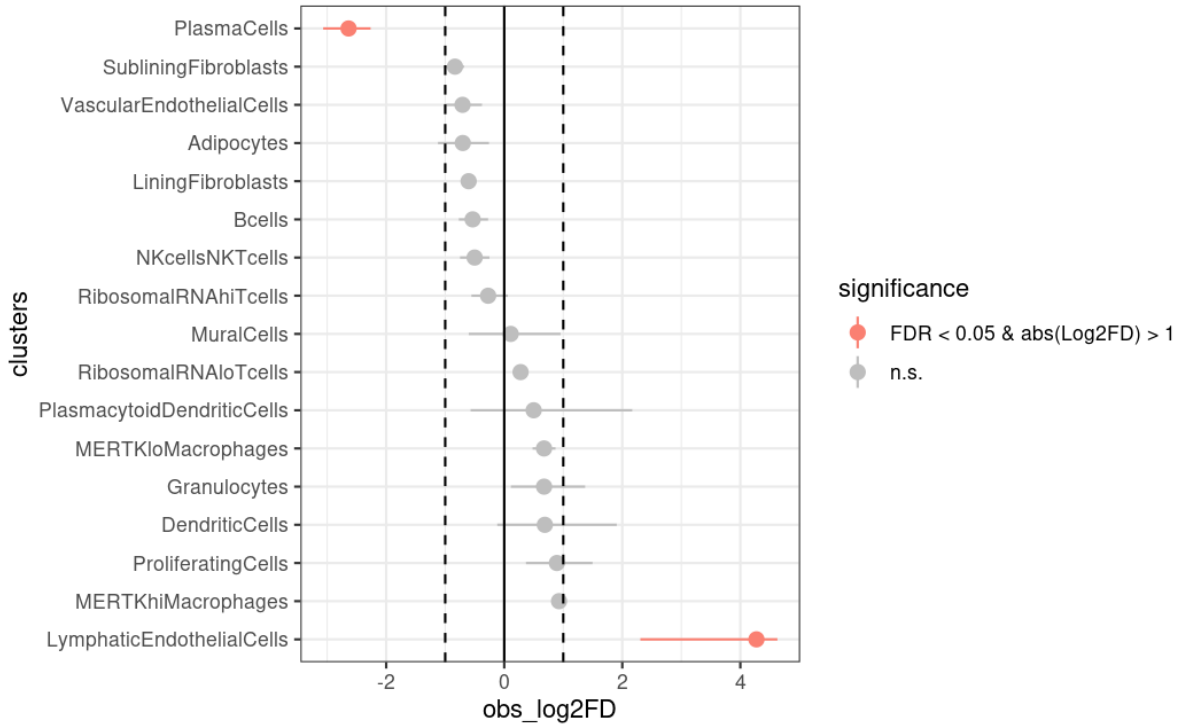

Figure 59 Differential cellular proportions in post-treatment RA (left) and PsA (right) synovial tissues

Differential gene expression analysis showed most differentially expressed genes between PsA and RA synovial tissue were in pre-treatment lining fibroblasts (Supplementary Table 3, Figure 60), but these were not present after glucocorticoid treatment (Figure 61). In pre-treatment lining fibroblasts, 27 genes were upregulated in RA and 56 genes were upregulated in PsA (padj < 0.05, log2FoldChange > 1) (Figure 60). Strikingly in pre-treatment lining fibroblasts, matrix Gla protein (*MGP*) was upregulated in RA and bone morphogenetic protein-binding endothelial cell precursor-derived regulator (*BMPER*) was upregulated in PsA with the lowest padj values (Figure 60).

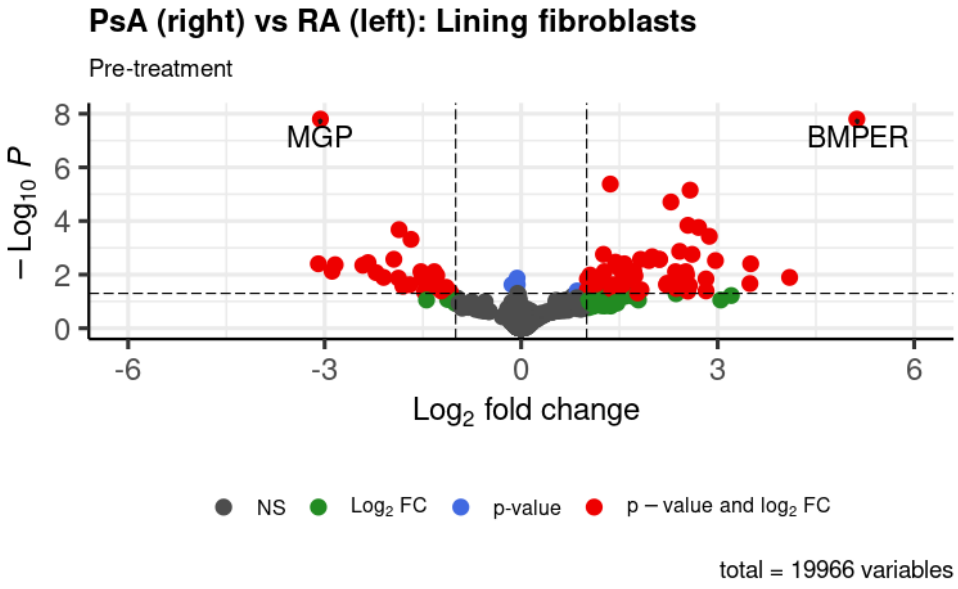

Figure 60 Differential gene expression in pre-treatment lining fibroblasts in RA and PsA (RA: n = 4; PsA: n = 4)

P values were corrected for multiple testing using the Benjamini and Hochberg method in DESeq2 by default (270, 272).

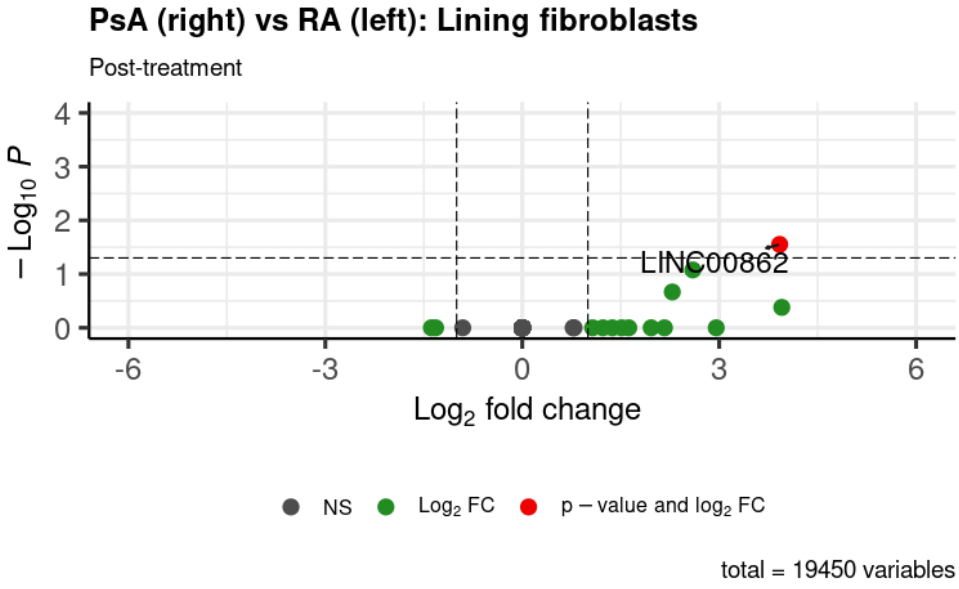

Figure 61 Differential gene expression in post-treatment lining fibroblasts in RA and PsA (RA: n = 4; PsA: n = 4)

P values were corrected for multiple testing using the Benjamini and Hochberg method in DESeq2 by default (270, 272).

Although *MGP* was upregulated in RA compared to PsA in pre-treatment lining fibroblasts, the trend towards increase in *MGP* in PsA after intra-articular methylprednisolone injection may account for the lack of difference seen between PsA and RA in post-treatment samples (Figure 62). Similarly, although *BMPER* was upregulated in PsA compared to RA in pre-treatment lining fibroblasts, the reduction in *BMPER* in PsA after treatment may account for the lack of inter-disease differences in post-treatment samples (Figure 63). Over-representation analysis using g:Profiler showed upregulated gene pathways in pre-treatment synovial tissue lining fibroblasts in PsA compared to RA (Table 13).

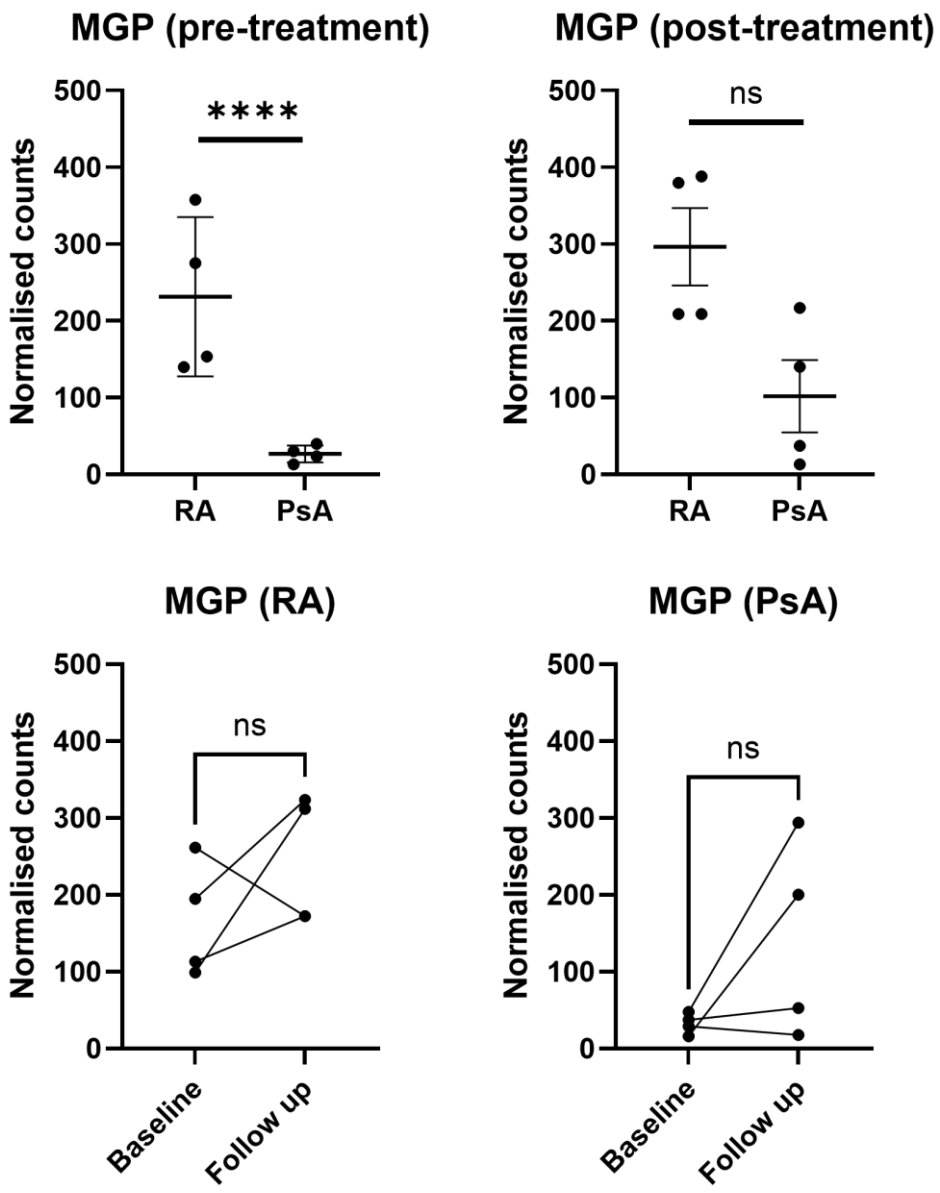

Figure 62 Comparison of lining fibroblast MGP gene expression across disease and treatment status.

***** denotes adjusted P value < 0.0001 and ns denotes non-statistically significant by DESeq2 analysis of pseudobulked data. P values were corrected for multiple testing using the Benjamini and Hochberg method in DESeq2 by default (270, 272).*

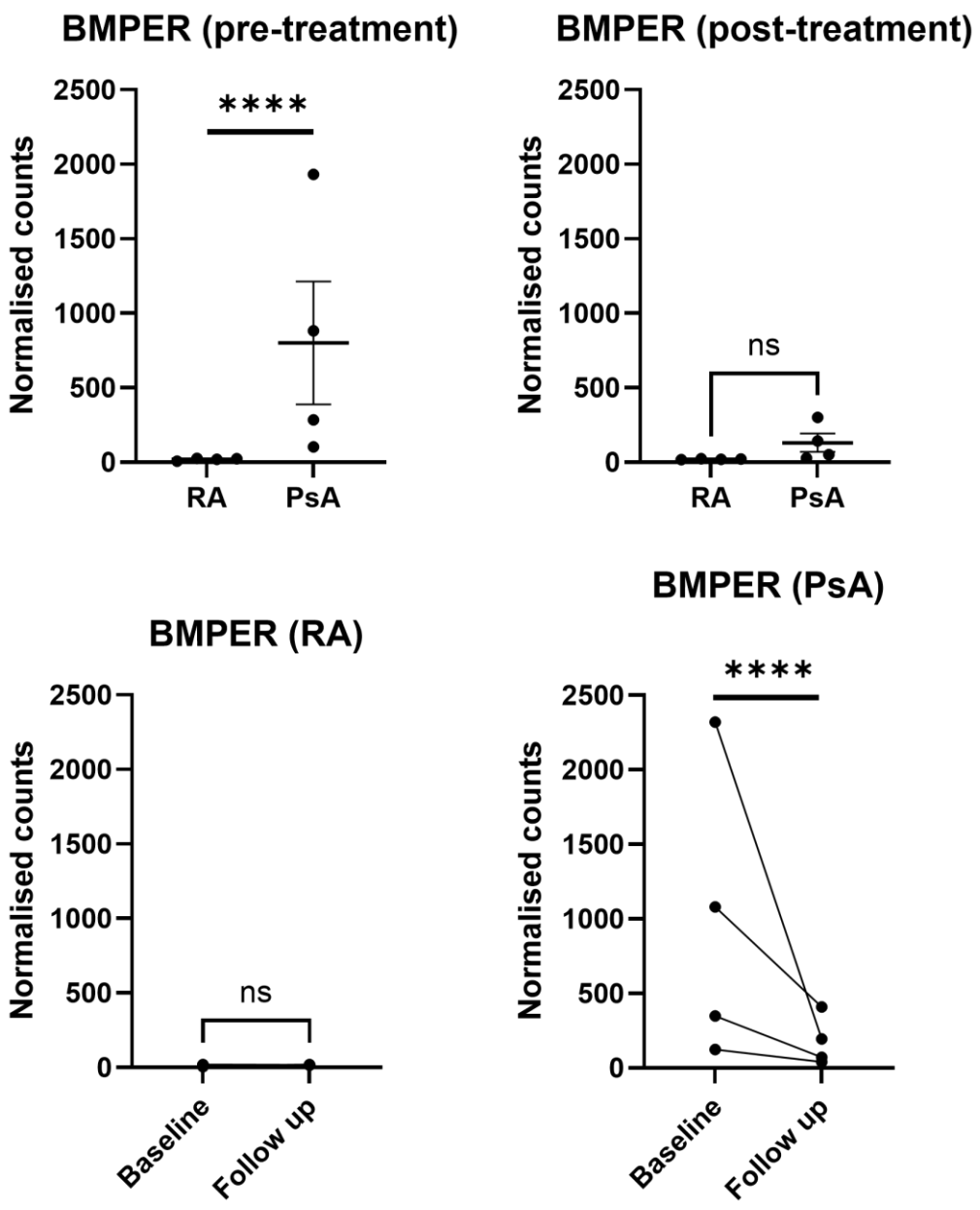

Figure 63 Comparison of lining fibroblast BMPER gene expression across disease and treatment status.

***** denotes adjusted P value < 0.0001 and ns denotes non-statistically significant by DESeq2 analysis of pseudobulked data. P values were corrected for multiple testing using the Benjamini and Hochberg method in DESeq2 by default (270, 272).*

Table 13 Over-representation analysis of upregulated gene pathways in PsA vs RA (pre-treatment synovial lining fibroblasts)

id	term_id	term_name		p_value
1	GO:0048731	system development		3.5e-06
2	GO:0007275	multicellular organism development		1.8e-04
3	GO:0007409	axonogenesis		3.2e-04
4	GO:0009653	anatomical structure morphogenesis		4.8e-04
5	GO:0048870	cell motility		6.4e-04
6	GO:0061564	axon development		1.0e-03
7	GO:0007399	nervous system development		3.5e-03
8	GO:0048667	cell morphogenesis involved in neuron differentiation		5.9e-03
9	GO:0048856	anatomical structure development		7.2e-03
10	GO:0048513	animal organ development		8.6e-03

g:Profiler (biit.cs.ut.ee/gprofiler)

4.3.10 Cell-cell communication in pre-treatment RA and PsA synovial tissues

CellChat is a computational tool to infer cell-cell communication from single cell transcriptomics data (357). Skeletal myocytes were excluded from cell-cell communication analysis as these originate from outside the joint capsule and their multinucleated nature is unsuitable for analysis with CellChat. There were similarities and differences in cell-cell communication patterns in pre-treatment RA and PsA synovial tissues (Figure 64, Figure 65, Supplementary Figure 9, Supplementary Figure 10, Supplementary Figure 11). For example, lining fibroblasts had the highest outgoing interaction strength in both RA and PsA (Figure 65). A striking difference was the greater signalling role of B cells and plasma cells in RA compared to PsA (Figure 64, Figure 65). This is in keeping with RA being distinguished for the role of adaptive immune system and seropositivity for RF and anti-CCP Ab. Conversely, there were more, and stronger interactions sent by lymphatic endothelial cells to other cell types in PsA compared to RA (Figure 64, Figure *65*).

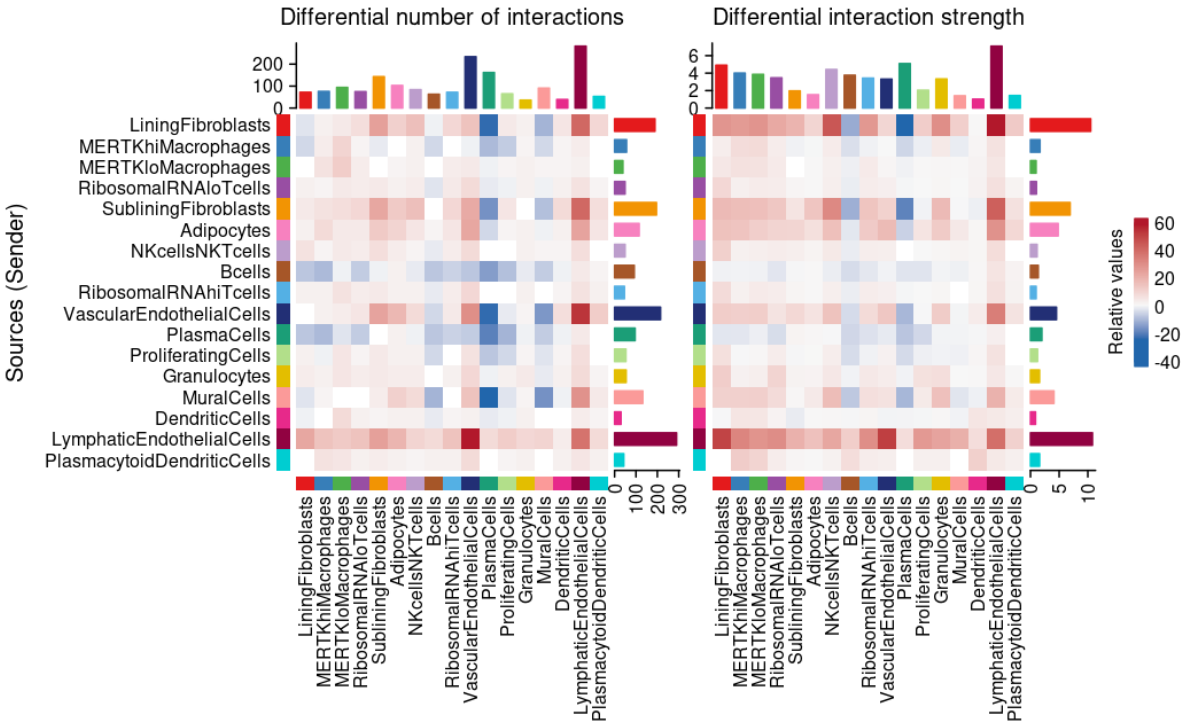

Figure 64 Heatmap of differential number of interactions and differential interaction strength in PsA vs RA synovial tissues (pre-treatment), with RA set as the reference

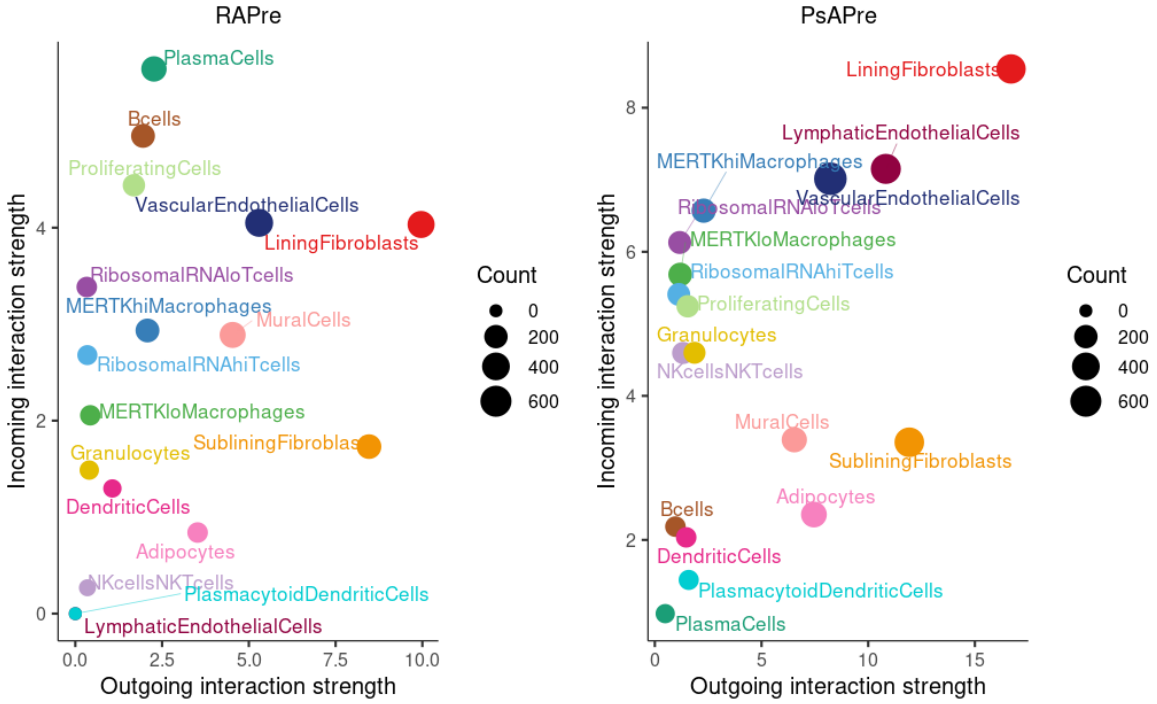

Figure 65 Scatter plot of sending and receiving signal strengths in pre-treatment RA (left) and PsA (right) synovial tissues

4.4 Discussion

4.4.1 Synovial tissue snRNA-seq profiles

Bulk sequencing of tissues results in cell-averaged expression profiles which misses the complexity of cell expression profile heterogeneity and changes in cell composition in response to treatment (363). snRNA-seq allows examination of gene expression at a single nucleus level to reveal states of heterogeneous cell populations. As expected, most cell clusters identified resembled those from previous single cell studies. For example, synovial fibroblasts subsets were easily distinguished by chloride intracellular channel protein 5 (*CLIC5*) (lining fibroblasts) and Thy-1 cell surface antigen (*THY1*) (sublining fibroblasts). Similarly, tissue resident and tissue infiltrating synovial macrophages were easily distinguished by the expression level of MER proto-oncogene tyrosine kinase (*MERTK*).

Some cell types such as adipocytes and myocytes are challenging to identify with scRNA-seq. Adipocytes as large buoyant cells are not easily identified with scRNA-seq. Skeletal myocytes are multinucleated cells. Identifying the cell origin of a nucleus in snRNA-seq studies is currently unfeasible and can result in biasing of sequencing data towards multinucleated cells (364). The large size of myocytes presents a challenge in droplet generation (364). The advantage of scRNA-seq over scRNA-seq is that snRNA-seq does not require preservation of cellular integrity during sample preparation such as dissociation (365). snRNA-seq here readily identified adipocytes and skeletal myocytes that otherwise would not be seen with scRNA-seq.

snRNA-seq analysis of synovial tissues from RA patients have previously been performed (366). The absence of myocytes and adipocytes in the study by Gupta *et al*. may be due to tissue disaggregation or their synovial tissues arising from surgical specimens instead of

ultrasound guided synovial tissue biopsies (366). My study was the first reported snRNA-seq study of longitudinal analysis of ultrasound guided synovial tissue needle biopsy from RA and PsA patients before and after intra-articular methylprednisolone injection. Ultrasound guided synovial tissue needle biopsy in my study was performed without a coaxial needle. In future, use of an outer coaxial needle may reduce trauma and accidental collection of skeletal myocytes.

4.4.2 Intra-articular methylprednisolone injection effects on cellular proportion of synovial tissues

After intra-articular methylprednisolone injection, the adipocyte cell proportion in synovial tissues was reduced whereas there was an increase in NK/NKT cells and ribosomal RNA high T cells (Figure 47). Although samples from patients with skeletal myocytes were excluded from cell proportion analysis to reduce confounding by extra-articular cells, there may nonetheless still be cells present from extra-articular tissues such as adipocytes from extra-articular fat pad.

The reduction in synovial tissue adipocyte cell proportion with intra-articular methylprednisolone injection is unsurprising given that decreased adipose tissue mass has been linked to glucocorticoids and associated lipolysis (367). The reduction in synovial tissue adipocytes may be a manifestation of the fat redistribution from the extremities to the trunk and the neck seen in Cushing syndrome. Acute exposure to glucocorticoids promotes lipolysis but chronic glucocorticoid exposure induces lipogenesis in adipocytes (367-369). While acute activation of glucocorticoid receptors stimulates lipolysis in adipose tissues, activation of mineralocorticoid receptors promotes adipogenesis, which together account for divergent lipid responses to glucocorticoids in adipose tissues (367,

368). Activation of glucocorticoid receptor-α leads to its phosphorylation, dissociation from HSP90, nuclear translocation, and binding to the GRE to upregulate transcription of lipolysis genes including adipose triglyceride lipase (*ATGL*) and *ANGPTL4*, and downregulate lipogenic genes such as phosphodiesterase 3B (*PDE3B*) (367). These effects increase cellular cyclic adenosine monophosphate and activate protein kinase A (PKA). Activated protein kinase A in turn phosphorylates hormone-sensitive lipase (HSL) and perilipins which result in lipid breakdown into glycerol and fatty acids (370, 371). Conversely, lipogenesis is mediated by glucocorticoids through induction of glucocorticoid resistance by the glucocorticoid receptor-β isoform and activation of the mineralocorticoid receptor (367).

Given that samples containing extra-capsular tissues such as skeletal muscle were excluded from this analysis, the reduction in synovial tissue adipocytes after intra-articular methylprednisolone injection likely reflects the changes in synovial tissue composition, in concordance with known glucocorticoid induced lipolysis effects. However, a limitation is that the cellular and molecular changes in adipocytes may be an artefact of extra-articular fat pad adipocytes being present in biopsy samples. The perturbation in cellular proportions could have been confirmed histologically if there were sufficient biopsy fragments remaining. However, the vast majority of the synovial tissue biopsy fragments were used for snRNA-seq analysis rather than for histological analysis. In hindsight, this turned out to be a fortunate decision as the droplet generation for snRNA-seq was affected by clogging which reduced the number of nuclei available for sequencing (Figure 43). If I had reserved more tissue biopsy fragments for confirmatory histology, the snRNA-seq analysis would have been compromised. As the snRNA-seq analysis was of greater priority, it was appropriate to process most of the synovial tissue fragments for snRNA-seq

rather than histology. As there were fewer than 4 fragments embedded in OCT from each synovial tissue biopsy, there are insufficient tissue fragments to ensure representativity of confirmatory histological analysis (372). A minimum of 6 fragments and the assessment an area of tissue of at least 2.5 mm^2 are necessary for histological analysis to be representative (373, 374). Therefore, the effects of intra-articular methylprednisolone injection on synovial tissue cell proportions need to be validated in a larger independent cohort using histological analysis, to confirm that synovial tissue adipocytes proportion is reduced by glucocorticoid. The distance between the synovial tissue lining and extra-articular fat pad may be a challenge to prove histologically that adipocytes are not intra-articular in origin because the synovial tissue lining, joint capsule and extra-articular fat pad would need to be visualised on the same slide.

Contrary to the reduction in synovial tissue adipocyte cell proportion, there was an increase in proportion of NK/NKT cells and ribosomal RNA high T cells in synovial tissues after intra-articular methylprednisolone injection (Figure 47). NK cells are cytotoxic lymphocytes that play a critical role in the innate immune response (375). Healthy joints contain few NK cells but abundant NK cells are found in inflamed joints in patients with RA and in mice with collagen-induced arthritis (376, 377).

Although glucocorticoids are widely known to suppress NK cell proliferation and cytokine production, they can also have a dichotomic effect on NK cells dependent on the local cytokine milieu (378-380). Indeed, glucocorticoids have also been shown to enhance the proliferation, survival and function of NK cells (379, 380). It is therefore intriguing to see an increase in the proportion of NK/NKT cells in synovial tissues after intra-articular methylprednisolone injection (Figure 47). Whilst previous reports of glucocorticoid

enhancing NK cell proliferation and survival may be congruent with my finding of increased proportion of synovial tissue NK/NKT cells, this finding needs to be confirmed in a larger independent cohort to establish the effects on intra-articular methylprednisolone injection on NK cells. If independent studies confirm an increase in synovial tissue NK/NKT cells after intra-articular methylprednisolone injection, future mechanistic studies would be helpful to investigate whether this increase is due to early effects of methylprednisolone or late effects of rebound reaction from methylprednisolone withdrawal.

Like NK/NKT cells, the proportion of ribosomal RNA high T cells in synovial tissues was also increased after intra-articular methylprednisolone injection (Figure 47). A concomitant trend towards increase in the proportion of ribosomal RNA low T cells suggests that there is an expansion of T cell numbers, rather than upregulation of ribosomal RNA transcription across T cells with reciprocal reduction in proportion of transcriptionally inactive T cells. Glucocorticoids are widely known to suppress and induce apoptosis in immune cells such as T cells (236, 381). However, glucocorticoids have also been reported to increase T cell populations (382-384).

In patients with sudden hearing loss without underlying inflammatory disease, high-dose intravenous prednisolone followed by oral prednisolone resulted in T cell lymphocytosis (385). Moreover, systemic glucocorticoid treatment in patients with asthma or relapse of multiple sclerosis increased the absolute number of Tregs in blood (384, 386). Both *in vitro* and *in vivo* studies of glucocorticoids demonstrate that glucocorticoids may induce expansion of T cell populations particularly in the context of inflammation (382-385, 387, 388).

It is therefore plausible that intra-articular methylprednisolone injection increased the proportion of transcriptionally active T cells in synovial tissues (Figure 47). The phenotypes of the expanded T cell populations require further investigation using techniques such as flow cytometry in a larger independent cohort to confirm and delineate whether glucocorticoid related T cell expansion in synovial tissues may be due to steroid withdrawal. Having evaluated the effects on cell proportion, I went on to investigate the perturbation effects of intra-articular methylprednisolone injection on gene expression.

4.4.3 Differential gene expression in synovial tissue fibroblasts after intra-articular methylprednisolone injection

NALF1

After intra-articular methylprednisolone injection, *NALF1* was downregulated in synovial sublining fibroblasts when samples containing skeletal myocytes were excluded (Table 10, Figure 48), and also in synovial lining fibroblasts when samples containing skeletal myocytes were included (Table 11, Figure 52). *NALF1* encodes an auxiliary component of the sodium leak channel non-selective (NALCN) sodium channel complex, a non-selective cation channel that regulates the resting membrane potential and excitability of neurons (389). *NALF1* has been shown to be a marker of activated sublining fibroblasts in RA (390). The downregulation of *NALF1*, a marker of activated sublining fibroblasts, is therefore congruent with anti-inflammatory treatment in the form of intra-articular methylprednisolone injection.

Furthermore, downregulation of *NALF1* may have important implications for the analgesic effects of intra-articular methylprednisolone injections. NALF1 is a pore-forming

subcomplex that regulate the gating of NALCN (391). In turn, the NALCN has been shown to contribute to neuronal sensitisation in neuropathic pain (392-394). This study therefore provides important novel insights into *NALF1* as a biomarker of treatment. Moreover, it generates the hypothesis as to whether *NALF1* expressing fibroblasts may be targeted therapeutically to treat pain and inflammation in inflammatory arthritis. A larger independent cohort is required to delineate whether intra-articular methylprednisolone downregulates *NALF1* in synovial lining and sublining fibroblasts, as downregulation was not consistent in analysis with and without samples from patients containing skeletal myocytes which may be due to the very small sample size (Supplementary Figure 6, Supplementary Figure 8).

ITGB8

As well as *NALF1*, the expression of *ITGB8* was also downregulated in sublining fibroblasts after intra-articular methylprednisolone injection when samples from patients containing skeletal myocytes were excluded (Table 10, Figure 48). *ITGB8* encodes a single-pass type I membrane protein with a von Willebrand factor type A domain and four cysteine-rich repeats (395). ITGB8 protein noncovalently binds to an alpha subunit to form integrin alpha-V:beta-8 (ITGAV:ITGB8), a receptor for fibronectin (396). The role of ITGB8 in extracellular matrix protein binding has been shown to be relevant in many functions including cell adhesion, cell invasion, angiogenesis and chondrogenesis (397-399). Although the analysis including samples from patients containing skeletal myocytes did not find a statistically significant difference in *ITGB8* expression after intra-articular methylprednisolone injection, this may be due to confounding by the presence of extra-articular fibroblasts (Supplementary Figure 7). The exploratory finding of *ITGB8* downregulation in sublining fibroblasts by intra-articular methylprednisolone is supported

by *in vitro* evidence of *ITGB8* downregulation in mesenchymal derived cells by methylprednisolone (300). The therapeutic perturbation of *ITGB8* in sublining fibroblasts highlights an unmet need for research into the role of *ITGB8* in the underlying pathogenesis of inflammatory arthritis and its potential as a therapeutic target.

TIMP1

Analysis of snRNA-seq data from 8 participants demonstrated that *TIMP1* transcription was persistently suppressed at four weeks in inflammatory arthritis synovial lining fibroblasts after intra-articular methylprednisolone injection (Figure 53). As the lining fibroblasts are most likely to be from the synovial tissue lining, even the inclusion of samples containing skeletal myocytes would not confound the differential gene expression analysis in lining fibroblasts. Previous studies showed that *TIMP* RNA and TIMP-1 protein levels were reduced in RA synovium up to two weeks after glucocorticoid treatment (329, 334). The downregulation of TIMP-1 by glucocorticoid may be specific to inflammatory arthritis as no difference in TIMP-1 immunostaining was observed for OA synovium after intra-articular methylprednisolone injection (328). The consistent finding of *TIMP1* downregulation in this snRNA-seq study with ground truth in previous studies reinforce the findings in this study (329, 334). Curiously, previous *in vitro* study showed *TIMP1* transcription in fibroblasts was not affected by methylprednisolone (300). The discrepancy between these *in vitro* and *in vivo* findings may be related to the follow-up timepoints (6 h vs 4 weeks) as well as the experimental context (*in vitro* cell culture of single cell type versus *in vivo* human arthritic joint). This demonstrated the limitations of *in vitro* experiments and the value of this *in vivo* therapeutic atlas.

Although TIMP-1 is known for its eponymous function to inhibit metalloproteinases which are widely understood to mediate joint tissue destruction, TIMP-1 also exhibits cytokine functions via interaction with cell surface receptors linked to inflammation (400). TIMP-1 has a metalloproteinase-inhibitor motif within the N-terminal domain, a CD63-binding C-terminal domain, which interacts with CD74 via its N-terminal domain (400). Diverse inflammatory cytokines including IL-1, IL-6, TNF upregulate *TIMP1* expression via transcription factors such as STAT-3, NF-κB and AP-1 (400). In my study, downregulation of *TIMP1* expression in synovial lining fibroblasts after intra-articular methylprednisolone may be due to its anti-inflammatory effects as evidenced by reduced IL-6 and TNF protein levels in PsA synovial fluid (Figure 35, Figure 37).

Elevated TIMP-1 levels are associated with worse prognosis in inflammatory diseases including cancer and infections (400). High circulating levels of TIMP-1 was associated with COVID-19 severity in patients (401). TIMP-1 activated neutrophils to release neutrophil extracellular traps (NETs) which was associated with COVID-19 progression (402, 403). It is therefore intriguing that perhaps *TIMP1* downregulation is one of the mechanisms by which glucocorticoid improves COVID-19 outcomes (404).

TIMP-1 has been shown to regulate diverse immune cell functions including T cells (anti-cytotoxic, anti-apoptotic), B cells (anti-apoptotic, pro-proliferative), neutrophils (anti-apoptotic, granulopoiesis, NET formation), macrophages (anti-angiogenic), dendritic cells (pro-migratory) and NK cells (anti-angiogenic) (400). Although the molecular mechanisms by which TIMP-1 mediates its effects on inflammation are poorly understood, TIMP-1 has been shown to interact with CD63, CD44 and CD74 to activate PI3K/AKT, ERK, HIF, p38 and ZAP70 signalling pathways (400).

In addition to immune functions, TIMP-1 also has a role in neuronal differentiation and plasticity (405). Neurons internalised TIMP-1 through low-density lipoprotein-related protein 1 (LRP-1) binding (406). This in turn inhibited neurite outgrowth and increased growth cone volume (406). This leads to speculation as to whether intra-articular methylprednisolone may relieve pain through TIMP-1 downregulation leading to neurite outgrowth inhibition. As the nuclei of neurons in synovial tissues lie in the dorsal root ganglion, even snRNA-seq is not able to capture information relating to neurons in synovial tissue biopsies. However, a recent study predicted cross-talk between synovial tissue lining fibroblasts with dorsal root ganglion neurons (407). This may account for the therapeutic effects of intra-articular methylprednisolone injection in both non-inflamed joints such as OA, as well as inflammatory arthritis. More investigations are needed to understand the role of TIMP-1 in pain modulation in setting of arthritis.

TIMP-1 binds to receptors CD63, CD74, CD82, LRP-1 and CD44 (408). CD63 is expressed ubiquitously whereas CD74 is restricted to lymphoid tissues and antigen presenting cells, indicating cell-type specific roles of TIMP-1 (400). Given that TIMP-1 may mediate pleiotropic effects including inhibition of metalloproteinases which may be protective in arthritis and pro-inflammatory effects through its cytokine role, targeting TIMP-1 receptors instead of TIMP-1 ligand directly may be a useful therapeutic strategy. Indeed, TIMP-1 receptor CD74 has been implicated in the pathogenesis of RA (409). Moreover, synovial tissue CD74 levels are higher in RA than OA (409). The p41 isoform of CD74 was also upregulated in affected paws of collagen-induced arthritis mice (409).

Given the roles of TIMP-1 in diseases, it is not surprising that its receptors have been targeted therapeutically. For example, milatuzumab is a monoclonal anti-CD74 antibody under investigation for treatment of B cell neoplasms (410). Since my study and others showed that glucocorticoids downregulate *TIMP1* in inflamed synovial tissues, it would be intriguing to see if targeting the TIMP-1 pathway with receptor antagonists such as milatuzumab, or antibodies against the C-terminal CD63-interacting domain of TIMP-1, may be efficacious in inflammatory arthritis without glucocorticoid associated adverse effects (411). A Phase 1b study of milatuzumab in systemic lupus erythematosus (SLE) showed some promise but the double-blind, placebo-controlled expansion phase to test efficacy was terminated early due to poor enrolment (412). CD74 has not been specifically targeted yet in inflammatory arthritis so the TIMP-1 pathway remains a potential therapeutic target of interest.

Although previous studies have shown that synovial tissue TIMP-1 was downregulated by glucocorticoid, the effects of TIMP-1 downregulation in synovial tissues were unknown. The power of single cell transcriptomic analysis is that it allows modelling of cell-cell communication. Using nichenet, I demonstrated that *TIMP1* downregulation in lining fibroblasts was predicted to target diverse range of genes including *DUSP1*, *H2AC6*, *JUND*, *MMP3*, *NCOA3*, *TNFAIP3*, *KLF6*, *RUNX1*, *SPP1*, *IL2RA*, *LMNA*, *AHNAK* and *ZFP36L2* (Figure 54). My dataset did not show significant changes in these TIMP-1 predicted target genes with treatment which may be due to other effects of intra-articular methylprednisolone injection and late follow-up timepoint. Future studies of TIMP-1 specific perturbation, such as TIMP-1 receptor monoclonal antibody inhibitor, would help delineate the role of TIMP-1 in the inflammatory arthritis synovial microenvironment.

4.4.4 Intra-articular methylprednisolone injection upregulated lipogenesis in adipocytes

The most striking effects of intra-articular methylprednisolone injection were reduction in adipocyte cell proportion and upregulation in lipogenesis by adipocytes (Figure 47, Table 11, Figure 49, Figure 51, Table 12). Lipogenesis is the conversion of acetyl-CoA into lipids, which occurs mainly in adipose and liver tissues. Initial analysis excluding samples from 3 participants containing skeletal myocytes showed no differential gene expression in adipocytes (Table 10), but exploratory analysis including all samples showed lipogenesis upregulation in adipocytes (Table 11, Figure 49, Table 12, Figure 51). The role of glucocorticoids in regulation of lipid metabolism has been reviewed previously (367, 413, 414).

Synovial tissues are known to contain adipocytes which store energy and have endocrine functions that regulate tissue metabolism (315). Recently, the Brenner group demonstrated that adipocytes regulate fibroblast function through cortisol signalling, and loss of adipocytes contributes to fibroblast dysfunction in inflammatory arthritis (415). I speculate that the reduction in synovial tissue adipocyte proportion with intra-articular methylprednisolone injection may contribute to the reactive flare that may begin 12 h after injection and resolve spontaneously after 3 days (416). A follow-up study with post-injection synovial tissue biopsy at an earlier timepoint such as 24 h would allow investigation of the mechanisms that cause glucocorticoid post-injection flare (417, 418).

Synovial metabolic perturbation by intra-articular methylprednisolone injection may affect the HIF pathway. For example, HIF1-α is stabilised by the accumulation of succinate, a key metabolite involved in many metabolic pathways (173). Succinate is abundant in

synovial fluids from patients with inflammatory arthritis, and these fluids elicit IL-1β release from macrophages which is dependent on succinate receptor 1 (SUCNR1), a sensor for extracellular succinate (150). Glucocorticoids have been shown to repress glycolysis in inflammatory myeloid cells and promote TCA cycle flux, promoting succinate metabolism and preventing intracellular accumulation of succinate (151, 419). Therefore, it is plausible that intra-articular methylprednisolone injection may impact the hypoxic pathway mediated by HIF-1α through succinate metabolism. Future studies of synovial tissues incorporating snRNA-seq with single cell metabolomics would provide insight into the role of metabolites as drivers and targets in inflammatory arthritis (173).

Lipid metabolism is regulated by pathways involving peroxisome proliferator-activated receptors (PPAR), liver X receptors (LXR) and SREBPs (173). SREBPs are encoded by *SREBF1* and *SREBF2*, and are master regulators of lipid biogenesis that are known to be upregulated by glucocorticoids (420). The trends toward increase in *SREBF1* and *SREBF2* expression in adipocytes after intra-articular methylprednisolone injection were not statistically significant (Figure 50). Not all synovial tissue biopsies captured adipocytes and the missing data that arose from this may have caused statistical analysis to be underpowered to look for a perturbation in *SREBF1* and *SREBF2*. Moreover, any differential expression in *SREBF1* and *SREBF2* genes in synovial adipocytes may have resolved at 4 weeks after intra-articular methylprednisolone injection, whereas an earlier follow-up may show statistically significant differential expression of *SREBF1* and *SREBF2* genes. SREBPs regulate triglyceride synthesis and cholesterol biogenesis. The upregulation of lipogenesis genes downstream of SREBPs implicate SREBPs in the adipocyte response to intra-articular methylprednisolone injection.

Lipids have structural and functional roles in maintaining cellular homeostasis (341). Both pro- and anti-inflammatory lipids are involved in the pathogenesis of arthritis (314). The lipidome profile in RA joint fluid is severely perturbed and this correlates with the extent of inflammation and severity of synovitis on ultrasound (421). Arthritis treatments such as hydroxychloroquine, methotrexate and biological therapies have beneficial effects on lipid metabolism, and it has been suggested that lipids are involved with pathogenesis of arthritis (422). Indeed, lipid metabolites have been shown to have functional relevance in RA and PsA (Figure 66) (173).

	Normal Role/Function	Rhuematoid Arthritis (RA)	Psoriatic Arthritis (PsA)
PPARγ	Nuclear receptor Molecular sensor of FAs and FA derivatives	↓Expression in synovial tissue Activation => modest decrease in disease	Activation showed amelioration in clinical disease
Pioglitazone	PPARγ agonist	↓Disease activity	↓Disease activity
LXR	Receptor Regulate intracellular cholesterol and lipid homeostasis	↑ Expression in RA SF macrophages ↑ regulates MERTK in macrophages, promoting phagocytosis ↓ Expression of IL-1β, IL-6, CXCL10, and MMP-3 in RAFLS	
Oxysterol	Cholesterol metabolite Works with LXR to regulate intracellular cholesterol and lipid homeostasis	Enriched in RA SF Potentiate DAMP induced IL-6, TNFα, and IL-1β	
SREBP	Transcription Factor in FA metabolism Activation assists fulfilling increased lipid requirements of T cells during blastogenesis	↑Inflammation activation in macrophages	
PUFA	Polyunsaturated fatty acids and their derived oxylipin metabolites	↑ Concentrations of eicosanoids in RA synovial fluid ↓ Percentages of eicosapentaenoic, linoleic, and α-linolenic acid	
Choline	Phospholipid	↑ Expression of choline kinase in RA synovial tissue. ↑ Upregulated choline kinase in RA FLS in response to TNFα ↑ Fatigue	Choline metabolite (TMAO) is associated with measures of joint and skin inflammation

Figure 66 Lipid metabolites and their functions in health, RA and PsA.

The presence of lipids such as cholesterol in inflammatory arthritis synovial fluid has long been recognised (423). For example, Ananth *et al*. showed that apolipoprotein A-I, apolipoprotein B and cholesterol levels were higher in synovial fluids from patients with RA than patients with degenerative joint disease (423). In a study of serial synovial fluid samples from two patients with RA, synovial fluid triglycerides and glycoproteins were found to correlate with disease activity (424). Cross-sectional analysis of synovial fluids from patients with RA using liquid chromatography-tandem mass spectrometry (LC-MS/MS) previously showed almost 70 different lipid components from distinct lipid classes including lysophosphatidylcholine and phosphatidycholine species (425). Key anti-inflammatory and pro-resolving lipid mediators including maresin 1, lipoxin A_4 and resolving D5 were found in these synovial fluids (425). The synovial fluid lipid profiles in my cohorts may be characterised to assess whether they correlate with changes in synovial fluid cytokines and synovial tissue snRNA-seq profiles.

Adipocytes are involved in regulation of adaptive immunity (342). Adipocytes exhibit properties of APCs such as expression of CD1d, MHC class I and II molecules. For example, lipid antigen presentation by adipocytes to NKT cells through CD1d modulates tissue inflammation (426). Moreover, adipokines produced by adipocytes regulate the survival, activation and differentiation of immune cells (342, 427). High fat diet fed mice have increased expression of MHC II molecules in adipocytes (428). This illustrates how lipid metabolism may influence cell-cell communication between adipocytes and CD4 T

cells and Tregs (428). Knockout of HIF-1α protected mice from high fat diet induced upregulation of MHC II genes in adipocytes and tissue inflammation (429). This suggests that hypoxia is involved in the crosstalk between lipid metabolism and immune pathways.

The interconnection between lipid metabolism and inflammation suggests that lipid metabolism may be targeted for anti-inflammatory effects. For example, PPARγ expression was decreased in RA synovial tissues compared to OA and normal synovium (430). PPARγ along with PPARα and PPARδ are subtypes of PPARs which regulate fatty acid metabolism (431). PPARγ agonist pioglitazone has been tested as a treatment for RA and PsA (432, 433). Pioglitazone treatment resulted in a modest reduction in DAS28-CRP in patients with RA (432). Pioglitazone also reduced tender and swollen joint counts in patients with PsA (433). However, both studies reported side effects including lower-extremity oedema which is known to occur with pioglitazone. Other strategies to target synovial tissue lipid metabolism need to be considered. The role of lipid metabolism in synovial tissues may depend on the microenvironment and the cell subsets involved (173). An understanding of the spatial distribution of lipid profiles in synovial tissues is therefore needed.

Spatial characterisation of synovial tissue lipid profiles in RA and PsA is emerging. Matrix-Assisted Laser Desorption Ionization Mass Spectrometry Imaging (MALDI-MSI) and matrix-enhanced secondary ion mass spectrometry (ME-SIMS) are established techniques to determine the relative abundance and the spatial distribution of proteins, lipids, metabolites or other organic compounds by their molecular masses (434, 435). Rocha *et al*. presented abstracts of their MALDI-MSI analysis which showed distinct synovial tissue lipid profiles in RA and PsA (436, 437). Lipid species including

sphingomyelins, phosphatidylcholines (PCs) and phosphatidylethanolamines (PEs) had the greatest separation power to classify RA and PsA tissue samples (436). Most significantly different lipid species were increased in RA and PsA compared to controls (436). Spatial distribution of PE was associated with increased vascularity and inflammatory cell infiltrates in the synovial sublining (436, 437). Proteomic analysis also found lipid metabolism related proteins in synovial tissues that distinguish between RA and PsA (436).

Although these cross-sectional studies provide useful insights as to how lipid profiles may differ in synovial tissues in different diseases, there is a knowledge gap relating to how the spatial distribution of lipids in synovial tissues change over time. My study demonstrated there were fewer synovial tissue adipocytes, and that lipogenesis genes in adipocytes were upregulated, after intra-articular methylprednisolone injection. MALDI-MSI/ME-SIMS analysis of synovial tissues before and after intra-articular methylprednisolone injection would characterise perturbation of lipid profiles spatially. Further studies in longitudinal samples are needed to address whether lipid metabolism may be therapeutically targeted in inflammatory arthritis by dissecting the immune and metabolic effects of lipid species on stromal and immune cells in synovial tissues.

Synovial tissue biopsy is limited in that only a small sample of the joint is available for analysis. Characterisation at the level of the anatomical joint, not just at the tissue lining, is needed to understand the pathological processes underlying inflammatory arthritis. Non-invasive *in vivo* evaluation of the immune-metabolic changes with detailed anatomical delineation using functional and molecular-based imaging (such as positron emission tomography, fluorescence optical imaging, optoacoustic imaging, contrast-enhanced

ultrasonography) would add to our understanding of immunometabolism in inflammatory arthritis (274).

4.4.5 Differential gene expression in B cells after intra-articular methylprednisolone injection

When samples containing skeletal myocytes were excluded from analysis, there were no differential gene expression in cell types such as B cells and macrophages (Table 10). This may be due to reduced sample size for analysis which may limit statistical power. Exploratory analysis including samples containing skeletal myocytes showed downregulation of versican (*VCAN*) and *IL2RA* gene expression in B cells, and downregulation of formyl peptide receptor 3 (*FPR3*) gene expression in MERTK low macrophages (Table 11). Interpretation of these exploratory analyses need to be treated with caution as analysis may be confounded by cells from outside the joint capsule.

The downregulation of *VCAN* by glucocorticoid has been shown previously (438, 439). *VCAN* encodes a large extracellular matrix proteoglycan called versican which is a member of the lectican protein family which includes aggrecan found in cartilage (440). Versican binds to leukocyte adhesion molecules L-selectin, P-selectin and CD44 (441). The effects of glucocorticoids on versican have been studied in the context of foetal lung maturation (438, 439). Glucocorticoid signalling represses *VCAN* gene expression and glucocorticoid administration reduces versican levels *in vivo* (438, 439). There is therefore precedent for glucocorticoid mediated downregulation of *VCAN* expression. However, B cells are not known to express *VCAN*. Fibroblasts are the predominant cells that express *VCAN* (442). Methylprednisolone has previously been shown to induce no differential gene expression of *VCAN* in B cells *in vitro* (300). Therefore, the downregulation of *VCAN*

in B cells in this study needs to be interpreted with scepticism and confirmed in a larger independent cohort using alternative assays such as flow cytometry.

Exploratory analysis including samples containing skeletal myocytes also showed downregulation of *IL2RA* gene expression in B cells (Table 11). IL2RA and IL2RB bind with the IL-2 receptor common gamma subunit (IL2RG) to form the IL-2 receptor (IL2R) (443). IL2R is involved in regulating immune tolerance by controlling Tregs which suppress the activation and expansion of autoreactive T cells. Due to its role in the development and function of Tregs, *IL2RA* is recognised as a general susceptibility gene for autoimmune diseases including RA, juvenile idiopathic arthritis (JIA), multiple sclerosis and type 1 diabetes mellitus (444). For example, the IL2RA-rs2104286 minor allele is associated with joint destruction and persistence of RA (445).

Glucocorticoids have been shown to downregulate *IL2RA* (446). In T cells, dexamethasone decreased *IL2RA* mRNA levels, reduced IL2RA protein expression, and inhibited IL-2 induced T cell proliferation (446). Although *IL2RA* is expressed by B cells, *IL2RA* has not been shown to be perturbed by glucocorticoids in B cells before (300, 447). Given the exploratory nature of this analysis and possible confounding by inclusion of samples containing extra-capsular tissues, this finding therefore needs to be corroborated in a hypothesis driven approach using flow cytometry in an independent cohort.

4.4.6 Differential gene expression in macrophages after intra-articular methylprednisolone injection

In the exploratory analysing including samples containing skeletal myocytes, *FPR3* was downregulated in MERTK low macrophages after intra-articular methylprednisolone

injection (Table 11). The formyl peptide receptor family (*FPR1*, *FPR2* and *FPR3*) encodes G-protein-coupled receptors that are expressed mainly by phagocytic leukocytes such as macrophages and are involved in antibacterial host defence and inflammation (448). Unlike FPR1 and FPR2 which are expressed on the cell surface, FPR3 is located in intracellular vesicles (449). FPR3 is known to be upregulated in the lympho-myeloid pathotype of synovial tissue biopsies of patients with RA (448). Although *FPR3* has previously been shown to be downregulated in monocytes *in vitro* by methylprednisolone, the effects of intra-articular methylprednisolone on *FPR3* expression in synovial tissue requires confirmation in an independent cohort to ensure this is not a spurious finding due to confounding by extra-capsular monocytes (300).

4.4.7 Intra-articular methylprednisolone effects on differential gene expression in RA and PsA subgroups

The difference in synovial fluid IL-6 and TNF responses to intra-articular methylprednisolone injection in RA and PsA subgroups suggested that there may be subgroup differences in synovial tissue response to treatment (Figure 35, Figure 37). There were scant differentially expressed genes in RA and PsA subgroups in cell types other than lining fibroblasts (Supplementary Table 2). In synovial lining fibroblasts, intra-articular methylprednisolone injection induced no differentially expressed genes in RA, whereas a perturbation response was noted in PsA (Figure 56, Figure 57). Genes related to inflammatory arthritis such as TNFAIP6 and JAK2 were downregulated in PsA lining fibroblasts after treatment with intra-articular methylprednisolone injection (Figure 57).

TNFAIP6 encodes a secretory protein containing a hyaluronan-binding domain which mediate extracellular matrix stability and cell migration. Pro-inflammatory cytokines such as TNF and IL-1 induce *TNFAIP6* transcription. The TNFAIP6 protein enhances the serine protease inhibitory activity of I alpha I, which is important in the protease network associated with inflammation. TNFAIP6 also enables binding of hyaluronan on the surface of macrophages to LYVE1 on lymphatic endothelium and facilitates macrophage extravasation (450). The downregulation of *TNFAIP6* in PsA synovial lining fibroblast was consistent with the downregulation of TNF protein in synovial fluid of the patients with PsA after intra-articular methylprednisolone injection (Figure 37, Figure 57).

Conversely, methylprednisolone upregulates *JAK2* transcription *in vitro* at 6 h whereas my study showed downregulation of *JAK2* in PsA lining fibroblasts four weeks after intra-articular methylprednisolone injection (Figure 57). This discrepancy was likely due to different acute and chronic effects of glucocorticoid, as well as the different context between an *in vitro* experiment and an *in vivo* setting. *JAK2* encodes a non-receptor tyrosine kinase with a central role in cytokine and growth factor signalling. Cytokine binding induces autophosphorylation and kinase activation, which then phosphorylates STAT proteins. *JAK2* is associated with myeloproliferative diseases including polycythaemia vera and thrombocythemia. JAK inhibitors are widely used to treat inflammatory arthritis include tofacitinib (inhibits JAK1/2/3), baricitinib (inhibits JAK1/2), upadacitinib (inhibits JAK1) and filgotinib (inhibits JAK1) (2).

In addition to downregulating conventional markers of inflammation in PsA synovial lining fibroblasts, intra-articular methylprednisolone injection also downregulated neuron related genes such as cholinergic receptor muscarinic 3 (*CHRM3*) (451), semaphorin 3D

(*SEMA3D*) (452), tumour protein p63 (*TP63*) (453), neuroligin 4 X-linked (*NLGN4X*) (454), TNF receptor associated factor 2 and NCK interacting kinase (*TNIK*) (455), Solute Carrier Family 24 Member 3 (*SLC24A3*) (456), basonuclin zinc finger protein 2 (*BNC2*) (457), mannosidase alpha class 2A member 1 (*MAN2A1*) (458), six-transmembrane epithelial antigen of prostate 4 (*STEAP4*) (459), and ABI family member 3 binding protein (*ABI3BP*) (Figure 57) (460). The role of the nervous system in mechanisms underlying peripheral pain and inflammation in inflammatory arthritis was reviewed recently and is described briefly here (461, 462).

Pain perception in the brain is relayed by activation of peripheral neurons and sensory circuits within the spinal cord and brain (463). These neurons extend axons to innervate peripheral tissues including synovium. The relevance of the nervous system as a therapeutic target in arthritis was exemplified by tanezumab, a monoclonal antibody against nerve growth factor (NGF), which was efficacious in reducing OA pain but had the adverse effect of rapidly progressive joint degeneration (464, 465).

As ion channels are emerging as important in the pathogenesis of arthritis and as therapeutic targets, it was particularly notable that *SLC24A3* was downregulated in PsA lining fibroblast after intra-articular methylprednisolone injection along with other inflammatory markers (Figure 57) (466). Ion channels are pore-forming proteins on cell membranes that regulate ion flux, membrane potential, osmoregulation and metabolism (467). The role of ion channels in arthritis and their potential as therapeutic targets were recently reviewed and are briefly described here (466, 468). Some ion channels typically associated with neurons are also expressed by immune cells and musculoskeletal cells of the joint (466). These ion channels have key functions that contribute to pathogenesis of

arthritis including synovial proliferation, cartilage destruction, inflammation and pain (466). However, the electrophysiological properties of ion channels in synovial tissues remain poorly understood and the factors underlying the contribution of ion channels to pathogenesis of arthritis are not fully elucidated (466).

Lipid metabolites including derivatives of phosphatidylcholine, a key component of nanobubbles invented by Professor Stride, may mediate effects through ion channels potentially leading to pain exacerbation. For example, lysophosphatidylcholine is released after hydrolysis of membrane phospholipid phosphatidylcholine by phospholipase A2 (469). Lysophosphatidylcholine, along with other endogenous lipid species, in turn can activate and potentiate acid-sensing ion channel (ASIC) 3 (470, 471). ASIC3 activation by lysophosphatidylcholine has been shown to contribute to chronic pain in musculoskeletal disorders (466, 470, 472). Inhibitors of ASIC3 were reported to reduce inflammatory pain, cartilage damage and mechanical hypersensitivity in animal models, highlighting the potential of ion channels as therapeutic targets (466).

It was therefore exciting that *SLC24A3* was revealed as a putative biomarker of disease in PsA lining fibroblast that was downregulated after intra-articular methylprednisolone injection (Figure 57). *SLC24A3*, otherwise known as sodium/potassium/calcium exchanger 3 (*NCKX3*), encodes a potassium-dependent sodium-calcium exchanger that transports one Ca^{2+} and one K^{+} in exchange for four Na^{+} (473). The role of solute carrier transporter family in metabolism and inflammation by RA fibroblasts has been previously reviewed extensively but SLC24A3 was not widely known to be relevant to arthritis (474).

SLC24A3 was previously shown to be unperturbed by glucocorticoid *in vitro* (300). My study showed lining fibroblast expression of *SLC24A3* was also unaffected by intra-articular methylprednisolone injection in the RA subgroup (Figure 56). The downregulation of *SLC24A3* was therefore associated with the resolution of inflammation in the synovium of patients with PsA, rather than with the administration of intra-articular methylprednisolone injection per se (Figure 57).

Whether *SLC24A3* downregulation contributed to the resolution of inflammation, or was a consequence of resolution of inflammation, requires investigation to distinguish *SLC24A3* as a biomarker of disease or a potential therapeutic target. Using dextran sodium sulphate induced experimental colitis mouse models with SLC24A3 KO mice, Tran *et al.* demonstrated that loss of SLC24A3 prevented resolution of inflammation (475). Furthermore, they demonstrated that loss of SLC24A3 exacerbated colitis through p53/NF-κB activation through calcium homeostasis. This supports SLC24A3 as more than a mere marker of inflammation, and instead actively mediates resolution of inflammation.

In addition to animal models of colitis, metal ion channels have also been described as relevant in human inflammatory arthritis synovium. In the aforementioned work by the Brenner group, metal ion homeostasis genes were found to be differentially expressed by synovial tissue fibroblasts from patients with inflammatory arthritis compared to fibroblasts from "healthy human synovial tissue" dissected at autopsy from subjects without history of arthritis, autoimmune disease or recorded traumatic injury (415). These findings implicate metal ion channels in synovial tissue inflammation.

SLC24A3 also regulates mast cell activation by controlling the sustained phase of Ca^{2+} gradient (476). Indeed, *SL24A3* was expressed by synovial tissue mast cells in my dataset (Supplementary Figure 12). Mast cells are known to have pleiotropic roles in synovial tissue inflammation, and may act as immunomodulatory cells (477). Mast cell expression of SLC24A3 may offer additional targets for modulation as mast cell ion channels have been viewed as potential therapeutic targets in immune mediated diseases (478). *SLC24A3* was shown to be upregulated in other settings including inflamed brain glial cells (479), and associated with the immune response and tumour immune microenvironment in cervical cancer (480, 481). Therefore, SLC24A3 modulators may have potential therapeutic value across different diseases.

Ion channel modulators have been tested in animal models of arthritis and in patients with arthritis, heralding their development as novel treatment strategies for arthritis. Clinical trials are already underway for ion channel modulators in OA (466, 468). Animal models of inflammatory arthritis may be used to investigate whether targeting SLC24A3 would be an effective treatment for treatment of inflammatory arthritis. A caveat is that there was no significant differential expression of *SLC24A3* in synovial tissues after treatment with either tocilizumab or rituximab in RA patients enrolled in the R4RA trial (Supplementary Figure 13) (336). The R4RA was a synovial biopsy-based biomarker analysis of rituximab versus tocilizumab in patients with RA (336). It may be that *SLC24A3* was not significantly differentially expressed in the R4RA dataset because *SLC24A3* was only expressed in select cell subtypes such as lining fibroblasts but not sublining fibroblasts (Supplementary Figure 12). The other challenge that SLC24A3 poses as a therapeutic target is that it is also expressed in the brain, aorta, uterus, intestine, smooth muscles, and

kidney tubules so intra-articular administration may be preferred to limit systemic exposure to a SLC24A3 modulator (408, 475, 482, 483).

Some neuron related genes were upregulated in PsA synovial lining fibroblasts with intra-articular methylprednisolone injection, such as heparin binding epidermal growth factor like growth factor (*HBEGF*) (484), SH3 and multiple ankyrin repeat domains 2 (*SHANK2*) (485), collagen type XXII alpha 1 chain (*COL22A1*) (486), and chemerin chemokine-like receptor 2 (*CMKLR2*) (487). While these genes have a myriad of functions beyond those related to neurons, it is intriguing that these genes have in common functions related to the nervous system. The previously reported association between rapidly progressive OA (RPOA) with tanezumab provides proof-of-concept that inhibition of neuronal pathways may exacerbate joint destruction, even if the mechanisms remain unexplained (464, 465). This association, along with my finding that some neuron related genes were upregulated in PsA lining fibroblasts in association with resolution of inflammation after intra-articular methylprednisolone injection, lead to the generation of the hypothesis as to whether specific neuron related molecules may in fact be beneficial in reducing joint destruction.

This study added novel insights into how intra-articular methylprednisolone affects neuron related gene expression in synovial lining fibroblasts. These findings may be confirmed by accessing other single cell therapeutic atlases of synovial tissues such as the R4RA dataset which compared rituximab with tocilizumab in the treatment of RA (336). Further investigation is needed to understand the significance of this therapeutic response. These may act as biomarkers of inflammation, or even therapeutic targets for pain modulation in arthritis. In animal models of perinatal stroke, methylprednisolone restored microglial,

astroglial and oligodendrocyte populations (241). There is therefore a precedent to support methylprednisolone effects on neuron related fibroblasts in hypoxic inflamed tissues.

The differential expression of neuron-related genes induced by methylprednisolone in PsA lining fibroblasts may provide mechanistic insights into how methylprednisolone affects the nervous system during hypoxia. Hypoxia was known to induce excitability loss in spinal cord axons (488, 489). Sasaki *et al*. showed that methylprednisolone protected spinal cord axons against hypoxia-induced excitability loss (488). One may speculate that the differentially expressed neuron related genes in fibroblasts induced by methylprednisolone in my study may account for the protective effects of methylprednisolone against hypoxia-induced excitability loss. Histological analysis of synovial tissues is needed to understand how intra-articular methylprednisolone injection affects neurons in synovial tissues. This could be further explored by using deep imaging techniques such as multiphoton microscopy to investigate whether the spatial distribution and density of synovial tissue lining innervation is perturbed with intra-articular methylprednisolone injection. Such experiments would clarify if the perturbed neuronal genes in PsA synovial lining fibroblasts with treatment has physiological effects on the synovial tissue nervous system.

4.4.8 Synovial tissue snRNA-seq therapeutic atlas of intra-articular methylprednisolone injection

This study was the first reported snRNA-seq therapeutic atlas in inflammatory arthritis characterising synovium before and after treatment, with intra-articular methylprednisolone injection as the model therapy. Cells respond to drugs differently *in vitro* compared to *in vivo*. The microenvironment niche, extracellular matrix and

adipocytes in the *in vivo* setting is missing from the *in vitro* experimental setup. The fact that *in vitro* cultures do not recapitulate the *in vivo* setting highlights why novel therapies may show promise in preclinical stages but fail to show clinical efficacy. Conversely, efficacious therapies in development may be erroneously abandoned due to poor preclinical testing. This *in vivo* therapeutic atlas of intra-articular methylprednisolone injection serves as a foundation for the investigation of other existing and emerging therapeutic agents for arthritis using synovial tissue snRNA-seq profiling.

One of the strengths of using snRNA-seq for evaluating longitudinal changes in synovium is its unbiased approach to genome-scale assessments of cellular identities and states. Most studies into synovial tissue sequencing at single cell level are scRNA-seq analyses. However, scRNA-seq requires tissue disaggregation by thermal and enzymatic means which may significantly bias gene expression and alter the observed cell types. The advantage of using snRNA-seq is that cells do not undergo thermal and enzymatic disaggregation, resulting in a more accurate picture of cell gene expression and cellular composition. For example, adipocyte data are frequently absent from scRNA-seq due to technical challenges relating to adipocytes as large buoyant cells (365, 490). The snRNA-seq therapeutic atlas described herein can not only characterise the adipocytes found in synovium but is also sufficiently sensitive enough to describe the therapeutic effects on cell abundance and differential gene expression in adipocytes longitudinally.

This therapeutic atlas provided important insights into the *in vivo* mechanisms of action in patients with inflammatory arthritis. Previous studies showed glucocorticoids mediate different anti-inflammatory effects via distinct cell types in different mouse models of arthritis (230). In the antigen-induced arthritis (AIA) model, deletion of the glucocorticoid

receptor abrogated the therapeutic effects of glucocorticoids, but deletion of the glucocorticoid in stromal cells did not (491). In the serum transfer-induced arthritis mouse model however, the anti-inflammatory effects of dexamethasone were found to be mediated by glucocorticoid receptors expressed by the stromal cell compartment rather than T cells or other haematopoietic cells (492). Given that intra-articular methylprednisolone injection was found to have profound different gene expression changes in PsA lining fibroblasts, my data therefore suggests that the serum transfer-induced arthritis mouse model may be more reflective than the AIA model of glucocorticoid effects in patients with PsA.

4.4.9 Molecular endotyping of synovial tissues between RA and PsA

Understanding the differences in the pathogenesis of RA and PsA may identify potential novel biomarkers and therapeutic targets. Differences between RA and PsA have previously been characterised at synovial tissue single cell transcriptomic level (346). I undertook an exploratory analysis to see if there was a difference between PsA and RA synovial tissues at single nucleus level, which has not been done before. The exploratory analysis between RA and PsA was hypothesis generating, especially since there may be confounders such as differences in age, gender, comorbidities, medications, disease stage, etc. Any findings would require validation using independent assays in independent cohorts.

In pre-treatment synovial tissues, there were greater proportions of adipocytes, ribsomal RNA high T cells, NK/NKT cells, B cells and mural cells in RA, and greater proportions of lymphatic endothelial cells and plasmacytoid dendritic cells in PsA (Figure 58). Synovial tissue B cells are known to have a pathogenic role in RA and their significance is

confirmed by the therapeutic efficacy of B cell depletion using rituximab to target CD20 (493). In this study, the greater proportion of synovial tissue B cells found in pre-treatment synovial tissues in RA compared to PsA was consistent with known preponderance of synovial tissue B cells in the pathophysiology of RA (494-496).

Synovial tissue single cell transcriptomic profiles have previously been characterised in RA and PsA but adipocytes are missing in their dataset (346). In pre-treatment synovial tissues, my dataset showed greater proportion of adipocytes in RA compared to PsA (Figure 58). This difference may reflect greater inflammation in the pre-treatment synovial tissues in PsA compared to RA, as suggested by the synovial fluid IL-6 reduction in response to intra-articular methylprednisolone injection in the PsA group but not the RA group (Figure 35). The presence of adipocytes in synovial tissues is known to be decreased with progression of arthritis (497). In my dataset, the difference in synovial tissue adipocyte composition in RA and PsA may be confounded by factors such as disease stage and severity. Future studies should compare synovial tissue biopsies from RA and PsA patients with similar characteristics, such as disease stage and severity, to delineate the molecular and cellular differences underlying their pathophysiology.

Curiously, lymphatic endothelial cells were noted to be greater in proportion in PsA synovial tissue compared to RA, in both pre- and post-treatment (Figure 58, Figure 59). The lymphatic system is important in maintaining interstitial fluid balance and immune cell transport (498). Antigen presenting cells such as dendritic cells travel from peripheral sites through the afferent lymphatics to lymph nodes where B and T cells are activated by foreign antigens, which then migrate via efferent lymphatics to mount an immune response (499). Moreover, the egress of T cells from inflamed tissues via lymphatics is important

for resolution of inflammation (500). Indeed, lymphatic drainage is known to be essential in regulating humoral immunity and peripheral tolerance (501, 502). In addition to facilitating transport of immune cells, lymphatic endothelial cells also secrete immunomodulatory signals including TGF-β to suppress dendritic cell maturation, IL-7 to increase IL-2-sensitivity in regulatory T cells, and macrophage-colony stimulating factor (M-CSF) to modulate macrophage differentiation (499, 503-505).

Rheumatoid lymphadenopathy was first described in 1896 and lymphatic involvement in RA has since been generally accepted (506). Lymphatic disorders such as lymphoedema have been described in RA, and there are case reports of lymphoedema in PsA too (507-509). The pathophysiology of RA is associated with dysregulated synovial lymphatic vasculature, including an expansion and collapsed phase (499).

Interestingly, lymphatic vessel length has previously been shown to be reduced in the hands of patients with active RA compared to healthy controls (510). Their clinical finding corroborated with my snRNA-seq finding that there were few lymphatic endothelial cells in synovium of patients with RA (Figure 58, Figure 59). My finding suggested that reduced proportion of lymphatic endothelial cells may be specific to RA and not PsA, highlighting potential discrepancy in the role of lymphatic endothelial cells in pathogenesis of RA and PsA. In animal models of inflammatory arthritis, inhibition of lymphangiogenesis and lymphatic drainage exacerbated inflammation and restoration of synovial tissue lymphatic system attenuated joint damage (511, 512). RA treatments alter the lymphatic vessels and nodes so the lymphatic system may represent a potential biomarker of disease and a therapeutic target for RA (513). *In vitro* organoid and *in vivo* animal studies are therefore warranted to investigate the role of synovial tissue lymphatics

in pathogenesis of inflammatory arthritis, and their potential as therapeutic targets especially for RA (499).

Having explored the differences in synovial tissue cellular composition, I then explored differentially expressed genes between synovial cell types in RA and PsA. Differential gene expression analysis showed only the pre-treatment lining fibroblasts were demonstrably different between RA and PsA (Figure 60). The post-treatment samples showed essentially no differences between diseases (Figure 61). This finding is consistent with the cellular composition being more similar after treatment (Figure 58, Figure 59). As this analysis is exploratory, confirmation of findings will be necessary to rule out confounders.

Differential gene expression analysis in pre-treatment synovial lining fibroblasts showed marked upregulation of *MGP* in RA compared to PsA. The *MGP* gene encodes a member of the osteocalcin/matrix Gla family of proteins which is activated by vitamin K dependent carboxylation (514). MGP has a pleiotropic role in bone metabolism as it promotes bone formation by upregulating Wnt/β-catenin signalling and exerts an inhibitor effect on bone mineralisation (514-517).

Previously, immunohistochemistry of synovial tissues showed that MGP was increased in RA compared to OA (518). My study results suggest that *MGP* upregulation in lining fibroblasts is specific to RA and not PsA (Figure 60). This is interesting because some studies suggested that bone erosions occur less frequently in PsA than RA (519, 520), although other studies found no difference (2, 521-523). This exploratory analysis generated the hypothesis as to whether lining fibroblast expression of *MGP* may explain

bony erosion as being more predominant in RA compared to PsA, by inhibiting calcification.

The role of MGP in osteoporosis is well known and polymorphism of the *MGP* locus is associated with bone mineral density in elderly women (514, 524). The use of an osteoporosis treatment denosumab (an anti-RANKL Ab) for treating RA provides proof-of-concept that treatments targeting bone mineralisation may be effective at treating RA (514, 525). Further studies are required to understand why *MGP* is upregulated in RA lining fibroblasts, and its potential as a therapeutic target.

On the other end of the spectrum, *BMPER* expression was markedly upregulated in pre-treatment synovial lining fibroblasts in PsA compared to RA (Figure 60) (526). Given that synovial tissue vasculature is known to be tortuous and bushy in PsA, it was interesting to note that *BMPER* may be involved in the pathogenesis of this pathological feature in PsA (344). Fromm *et al*. showed that conditioned media from fibroblasts from PsA synovial tissues enhanced endothelial tube formation and endothelial cell migration *in vitro* compared to fibroblasts from RA synovial tissues (527). The pro-angiogenic phenotype in PsA was attributed to increased secretion of VEGF and thymic stromal lymphopoietin (TSLP) by PsA synovial fibroblasts but there may be other secreted factors involved that were unaccounted for such as BMPER.

BMPER, also known as Crossveinless-2 (*CV2*), was first identified in *Drosophila* to be required for the formation of wing crossveins (528, 529). This gene encodes a secreted protein that contains five cysteine-rich domains followed by a von Willebrand D domain and a trypsin-inhibitor domain (530). *BMPER* has been shown to have a conserved

function across species for pattern guidance of interconnecting blood vessels. In *Drosophila*, deficiency in BMPER resulted in a phenotype lacking crossveins which are interconnecting veins between the longitudinal veins of the wing (529). Moreover in zebrafish, *BMPER* knockdown compromised the caudal vein development and the pattern guiding of intersomitic vessels, demonstrating that *BMPER* is required in vascular pattern formation (531). BMPER has also been implicated in retinal angiogenesis in oxygen induced retinopathy, and cardiovascular development (532, 533).

BMPER interacts with and modulate bone morphogenetic proteins (BMP), including BMP2, BMP4 and BMP6, which are important in blood vessel formation and vascular disease (530, 534, 535). As well as extracellular modulation of BMP, BMPER may also impact endothelial cells through LRP-1 signalling, similarly to TIMP-1 (406, 536). The functions of BMPER include both pro- and anti-BMP signalling effects in different experimental settings (532). In particular, the concentration of BMPER relative to BMP may be important in determining its effects (537). At low concentrations, BMPER enhances sprouting and vasculature formation whereas high concentrations of BMPER inhibit these processes (532).

The role of BMPER expression by synovial tissue lining fibroblasts in the pathogenesis of PsA is likely to be multifaceted. In gain-of-function assays, BMPER antagonises BMP but in loss-of-function models, BMPER has pro-BMP functions (526). BMPER has also been reported to inhibit angiogenesis and inflammation which in turn have therapeutic implications. For examples, BMPER inhibits endothelial inflammation by inhibiting TNF-induced endothelial inflammation (526, 538). An anti-inflammatory role for BMPER was confirmed when small interfering RNA (siRNA) knockdown of *BMPER* in HUVECs

increased inflammatory markers intracellular adhesion molecule 1 (ICAM-1) and vascular cell adhesion molecule 1 (VCAM-1) expression (526, 539).

Although lining fibroblast expression of *MGP* and *BMPER* may be novel endotypes of RA and PsA, respectively, MGP and BMPER are also inextricably linked through shared molecular mechanisms. In *Apoe*$^{-/-}$ mouse models of atherosclerosis, overexpression of MGP downregulated BMPER and loss of MGP strongly upregulated BMPER (540). This reciprocal relationship between MGP and BMPER likely reflect their shared and opposing roles in BMP signalling. Excessive MGP expression has been shown to inhibit pulmonary vascular development through interference with BMP-4 signalling (541). Specifically, overexpression of *Mgp* transgene in mouse models inhibited side branching of the vascular endothelium (541). This appears to be analogous to the straight, linear blood vessels seen in RA synovial tissues, and may also be driven by overexpression of MGP by synovial tissue lining fibroblasts. Increased MGP expression suppresses VEGF expression, whereas VEGF expression is increased in the absence of MGP (540). Therefore, the disparate appearance of linear blood vessels in RA joints and tortuous bushy vasculature in PsA joints may be driven by opposing effects of MGP and BMPER, not only on each other, but also on VEGF and BMP signalling (Figure 67) (540).

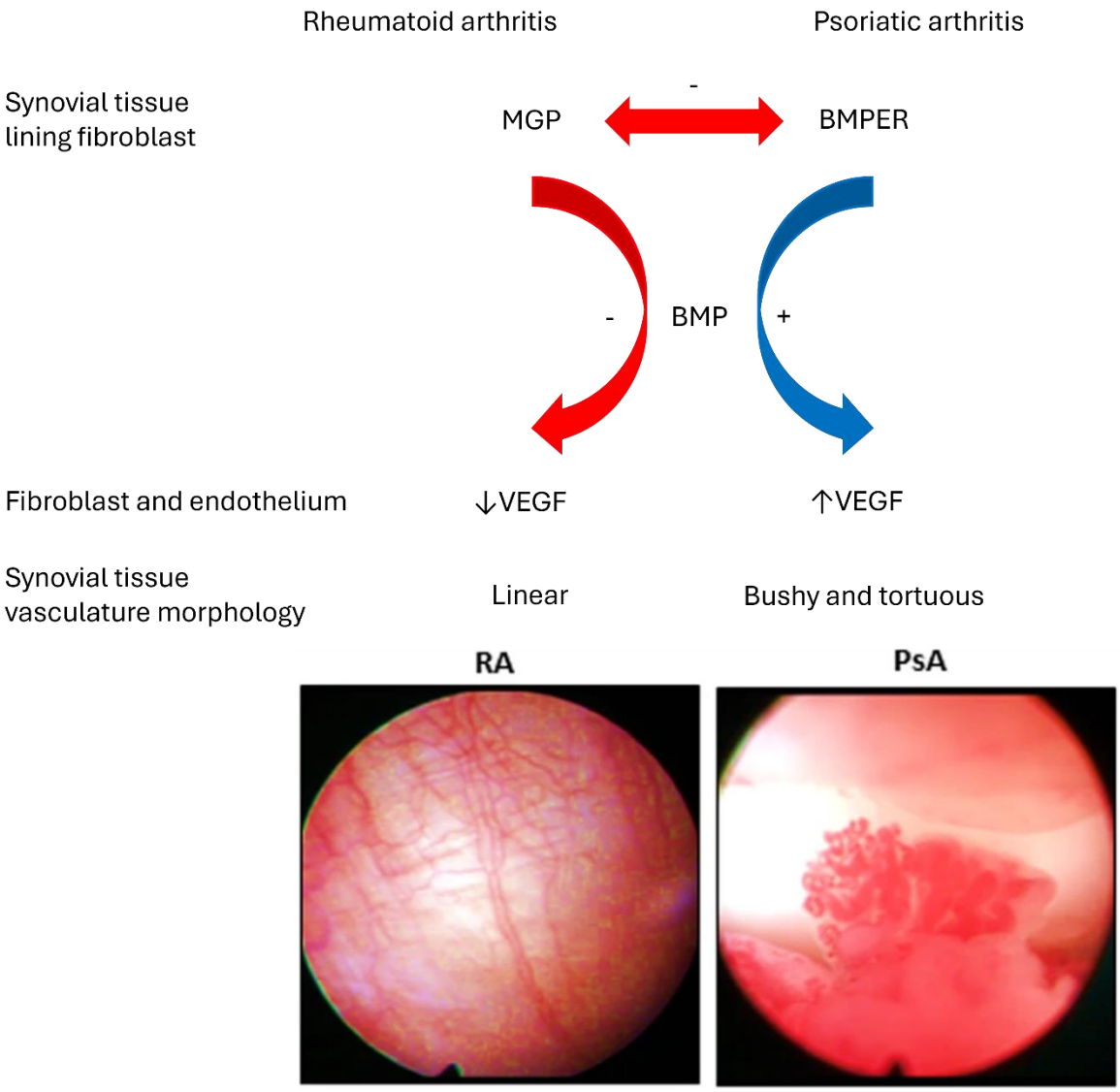

Figure 67 Proposed mechanistic model by which the negative reciprocal relationship between MGP and BMPER drives divergent synovial tissue vasculature morphology in RA and PsA through BMP and VEGF signalling. Red arrow denotes negative effects. Blue arrow denotes positive effects.

Photomicrographs of distinct vascular patterns in the synovium of patients with PsA as compared to patients with RA reprinted in accordance with the Creative Commons Attribution Non-Commercial (CC BY-NC 4.0) license (https://creativecommons.org/licenses/by-nc/4.0/) from Fromm et al. (527)

ELISA of BMPER in synovial fluids from my study to determine whether BMPER is higher in synovial fluids from patients with PsA than patients with RA, would provide protein confirmation of the transcriptomic difference seen. The dataset shared by Floudas *et al*. may be interrogated to see whether lining fibroblast expression of BMPER was indeed higher in patients with PsA compared to RA in an independent cohort (346).

As well as using differential gene expression to explore molecular endotypes of lining fibroblasts in RA and PsA, I also examined differences in gene pathways between these diseases. Exploratory gene set enrichment analysis comparison of pre-treatment synovial lining fibroblasts showed upregulation of neuron differentiation pathways in PsA compared to RA (Table 13). Recently, the association between synovial fibroblast expression with sensory nerve growth and pain has been characterised (407). Synovial lining fibroblasts were predicted to express genes associated with pain that enhance the growth of dorsal root ganglion nociceptive neurons into synovial hypertrophy regions in RA (407). The differences seen in my dataset between RA and PsA may be confounded by factors such as disease stage and severity. Further studies are required to understand how synovial lining fibroblasts contribute to pain in RA and PsA.

4.4.10 Cell-cell communication in RA and PsA synovial tissues

Previously, single cell transcriptomic studies that characterised differences in cell-cell communication networks in RA and PsA patients have been limited (346). Floudas *et al*. was the first study to characterise single cell transcriptomic profiling of synovial tissues from RA and PsA inflamed joints without prior sorting of immune and stromal cells (346). My study found similarities and differences in cell-cell communication in pre-treatment synovial tissues from patients with RA and PsA (Figure 64, Figure 65, Supplementary

Figure 9, Supplementary Figure 10, Supplementary Figure 11). For example, lining fibroblasts had the highest outgoing interaction strength in both RA and PsA (Figure 65). Stronger and greater number of interactions mediated by B cells and plasma cells, and weaker interactions mediated by lymphatic endothelial cells, in RA compared to PsA may define the distinct synovial tissue immune-stromal cell crosstalk. Understanding the distinct pathogenesis allows targeted therapies for treating inflammatory arthritis, such as the use of rituximab for B cell depletion in the treatment of RA but not PsA.

Further work is required to elucidate the role of synovial tissue immune-stromal cell crosstalk in the pathogenesis and resolution of inflammatory arthritis. scRNA-seq and snRNA-seq provide deep, high-resolution understanding of cell populations and states but lack the spatial context which would otherwise inform analyses of cell identity and function. Spatial multi-omics approaches (e.g. transcriptomic, metabolomic and proteomic) would provide geographic colocalization information relating to interactions in cellular niches (364). Integration of spatial multi-omics approaches to dissect the spatiotemporal dynamics of cellular microenvironments would identify extracellular and intercellular signalling networks and decipher how these determine resolution of inflammation.

4.4.11 Limitations

The small sample size in this study may be insufficiently powered to detect subtle differences. The sample size could have been increased if all the synovial tissue samples were analysed with snRNA-seq. However, snRNA-seq analysis is expensive and financial restraints limited the number of synovial tissue biopsy samples that could be analysed to 8 pairs. To maximise statistical power for subgroup analysis of RA versus PsA, paired pre-

and post-treatment samples from 4 patients with RA and 4 patients with PsA were analysed. As not all the paired samples from patients with PsA were analysed, 4 patients with PsA were randomly chosen for snRNA-seq analysis to prevent skewing of data.

Glucocorticoids are known to have short- and long-term effects. Follow-up at a single timepoint allows only a snapshot of the glucocorticoid effects. The short-term effects of intra-articular methylprednisolone injection would be expected to have resolved at 4-week follow-up. Future studies with multiple follow-up timepoints would allow dynamic characterisation of therapeutic effects.

Compared with scRNA-seq, a potential disadvantage with snRNA-seq is that it only captures approximately 10% of the transcriptome as snRNA-seq sequences only the RNA in the nucleus and not the cytoplasm (363). Previous studies of snRNA-seq in other tissue types demonstrated that snRNA-seq may struggle to detect cellular state compared to scRNA-seq. For example, compared to scRNA-seq, snRNA-seq was found to have low sensitivity and be unsuitable for detecting cellular activation in microglia (542). The snRNA-seq therapeutic atlas described herein showed that snRNA-seq was sensitive enough to detect changes in many glucocorticoid related genes in different synovial cell types. Nonetheless, there may be differentially expressed genes that snRNA-seq was insufficiently sensitive to detect.

A study limitation is that not all cell types from the synovium are represented in the snRNA-seq analysis of frozen synovial tissue biopsy samples. For example, neutrophils are notoriously challenging to be analysed using snRNA-seq or scRNA-seq from frozen tissue samples. Neutrophils are highly sensitive to degradation after collection and with

freezing. Moreover, neutrophils have relatively low RNA content and high levels of RNases. Therefore, this snRNA-seq therapeutic atlas maps out the therapeutic response of most but not all cell types in synovial tissues. scRNA-seq or flow cytometry analysis of fresh synovial tissue biopsy samples would provide a more accurate representation of cell types including neutrophils but may be confounded by batch effects.

Sample clogging in GEM preparation led to fewer recovered cells which may have impacted downstream analysis. Sample clogs may have been due to suboptimal sample preparations, non-sterile work environments, clumping of gel beads, or slow chip loading. Strategies to minimize sample clogging include cell debris removal using cell strainers, visually inspecting single cell suspension before loading onto the chip and avoid overloading chip with excess cells. Grounding frozen synovial tissues into powder quickly in mortar may also yield higher nuclei recovery with less clogging (543).

Myocytes expressing striated muscle genes were also found in greater numbers in my study than expected compared to previous scRNA-seq studies of synovial tissue biopsies (336, 355). This may have been due to poor biopsy technique resulting in collection of extra-articular muscle tissues. However, perhaps it should not be too surprising for myocytes to be found given that the biopsy needle passes through muscle tissues. Since skeletal myocytes are multinucleated, the inclusion of skeletal muscle fibres may give disproportionately large number of skeletal myocyte nuclei. Myocytes may be underestimated in scRNA-seq studies as they are multinucleated cells that may be too large to be captured in microfluidic droplets for scRNA-seq analysis. Although exploratory analysis without samples from participants containing skeletal myocytes was performed to limit confounding by extra-articular cells, this nonetheless does not exclude the possibility

of extra-articular cells being present in biopsy samples such as adipocytes from extra-articular fat pads.

Cell-free RNA molecules in the cell suspension (ambient RNA) may lead to inflated UMI counts. Ambient RNA sources include ruptured, dead or dying cells, or other exogenous contamination sources. If not accounted for, background UMI counts may lead to systematic biases or batch effects in downstream analyses. Increased background RNA led to the barcode rank plot not having a steep cliff, which is not unusual with snRNA-seq datasets (Supplementary Figure 14). DecontX and automated SoupX methods were used to remove ambient RNA but manual soupX settings or CellBender may be more effective at removing background noise (349, 544). I attempted to apply SoupX using manual settings to estimate the cell contamination fraction. Although this manual strategy improved background removal such as haemoglobin genes, it distorted the fine structure of the dataset making the automated method preferable (data not shown) (544). Further finetuning of manual soupX settings may allow more effective ambient removal without erroneous data distortion. CellBender is an alternative automated method but it has the disadvantage of heavy computational cost.

Read counts were normalised in the pre-processing pipeline using log normalisation to ensure that measurements are comparable across cells of different library sizes (363). However, other normalisation methods exist and may be preferable. SCTransform has been shown to improve performance of single cell pathway scoring tools (545). SCTransform normalises counts based on one group of genes at a time, with each group selected so that all the genes have similar abundances. This approach allows variation in total library size rather than enforcing it as a constant metric. Re-analysis using

SCTransform would assess whether the normalisation method affects analysis results. Paired differential gene expression here was performed using DESeq2 but other methods are available. Further work involves analysing differential expression using other single cell RNA sequencing differential analysis methods such as MAST to confirm findings (546).

Despite these limitations, snRNA-seq analysis was able to demonstrate the effects of intra-articular methylprednisolone on synovial tissues at single nucleus level. The downregulation of *TIMP1* expression in synovial tissue lining fibroblast after intra-articular methylprednisolone injection is consistent with other studies. This therapeutic atlas of intra-articular methylprednisolone injection effects also identified potential novel therapeutic targets in inflammatory arthritis. snRNA-seq analysis of synovial tissue biopsy before and after treatment may be a useful tool in the future to study novel therapeutics.

5. Conclusion and future work

Hypoxia in the joint is a feature of inflammatory arthritis and may contribute to the pathogenesis of inflammation. This DPhil initially had set out to investigate whether oxygen nanobubbles could relieve joint hypoxia in patients with inflammatory arthritis as a therapeutic intervention. Upon further *in vitro* investigation, I found that the oxygen nanobubbles may mediate effects through its chemical components independently of gaseous effects. Due to the uncertainty underlying the nature of oxygen nanobubbles and their mechanisms of action, the clinical study of oxygen nanobubbles in patients with inflammatory arthritis was cancelled. Instead, I proceeded with the parallel perturbation study of intra-articular methylprednisolone injection that was originally planned to provide context for the nanobubble study. This study of intra-articular methylprednisolone injection provides a platform to advance understanding of the mechanism of action of this widely used but incompletely understood treatment.

Intra-articular methylprednisolone injection is a widely used therapy for treating inflammatory arthritis, especially when a single joint is involved. Inflammatory arthritis patients who responded to TNFi were found to have higher synovial tissue oxygen with treatment. My study found no change in synovial fluid oxygen with intra-articular methylprednisolone injection. This discrepancy may be due to numerous factors such as the measurement of oxygen levels in the synovial fluid instead of the synovial tissue and not having a sample size large enough to have sufficient treatment responders for subgroup analysis. Single nucleus transcriptomic analysis of the synovial tissues also found no changes in hypoxia markers with intra-articular methylprednisolone injection.

Our understanding of inflammatory arthritis has been greatly advanced by single cell transcriptomic analysis. Synovial tissue adipocytes were not sequenced in previous single cell transcriptomic studies due to their buoyancy and so would be lost during the tissue disaggregation process. Single nucleus transcriptomic analysis has the advantage of not needing tissue disaggregation for nuclei extraction. My study provided unique insights into longitudinal effects of intra-articular methylprednisolone injection on single nucleus transcriptomic profiles of inflammatory arthritis synovial tissues. Known methylprednisolone effects such as *TIMP1* downregulation were demonstrated in my study, providing biological correlation between this exploratory study with known ground truths. In particular, I discovered neuron-related genes expressed by lining fibroblasts that may be novel therapeutic targets in patients with PsA.

For instance, I found downregulation of *TNFAIP6* and *JAK2* in synovial tissue lining fibroblasts of patients with PsA after intra-articular methylprednisolone injection. The importance of TNF and JAK pathways in PsA is exemplified by the widespread use of inhibitors that target TNF and JAK in the treatment of PsA. This provides evidence that the perturbed gene expression by intra-articular methylprednisolone injection may identify established as well as novel therapeutic targets. For example, it is intriguing that *SLC24A3* was also downregulated after intra-articular methylprednisolone injection in synovial tissue lining fibroblasts of patients with PsA. The sodium/potassium/calcium exchanger encoded by *SLC24A3* has previously been implicated in inflammatory bowel disease, suggesting *SLC24A3* may play a shared mechanistic role in inflammation across tissues involving synovium as well as the gastrointestinal tract.

Whether *SLC24A3* in synovial tissue lining fibroblasts is also perturbed by TNFi treatment may be explored by interrogating the dataset provided by Thomas *et al*. (547). Publicly available GWAS datasets may also be leveraged to investigate whether *SLC24A3* alleles are associated with immune mediated inflammatory diseases. Although my work has demonstrated downregulation of *SLC24A3* expression in lining fibroblasts of 4 patients with PsA after intra-articular methylprednisolone injection, this synovial tissue finding needs to be confirmed in a larger independent study with multiple follow up timepoints at protein level. Spatial proteomic analysis of synovial tissues would confirm SLC24A3 as a disease biomarker and facilitate understanding of its role in cellular interactions within tissue microenvironments. Further mechanistic studies are needed understand the cellular and molecular role of *SLC24A3* in the pathogenesis and resolution of inflammatory disease. *Slc24a3* KO mice have already demonstrated that SLC24A3 plays a critical role in the immune response through regulation of p53 and NF-κB signalling (475). Inflammatory arthritis models in *Slc24a3* KO mice would delineate the role of SLC24A3 in inflammatory arthritis. SLC24A3 in the mouse joint may also be directly targeted using agonists and antagonists to understand its role in health and disease.

The importance of synovial tissue adipocytes in the pathogenesis and resolution of inflammatory arthritis is demonstrated by their response to treatment. I showed that intra-articular methylprednisolone injection reduced the proportion of adipocytes in the synovial tissue composition, and upregulated lipogenesis genes and gene set pathways. Intra-articular methylprednisolone injections may not be repeated within three months due to their long-lasting effects. Most previous perturbation studies of glucocorticoid effects on synovial tissues have follow-up of less than two weeks. The longer follow-up of four weeks in my study allows study of the prolonged effects of intra-articular

methylprednisolone injection. The perturbation effects on adipocyte composition and gene expression suggest that synovial tissue adipocytes may be important drivers underlying the long-term effects of intra-articular methylprednisolone injection.

This study provided unique insights into adipocytes in cell-cell communication in inflammatory arthritis synovial tissues. I found that adipocytes are major signalling players that send diverse signalling pathways to diverse stromal and immune cell types in inflammatory arthritis synovial tissues. This provided unique insights into the role of adipocytes in inflammatory arthritis synovial tissues. Spatial analysis would confirm these adipocyte findings.

Exploratory comparison of pre-treatment synovial tissue identified *MGP* and *BMPER* as molecular endotypes for lining fibroblasts in RA and PsA, respectively. Given that the *MGP* pathway may inhibit bone mineralisation, and that lining fibroblasts have been implicated in tissue damage in RA, together these results suggest that the *MGP* pathway may be a novel therapeutic target for preventing bony erosions in RA but not PsA. Conversely, the upregulation of *BMPER* in PsA lining fibroblasts may account for the bushy tortuous vasculature and bony proliferation characteristics of PsA. Use of animal models would delineate the roles of *MGP* and *BMPER* in the pathogenesis of inflammatory arthritis and their potential as therapeutic targets.

Overexpression of *MGP* transgene in mouse models inhibited side branching of the vascular endothelium (541). This appears to be analogous to the straight, linear blood vessels seen in RA synovial tissues, and may also be driven by overexpression of MGP by synovial tissue lining fibroblasts. MGP loss-of-function or gain-of-function experiments

using *Mgp*$^{-/-}$ KO mice and *MGP*$^{tg/wt}$ transgenic mice would enhance understanding of how MGP affects synovial tissue vasculature morphology and bony erosions in RA (540, 541, 548).

Synovial tissue angiogenesis is characteristic of both RA and PsA, but PsA synovial blood vessels have a tortuous, elongated and dilated morphology like that observed in tumour vasculature (527). PsA synovial fibroblasts have been shown to promote angiogenesis through regulation of endothelial cells (527). My study revealed *BMPER* as a potentially novel transcriptional biomarker of PsA synovial tissue lining fibroblasts.

Publicly available single cell atlas of synovial tissues, such as the dataset provided by Floudas *et al*., may provide insight as to whether *BMPER* is upregulated in synovial tissue lining fibroblasts from patients with PsA compared to RA (346). Animal models of inflammatory arthritis are needed to investigate the mechanistic role of BMPER in PsA and its potential as a therapeutic target. Mice missing one allele of *Bmper* (*Bmper*$^{+/-}$ mice) have demonstrated the pivotal role of BMPER in an animal model of pulmonary inflammatory response (536). *Bmper*$^{-/-}$ mice die at birth so *Bmper*$^{+/-}$ mice are used instead to study the role of *Bmper* (537). BMPER has been shown to regulate inflammatory responses in endothelial cells in a lipopolysaccharide (LPS) challenge, suggesting BMPER may be a therapeutic target in setting of inflammation. *Bmper*$^{+/-}$ mice should be used to investigate the role of BMPER in not only CIA but especially *Saccharomyces cerevisiae* mannan-induced psoriatic arthritis (MIP) (549). Inducing MIP in wildtype and *Bmper*$^{+/-}$ mice would reveal if *Bmper* haploinsufficiency would affect development of experimental PsA.

The mechanistic role of BMPER in angiogenesis has been studied previously (535). BMPER promotes endothelial cell sprouting and migration *in vitro* and *in vivo*. Using the chick chorioallantois membrane assay, Heinke *et al*. demonstrated that application of BMPER protein resulted in a denser capillary network with greater capillary diameters, similar to the addition of VEGF (535). This may be analogous to the bushy tortuous vasculature seen in PsA so it would be interesting to see whether intra-articular administration of BMPER protein in mouse joints would be sufficient to recapitulate the vasculature phenotype seen in PsA.

In conclusion, this thesis explored therapeutic effects on hypoxic pathways in inflammatory arthritis. Although a clinical study of oxygen nanobubbles effects on joint hypoxia was planned, this did not come to fruition as *in vitro* experiments showed the nanobubbles mediate effects through biochemical rather than gaseous means. The parallel study of intra-articular methylprednisolone injection showed no effects on hypoxic pathways in inflammatory arthritis. Exploratory analysis of synovial tissue using single nucleus transcriptomics provided known and novel insights into the therapeutic effects of intra-articular methylprednisolone injection.

6. References

1. Strand V, Sharp V, Koenig AS, Park G, Shi YF, Wang B, et al. Comparison of health-related quality of life in rheumatoid arthritis, psoriatic arthritis and psoriasis and effects of etanercept treatment. Annals of the Rheumatic Diseases. 2012;71(7):1143-50. doi: 10.1136/annrheumdis-2011-200387. PubMed PMID: WOS:000305293400007.
2. Merola J, Espinoza L, Fleischmann R. Distinguishing rheumatoid arthritis from psoriatic arthritis. RMD OPEN. 2018;4. doi: 10.1136/rmdopen-2018-000656. PubMed PMID: WOS:000442552300011.
3. Alamanos Y, Drosos AA. Epidemiology of adult rheumatoid arthritis. Autoimmunity Reviews. 2005;4(3):130-6. doi: 10.1016/j.autrev.2004.09.002. PubMed PMID: WOS:000229062300003.
4. Aletaha D, Neogi T, Silman A, Funovits J, Felson D, Bingham C, et al. 2010 Rheumatoid Arthritis Classification Criteria An American College of Rheumatology/European League Against Rheumatism Collaborative Initiative. ARTHRITIS AND RHEUMATISM. 2010;62:2569-81. doi: 10.1002/art.27584. PubMed PMID: WOS:000283059100001.
5. Gelfand JM, Gladman DD, Mease PJ, Smith N, Margolis DJ, Nijsten T, et al. Epidemiology of psoriatic arthritis in the population of the United States. Journal of the American Academy of Dermatology. 2005;53(4):573-7. doi: 10.1016/j.jaad.2005.03.046. PubMed PMID: WOS:000232067800002.
6. Taylor W, Gladman D, Helliwell P, Marchesoni A, Mease P, Mielants H, et al. Classification criteria for psoriatic arthritis - Development of new criteria from a large international study. ARTHRITIS AND RHEUMATISM. 2006;54:2665-73. doi: 10.1002/art.21972. PubMed PMID: WOS:000239641400037.
7. Coates L, FitzGerald O, Helliwell P, Paul C. Psoriasis, psoriatic arthritis, and rheumatoid arthritis: Is all inflammation the same? SEMINARS IN ARTHRITIS AND RHEUMATISM. 2016;46:291-304. doi: 10.1016/j.semarthrit.2016.05.012. PubMed PMID: WOS:000390979200006.
8. Felquer M, FitzGerald O. Peripheral joint involvement in psoriatic arthritis patients. CLINICAL AND EXPERIMENTAL RHEUMATOLOGY. 2015;33:S26-S30. PubMed PMID: WOS:000364357100006.
9. Smolen J, Landewe R, Bergstra S, Kerschbaumer A, Sepriano A, Aletaha D, et al. EULAR recommendations for the management of rheumatoid arthritis with synthetic and biological disease-modifying antirheumatic drugs: 2022 update. ANNALS OF THE RHEUMATIC DISEASES. 2023;82:3-18. doi: 10.1136/ard-2022-223356. PubMed PMID: WOS:000885543600001.
10. Gossec L, Kerschbaumer A, Ferreira R, Aletaha D, Baraliakos X, Bertheussen H, et al. EULAR recommendations for the management of psoriatic arthritis with pharmacological therapies: 2023 update. ANNALS OF THE RHEUMATIC DISEASES. 2024;83:706-19. doi: 10.1136/ard-2024-225531. PubMed PMID: WOS:001189118000001.
11. Rein P, Mueller RB. Treatment with Biologicals in Rheumatoid Arthritis: An Overview. Rheumatology and Therapy. 2017;4(2):247-61. doi: 10.1007/s40744-017-0073-3. PubMed PMID: WOS:000416125000004.
12. Ogdie A, Coates LC, Gladman DD. Treatment guidelines in psoriatic arthritis. Rheumatology. 2020;59:I37-I46. doi: 10.1093/rheumatology/kez383. PubMed PMID: WOS:000531538500007.

13. Germano V, Cattaruzza M, Osborn J, Tarantino A, Di Rosa R, Salemi S, et al. Infection risk in Rheumatoid Arthritis and Spondyloarthropathy patients under treatment with DMARDs, Corticosteroids and TNF-α antagonists. J Transl Med. 2014;12. doi: 10.1186/1479-5876-12-77. PubMed PMID: WOS:000336922200003.
14. Winthrop K, Mease P, Kerschbaumer A, Voll R, Breedveld F, Smolen J, et al. Unmet need in rheumatology: reports from the Advances in Targeted Therapies meeting, 2023. ANNALS OF THE RHEUMATIC DISEASES. 2024;83:409-16. doi: 10.1136/ard-2023-224916. PubMed PMID: WOS:001143651300001.
15. Thomas J, Bansback N, Barber C, Wells G, Hazlewood G. Personalized medicine in rheumatoid arthritis: Combining biomarkers and patient preferences to guide therapeutic decisions. BEST PRACTICE & RESEARCH IN CLINICAL RHEUMATOLOGY. 2022;36. doi: 10.1016/j.berh.2022.101812. PubMed PMID: WOS:001053216100001.
16. Lundolesen K. OXYGEN TENSION IN SYNOVIAL FLUIDS. Arthritis and Rheumatism. 1970;13(6):769-+. doi: 10.1002/art.1780130606. PubMed PMID: WOS:A1970H953900006.
17. McGarry T, Biniecka M, Veale DJ, Fearon U. Hypoxia, oxidative stress and inflammation. Free Radic Biol Med. 2018;125:15-24. Epub 2018/03/31. doi: 10.1016/j.freeradbiomed.2018.03.042. PubMed PMID: 29601945.
18. Hitchon C, Wong K, Ma G, Reed J, Lyttle D, El-Gabalawy H. Hypoxia-induced production of stromal cell-derived factor 1 (CXCL12) and vascular endothelial growth factor by synovial fibroblasts. Arthritis Rheum. 2002;46(10):2587-97. Epub 2002/10/18. doi: 10.1002/art.10520. PubMed PMID: 12384916.
19. Makino Y, Nakamura H, Ikeda E, Ohnuma K, Yamauchi K, Yabe Y, et al. Hypoxia-Inducible Factor Regulates Survival of Antigen Receptor-Driven T Cells. Journal of Immunology. 2003;171(12):6534-40. doi: http://dx.doi.org/10.4049/jimmunol.171.12.6534.
20. Hollander AP, Corke KP, Freemont AJ, Lewis CE. Expression of hypoxia-inducible factor 1alpha by macrophages in the rheumatoid synovium: implications for targeting of therapeutic genes to the inflamed joint. Arthritis Rheum. 2001;44(7):1540-4. Epub 2001/07/24. doi: 10.1002/1529-0131(200107)44:7<1540::aid-art277>3.0.co;2-7. PubMed PMID: 11465705.
21. Murdoch C, Muthana M, Lewis CE. Hypoxia regulates macrophage functions in inflammation. J Immunol. 2005;175(10):6257-63. Epub 2005/11/08. doi: 10.4049/jimmunol.175.10.6257. PubMed PMID: 16272275.
22. Kaelin WG, Jr., Ratcliffe PJ. Oxygen sensing by metazoans: The central role of the HIF hydroxylase pathway. Molecular Cell. 2008;30(4):393-402. doi: 10.1016/j.molcel.2008.04.009. PubMed PMID: WOS:000256266900001.
23. Semenza G. Hypoxia-Inducible Factors in Physiology and Medicine. CELL. 2012;148:399-408. doi: 10.1016/j.cell.2012.01.021. PubMed PMID: WOS:000300225000010.
24. Quiñonez-Flores CM, González-Chávez SA, Pacheco-Tena C. Hypoxia and its implications in rheumatoid arthritis. J Biomed Sci. 2016;23(1):62. Epub 2016/08/24. doi: 10.1186/s12929-016-0281-0. PubMed PMID: 27549205; PubMed Central PMCID: PMC4994473.
25. Berra E, Benizri E, Ginouvès A, Volmat V, Roux D, Pouysségur J. HIF prolyl-hydroxylase 2 is the key oxygen sensor setting low steady-state levels of HIF-1alpha in normoxia. EMBO J. 2003;22(16):4082-90. doi: 10.1093/emboj/cdg392. PubMed PMID: 12912907; PubMed Central PMCID: PMC175782.
26. Appelhoff R, Tian Y, Raval R, Turley H, Harris A, Pugh C, et al. Differential function of the prolyl hydroxylases PHD1, PHD2, and PHD3 in the regulation of hypoxia-

inducible factor. J Biol Chem. 2004;279:38458-65. doi: 10.1074/jbc.M406026200. PubMed PMID: WOS:000223684100049.
27. Paradowska-Gorycka A, Stypinska B, Pawlik A, Haladyj E, Romanowska-Prochnicka K, Olesinska M. HIF-1A gene polymorphisms and its protein level in patients with rheumatoid arthritis: a case-control study. Inflammation Research. 2018;67(5):423-33. doi: 10.1007/s00011-018-1134-y. PubMed PMID: WOS:000429923700005.
28. Ahn JK, Koh EM, Cha HS, Lee YS, Kim J, Bae EK, et al. Role of hypoxia-inducible factor-1alpha in hypoxia-induced expressions of IL-8, MMP-1 and MMP-3 in rheumatoid fibroblast-like synoviocytes. Rheumatology. 2008;47(6):834-9. doi: http://dx.doi.org/10.1093/rheumatology/ken086.
29. Cramer T, Yamanishi Y, Clausen BE, Forster I, Pawlinski R, Mackman N, et al. HIF-1 alpha is essential for myeloid cell-mediated inflammation. Cell. 2003;112(5):645-57. doi: 10.1016/s0092-8674(03)00154-5. PubMed PMID: WOS:000181443600008.
30. Christensen A, Haase C, Cook A, Hamilton J. K/BxN Serum-Transfer Arthritis as a Model for Human inflammatory Arthritis. Front Immunol. 2016;7. doi: 10.3389/fimmu.2016.00213. PubMed PMID: WOS:000376843300001.
31. Matsumoto I, Staub A, Benoist C, Mathis D. Arthritis provoked by linked T and B cell recognition of a glycolytic enzyme. SCIENCE. 1999;286(5445):1732-5. PubMed PMID: WOS:000083912200037.
32. Giatromanolaki A, Sivridis E, Maltezos E, Athanassou N, Papazoglou D, Gatter KC, et al. Upregulated hypoxia inducible factor-1alpha and -2alpha pathway in rheumatoid arthritis and osteoarthritis. Arthritis Res Ther. 2003;5(4):R193-201. Epub 2003/06/26. doi: 10.1186/ar756. PubMed PMID: 12823854; PubMed Central PMCID: PMC165055.
33. Ratcliffe PJ. HIF-1 and HIF-2: working alone or together in hypoxia? Journal of Clinical Investigation. 2007;117(4):862-5. doi: 10.1172/jci31750. PubMed PMID: WOS:000245451700005.
34. Ryu JH, Chae CS, Kwak JS, Oh H, Shin Y, Huh YH, et al. Hypoxia-inducible factor-2α is an essential catabolic regulator of inflammatory rheumatoid arthritis. PLoS Biol. 2014;12(6):e1001881. Epub 2014/06/11. doi: 10.1371/journal.pbio.1001881. PubMed PMID: 24914685; PubMed Central PMCID: PMC4051611.
35. Sivakumar B, Akhavani MA, Winlove CP, Taylor PC, Paleolog EM, Kang N. Synovial hypoxia as a cause of tendon rupture in rheumatoid arthritis. J Hand Surg Am. 2008;33(1):49-58. Epub 2008/02/12. doi: 10.1016/j.jhsa.2007.09.002. PubMed PMID: 18261665.
36. Brand D, Latham K, Rosloniec E. Collagen-induced arthritis. NATURE PROTOCOLS. 2007;2(5):1269-75. doi: 10.1038/nprot.2007.173. PubMed PMID: WOS:000253138700026.
37. Yang S, Kim J, Ryu J, Oh H, Chun C, Kim B, et al. Hypoxia-inducible factor-2α is a catabolic regulator of osteoarthritic cartilage destruction. NATURE MEDICINE. 2010;16(6):687-U91. doi: 10.1038/nm.2153. PubMed PMID: WOS:000278394200035.
38. Ryu J, Yang S, Shin Y, Rhee J, Chun C, Chun J. Interleukin-6 Plays an Essential Role in Hypoxia-Inducible Factor 2α-Induced Experimental Osteoarthritic Cartilage Destruction in Mice. ARTHRITIS AND RHEUMATISM. 2011;63(9):2732-43. doi: 10.1002/art.30451. PubMed PMID: WOS:000295005000022.
39. Deng W, Feng X, Li X, Wang D, Sun L. Hypoxia-inducible factor 1 in autoimmune diseases. CELLULAR IMMUNOLOGY. 2016;303:7-15. doi: 10.1016/j.cellimm.2016.04.001. PubMed PMID: WOS:000375821900002.
40. Hu F, Liu H, Xu L, Li Y, Liu X, Shi L, et al. Hypoxia-inducible factor-1alpha perpetuates synovial fibroblast interactions with T cells and B cells in rheumatoid arthritis.

European Journal of Immunology. 2016;46(3):742-51. doi: http://dx.doi.org/10.1002/eji.201545784.
41. Hua S, Dias TH. Hypoxia-Inducible Factor (HIF) as a Target for Novel Therapies in Rheumatoid Arthritis. Front Pharmacol. 2016;7:184. Epub 2016/07/23. doi: 10.3389/fphar.2016.00184. PubMed PMID: 27445820; PubMed Central PMCID: PMC4921475.
42. Gaber T, Dziurla R, Tripmacher R, Burmester GR, Buttgereit F. Hypoxia inducible factor (HIF) in rheumatology: Low O2! See what HIF can do! Annals of the Rheumatic Diseases. 2005;64(7):971-80. doi: http://dx.doi.org/10.1136/ard.2004.031641.
43. Brouwer E, Gouw AS, Posthumus MD, van Leeuwen MA, Boerboom AL, Bijzet J, et al. Hypoxia inducible factor-1-alpha (HIF-1alpha) is related to both angiogenesis and inflammation in rheumatoid arthritis. Clin Exp Rheumatol. 2009;27(6):945-51. Epub 2010/02/13. PubMed PMID: 20149310.
44. Maruotti N, Cantatore FP, Crivellato E, Vacca A, Ribatti D. Angiogenesis in rheumatoid arthritis. Histology and Histopathology. 2006;21(4-6):557-66.
45. Takeda N, Maemura K, Imai Y, Harada T, Kawanami D, Nojiri T, et al. Endothelial PAS domain protein 1 gene promotes angiogenesis through the transactivation of both vascular endothelial growth factor and its receptor, Flt-1. CIRCULATION RESEARCH. 2004;95:146-53. doi: 10.1161/01.RES.0000134920.10128.b4. PubMed PMID: WOS:000222835600006.
46. Bosco MC, Delfino S, Ferlito F, Battaglia F, Puppo M, Gregorio A, et al. Hypoxic synovial environment and expression of macrophage inflammatory protein 3alpha/CCL20 in juvenile idiopathic arthritis. Arthritis and Rheumatism. 2008;58(6):1833-8. doi: http://dx.doi.org/10.1002/art.23516.
47. Santiago B, Calonge E, Del Rey MJ, Gutierrez-Cañas I, Izquierdo E, Usategui A, et al. CXCL12 gene expression is upregulated by hypoxia and growth arrest but not by inflammatory cytokines in rheumatoid synovial fibroblasts. Cytokine. 2011;53(2):184-90. Epub 2010/07/09. doi: 10.1016/j.cyto.2010.06.006. PubMed PMID: 20609598.
48. Koch AE. Angiogenesis as a target in rheumatoid arthritis. Annals of the Rheumatic Diseases. 2003;62:60-7. doi: 10.1136/ard.62.suppl_2.ii60. PubMed PMID: WOS:000185766200016.
49. Walsh D, Pearson C. Angiogenesis in the pathogenesis of inflammatory joint and lung diseases. ARTHRITIS RESEARCH. 2001;3:147-53. PubMed PMID: WOS:000167775100004.
50. Brenchley P. Antagonising angiogenesis in rheumatoid arthritis. ANNALS OF THE RHEUMATIC DISEASES. 2001;60:III71-III4. PubMed PMID: WOS:000171874400017.
51. Akhavani MA, Madden L, Buysschaert I, Sivakumar B, Kang N, Paleolog EM. Hypoxia upregulates angiogenesis and synovial cell migration in rheumatoid arthritis. Arthritis Res Ther. 2009;11(3):R64. Epub 2009/05/12. doi: 10.1186/ar2689. PubMed PMID: 19426483; PubMed Central PMCID: PMC2714109.
52. Munoz-Najar UM, Neurath KM, Vumbaca F, Claffey KP. Hypoxia stimulates breast carcinoma cell invasion through MT1-MMP and MMP-2 activation. Oncogene. 2006;25(16):2379-92. doi: 10.1038/sj.onc.1209273. PubMed PMID: WOS:000236764300010.
53. Bauer AT, Burgers HF, Rabie T, Marti HH. Matrix metalloproteinase-9 mediates hypoxia-induced vascular leakage in the brain via tight junction rearrangement. Journal of Cerebral Blood Flow and Metabolism. 2010;30(4):837-48. doi: 10.1038/jcbfm.2009.248. PubMed PMID: WOS:000276197200018.

54. Blades M, Ingegnoli F, Wheller S, Manzo A, Wahid S, Panayi G, et al. Stromal cell-derived factor 1 (CXCL12) induces monocyte migration into human synovium transplanted onto SCID mice. ARTHRITIS AND RHEUMATISM. 2002;46:824-36. doi: 10.1002/art.10102. PubMed PMID: WOS:000174409200032.
55. Nanki T, Hayashida K, El-Gabalawy H, Suson S, Shi K, Girschick H, et al. Stromal cell-derived factor-1-CXC chemokine receptor 4 interactions play a central role in CD4⁺ T cell accumulation in rheumatoid arthritis synovium. JOURNAL OF IMMUNOLOGY. 2000;165:6590-8. PubMed PMID: WOS:000165467100073.
56. Ceradini D, Kulkarni A, Callaghan M, Tepper O, Bastidas N, Kleinman M, et al. Progenitor cell trafficking is regulated by hypoxic gradients through HIF-1 induction of SDF-1. NATURE MEDICINE. 2004;10:858-64. doi: 10.1038/nm1075. PubMed PMID: WOS:000223055700041.
57. Staller P, Sulitkova J, Liszlwan J, Moch H, Oakeley E, Krek W. Chemokine receptor CXCR4 downregulated by von Hippel-Lindau tumour suppressor pVHL. NATURE. 2003;425:307-11. doi: 10.1038/nature01874. PubMed PMID: WOS:000185370900048.
58. Kong T, Eltzschig H, Karhausen J, Colgan S, Shelley C. Leukocyte adhesion during hypoxia is mediated by HIF-1-dependent induction Of β2 integrin gene expression. PROCEEDINGS OF THE NATIONAL ACADEMY OF SCIENCES OF THE UNITED STATES OF AMERICA. 2004;101:10440-5. doi: 10.1073/pnas.0401339101. PubMed PMID: WOS:000222664200036.
59. Oikawa M, Abe M, Kurosawa H, Hida W, Shirato K, Sato Y. Hypoxia induces transcription factor ETS-1 via the activity of hypoxia-inducible factor-1. BIOCHEMICAL AND BIOPHYSICAL RESEARCH COMMUNICATIONS. 2001;289:39-43. doi: 10.1006/bbrc.2001.5927. PubMed PMID: WOS:000172451100007.
60. Peters CL, Morris CJ, Mapp PI, Blake DR, Lewis CE, Winrow VR. The transcription factors hypoxia-inducible factor 1alpha and Ets-1 colocalize in the hypoxic synovium of inflamed joints in adjuvant-induced arthritis. Arthritis Rheum. 2004;50(1):291-6. Epub 2004/01/20. doi: 10.1002/art.11473. PubMed PMID: 14730627.
61. Sato Y. Role of ETS family transcription factors in vascular development and angiogenesis. CELL STRUCTURE AND FUNCTION. 2001;26:19-24. PubMed PMID: WOS:000168417400004.
62. Cha HS, Ahn KS, Jeon CH, Kim J, Song YW, Koh EM. Influence of hypoxia on the expression of matrix metalloproteinase-1, -3 and tissue inhibitor of metalloproteinase-1 in rheumatoid synovial fibroblasts. Clin Exp Rheumatol. 2003;21(5):593-8. Epub 2003/11/13. PubMed PMID: 14611107.
63. Swales C, Athanasou NA, Knowles HJ. Angiopoietin-like 4 is over-expressed in rheumatoid arthritis patients: association with pathological bone resorption. PLoS One. 2014;9(10):e109524. Epub 2014/10/08. doi: 10.1371/journal.pone.0109524. PubMed PMID: 25289668; PubMed Central PMCID: PMC4188739.
64. Kim K, Bang S, Lee H, Bae S. Update on the genetic architecture of rheumatoid arthritis. NATURE REVIEWS RHEUMATOLOGY. 2017;13(1):13-24. doi: 10.1038/nrrheum.2016.176. PubMed PMID: WOS:000391344100005.
65. Stahl E, Raychaudhuri S, Remmers E, Xie G, Eyre S, Thomson B, et al. Genome-wide association study meta-analysis identifies seven new rheumatoid arthritis risk loci. NATURE GENETICS. 2010;42(6):508-U56. doi: 10.1038/ng.582. PubMed PMID: WOS:000278081500016.
66. Okada Y, Wu D, Trynka G, Raj T, Terao C, Ikari K, et al. Genetics of rheumatoid arthritis contributes to biology and drug discovery. NATURE. 2014;506(7488):376-+. doi: 10.1038/nature12873. PubMed PMID: WOS:000331477800043.

67. Ha E, Bae S, Kim K. Large-scale meta-analysis across East Asian and European populations updated genetic architecture and variant-driven biology of rheumatoid arthritis, identifying 11 novel susceptibility loci. ANNALS OF THE RHEUMATIC DISEASES. 2021;80(5):558-65. doi: 10.1136/annrheumdis-2020-219065. PubMed PMID: WOS:000641486900026.
68. Ishigaki K, Sakaue S, Terao C, Luo Y, Sonehara K, Yamaguchi K, et al. Multi-ancestry genome-wide association analyses identify novel genetic mechanisms in rheumatoid arthritis. NATURE GENETICS. 2022;54(11):1640-+. doi: 10.1038/s41588-022-01213-w. PubMed PMID: WOS:000878933800001.
69. Oliver KM, Taylor CT, Cummins EP. Hypoxia. Regulation of NFkappaB signalling during inflammation: The role of hydroxylases. Arthritis Research and Therapy. 2009;11(1):215. doi: http://dx.doi.org/10.1186/ar2575.
70. Cummins E, Keogh C, Crean D, Taylor C. The role of HIF in immunity and inflammation. MOLECULAR ASPECTS OF MEDICINE. 2016;47-48:24-34. doi: 10.1016/j.mam.2015.12.004. PubMed PMID: WOS:000369638000004.
71. Rius J, Guma M, Schachtrup C, Akassoglou K, Zinkernagel AS, Nizet V, et al. NF-kappaB links innate immunity to the hypoxic response through transcriptional regulation of HIF-1alpha. Nature. 2008;453(7196):807-11. Epub 20080423. doi: 10.1038/nature06905. PubMed PMID: 18432192; PubMed Central PMCID: PMC2669289.
72. Razani B, Reichardt A, Cheng G. Non-canonical NF-κB signaling activation and regulation: principles and perspectives. Immunol Rev. 2011;244:44-54. doi: 10.1111/j.1600-065X.2011.01059.x. PubMed PMID: WOS:000297507300004.
73. Hu F, Mu R, Zhu J, Shi L, Li Y, Liu X, et al. Hypoxia and hypoxia-inducible factor-1α provoke toll-like receptor signalling-induced inflammation in rheumatoid arthritis. Ann Rheum Dis. 2014;73(5):928-36. Epub 2013/05/07. doi: 10.1136/annrheumdis-2012-202444. PubMed PMID: 23644550.
74. Benito M, Murphy E, Murphy E, van den Berg W, FitzGerald O, Bresnihan B. Increased synovial tissue NF-κB1 expression at sites adjacent to the cartilage-pannus junction in rheumatoid arthritis. ARTHRITIS AND RHEUMATISM. 2004;50:1781-7. doi: 10.1002/art.20260. PubMed PMID: WOS:000221876000012.
75. Simmonds R, Foxwell B. Signalling, inflammation and arthritis -: NF-κB and its relevance to arthritis and inflammation. Rheumatology. 2008;47:584-90. doi: 10.1093/rheumatology/kem298. PubMed PMID: WOS:000255315700006.
76. Oliver KM, Garvey JF, Ng CT, Veale DJ, Fearon U, Cummins EP, et al. Hypoxia activates NF-kappaB-dependent gene expression through the canonical signaling pathway. Antioxid Redox Signal. 2009;11(9):2057-64. Epub 2009/05/09. doi: 10.1089/ars.2008.2400. PubMed PMID: 19422287.
77. Bruning U, Fitzpatrick S, Frank T, Birtwistle M, Taylor C, Cheong A. NFκB and HIF display synergistic behaviour during hypoxic inflammation. CELLULAR AND MOLECULAR LIFE SCIENCES. 2012;69:1319-29. doi: 10.1007/s00018-011-0876-2. PubMed PMID: WOS:000302258700006.
78. van Uden P, Kenneth N, Rocha S. Regulation of hypoxia-inducible factor-1α by NF-κB. BIOCHEMICAL JOURNAL. 2008;412:477-84. doi: 10.1042/BJ20080476. PubMed PMID: WOS:000256946500008.
79. Park SY, Lee SW, Kim HY, Lee WS, Hong KW, Kim CD. HMGB1 induces angiogenesis in rheumatoid arthritis via HIF-1α activation. Eur J Immunol. 2015;45(4):1216-27. Epub 2014/12/30. doi: 10.1002/eji.201444908. PubMed PMID: 25545169.

80. Elia A, Cappello P, Puppo M, Fraone T, Vanni C, Eva A, et al. Human dendritic cells differentiated in hypoxia down-modulate antigen uptake and change their chemokine expression profile. J Leukoc Biol. 2008;84:1472-82. doi: 10.1189/jlb.0208082. PubMed PMID: WOS:000261032300014.
81. Naldini A, Morena E, Pucci A, Miglietta D, Riboldi E, Sozzani S, et al. Hypoxia affects dendritic cell survival: Role of the hypoxia-inducible factor-1a and lipopolysaccharide. J Cell Physiol. 2012;227:587-95. doi: 10.1002/jcp.22761. PubMed PMID: WOS:000298092800021.
82. Mancino A, Schioppa T, Larghi P, Pasqualini F, Nebuloni M, Chen I, et al. Divergent effects of hypoxia on dendritic cell functions. BLOOD. 2008;112:3723-34. doi: 10.1182/blood-2008-02-142091. PubMed PMID: WOS:000260301800032.
83. Palazon A, Goldrath A, Nizet V, Johnson R. HIF Transcription Factors, Inflammation, and Immunity. IMMUNITY. 2014;41:518-28. doi: 10.1016/j.immuni.2014.09.008. PubMed PMID: WOS:000345504300007.
84. Dang E, Barbi J, Yang H, Jinasena D, Yu H, Zheng Y, et al. Control of T_H17/T_{reg} Balance by Hypoxia-Inducible Factor 1. CELL. 2011;146:772-84. doi: 10.1016/j.cell.2011.07.033. PubMed PMID: WOS:000294477500017.
85. Kojima H, Gu H, Nomura S, Caldwell C, Kobata T, Carmeliet P, et al. Abnormal B lymphocyte development and autoimmunity in hypoxia-inducible factor 1α-deficient chimeric mice. PROCEEDINGS OF THE NATIONAL ACADEMY OF SCIENCES OF THE UNITED STATES OF AMERICA. 2002;99:2170-4. doi: 10.1073/pnas.052706699. PubMed PMID: WOS:000174031100076.
86. Kojima H, Kobayashi A, Sakurai D, Kanno Y, Hase H, Takahashi R, et al. Differentiation Stage-Specific Requirement in Hypoxia-Inducible Factor-1α-Regulated Glycolytic Pathway during Murine B Cell Development in Bone Marrow. JOURNAL OF IMMUNOLOGY. 2010;184:154-63. doi: 10.4049/jimmunol.0800167. PubMed PMID: WOS:000272985300020.
87. Jeon CH, Ahn JK, Chai JY, Kim HJ, Bae EK, Park SH, et al. Hypoxia appears at pre-arthritic stage and shows co-localization with early synovial inflammation in collagen induced arthritis. Clin Exp Rheumatol. 2008;26(4):646-8. Epub 2008/09/19. PubMed PMID: 18799097.
88. Etherington PJ, Winlove P, Taylor P, Paleolog E, Miotla JM. VEGF release is associated with reduced oxygen tensions in experimental inflammatory arthritis. Clin Exp Rheumatol. 2002;20(6):799-805. Epub 2003/01/02. PubMed PMID: 12508771.
89. Cousins FL, Murray AA, Scanlon JP, Saunders PT. Hypoxyprobe™ reveals dynamic spatial and temporal changes in hypoxia in a mouse model of endometrial breakdown and repair. BMC Res Notes. 2016;9:30. Epub 20160119. doi: 10.1186/s13104-016-1842-8. PubMed PMID: 26780953; PubMed Central PMCID: PMC4717617.
90. Jankovic B, Aquino-Parsons C, Raleigh J, Stanbridge E, Durand R, Banath J, et al. Comparison between pimonidazole binding, oxygen electrode measurements, and expression of endogenous hypoxia markers in cancer of the uterine cervix. CYTOMETRY PART B-CLINICAL CYTOMETRY. 2006;70B:45-55. doi: 10.1002/cyto.b.20086. PubMed PMID: WOS:000235931400001.
91. Shi M, Cui F, Liu AJ, Ma HJ, Cheng M, Song SX, et al. The protective effects of chronic intermittent hypobaric hypoxia pretreatment against collagen-induced arthritis in rats. J Inflamm (Lond). 2015;12:23. Epub 2015/04/11. doi: 10.1186/s12950-015-0068-1. PubMed PMID: 25861246; PubMed Central PMCID: PMC4389442.
92. Hu F, Shi L, Mu R, Zhu J, Li Y, Ma X, et al. Hypoxia-inducible factor-1α and interleukin 33 form a regulatory circuit to perpetuate the inflammation in rheumatoid

arthritis. PLoS One. 2013;8(8):e72650. Epub 2013/08/24. doi: 10.1371/journal.pone.0072650. PubMed PMID: 23967327; PubMed Central PMCID: PMC3744448.
93. SAGONE A, LAWRENCE T, BALCERZAK S. EFFECT OF SMOKING ON TISSUE OXYGEN SUPPLY. BLOOD. 1973;41(6):845-51. PubMed PMID: WOS:A1973P919600011.
94. Daijo H, Hoshino Y, Kai S, Suzuki K, Nishi K, Matsuo Y, et al. Cigarette smoke reversibly activates hypoxia-inducible factor 1 in a reactive oxygen species-dependent manner. SCIENTIFIC REPORTS. 2016;6. doi: 10.1038/srep34424. PubMed PMID: WOS:000384189700001.
95. Källberg H, Ding B, Padyukov L, Bengtsson C, Rönnelid J, Klareskog L, et al. Smoking is a major preventable risk factor for rheumatoid arthritis: estimations of risks after various exposures to cigarette smoke. ANNALS OF THE RHEUMATIC DISEASES. 2011;70(3):508-11. doi: 10.1136/ard.2009.120899. PubMed PMID: WOS:000286927800017.
96. HELIOVAARA M, AHO K, AROMAA A, KNEKT P, REUNANEN A. SMOKING AND RISK OF RHEUMATOID-ARTHRITIS. JOURNAL OF RHEUMATOLOGY. 1993;20(11):1830-5. PubMed PMID: WOS:A1993ML97300005.
97. Silman A, Newman J, MacGregor A. Cigarette smoking increases the risk of rheumatoid arthritis - Results from a nationwide study of disease-discordant twins. ARTHRITIS AND RHEUMATISM. 1996;39(5):732-5. PubMed PMID: WOS:A1996UJ81300003.
98. Hutchinson D, Shepstone L, Moots R, Lear J, Lynch M. Heavy cigarette smoking is strongly associated with rheumatoid arthritis (RA), particularly in patients without a family history of RA. ANNALS OF THE RHEUMATIC DISEASES. 2001;60(3):223-7. PubMed PMID: WOS:000167210300008.
99. VESSEY M, VILLARDMACKINTOSH L, YEATES D. ORAL-CONTRACEPTIVES, CIGARETTE-SMOKING AND OTHER FACTORS IN RELATION TO ARTHRITIS. CONTRACEPTION. 1987;35(5):457-64. PubMed PMID: WOS:A1987J587600005.
100. Hussain M, Tripathi V. Smoking under hypoxic conditions: a potent environmental risk factor for inflammatory and autoimmune diseases. MILITARY MEDICAL RESEARCH. 2018;5. doi: 10.1186/s40779-018-0158-5. PubMed PMID: WOS:000429071700001.
101. Kent B, Mitchell P, McNicholas W. Hypoxemia in patients with COPD: cause, effects, and disease progression. INTERNATIONAL JOURNAL OF CHRONIC OBSTRUCTIVE PULMONARY DISEASE. 2011;6:199-208. doi: 10.2147/COPD.S10611. PubMed PMID: WOS:000208709800022.
102. Kang J, Jeong S, Lee K, Park N, Jung H, Lee K, et al. Exacerbation of symptomatic arthritis by cigarette smoke in experimental arthritis. PLOS ONE. 2020;15(3). doi: 10.1371/journal.pone.0230719. PubMed PMID: WOS:000535935400020.
103. Ratcliffe P, Koivunen P, Myllyharju J, Ragoussis J, Bovée J, Batinic-Haberle I, et al. Update on hypoxia-inducible factors and hydroxylases in oxygen regulatory pathways: from physiology to therapeutics. HYPOXIA. 2017;5:11-20. doi: 10.2147/HP.S127042. PubMed PMID: WOS:000399117900002.
104. Post T, Denney C, Cohen A, Jordan J, Limper U. Human hypoxia models in aerospace medicine: Potential applications for human pharmacological research. BRITISH JOURNAL OF CLINICAL PHARMACOLOGY. 2024. doi: 10.1111/bcp.16040. PubMed PMID: WOS:001193931400001.

105. Beuck S, Schänzer W, Thevis M. Hypoxia-inducible factor stabilizers and other small-molecule erythropoiesis-stimulating agents in current and preventive doping analysis. DRUG TESTING AND ANALYSIS. 2012;4:830-45. doi: 10.1002/dta.390. PubMed PMID: WOS:000311436000005.
106. Elliott S. Erythropoiesis-stimulating agents and other methods to enhance oxygen transport. BRITISH JOURNAL OF PHARMACOLOGY. 2008;154:529-41. doi: 10.1038/bjp.2008.89. PubMed PMID: WOS:000256133600005.
107. Skalny A, Zaitseva I, Gluhcheva Y, Skalny A, Achkasov E, Skalnaya M, et al. Cobalt in athletes: hypoxia and doping - new crossroads. JOURNAL OF APPLIED BIOMEDICINE. 2019;17:21-8. doi: 10.32725/jab.2018.003. PubMed PMID: WOS:000493806600003.
108. Viscor G, Torrella J, Corral L, Ricart A, Javierre C, Pages T, et al. Physiological and Biological Responses to Short-Term Intermittent Hypobaric Hypoxia Exposure: From Sports and Mountain Medicine to New Biomedical Applications. FRONTIERS IN PHYSIOLOGY. 2018;9. doi: 10.3389/fphys.2018.00814. PubMed PMID: WOS:000437894300001.
109. McLaughlin C, Skabelund A, George A. Impact of High Altitude on Military Operations. CURRENT PULMONOLOGY REPORTS. 2017;6:146-54. doi: 10.1007/s13665-017-0181-0. PubMed PMID: WOS:000405858100009.
110. Bitterman H. Bench-to-bedside review: Oxygen as a drug. CRITICAL CARE. 2009;13. doi: 10.1186/cc7151. PubMed PMID: WOS:000264351600054.
111. Wingelaar T, van Ooij P, van Hulst R. Oxygen Toxicity and Special Operations Forces Diving: Hidden and Dangerous. FRONTIERS IN PSYCHOLOGY. 2017;8. doi: 10.3389/fpsyg.2017.01263. PubMed PMID: WOS:000406403000001.
112. Bitterman N. CNS oxygen toxicity. UNDERSEA AND HYPERBARIC MEDICINE. 2004;31:63-72. PubMed PMID: WOS:000222000700007.
113. Hartnett M, Lane R. Effects of oxygen on the development and severity of retinopathy of prematurity. JOURNAL OF AAPOS. 2013;17(3):229-34. doi: 10.1016/j.jaapos.2012.12.155. PubMed PMID: WOS:000321224900001.
114. Chen M, Guo L, Smith L, Dammann C, Dammann O. High or Low Oxygen Saturation and Severe Retinopathy of Prematurity: A Meta-analysis. PEDIATRICS. 2010;125(6):E1483-E92. doi: 10.1542/peds.2009-2218. PubMed PMID: WOS:000278268600056.
115. GARNER A. AN INTERNATIONAL CLASSIFICATION OF RETINOPATHY OF PREMATURITY. ARCHIVES OF OPHTHALMOLOGY. 1984;102(8):1130-4. PubMed PMID: WOS:A1984TC45900010.
116. Sankar M, Sankar J, Chandra P. Anti-vascular endothelial growth factor (VEGF) drugs for treatment of retinopathy of prematurity. COCHRANE DATABASE OF SYSTEMATIC REVIEWS. 2018(1). doi: 10.1002/14651858.CD009734.pub3. PubMed PMID: WOS:000423977300032.
117. Owen J, Logan K, Nesbitt H, Able S, Vasilyeva A, Bluemke E, et al. [Orally administered oxygen nanobubbles enhance tumor response to sonodynamic therapy]. NANO SELECT2022. p. 394-401.
118. King D, Stride E, Mendis J, Gurton W, Macrae H, Jones L, et al. [A Double-Blind, Randomized, Placebo-Controlled Pilot Study examining an Oxygen Nanobubble Beverage for 16.1-km Time Trial and Repeated Sprint Cycling Performance]. JOURNAL OF DIETARY SUPPLEMENTS2024. p. 167-81.
119. Riess JG. Understanding the fundamentals of perfluorocarbons and perfluorocarbon emulsions relevant to in vivo oxygen delivery. Artificial Cells Blood

Substitutes and Biotechnology. 2005;33(1):47-63. doi: 10.1081/bio-200046659. PubMed PMID: WOS:000227360400005.
120. Owen J, McEwan C, Nesbitt H, Bovornchutichai P, Averre R, Borden M, et al. Reducing Tumour Hypoxia via Oral Administration of Oxygen Nanobubbles. Plos One. 2016;11(12):12. doi: 10.1371/journal.pone.0168088. PubMed PMID: WOS:000391229300011.
121. Munn Z, Peters M, Stern C, Tufanaru C, McArthur A, Aromataris E. Systematic review or scoping review? Guidance for authors when choosing between a systematic or scoping review approach. BMC MEDICAL RESEARCH METHODOLOGY. 2018;18. doi: 10.1186/s12874-018-0611-x. PubMed PMID: WOS:000451310200002.
122. Tricco AC, Lillie E, Zarin W, O'Brien KK, Colquhoun H, Levac D, et al. PRISMA Extension for Scoping Reviews (PRISMA-ScR): Checklist and Explanation. Annals of Internal Medicine. 2018;169(7):467-+. doi: 10.7326/m18-0850. PubMed PMID: WOS:000446042400006.
123. Lee YA, Kim JY, Hong SJ, Lee SH, Yoo MC, Kim KS, et al. Synovial proliferation differentially affects hypoxia in the joint cavities of rheumatoid arthritis and osteoarthritis patients. Clin Rheumatol. 2007;26(12):2023-9. Epub 2007/03/30. doi: 10.1007/s10067-007-0605-2. PubMed PMID: 17393234.
124. Stewart C, Haitsma I, Zador Z, Hemphill J, Morabito D, Manley G, et al. THE NEW LICOX COMBINED BRAIN TISSUE OXYGEN AND BRAIN TEMPERATURE MONITOR: ASSESSMENT OF IN VITRO ACCURACY AND CLINICAL EXPERIENCE IN SEVERE TRAUMATIC BRAIN INJURY. NEUROSURGERY. 2008;63:1159-64. doi: 10.1227/01.NEU.0000333265.19131.7C. PubMed PMID: WOS:000261643400047.
125. Falchuk KH, Goetzl EJ, Kulka JP. RESPIRATORY GASES OF SYNOVIAL FLUIDS - AN APPROACH TO SYNOVIAL TISSUE CIRCULATORY-METABOLIC IMBALANCE IN RHEUMATOID ARTHRITIS. American Journal of Medicine. 1970;49(2):223-&. doi: 10.1016/s0002-9343(70)80078-x. PubMed PMID: WOS:A1970H264200010.
126. Treuhaft PS, McCarty DJ. SYNOVIAL FLUID PH, LACTATE, OXYGEN AND CARBON DIOXIDE PARTIAL PRESSURE IN VARIOUS JOINT DISEASES. Arthritis and Rheumatism. 1971;14(4):475-&. doi: 10.1002/art.1780140407. PubMed PMID: WOS:A1971K218600006.
127. Goetzl EJ, Rynes RI, Stillman JS. Abnormalities of respiratory gases in synovial fluid of patients with juvenile rheumatoid arthritis. Arthritis and Rheumatism. 1974;17(4):450-4. doi: http://dx.doi.org/10.1002/art.1780170416.
128. Richman AI, Su EY, Ho Jr G. Reciprocal relationship of synovial fluid volume and oxygen tension. Arthritis and Rheumatism. 1981;24(5):701-5. doi: http://dx.doi.org/10.1002/art.1780240512.
129. Geborek P, Lindoff B, Valind SO. Measurement of oxygen and carbon dioxide partial pressures in synovial fluid after tonometry. Clinical Physiology. 1988;8(4):427-32.
130. Bosco MC, Blengio F, Varesio L. Hypoxia and inflammation. European Journal of Immunology. 2009;39(SUPPL. 1):S478. doi: http://dx.doi.org/10.1002/eji.200990184.
131. Biniecka M, Kennedy A, Fearon U, Ng CT, Veale DJ, O'Sullivan JN. Oxidative damage in synovial tissue is associated with in vivo hypoxic status in the arthritic joint. Ann Rheum Dis. 2010;69(6):1172-8. Epub 2009/08/27. doi: 10.1136/ard.2009.111211. PubMed PMID: 19706618.
132. Ng CT, Biniecka M, Kennedy A, McCormick J, Fitzgerald O, Bresnihan B, et al. Synovial tissue hypoxia and inflammation in vivo. Ann Rheum Dis. 2010;69(7):1389-95.

Epub 2010/05/05. doi: 10.1136/ard.2009.119776. PubMed PMID: 20439288; PubMed Central PMCID: PMC2946116.
133. Biniecka M, Kennedy A, Ng CT, Chang TC, Balogh E, Fox E, et al. Successful tumour necrosis factor (TNF) blocking therapy suppresses oxidative stress and hypoxia-induced mitochondrial mutagenesis in inflammatory arthritis. Arthritis Res Ther. 2011;13(4):R121. Epub 2011/07/27. doi: 10.1186/ar3424. PubMed PMID: 21787418; PubMed Central PMCID: PMC3239359.
134. Kennedy A, Ng CT, Chang TC, Biniecka M, O'Sullivan JN, Heffernan E, et al. Tumor Necrosis Factor Blocking Therapy Alters Joint Inflammation and Hypoxia. Arthritis and Rheumatism. 2011;63(4):923-32. doi: 10.1002/art.30221. PubMed PMID: WOS:000289421100010.
135. Balogh E, Ng CT, Veale DJ, Fearon U, Biniecka M. A novel angiopoetin2/tek tyrosine kinase receptor mediated effect on leukocyte cell influx and oxidative damage in inflammatory arthritis. Arthritis and Rheumatism. 2012;64(SUPPL. 10):S769. doi: http://dx.doi.org/10.1002/art.37735.
136. Biniecka M, Gao W, Ng CT, Balogh E, Veale DJ, Fearon U. Nicotinamide adenine dinucleotide phosphate oxidase mediated angiogenesis and inflammation in the arthritic joint. Arthritis and Rheumatism. 2012;64(SUPPL. 10):S510. doi: http://dx.doi.org/10.1002/art.37735.
137. !!! INVALID CITATION !!! .
138. Balogh E, Veale DJ, McCormick J, Szekanecz Z, Ng CT, Fearon U, et al. Hypoxia drives angiogenesis in inflammatory arthritis. Annals of the Rheumatic Diseases. 2013;72(SUPPL. 3). doi: http://dx.doi.org/10.1136/annrheumdis-2013-eular.603.
139. Hardy W, Wright F, Hawtree S, Fearon U, Veale D, Perretti M, et al. Hypoxia-inducible factor 2a regulates macrophage function in rheumatoid arthritis. Annals of the Rheumatic Diseases. 2014;73(SUPPL. 2). doi: http://dx.doi.org/10.1136/annrheumdis-2014-eular.4257.
140. Fisher BA, Donatien P, Filer A, Winlove CP, McInnes IB, Buckley CD, et al. Decrease in articular hypoxia and synovial blood flow at early time points following infliximab and etanercept treatment in rheumatoid arthritis. Clin Exp Rheumatol. 2016;34(6):1072-6. Epub 2016/10/18. PubMed PMID: 27749236.
141. Biniecka M, Canavan M, Balogh E, McGarry T, Orr C, Veale D, et al. Impaired cellular energy metabolism contributes to joint pathogenesis in rheumatoid arthritis. FEBS Open Bio. 2019;9(Supplement 1):73. doi: http://dx.doi.org/10.1002/2211-5463.12675.
142. Goetzl EJ, Falchuk KH, Zeiger LS, Sullivan AL, Hebert CL, Adams JP, et al. A physiological approach to the assessment of disease activity in rheumatoid arthritis. J Clin Invest. 1971;50(6):1167-80. Epub 1971/06/01. doi: 10.1172/jci106594. PubMed PMID: 5578228; PubMed Central PMCID: PMC292046.
143. THOMAS D, DINGLE J. INVITRO STUDIES OF RHEUMATOID SYNOVIUM - PRELIMINARY METABOLIC COMPARISON BETWEEN SYNOVIAL MEMBRANE AND VILLI. BRITISH JOURNAL OF EXPERIMENTAL PATHOLOGY. 1955;36:195-8. PubMed PMID: WOS:A1955WV34900012.
144. Dingle JTM, Thomas DPP. INVITRO STUDIES ON HUMAN SYNOVIAL MEMBRANE - A METABOLIC COMPARISON OF NORMAL AND RHEUMATOID TISSUE. British Journal of Experimental Pathology. 1956;37(4):318-&. PubMed PMID: WOS:A1956WY00900002.
145. Roberts JE, McLees BD, Kerby GP. PATHWAYS OF GLUCOSE METABOLISM IN RHEUMATOID AND NONRHEUMATOID SYNOVIAL MEMBRANE. Journal of Laboratory and Clinical Medicine. 1967;70(3):503-+. PubMed PMID: WOS:A19679886600018.

146. Blake DR, Merry P, Unsworth J, Kidd BL, Outhwaite JM, Ballard R, et al. Hypoxic-reperfusion injury in the inflamed human joint. Lancet. 1989;1(8633):289-93.
147. Shime H, Yabu M, Akazawa T, Kodama K, Matsumoto M, Seya T, et al. Tumor-secreted lactic acid promotes IL-23/IL-17 proinflammatory pathway. Journal of Immunology. 2008;180(11):7175-83. doi: 10.4049/jimmunol.180.11.7175. PubMed PMID: WOS:000257507300013.
148. Haas R, Smith J, Rocher-Ros V, Nadkarni S, Montero-Melendez T, D'Acquisto F, et al. Lactate Regulates Metabolic and Proinflammatory Circuits in Control of T Cell Migration and Effector Functions. Plos Biology. 2015;13(7). doi: 10.1371/journal.pbio.1002202. PubMed PMID: WOS:000360617100015.
149. Biniecka M, Canavan M, McGarry T, Gao W, McCormick J, Cregan S, et al. Dysregulated bioenergetics: a key regulator of joint inflammation. Ann Rheum Dis. 2016;75(12):2192-200. Epub 2016/03/26. doi: 10.1136/annrheumdis-2015-208476. PubMed PMID: 27013493; PubMed Central PMCID: PMC5136702.
150. Littlewood-Evans A, Sarret S, Apfel V, Loesle P, Dawson J, Zhang J, et al. GPR91 senses extracellular succinate released from inflammatory macrophages and exacerbates rheumatoid arthritis. JOURNAL OF EXPERIMENTAL MEDICINE. 2016;213:1655-62. doi: 10.1084/jem.20160061. PubMed PMID: WOS:000382520900002.
151. Tannahill GM, Curtis AM, Adamik J, Palsson-McDermott EM, McGettrick AF, Goel G, et al. Succinate is an inflammatory signal that induces IL-1β through HIF-1α. Nature. 2013;496(7444):238-42. Epub 20130324. doi: 10.1038/nature11986. PubMed PMID: 23535595; PubMed Central PMCID: PMC4031686.
152. Li Y, Zheng JY, Liu JQ, Yang J, Liu Y, Wang C, et al. Succinate/NLRP3 Inflammasome Induces Synovial Fibroblast Activation: Therapeutical Effects of Clematichinenoside AR on Arthritis. Front Immunol. 2016;7:532. Epub 2016/12/23. doi: 10.3389/fimmu.2016.00532. PubMed PMID: 28003810; PubMed Central PMCID: PMC5141240.
153. Li Y, Liu Y, Wang C, Xia WR, Zheng JY, Yang J, et al. Succinate induces synovial angiogenesis in rheumatoid arthritis through metabolic remodeling and HIF-1α/VEGF axis. Free Radic Biol Med. 2018;126:1-14. Epub 2018/07/22. doi: 10.1016/j.freeradbiomed.2018.07.009. PubMed PMID: 30030103.
154. Michopoulos F, Karagianni N, Whalley N, Firth M, Nikolaou C, Wilson I, et al. Targeted Metabolic Profiling of the Tg197 Mouse Model Reveals Itaconic Acid as a Marker of Rheumatoid Arthritis. JOURNAL OF PROTEOME RESEARCH. 2016;15:4579-90. doi: 10.1021/acs.jproteome.6b00654. PubMed PMID: WOS:000389396500035.
155. Lampropoulou V, Sergushichev A, Bambouskova M, Nair S, Vincent E, Loginicheva E, et al. Itaconate Links Inhibition of Succinate Dehydrogenase with Macrophage Metabolic Remodeling and Regulation of Inflammation. CELL METABOLISM. 2016;24:158-66. doi: 10.1016/j.cmet.2016.06.004. PubMed PMID: WOS:000380793400020.
156. Balaba TJ, Zhigalova LF, Farhadi VR. Study of some indices of the oxidation metabolism and effect on them of intraarticular oxygenotherapy in the experimental arthrosis of the knee joint. Ortopediya Travmatologiya i Protezirovanie. 1978;NO.10:30-5.
157. Leach R, Rees P, Wilmshurst P. ABC of oxygen - Hyperbaric oxygen therapy. BRITISH MEDICAL JOURNAL. 1998;317(7166):1140-3. PubMed PMID: WOS:000076755100037.
158. Harnanik T, Soeroso J, Suryokusumo MG, Juliandhy T. Effects of Hyperbaric Oxygen on T helper 17/regulatory T Polarization in Antigen and Collagen-induced Arthritis: Hypoxia-inducible Factor-1α as a Target. Oman Med J. 2020;35(1):e90. Epub

2020/01/30. doi: 10.5001/omj.2020.08. PubMed PMID: 31993228; PubMed Central PMCID: PMC6982795.
159. Harnanik T, Soeroso J, Guritno Suryokusumo M, Juliandhy T. Hyperbaric oxygen effect on switching phenotype M1-M2 macrophage expression in antigen and collagen-induced arthritis. International Medical Journal. 2019;26(6):479-82.
160. Gouveia D, Chichorro M, Cardoso A, Carvalho C, Silva C, Coelho T, et al. Hyperbaric Oxygen Therapy in Systemic Inflammatory Response Syndrome. VETERINARY SCIENCES. 2022;9(2). doi: 10.3390/vetsci9020033. PubMed PMID: WOS:000762021000001.
161. Oley M, Oley M, Islam A, Hatta M, Faruk M, Noersasongko A, et al. Hyperbaric oxygen therapy in managing systemic inflammatory response syndrome caused by ischemia-reperfusion injury following hand replantation and long-term outcomes: A report of two cases. ANNALS OF MEDICINE AND SURGERY. 2020;60:155-61. doi: 10.1016/j.amsu.2020.10.023. PubMed PMID: WOS:000604743400005.
162. Comstedt P, Storgaard M, Lassen A. The Systemic Inflammatory Response Syndrome (SIRS) in acutely hospitalised medical patients: a cohort study. SCANDINAVIAN JOURNAL OF TRAUMA RESUSCITATION & EMERGENCY MEDICINE. 2009;17. doi: 10.1186/1757-7241-17-67. PubMed PMID: WOS:000283036800001.
163. Al-Waili N, Butler G. Effects of hyperbaric oxygen on inflammatory response to wound and trauma: Possible mechanism of action. THESCIENTIFICWORLDJOURNAL. 2006;6:425-41. doi: 10.1100/tsw.2006.78. PubMed PMID: WOS:000242386800002.
164. Sen S, Sen S. Therapeutic effects of hyperbaric oxygen: integrated review. MEDICAL GAS RESEARCH. 2021;11:30-3. doi: 10.4103/2045-9912.310057. PubMed PMID: WOS:000624630500006.
165. Cuzzocrea S, Mazzon E, di Paola R, Genovese T, Patel NS, Britti D, et al. Erythropoietin reduces the degree of arthritis caused by type II collagen in the mouse. Arthritis Rheum. 2005;52(3):940-50. Epub 2005/03/08. doi: 10.1002/art.20875. PubMed PMID: 15751086.
166. Cao Y. Erythropoietin in cancer: a dilemma in risk therapy. TRENDS IN ENDOCRINOLOGY AND METABOLISM. 2013;24:190-9. doi: 10.1016/j.tem.2012.10.007. PubMed PMID: WOS:000317948300004.
167. Jonasch E, Donskov F, Iliopoulos O, Rathmell W, Narayan V, Maughan B, et al. Belzutifan for Renal Cell Carcinoma in von Hippel-Lindau Disease. NEW ENGLAND JOURNAL OF MEDICINE. 2021;385:2036-46. doi: 10.1056/NEJMoa2103425. PubMed PMID: WOS:000721915400008.
168. Maruotti N, Cantatore F, Ribatti D. Putative effects of potentially anti-angiogenic drugs in rheumatic diseases. EUROPEAN JOURNAL OF CLINICAL PHARMACOLOGY. 2014;70:135-40. doi: 10.1007/s00228-013-1605-6. PubMed PMID: WOS:000330035900002.
169. Lu J, Kasama T, Kobayashi K, Yoda Y, Shiozawa F, Hanyuda M, et al. Vascular endothelial growth factor expression and regulation of murine collagen-induced arthritis. JOURNAL OF IMMUNOLOGY. 2000;164:5922-7. PubMed PMID: WOS:000087154800048.
170. Cope AP, Jasenecova M, Vasconcelos JC, Filer A, Raza K, Qureshi S, et al. Abatacept in individuals at high risk of rheumatoid arthritis (APIPPRA): a randomised, double-blind, multicentre, parallel, placebo-controlled, phase 2b clinical trial. Lancet. 2024;403(10429):838-49. Epub 20240213. doi: 10.1016/S0140-6736(23)02649-1. PubMed PMID: 38364839.

171. Meadows K, Hurwitz H. Anti-VEGF Therapies in the Clinic. COLD SPRING HARBOR PERSPECTIVES IN MEDICINE. 2012;2. doi: 10.1101/cshperspect.a006577. PubMed PMID: WOS:000314281700006.
172. Brown D, Michels M, Kaiser P, Heier J, Sy J, Ianchulev T. Ranibizumab versus Verteporfin Photodynamic Therapy for Neovascular Age-Related Macular Degeneration: Two-Year Results of the ANCHOR Study. OPHTHALMOLOGY. 2009;116:57-65. doi: 10.1016/j.ophtha.2008.10.018. PubMed PMID: WOS:000262276700010.
173. Hanlon M, Canavan M, Barker B, Fearon U. Metabolites as drivers and targets in rheumatoid arthritis. CLINICAL AND EXPERIMENTAL IMMUNOLOGY. 2022;208:167-80. doi: 10.1093/cei/uxab021. PubMed PMID: WOS:000789312500001.
174. Momaya A, Fawal M, Estes R. Performance-Enhancing Substances in Sports: A Review of the Literature. SPORTS MEDICINE. 2015;45:517-31. doi: 10.1007/s40279-015-0308-9. PubMed PMID: WOS:000352165100006.
175. Bennett C, Silver S, Djulbegovic B, Samaras A, Blau C, Gleason K, et al. Venous thromboembolism and mortality associated with recombinant erythropoietin and darbepoetin administration for the treatment of cancer-associated anemia. JAMA-JOURNAL OF THE AMERICAN MEDICAL ASSOCIATION. 2008;299:914-24. PubMed PMID: WOS:000253413200020.
176. Salamin O, Kuuranne T, Saugy M, Leuenberger N. Erythropoietin as a performance-enhancing drug: Its mechanistic basis, detection, and potential adverse effects. MOLECULAR AND CELLULAR ENDOCRINOLOGY. 2018;464:75-87. doi: 10.1016/j.mce.2017.01.033. PubMed PMID: WOS:000427666200010.
177. Fine bubble technology — General principles for usage and measurement of fine bubbles International Organization for Standardization: British Standards Institution; 2024.
178. Agarwal A, Ng W, Liu Y. Principle and applications of microbubble and nanobubble technology for water treatment. CHEMOSPHERE. 2011;84:1175-80. doi: 10.1016/j.chemosphere.2011.05.054. PubMed PMID: WOS:000294145400002.
179. Khuntia S, Majumder S, Ghosh P. Microbubble-aided water and wastewater purification: a review. REVIEWS IN CHEMICAL ENGINEERING. 2012;28:191-221. doi: 10.1515/revce-2012-0007. PubMed PMID: WOS:000311992000001.
180. Takahashi M, Chiba K, Li P. Free-radical generation from collapsing microbubbles in the absence of a dynamic stimulus. JOURNAL OF PHYSICAL CHEMISTRY B. 2007;111:1343-7. doi: 10.1021/jp0669254. PubMed PMID: WOS:000244039700014.
181. Alheshibri M, Qian J, Jehannin M, Craig V. [A History of Nanobubbles]. Langmuir2016. p. 11086-100.
182. Ning J, Zhao H, Chen B, Mi E, Yang Z, Qing W, et al. Argon Mitigates Impaired Wound Healing Process and Enhances Wound Healing In Vitro and In Vivo. THERANOSTICS. 2019;9:477-90. doi: 10.7150/thno.29361. PubMed PMID: WOS:000456291500013.
183. Höllig A, Weinandy A, Liu J, Clusmann H, Rossaint R, Coburn M. Beneficial Properties of Argon After Experimental Subarachnoid Hemorrhage: Early Treatment Reduces Mortality and Influences Hippocampal Protein Expression. CRITICAL CARE MEDICINE. 2016;44:E520-E9. doi: 10.1097/CCM.0000000000001561. PubMed PMID: WOS:000378080400008.
184. Tiller N, Jeukendrup A. Comment On: "A Double-Blind, Randomized, Placebo-Controlled Pilot Study Examining an Oxygen Nanobubble Beverage for 16.1-km Time Trial and Repeated Sprint Cycling Performance". JOURNAL OF DIETARY SUPPLEMENTS. 2024;21:207-9. doi: 10.1080/19390211.2023.2263563. PubMed PMID: WOS:001169115200001.

185. Kimmich R, Peters A. SOLVATION OF OXYGEN IN LECITHIN BILAYERS. Chemistry and Physics of Lipids. 1975;14(4):350-62. doi: 10.1016/0009-3084(75)90072-9. PubMed PMID: WOS:A1975AN83000011.
186. Kimmich R, Peters A, Spohn KH. SOLUBILITY OF OXYGEN IN LECITHIN BILAYERS AND OTHER HYDROCARBON LAMELLAE AS A PROBE FOR FREE-VOLUME AND TRANSPORT-PROPERTIES. Journal of Membrane Science. 1981;9(3):313-36. doi: 10.1016/s0376-7388(00)80272-0. PubMed PMID: WOS:A1981MR04800008.
187. Peters A, Kimmich R. HETEROGENEOUS SOLUBILITY OF OXYGEN IN AQUEOUS LECITHIN DISPERSIONS AND ITS RELATION TO CHAIN MOBILITY - NMR RELAXATION AND WIDE-LINE STUDY. Biophysics of Structure and Mechanism. 1978;4(1):67-85. doi: 10.1007/bf00538841. PubMed PMID: WOS:A1978EG15600006.
188. SUBCZYNSKI W, HYDE J, KUSUMI A. OXYGEN PERMEABILITY OF PHOSPHATIDYLCHOLINE CHOLESTEROL MEMBRANES. PROCEEDINGS OF THE NATIONAL ACADEMY OF SCIENCES OF THE UNITED STATES OF AMERICA. 1989;86:4474-8. PubMed PMID: WOS:A1989AB24900030.
189. Widomska J, Raguz M, Subczynski WK. Oxygen permeability of the lipid bilayer membrane made of calf lens lipids. Biochimica Et Biophysica Acta-Biomembranes. 2007;1768(10):2635-45. doi: 10.1016/j.bbamem.2007.06.018. PubMed PMID: WOS:000250663400031.
190. Knowles H, Vasilyeva A, Sheth M, Pattinson O, May J, Rumney R, et al. [Use of oxygen-loaded nanobubbles to improve tissue oxygenation: Bone-relevant mechanisms of action and effects on osteoclast differentiation]. BIOMATERIALS2024.
191. Feoktistova M, Geserick P, Leverkus M. Crystal Violet Assay for Determining Viability of Cultured Cells. Cold Spring Harb Protoc. 2016;2016(4):pdb.prot087379. Epub 20160401. doi: 10.1101/pdb.prot087379. PubMed PMID: 27037069.
192. Al-Nasiry S, Geusens N, Hanssens M, Luyten C, Pijnenborg R. The use of Alamar Blue assay for quantitative analysis of viability, migration and invasion of choriocarcinoma cells. HUMAN REPRODUCTION. 2007;22:1304-9. doi: 10.1093/humrep/dem011. PubMed PMID: WOS:000246802500017.
193. Elshabrawy HA, Chen Z, Volin MV, Ravella S, Virupannavar S, Shahrara S. The pathogenic role of angiogenesis in rheumatoid arthritis. Angiogenesis. 2015;18(4):433-48. Epub 2015/07/23. doi: 10.1007/s10456-015-9477-2. PubMed PMID: 26198292; PubMed Central PMCID: PMC4879881.
194. Radstake W, Gautam K, Van Rompay C, Vermeesen R, Tabury K, Verslegers M, et al. Comparison of in vitro scratch wound assay experimental procedures. BIOCHEMISTRY AND BIOPHYSICS REPORTS. 2023;33. doi: 10.1016/j.bbrep.2023.101423. PubMed PMID: WOS:000925080500001.
195. McNabb D, Reed R, Marciniak R. Dual luciferase assay system for rapid assessment of gene expression in Saccharomyces cerevisiae. EUKARYOTIC CELL. 2005;4:1539-49. doi: 10.1128/EC.4.9.1539-1549.2005. PubMed PMID: WOS:000231942100004.
196. Ferrer I, Alcantara S, Ballabriga J, Olive M, Blanco R, Rivera R, et al. Transforming growth factor-alpha (TGF-alpha) and epidermal growth factor-receptor (EGF-R) immunoreactivity in normal and pathologic brain. PROGRESS IN NEUROBIOLOGY. 1996;49:99-&. PubMed PMID: WOS:A1996VB24800001.
197. Leker R, Toth Z, Shahar T, Cassiani-Ingoni R, Szalayova I, Key S, et al. TRANSFORMING GROWTH FACTOR α INDUCES ANGIOGENESIS AND

NEUROGENESIS FOLLOWING STROKE. NEUROSCIENCE. 2009;163:233-43. doi: 10.1016/j.neuroscience.2009.05.050. PubMed PMID: WOS:000269404600021.
198. SALOMON D, KIM N, SAEKI T, CIARDIELLO F. TRANSFORMING GROWTH FACTOR-ALPHA - AN ONCODEVELOPMENTAL GROWTH-FACTOR. CANCER CELLS-A MONTHLY REVIEW. 1990;2:389-97. PubMed PMID: WOS:A1990EP81900003.
199. ROSENTHAL A, LINDQUIST P, BRINGMAN T, GOEDDEL D, DERYNCK R. EXPRESSION IN RAT FIBROBLASTS OF A HUMAN TRANSFORMING GROWTH FACTOR-ALPHA CDNA RESULTS IN TRANSFORMATION. CELL. 1986;46:301-9. PubMed PMID: WOS:A1986D253300017.
200. Halliwell B, Whiteman M. Measuring reactive species and oxidative damage in vivo and in cell culture:: how should you do it and what do the results mean? BRITISH JOURNAL OF PHARMACOLOGY. 2004;142:231-55. doi: 10.1038/sj.bjp.0705776. PubMed PMID: WOS:000221799400001.
201. Hu T, RamachandraRao S, Siva S, Valancius C, Zhu Y, Mahadev K, et al. Reactive oxygen species production via NADPH oxidase mediates TGF-β induced cytoskeletal alterations in endothelial cells. AMERICAN JOURNAL OF PHYSIOLOGY-RENAL PHYSIOLOGY. 2005;289:F816-F25. PubMed PMID: WOS:000231833300019.
202. BILLIAU A, EDY V, HEREMANS H, VANDAMME J, DESMYTER J, GEORGIADES J, et al. HUMAN INTERFERON - MASS-PRODUCTION IN A NEWLY ESTABLISHED CELL LINE, MG-63. ANTIMICROBIAL AGENTS AND CHEMOTHERAPY. 1977;12(1):11-5. PubMed PMID: WOS:A1977DN24400003.
203. Pautke C, Schieker M, Tischer T, Kolk A, Neth P, Mutschler W, et al. Characterization of osteosarcoma cell lines MG-63, Saos-2 and U-2OS in comparison to human osteoblasts. ANTICANCER RESEARCH. 2004;24(6):3743-8. PubMed PMID: WOS:000227014500008.
204. Jiménez N, Krouwer V, Post J. A new, rapid and reproducible method to obtain high quality endothelium in vitro. CYTOTECHNOLOGY. 2013;65(1):1-14. doi: 10.1007/s10616-012-9459-9. PubMed PMID: WOS:000313074500001.
205. Kocherova I, Bryja A, Mozdziak P, Volponi A, Dyszkiewicz-Konwinska M, Piotrowska-Kempisty H, et al. Human Umbilical Vein Endothelial Cells (HUVECs) Co-Culture with Osteogenic Cells: From Molecular Communication to Engineering Prevascularised Bone Grafts. JOURNAL OF CLINICAL MEDICINE. 2019;8(10). doi: 10.3390/jcm8101602. PubMed PMID: WOS:000498398500100.
206. She F, Wang WB, Wang Y, Tang PF, Wei JQ, Chen H, et al. Melatonin protects MG63 osteoblast- like cells from hydrogen peroxide- induced cytotoxicity by maintaining mitochondrial function. Mol Med Rep. 2014;9(2):493-8. doi: 10.3892/mmr.2013.1832. PubMed PMID: WOS:000332694100017.
207. Gunaratnam L, Morley M, Franovic A, de Paulsen N, Mekhail K, Parolin DAE, et al. Hypoxia inducible factor activates the transforming growth factor-alpha/epidermal growth factor receptor growth stimulatory pathway in VHL-/- renal cell carcinoma cells. J Biol Chem. 2003;278(45):44966-74. doi: 10.1074/jbc.M305502200. PubMed PMID: WOS:000186306700133.
208. Hunt MA, Currie MJ, Robinson BA, Dachs GU. Optimizing transfection of primary human umbilical vein endothelial cells using commercially available chemical transfection reagents. J Biomol Tech. 2010;21(2):66-72. PubMed PMID: 20592869; PubMed Central PMCID: PMC2884313.
209. Chong ZX, Yeap SK, Ho WY. Transfection types, methods and strategies: a technical review. PeerJ. 2021;9:e11165. Epub 20210421. doi: 10.7717/peerj.11165. PubMed PMID: 33976969; PubMed Central PMCID: PMC8067914.

210. Villemejane J, Mir LM. Physical methods of nucleic acid transfer: general concepts and applications. Br J Pharmacol. 2009;157(2):207-19. Epub 20090121. doi: 10.1111/j.1476-5381.2009.00032.x. PubMed PMID: 19154421; PubMed Central PMCID: PMC2697808.
211. Kamaruddin NAB, Fong LY, Tan JJ, Abdullah MNH, Cheema MS, Bin Yakop F, et al. Cytoprotective Role of Omentin Against Oxidative Stress-Induced Vascular Endothelial Cells Injury. Molecules. 2020;25(11). doi: 10.3390/molecules25112534. PubMed PMID: WOS:000553858800071.
212. Hras A, Hadolin M, Knez Z, Bauman D. Comparison of antioxidative and synergistic effects of rosemary extract with α-tocopherol, ascorbyl palmitate and citric acid in sunflower oil. FOOD CHEMISTRY. 2000;71:229-33. PubMed PMID: WOS:000089542200011.
213. Wang H, Zhang M, Ma Y, Wang B, Huang H, Liu Y, et al. Carbon Dots Derived from Citric Acid and Glutathione as a Highly Efficient Intracellular Reactive Oxygen Species Scavenger for Alleviating the Lipopolysaccharide-Induced Inflammation in Macrophages. ACS APPLIED MATERIALS & INTERFACES. 2020;12:41088-95. doi: 10.1021/acsami.0c11735. PubMed PMID: WOS:000572965700011.
214. Ageeva A, Kruppa A, Magin I, Babenko S, Leshina T, Polyakov N. New Aspects of the Antioxidant Activity of Glycyrrhizin Revealed by the CIDNP Technique. ANTIOXIDANTS. 2022;11(8). doi: 10.3390/antiox11081591. PubMed PMID: WOS:000846214700001.
215. Wing-Gaia S, Subudhi A, Askew E. Effects of purified oxygenated water on exercise performance during acute hypoxic exposure. INTERNATIONAL JOURNAL OF SPORT NUTRITION AND EXERCISE METABOLISM. 2005;15:680-8. PubMed PMID: WOS:000234235800008.
216. McNaughton L, Kenney S, Siegler J, Midgley A, Lovell R, Bentley D. The Effect of Superoxygenated Water on Blood Gases, Lactate, and Aerobic Cycling Performance. INTERNATIONAL JOURNAL OF SPORTS PHYSIOLOGY AND PERFORMANCE. 2007;2:377-85. PubMed PMID: WOS:000207535600005.
217. Fleming N, Vaughan J, Feeback M. Ingestion of oxygenated water enhances lactate clearance kinetics in trained runners. J Int Soc Sport Nutr. 2017;14. doi: 10.1186/s12970-017-0166-y. PubMed PMID: WOS:000397813100001.
218. Li Y, Wu CL, Liu J, Zhu Y, Zhang XY, Jiang LZ, et al. Soy Protein Isolate-Phosphatidylcholine Nanoemulsions Prepared Using High-Pressure Homogenization. Nanomaterials. 2018;8(5). doi: 10.3390/nano8050307. PubMed PMID: WOS:000435198300038.
219. Shao W, Hwang J, Liu CE, Mukhopadhyay D, Zhao S, Shen MC, et al. Serum lipoprotein-derived fatty acids regulate hypoxia-inducible factor. J Biol Chem. 2020;295(52):18284-300. doi: 10.1074/jbc.RA120.015238. PubMed PMID: WOS:000603645900030.
220. Dodd M, Fialho M, Aparicio C, Kerr M, Timm K, Griffin J, et al. Fatty Acids Prevent Hypoxia-Inducible Factor-1α Signaling Through Decreased Succinate in Diabetes. JACC-BASIC TO TRANSLATIONAL SCIENCE. 2018;3:485-98. doi: 10.1016/j.jacbts.2018.04.005. PubMed PMID: WOS:000601125900005.
221. Seo J, Jeong D, Park J, Lee K, Fukuda J, Chun Y. Fatty-acid-induced FABP5/HIF-1 reprograms lipid metabolism and enhances the proliferation of liver cancer cells. COMMUNICATIONS BIOLOGY. 2020;3. doi: 10.1038/s42003-020-01367-5. PubMed PMID: WOS:000588120400013.

222. German JB, Smilowitz JT, Zivkovic AM. Lipoproteins: When size really matters. Curr Opin Colloid Interface Sci. 2006;11(2-3):171-83. doi: 10.1016/j.cocis.2005.11.006. PubMed PMID: 20592953; PubMed Central PMCID: PMC2893739.
223. Doyle LM, Wang MZ. Overview of Extracellular Vesicles, Their Origin, Composition, Purpose, and Methods for Exosome Isolation and Analysis. Cells. 2019;8(7). Epub 20190715. doi: 10.3390/cells8070727. PubMed PMID: 31311206; PubMed Central PMCID: PMC6678302.
224. Sheth M, Saunders P, Kanellakis N, Talbot N, Turnbull C, Handa A, et al. A randomised crossover trial to investigate the clinical utility of orally delivered oxygen nanobubbles in Pulmonary Fibrosis. EUROPEAN RESPIRATORY JOURNAL. 2024;64. doi: 10.1183/13993003.congress-2024.PA2609. PubMed PMID: WOS:001360064300037.
225. Qi YJ, Liu GX. Berberine-10-hydroxy camptothecine-loaded lipid microsphere for the synergistic treatment of liver cancer by inhibiting topoisomerase and HIF-1 alpha. Drug Delivery. 2021;28(1):171-82. doi: 10.1080/10717544.2020.1870020. PubMed PMID: WOS:000606897800001.
226. Vanderhaeghen T, Beyaert R, Libert C. Bidirectional Crosstalk Between Hypoxia Inducible Factors and Glucocorticoid Signalling in Health and Disease. Front Immunol. 2021;12. doi: 10.3389/fimmu.2021.684085. PubMed PMID: WOS:000662953900001.
227. Biniecka M, Canavan M, McGarry T, Gao W, McCormick J, Cregan S, et al. Dysregulated bioenergetics: a key regulator of joint inflammation. Annals of the Rheumatic Diseases. 2016;75(12):2192-200. doi: 10.1136/annrheumdis-2015-208476. PubMed PMID: WOS:000389338900030.
228. HENCH P, KENDALL E, SLOCUMB C, POLLEY H. THE EFFECT OF A HORMONE OF THE ADRENAL CORTEX (17-HYDROXY-11-DEHYDROCORTICOSTERONE - COMPOUND-E) AND OF PITUITARY ADRENOCORTICOTROPIC HORMONE ON RHEUMATOID ARTHRITIS - PRELIMINARY REPORT. PROCEEDINGS OF THE STAFF MEETINGS OF THE MAYO CLINIC. 1949;24:181-97. PubMed PMID: WOS:A1949UN50000001.
229. Paragliola RM, Papi G, Pontecorvi A, Corsello SM. Treatment with Synthetic Glucocorticoids and the Hypothalamus-Pituitary-Adrenal Axis. Int J Mol Sci. 2017;18(10). Epub 20171020. doi: 10.3390/ijms18102201. PubMed PMID: 29053578; PubMed Central PMCID: PMC5666882.
230. Hardy R, Raza K, Cooper M. Therapeutic glucocorticoids: mechanisms of actions in rheumatic diseases. NATURE REVIEWS RHEUMATOLOGY. 2020;16:133-44. doi: 10.1038/s41584-020-0371-y. PubMed PMID: WOS:000511754200002.
231. Uson J, Rodriguez-García S, Castellanos-Moreira R, O'Neill T, Doherty M, Boesen M, et al. EULAR recommendations for intra-articular therapies. ANNALS OF THE RHEUMATIC DISEASES. 2021;80:1299-305. doi: 10.1136/annrheumdis-2021-220266. PubMed PMID: WOS:000698436800024.
232. HOLLANDER JL, BROWN EM, JESSAR RA, BROWN CY. Hydrocortisone and cortisone injected into arthritic joints; comparative effects of and use of hydrocortisone as a local antiarthritic agent. J Am Med Assoc. 1951;147(17):1629-35. doi: 10.1001/jama.1951.03670340019005. PubMed PMID: 14880415.
233. Furtado R, Oliveira L, Natour J. Polyarticular corticosteroid injection versus systemic administration in treatment of rheumatoid arthritis patients: A randomized controlled study. JOURNAL OF RHEUMATOLOGY. 2005;32:1691-8. PubMed PMID: WOS:000231921300011.
234. Kumar A, Dhir V, Sharma S, Sharma A, Singh S. Efficacy of Methylprednisolone Acetate Versus Triamcinolone Acetonide Intra-articular Knee Injection in Patients With Chronic Inflammatory Arthritis: A 24-Week Randomized Controlled Trial. CLINICAL

THERAPEUTICS. 2017;39:150-8. doi: 10.1016/j.clinthera.2016.11.023. PubMed PMID: WOS:000394412000015.
235. Centeno LM, Moore ME. Preferred intraarticular corticosteroids and associated practice: a survey of members of the American College of Rheumatology. Arthritis Care Res. 1994;7(3):151-5. doi: 10.1002/art.1790070309. PubMed PMID: 7727555.
236. Timmermans S, Souffriau J, Libert C. A General Introduction to Glucocorticoid Biology. Front Immunol. 2019;10. doi: 10.3389/fimmu.2019.01545. PubMed PMID: WOS:000474208200001.
237. Meduri G, Chrousos G. General Adaptation in Critical Illness: Glucocorticoid Receptor-alpha Master Regulator of Homeostatic Corrections. FRONTIERS IN ENDOCRINOLOGY. 2020;11. doi: 10.3389/fendo.2020.00161. PubMed PMID: WOS:000533862800001.
238. Czock D, Keller F, Rasche FM, Häussler U. Pharmacokinetics and pharmacodynamics of systemically administered glucocorticoids. Clin Pharmacokinet. 2005;44(1):61-98. doi: 10.2165/00003088-200544010-00003. PubMed PMID: 15634032.
239. Auger J, Zimmermann M, Faas M, Stifel U, Chambers D, Krishnacoumar B, et al. Metabolic rewiring promotes anti-inflammatory effects of glucocorticoids. NATURE. 2024. doi: 10.1038/s41586-024-07282-7. PubMed PMID: WOS:001201403000022.
240. Tuor U. Glucocorticoids and the prevention of hypoxic-ischemic brain damage. NEUROSCIENCE AND BIOBEHAVIORAL REVIEWS. 1997;21:175-9. PubMed PMID: WOS:A1997WL70100008.
241. Altamentova S, Rumajogee P, Hong J, Beldick S, Park S, Yee A, et al. Methylprednisolone Reduces Persistent Post-ischemic Inflammation in a Rat Hypoxia-Ischemia Model of Perinatal Stroke. TRANSLATIONAL STROKE RESEARCH. 2020;11:1117-36. doi: 10.1007/s12975-020-00792-2. PubMed PMID: WOS:000561632500001.
242. Tuor UI, Chumas PD, Del Bigio MR. Prevention of hypoxic-ischemic damage with dexamethasone is dependent on age and not influenced by fasting. Exp Neurol. 1995;132(1):116-22. doi: 10.1016/0014-4886(95)90065-9. PubMed PMID: 7720820.
243. Tuor UI, Del Bigio MR. Protection against hypoxic-ischemic damage with corticosterone and dexamethasone: inhibition of effect by a glucocorticoid antagonist RU38486. Brain Res. 1996;743(1-2):258-62. doi: 10.1016/s0006-8993(96)01054-2. PubMed PMID: 9017253.
244. Wells G, Becker J, Teng J, Dougados M, Schiff M, Smolen J, et al. Validation of the 28-joint Disease Activity Score (DAS28) and European League Against Rheumatism response criteria based on C-reactive protein against disease progression in patients with rheumatoid arthritis, and comparison with the DAS28 based on erythrocyte sedimentation rate. ANNALS OF THE RHEUMATIC DISEASES. 2009;68:954-60. doi: 10.1136/ard.2007.084459. PubMed PMID: WOS:000266917100031.
245. Schoels M, Aletaha D, Alasti F, Smolen J. Disease activity in psoriatic arthritis (PsA): defining remission and treatment success using the DAPSA score. ANNALS OF THE RHEUMATIC DISEASES. 2016;75:811-8. doi: 10.1136/annrheumdis-2015-207507. PubMed PMID: WOS:000375091500011.
246. van Gestel A, Haagsma C, Riel P. Validation of rheumatoid arthritis improvement criteria that include simplified joint counts. ARTHRITIS AND RHEUMATISM. 1998;41:1845-50. PubMed PMID: WOS:000076341300016.
247. Gossec L, Smolen J, Ramiro S, de Wit M, Cutolo M, Dougados M, et al. European League Against Rheumatism (EULAR) recommendations for the management of psoriatic arthritis with pharmacological therapies: 2015 update. ANNALS OF THE RHEUMATIC

DISEASES. 2016;75:499-510. doi: 10.1136/annrheumdis-2015-208337. PubMed PMID: WOS:000371077700004.
248. Jüni P, Hari R, Rutjes AW, Fischer R, Silletta MG, Reichenbach S, et al. Intra-articular corticosteroid for knee osteoarthritis. Cochrane Database Syst Rev. 2015;2015(10):CD005328. Epub 20151022. doi: 10.1002/14651858.CD005328.pub3. PubMed PMID: 26490760; PubMed Central PMCID: PMC8884338.
249. Knych H, Harrison L, Casbeer H, McKemie D. Disposition of methylprednisolone acetate in plasma, urine, and synovial fluid following intra-articular administration to exercised thoroughbred horses. JOURNAL OF VETERINARY PHARMACOLOGY AND THERAPEUTICS. 2014;37:125-32. doi: 10.1111/jvp.12070. PubMed PMID: WOS:000332307100002.
250. AUTEFAGE A, ALVINERIE M, TOUTAIN P. SYNOVIAL-FLUID AND PLASMA KINETICS OF METHYLPREDNISOLONE AND METHYLPREDNISOLONE ACETATE IN HORSES FOLLOWING INTRAARTICULAR ADMINISTRATION OF METHYLPREDNISOLONE ACETATE. EQUINE VETERINARY JOURNAL. 1986;18:193-8. PubMed PMID: WOS:A1986C586100010.
251. Bhat MY, Solanki HS, Advani J, Khan AA, Keshava Prasad TS, Gowda H, et al. Comprehensive network map of interferon gamma signaling. J Cell Commun Signal. 2018;12(4):745-51. Epub 20180906. doi: 10.1007/s12079-018-0486-y. PubMed PMID: 30191398; PubMed Central PMCID: PMC6235777.
252. Schoenborn JR, Wilson CB. Regulation of interferon-gamma during innate and adaptive immune responses. Adv Immunol. 2007;96:41-101. doi: 10.1016/S0065-2776(07)96002-2. PubMed PMID: 17981204.
253. Artis D, Spits H. The biology of innate lymphoid cells. Nature. 2015;517(7534):293-301. doi: 10.1038/nature14189. PubMed PMID: 25592534.
254. Dai H, Adamopoulos I. Psoriatic arthritis under the influence of IFNγ. CLINICAL IMMUNOLOGY. 2020;218. doi: 10.1016/j.clim.2020.108513. PubMed PMID: WOS:000558530700014.
255. Schiff M. Role of interleukin 1 and interleukin 1 receptor antagonist in the mediation of rheumatoid arthritis. ANNALS OF THE RHEUMATIC DISEASES. 2000;59:103-8. PubMed PMID: WOS:000165408900024.
256. Vincent TL. IL-1 in osteoarthritis: time for a critical review of the literature. F1000Res. 2019;8. Epub 20190621. doi: 10.12688/f1000research.18831.1. PubMed PMID: 31249675; PubMed Central PMCID: PMC6589928.
257. Ruscitti P, Cipriani P, Carubbi F, Liakouli V, Zazzeroni F, Di Benedetto P, et al. The Role of IL-1β in the Bone Loss during Rheumatic Diseases. MEDIATORS OF INFLAMMATION. 2015;2015. doi: 10.1155/2015/782382. PubMed PMID: WOS:000353494500001.
258. Wu R, Li N, Zhao X, Ding T, Xue H, Gao C, et al. Low-dose Interleukin-2: Biology and therapeutic prospects in rheumatoid arthritis. Autoimmun Rev. 2020;19(10):102645. Epub 20200813. doi: 10.1016/j.autrev.2020.102645. PubMed PMID: 32801037.
259. Zhang X, Miao M, Zhang R, Liu X, Zhao X, Shao M, et al. Efficacy and safety of low-dose interleukin-2 in combination with methotrexate in patients with active rheumatoid arthritis: a randomized, double-blind, placebo-controlled phase 2 trial. SIGNAL TRANSDUCTION AND TARGETED THERAPY. 2022;7. doi: 10.1038/s41392-022-00887-2. PubMed PMID: WOS:000765124300001.
260. Iwaszko M, Biały S, Bogunia-Kubik K. Significance of Interleukin (IL)-4 and IL-13 in Inflammatory Arthritis. Cells. 2021;10(11). Epub 20211103. doi:

10.3390/cells10113000. PubMed PMID: 34831223; PubMed Central PMCID: PMC8616130.
261. Ghoreschi K, Thomas P, Breit S, Dugas M, Mailhammer R, van Eden W, et al. Interleukin-4 therapy of psoriasis induces Th2 responses and improves human autoimmune disease. Nat Med. 2003;9(1):40-6. Epub 20021202. doi: 10.1038/nm804. PubMed PMID: 12461524.
262. Gabay C. Interleukin-6 and chronic inflammation. ARTHRITIS RESEARCH & THERAPY. 2006;8. doi: 10.1186/ar1917. PubMed PMID: WOS:000241022000003.
263. Choy E, De Benedetti F, Takeuchi T, Hashizume M, John M, Kishimoto T. Translating IL-6 biology into effective treatments. NATURE REVIEWS RHEUMATOLOGY. 2020;16:335-45. doi: 10.1038/s41584-020-0419-z. PubMed PMID: WOS:000528511900001.
264. Gremese E, Tolusso B, Bruno D, Perniola S, Ferraccioli G, Alivernini S. The forgotten key players in rheumatoid arthritis: IL-8 and IL-17 - Unmet needs and therapeutic perspectives. Front Med (Lausanne). 2023;10:956127. Epub 20230322. doi: 10.3389/fmed.2023.956127. PubMed PMID: 37035302; PubMed Central PMCID: PMC10073515.
265. Hernández-Bello J, Oregón-Romero E, Vázquez-Villamar M, García-Arellano S, Valle Y, Padilla-Gutiérrez J, et al. Aberrant expression of interleukin-10 in rheumatoid arthritis: Relationship with IL10 haplotypes and autoantibodies. CYTOKINE. 2017;95:88-96. doi: 10.1016/j.cyto.2017.02.022. PubMed PMID: WOS:000405054600013.
266. van Roon J, Wijngaarden S, Lafeber FP, Damen C, van de Winkel J, Bijlsma JW. Interleukin 10 treatment of patients with rheumatoid arthritis enhances Fc gamma receptor expression on monocytes and responsiveness to immune complex stimulation. J Rheumatol. 2003;30(4):648-51. PubMed PMID: 12672180.
267. Kimball AB, Kawamura T, Tejura K, Boss C, Hancox AR, Vogel JC, et al. Clinical and immunologic assessment of patients with psoriasis in a randomized, double-blind, placebo-controlled trial using recombinant human interleukin 10. Arch Dermatol. 2002;138(10):1341-6. doi: 10.1001/archderm.138.10.1341. PubMed PMID: 12374540.
268. Tilg H, van Montfrans C, van den Ende A, Kaser A, van Deventer SJ, Schreiber S, et al. Treatment of Crohn's disease with recombinant human interleukin 10 induces the proinflammatory cytokine interferon gamma. Gut. 2002;50(2):191-5. doi: 10.1136/gut.50.2.191. PubMed PMID: 11788558; PubMed Central PMCID: PMC1773093.
269. Cribbs AP, Luna-Valero S, George C, Sudbery IM, Berlanga-Taylor AJ, Sansom SN, et al. CGAT-core: a python framework for building scalable, reproducible computational biology workflows. *F1000Research*; 2019.
270. Love MI, Huber W, Anders S. Moderated estimation of fold change and dispersion for RNA-seq data with DESeq2. Genome Biology. 2014;15(12). doi: 10.1186/s13059-014-0550-8. PubMed PMID: WOS:000346609500022.
271. Zhu AQ, Ibrahim JG, Love MI. Heavy-tailed prior distributions for sequence count data: removing the noise and preserving large differences. Bioinformatics. 2019;35(12):2084-92. doi: 10.1093/bioinformatics/bty895. PubMed PMID: WOS:000474844600014.
272. BENJAMINI Y, HOCHBERG Y. CONTROLLING THE FALSE DISCOVERY RATE - A PRACTICAL AND POWERFUL APPROACH TO MULTIPLE TESTING. JOURNAL OF THE ROYAL STATISTICAL SOCIETY SERIES B-STATISTICAL METHODOLOGY. 1995;57(1):289-300. PubMed PMID: WOS:A1995QE45300017.

273. Salem R, El-deeb A, Elsergany M, Elsaadany H, El-khouly R. Intra-articular injection of etanercept versus glucocorticoids in rheumatoid arthritis patients. CLINICAL RHEUMATOLOGY. 2021;40(2):557-64. doi: 10.1007/s10067-020-05235-9. PubMed PMID: WOS:000545292600001.
274. Minopoulou I, Kleyer A, Yalcin-Mutlu M, Fagni F, Kemenes S, Schmidkonz C, et al. Imaging in inflammatory arthritis: progress towards precision medicine. NATURE REVIEWS RHEUMATOLOGY. 2023;19:650-65. doi: 10.1038/s41584-023-01016-1. PubMed PMID: WOS:001064447500002.
275. Hallasch S, Giese N, Stoffels I, Klode J, Sondermann W. Multispectral optoacoustic tomography might be a helpful tool for noninvasive early diagnosis of psoriatic arthritis. PHOTOACOUSTICS. 2021;21. doi: 10.1016/j.pacs.2020.100225. PubMed PMID: WOS:000659477300011.
276. Tascilar K, Fagni F, Kleyer A, Bayat S, Heidemann R, Steiger F, et al. Non-invasive metabolic profiling of inflammation in joints and entheses by multispectral optoacoustic tomography. Rheumatology. 2023;62:841-9. doi: 10.1093/rheumatology/keac346. PubMed PMID: WOS:000823477600001.
277. Ohrndorf S, Glimm A, Ammitzboll-Danielsen M, Ostergaard M, Burmester G. Fluorescence optical imaging: ready for prime time? RMD OPEN. 2021;7. doi: 10.1136/rmdopen-2020-001497. PubMed PMID: WOS:000764052500001.
278. Frinking P, Segers T, Luan Y, Tranquart F. THREE DECADES OF ULTRASOUND CONTRAST AGENTS: A REVIEW OF THE PAST, PRESENT AND FUTURE IMPROVEMENTS. ULTRASOUND IN MEDICINE AND BIOLOGY. 2020;46:892-908. doi: 10.1016/j.ultrasmedbio.2019.12.008. PubMed PMID: WOS:000514215100002.
279. Diao X, Shen Y, Chen L, Zhan J, Fang L, Liu Y, et al. Superb microvascular imaging is as sensitive as contrast-enhanced ultrasound for detecting synovial vascularity in rheumatoid arthritis. QUANTITATIVE IMAGING IN MEDICINE AND SURGERY. 2022;12:2866-76. doi: 10.21037/qims-21-859. PubMed PMID: WOS:000765749800001.
280. Motoyama S, Saito S, Minamiya Y, Saito R, Nakamura M, Okuyama M, et al. Methylprednisolone inhibits low-flow hypoxia-induced mitochondrial dysfunction in isolated perfused rat liver. CRITICAL CARE MEDICINE. 2003;31:1468-74. doi: 10.1097/01.CCM.0000066176.49774.CC. PubMed PMID: WOS:000182981300027.
281. Mihailova A. Interleukin 6 Concentration in Synovial Fluid of Patients with Inflammatory and Degenerative Arthritis. CURRENT RHEUMATOLOGY REVIEWS. 2022;18:230-3. doi: 10.2174/1874471015666220128113319. PubMed PMID: WOS:000854087100008.
282. WAAGE A, KAUFMANN C, ESPEVIK T, HUSBY G. INTERLEUKIN-6 IN SYNOVIAL-FLUID FROM PATIENTS WITH ARTHRITIS. CLINICAL IMMUNOLOGY AND IMMUNOPATHOLOGY. 1989;50:394-8. PubMed PMID: WOS:A1989T477200011.
283. SACK U, KINNE R, MARX T, HEPPT P, BENDER S, EMMRICH F. INTERLEUKIN-6 IN SYNOVIAL-FLUID IS CLOSELY ASSOCIATED WITH CHRONIC SYNOVITIS IN RHEUMATOID-ARTHRITIS. RHEUMATOLOGY INTERNATIONAL. 1993;13:45-51. PubMed PMID: WOS:A1993LY30500001.
284. HOUSSIAU F, DEVOGELAER J, VANDAMME J, DEDEUXCHAISNES C, VANSNICK J. INTERLEUKIN-6 IN SYNOVIAL-FLUID AND SERUM OF PATIENTS WITH RHEUMATOID-ARTHRITIS AND OTHER INFLAMMATORY ARTHRITIDES. ARTHRITIS AND RHEUMATISM. 1988;31:784-8. PubMed PMID: WOS:A1988N997500014.

285. Raza K, Falciani F, Curnow SJ, Ross EJ, Lee CY, Akbar AN, et al. Early rheumatoid arthritis is characterized by a distinct and transient synovial fluid cytokine profile of T cell and stromal cell origin. Arthritis Res Ther. 2005;7(4):R784-95. Epub 20050407. doi: 10.1186/ar1733. PubMed PMID: 15987480; PubMed Central PMCID: PMC1175027.
286. TETTA C, CAMUSSI G, MODENA V, DIVITTORIO C, BAGLIONI C. TUMOR-NECROSIS-FACTOR IN SERUM AND SYNOVIAL-FLUID OF PATIENTS WITH ACTIVE AND SEVERE RHEUMATOID-ARTHRITIS. ANNALS OF THE RHEUMATIC DISEASES. 1990;49:665-7. PubMed PMID: WOS:A1990DW96700003.
287. BERTAZZOLO N, PUNZI L, STEFANI M, CESARO G, PIANON M, FINCO B, et al. INTERRELATIONSHIPS BETWEEN INTERLEUKIN (IL)-1, IL-6 AND IL-8 IN SYNOVIAL-FLUID OF VARIOUS ARTHROPATHIES. AGENTS AND ACTIONS. 1994;41(1-2):90-2. PubMed PMID: WOS:A1994NG75300020.
288. Bommarito D, Hall C, Taams L, Corrigall V. Inflammatory cytokines compromise programmed cell death-1(PD-1)-mediated T cell suppression in inflammatory arthritis through up-regulation of soluble PD-1. CLINICAL AND EXPERIMENTAL IMMUNOLOGY. 2017;188(3):455-66. doi: 10.1111/cei.12949. PubMed PMID: WOS:000400993000016.
289. HOLT I, COOPER R, HOPKINS S. RELATIONSHIPS BETWEEN LOCAL INFLAMMATION, INTERLEUKIN-6 CONCENTRATION AND THE ACUTE PHASE PROTEIN RESPONSE IN ARTHRITIS PATIENTS. EUROPEAN JOURNAL OF CLINICAL INVESTIGATION. 1991;21(5):479-84. PubMed PMID: WOS:A1991GK00300005.
290. Partsch G, Steiner G, Leeb B, Dunky A, Broll H, Smolen J. Highly increased levels of tumor necrosis factor-alpha and other proinflammatory cytokines in psoriatic arthritis synovial fluid. JOURNAL OF RHEUMATOLOGY. 1997;24(3):518-23. PubMed PMID: WOS:A1997WM00100019.
291. Fiocco U, Martini V, Accordi B, Caso F, Costa L, Oliviero F, et al. Transcriptional network profile on synovial fluid T cells in psoriatic arthritis. CLINICAL RHEUMATOLOGY. 2015;34(9):1571-80. doi: 10.1007/s10067-015-3002-2. PubMed PMID: WOS:000360288800012.
292. van Kuijk A, Reinders-Blankert P, Smeets T, Dijkmans B, Tak P. Detailed analysis of the cell infiltrate and the expression of mediators of synovial inflammation and joint destruction in the synovium of patients with psoriatic arthritis: implications for treatment. ANNALS OF THE RHEUMATIC DISEASES. 2006;65(12):1551-7. doi: 10.1136/ard.2005.050963. PubMed PMID: WOS:000242048100003.
293. Barbarroja N, López-Montilla MD, Cuesta-López L, Pérez-Sánchez C, Ruiz-Ponce M, López-Medina C, et al. Characterization of the inflammatory proteome of synovial fluid from patients with psoriatic arthritis: Potential treatment targets. Front Immunol. 2023;14:1133435. Epub 20230322. doi: 10.3389/fimmu.2023.1133435. PubMed PMID: 37033920; PubMed Central PMCID: PMC10073963.
294. Fiocco U, Sfriso P, Oliviero F, Roux-Lombard P, Scagliori E, Cozzi L, et al. Synovial effusion and synovial fluid biomarkers in psoriatic arthritis to assess intraarticular tumor necrosis factor-α blockade in the knee joint. ARTHRITIS RESEARCH & THERAPY. 2010;12. doi: 10.1186/ar3090. PubMed PMID: WOS:000283841500022.
295. Fiocco U, Oliviero F, Sfriso P, Calabrese F, Lunardi F, Scagliori E, et al. Synovial Biomarkers in Psoriatic Arthritis. JOURNAL OF RHEUMATOLOGY. 2012;39:61-4. doi: 10.3899/jrheum.120246. PubMed PMID: WOS:000306388500017.
296. af Klint E, Grundtman C, Engstrom M, Catrina AI, Makrygiannakis D, Klareskog L, et al. Intraarticular glucocorticoid treatment reduces inflammation in synovial cell

infiltrations more efficiently than in synovial blood vessels. Arthritis and Rheumatism. 2005;52(12):3880-9. doi: 10.1002/art.21488. PubMed PMID: WOS:000234131500026.
297. Alex P, Szodoray P, Arthur E, Willis L, Hynd R, Flinn D, et al. Influence of intraarticular corticosteroid administration on serum cytokines in rheumatoid arthritis. CLINICAL RHEUMATOLOGY. 2007;26(5):845-8. doi: 10.1007/s10067-006-0419-7. PubMed PMID: WOS:000245428100046.
298. Kim W, Min S, Cho M, Youn J, Min J, Lee S, et al. The role of IL-12 in inflammatory activity of patients with rheumatoid arthritis (RA). Clin Exp Immunol. 2000;119(1):175-81. doi: 10.1046/j.1365-2249.2000.01095.x. PubMed PMID: 10606980; PubMed Central PMCID: PMC1905529.
299. Brennan F, McInnes I. Evidence that cytokines play a role in rheumatoid arthritis. JOURNAL OF CLINICAL INVESTIGATION. 2008;118:3537-45. doi: 10.1172/JCI36389. PubMed PMID: WOS:000260622600006.
300. Cao QL, Irizarry YB, Yazhuk S, Tran T, Gadkari M, Franco LM. GCgx: transcriptome-wide exploration of the response to glucocorticoids. Journal of Molecular Endocrinology. 2022;68(2):B1-B4. doi: 10.1530/jme-21-0107. PubMed PMID: WOS:000760813600001.
301. Brennan FM, Zachariae CO, Chantry D, Larsen CG, Turner M, Maini RN, et al. Detection of interleukin 8 biological activity in synovial fluids from patients with rheumatoid arthritis and production of interleukin 8 mRNA by isolated synovial cells. Eur J Immunol. 1990;20(9):2141-4. doi: 10.1002/eji.1830200938. PubMed PMID: 2209707.
302. SYMONS J, WONG W, PALLADINO M, DUFF G. INTERLEUKIN-8 IN RHEUMATOID AND OSTEOARTHRITIS. SCANDINAVIAN JOURNAL OF RHEUMATOLOGY. 1992;21:92-4. PubMed PMID: WOS:A1992HQ08400009.
303. Heard B, Barton K, Chung M, Achari Y, Shrive N, Frank C, et al. Single intra-articular dexamethasone injection immediately post-surgery in a rabbit model mitigates early inflammatory responses and post-traumatic osteoarthritis-like alterations. JOURNAL OF ORTHOPAEDIC RESEARCH. 2015;33(12):1826-34. doi: 10.1002/jor.22972. PubMed PMID: WOS:000364239400013.
304. Schlaak JF, Pfers I, Meyer Zum Büschenfelde KH, Märker-Hermann E. Different cytokine profiles in the synovial fluid of patients with osteoarthritis, rheumatoid arthritis and seronegative spondylarthropathies. Clin Exp Rheumatol. 1996;14(2):155-62. PubMed PMID: 8737721.
305. Isomäki P, Luukkainen R, Toivanen P, Punnonen J. The presence of interleukin-13 in rheumatoid synovium and its antiinflammatory effects on synovial fluid macrophages from patients with rheumatoid arthritis. Arthritis Rheum. 1996;39(10):1693-702. doi: 10.1002/art.1780391012. PubMed PMID: 8843860.
306. Spadaro A, Rinaldi T, Riccieri V, Valesini G, Taccari E. Interleukin 13 in synovial fluid and serum of patients with psoriatic arthritis. ANNALS OF THE RHEUMATIC DISEASES. 2002;61:174-6. PubMed PMID: WOS:000173456100017.
307. Tokayer A, Carsons S, Chokshi B, Santiago-Schwarz F. High levels of interleukin 13 in rheumatoid arthritis sera are modulated by tumor necrosis factor antagonist therapy: Association with dendritic cell growth activity. JOURNAL OF RHEUMATOLOGY. 2002;29:454-61. PubMed PMID: WOS:000174214100007.
308. Woods J, Haines G, Shah M, Rayan G, Koch A. Low-level production of interleukin-13 in synovial fluid and tissue from patients with arthritis. CLINICAL IMMUNOLOGY AND IMMUNOPATHOLOGY. 1997;85:210-20. PubMed PMID: WOS:A1997YG86400013.
309. Gartshteyn Y, Askanase AD, Mor A. SLAM Associated Protein Signaling in T Cells: Tilting the Balance Toward Autoimmunity. Front Immunol. 2021;12:654839. Epub

20210416. doi: 10.3389/fimmu.2021.654839. PubMed PMID: 33936082; PubMed Central PMCID: PMC8086963.
310. Farhangnia P, Ghomi S, Mollazadehghomi S, Nickho H, Akbarpour M, Delbandi A. SLAM-family receptors come of age as a potential molecular target in cancer immunotherapy. Front Immunol. 2023;14. doi: 10.3389/fimmu.2023.1174138. PubMed PMID: WOS:000994852900001.
311. Hadley B, Litfin T, Day C, Haselhorst T, Zhou Y, Tiralongo J. Nucleotide Sugar Transporter SLC35 Family Structure and Function. COMPUTATIONAL AND STRUCTURAL BIOTECHNOLOGY JOURNAL. 2019;17:1123-34. doi: 10.1016/j.csbj.2019.08.002. PubMed PMID: WOS:000504205700112.
312. van den Boom J, Heider D, Martin SR, Pastore A, Mueller JW. 3'-Phosphoadenosine 5'-phosphosulfate (PAPS) synthases, naturally fragile enzymes specifically stabilized by nucleotide binding. J Biol Chem. 2012;287(21):17645-55. Epub 20120326. doi: 10.1074/jbc.M111.325498. PubMed PMID: 22451673; PubMed Central PMCID: PMC3366831.
313. Orr C, Vieira-Sousa E, Boyle DL, Buch MH, Buckley CD, Cañete JD, et al. Synovial tissue research: a state-of-the-art review. Nat Rev Rheumatol. 2017;13(8):463-75. Epub 20170713. doi: 10.1038/nrrheum.2017.115. PubMed PMID: 28701760.
314. Coras R, Murillo-Saich JD, Singh AG, Kavanaugh A, Guma M. Lipidomic Profiling in Synovial Tissue. Front Med. 2022;9. doi: 10.3389/fmed.2022.857135. PubMed PMID: WOS:000810104600001.
315. Smith MD. The Normal Synovium. The Open Rheumatology Journal: Bentham Open; 2011. p. 100-6.
316. Kino T, Su Y, Chrousos G. Human glucocorticoid receptor isoform β: recent understanding of its potential implications in physiology and pathophysiology. CELLULAR AND MOLECULAR LIFE SCIENCES. 2009;66:3435-48. doi: 10.1007/s00018-009-0098-z. PubMed PMID: WOS:000270632600004.
317. Cain D, Cidlowski J. Immune regulation by glucocorticoids. NATURE REVIEWS IMMUNOLOGY. 2017;17:233-47. doi: 10.1038/nri.2017.1. PubMed PMID: WOS:000397385600009.
318. Oakley R, Ramamoorthy S, Foley J, Busada J, Lu N, Cidlowski J. Glucocorticoid receptor isoform-specific regulation of development, circadian rhythm, and inflammation in mice. FASEB JOURNAL. 2018;32:5258-71. doi: 10.1096/fj.201701153R. PubMed PMID: WOS:000447972500006.
319. Makrygiannakis D, Revu S, Engstrom M, Af Klint E, Nicholas AP, Pruijn GJM, et al. Local administration of glucocorticoids decreases synovial citrullination in rheumatoid arthritis. Arthritis Research & Therapy. 2012;14(1). doi: 10.1186/ar3702. PubMed PMID: WOS:000304698800034.
320. van der Goes MC, Straub RH, Wenting MJG, Capellino S, Jacobs JWG, Jahangier ZN, et al. Intra-articular glucocorticoid injections decrease the number of steroid hormone receptor positive cells in synovial tissue of patients with persistent knee arthritis. Annals of the Rheumatic Diseases. 2012;71(9):1552-8. doi: 10.1136/annrheumdis-2011-201019. PubMed PMID: WOS:000307646500022.
321. Gheorghe KR, Korotkova M, Catrina AI, Backman L, Af Klint E, Claesson HE, et al. Expression of 5-lipoxygenase and 15-lipoxygenase in rheumatoid arthritis synovium and effects of intraarticular glucocorticoids. Arthritis Research & Therapy. 2009;11(3). doi: 10.1186/ar2717. PubMed PMID: WOS:000269019300049.
322. Makrygiannakis D, Revu S, Neregard P, af Klint E, Snir O, Grundtman C, et al. Monocytes are essential for inhibition of synovial T-cell glucocorticoid-mediated

apoptosis in rheumatoid arthritis. Arthritis Research & Therapy. 2008;10(6). doi: 10.1186/ar2582. PubMed PMID: WOS:000263570300033.
323. Vandooren B, Cantaert T, ter Borg M, Noordenbos T, Kuhlman R, Gerlag D, et al. Tumor Necrosis Factor alpha Drives Cadherin 11 Expression in Rheumatoid Inflammation. Arthritis and Rheumatism. 2008;58(10):3051-62. doi: 10.1002/art.23886. PubMed PMID: WOS:000260024400015.
324. Makrygiannakis D, af Klint E, Catrina SB, Botusan IR, Klareskog E, Klareskog L, et al. Intraarticular corticosteroids decrease synovial RANKL expression in inflammatory arthritis. Arthritis and Rheumatism. 2006;54(5):1463-72. doi: 10.1002/art.21767. PubMed PMID: WOS:000237533100015.
325. Korotkova M, Westman M, Gheorghe KR, af Klint E, Trollmo C, Ulfgren AK, et al. Effects of antirheumatic treatments on the prostaglandin E-2 Biosynthetic pathway. Arthritis and Rheumatism. 2005;52(11):3439-47. doi: 10.1002/art.21390. PubMed PMID: WOS:000233285400015.
326. Gerlag DM, Haringman JJ, Smeets TJM, Zwinderman AH, Kraan MC, Laud PJ, et al. Effects of oral prednisolone on biomarkers in synovial tissue and clinical improvement in rheumatoid arthritis. Arthritis and Rheumatism. 2004;50(12):3783-91. doi: 10.1002/art.20664. PubMed PMID: WOS:000225750200008.
327. Wong PKK, Cuello C, Bertouch JV, Roberts-Thomson PJ, Ahern MJ, Smith MD, et al. Effects of pulse methylprednisolone on macrophage chemotactic protein-1 and macrophage inflammatory protein-1 alpha in rheumatoid synovium. Journal of Rheumatology. 2001;28(12):2634-6. PubMed PMID: WOS:000172517800012.
328. Young L, Katrib A, Cuello C, Vollmer-Conna U, Bertouch JV, Roberts-Thomson PJ, et al. Effects of intraarticular glucocorticoids on macrophage infiltration and mediators of joint damage in osteoarthritis synovial membranes - Findings in a double-blind, placebo-controlled study. Arthritis and Rheumatism. 2001;44(2):343-50. doi: 10.1002/1529-0131(200102)44:2<343::aid-anr52>3.0.co;2-q. PubMed PMID: WOS:000171750600013.
329. Wong P, Cuello C, Bertouch JV, Roberts-Thomson PJ, Ahern MJ, Smith MD, et al. The effects of pulse methylprednisolone on matrix metalloproteinase and tissue inhibitor of metalloproteinase-1 expression in rheumatoid arthritis. Rheumatology. 2000;39(10):1067-73. doi: 10.1093/rheumatology/39.10.1067. PubMed PMID: WOS:000089971500004.
330. Youssef PP, Haynes DR, Triantafillou S, Parker A, Gamble JR, RobertsThomson PJ, et al. Effects of pulse methylprednisolone on inflammatory mediators in peripheral blood, synovial. Fluid, and synovial membrane in rheumatoid arthritis. Arthritis and Rheumatism. 1997;40(8):1400-8. doi: 10.1002/art.1780400807. PubMed PMID: WOS:A1997XP45600006.
331. Youssef PP, Triantafillou S, Parker A, Coleman M, RobertsThomson PJ, Ahern MJ, et al. Effects of pulse methylprednisolone on cell adhesion molecules in the synovial membrane in rheumatoid arthritis - Reduced E-selectin and intercellular adhesion molecule 1 expression. Arthritis and Rheumatism. 1996;39(12):1970-9. doi: 10.1002/art.1780391205. PubMed PMID: WOS:A1996VX90100004.
332. Debois MHW, Arndt JW, Tak PP, Kluin PM, Vandervelde EA, Pauwels EKJ, et al. TC-99M-LABELED POLYCLONAL HUMAN IMMUNOGLOBULIN-G SCINTIGRAPHY BEFORE AND AFTER INTRAARTICULAR KNEE INJECTION OF TRIAMCINOLONE HEXACETONIDE IN PATIENTS WITH RHEUMATOID-ARTHRITIS. Nuclear Medicine Communications. 1993;14(10):883-7. doi: 10.1097/00006231-199310000-00009. PubMed PMID: WOS:A1993MB06400009.

333. Corkill MM, Kirkham BW, Haskard DO, Barbatis C, Gibson T, Panayi GS. GOLD TREATMENT OF RHEUMATOID-ARTHRITIS DECREASES SYNOVIAL EXPRESSION OF THE ENDOTHELIAL LEUKOCYTE ADHESION RECEPTOR ELAM-1. Journal of Rheumatology. 1991;18(10):1453-60. PubMed PMID: WOS:A1991GP89600007.
334. Firestein GS, Paine MM, Littman BH. GENE-EXPRESSION (COLLAGENASE, TISSUE INHIBITOR OF METALLOPROTEINASES, COMPLEMENT, AND HLA DR) IN RHEUMATOID-ARTHRITIS AND OSTEOARTHRITIS SYNOVIUM - QUANTITATIVE-ANALYSIS AND EFFECT OF INTRAARTICULAR CORTICOSTEROIDS. Arthritis and Rheumatism. 1991;34(9):1094-105. doi: 10.1002/art.1780340905. PubMed PMID: WOS:A1991GG33700004.
335. Nerviani A, Di Cicco M, Mahto A, Lliso-Ribera G, Rivellese F, Thorborn G, et al. A Pauci-Immune Synovial Pathotype Predicts Inadequate Response to TNF alpha-Blockade in Rheumatoid Arthritis Patients. Front Immunol. 2020;11. doi: 10.3389/fimmu.2020.00845. PubMed PMID: WOS:000536358300001.
336. Rivellese F, Surace AEA, Goldmann K, Sciacca E, Cubuk C, Giorli G, et al. Rituximab versus tocilizumab in rheumatoid arthritis: synovial biopsy-based biomarker analysis of the phase 4 R4RA randomized trial. Nature Medicine. 2022;28(6):1256-+. doi: 10.1038/s41591-022-01789-0. PubMed PMID: WOS:000797762900001.
337. Rivellese F, Rossi FW, Giorli G, Napolitano F, de Paulis A, Pitzalis C. Persistence of Mast Cell-Positive Synovitis in Early Rheumatoid Arthritis Following Treatment With Conventional Synthetic Disease Modifying Anti-Rheumatic Drugs. Frontiers in Pharmacology. 2020;11. doi: 10.3389/fphar.2020.01051. PubMed PMID: WOS:000556637600001.
338. Triaille C, Durez P, Sokolova T, Tilman G, de Bellefon LM, Galant C, et al. Common Transcriptomic Effects of Abatacept and Other DMARDs on Rheumatoid Arthritis Synovial Tissue. Front Immunol. 2021;12. doi: 10.3389/fimmu.2021.724895. PubMed PMID: WOS:000697995400001.
339. Tang S, Yao L, Ruan J, Kang J, Cao Y, Nie X, et al. [Single-cell atlas of human infrapatellar fat pad and synovium implicates APOE signaling in osteoarthritis pathology]. SCIENCE TRANSLATIONAL MEDICINE2024.
340. Emont MP, Jacobs C, Essene AL, Pant D, Tenen D, Colleluori G, et al. A single-cell atlas of human and mouse white adipose tissue. Nature. 2022;603(7903):926-+. doi: 10.1038/s41586-022-04518-2. PubMed PMID: WOS:000769827000023.
341. Muro E, Atilla-Gokcumen GE, Eggert US. Lipids in cell biology: how can we understand them better? Mol Biol Cell. 2014;25(12):1819-23. doi: 10.1091/mbc.E13-09-0516. PubMed PMID: WOS:000339651500001.
342. Song JF, Deng T. The Adipocyte and Adaptive Immunity. Front Immunol. 2020;11. doi: 10.3389/fimmu.2020.593058. PubMed PMID: WOS:000597280300001.
343. Ichikawa N, Taniguchi A, Kobayashi S, Yamanaka H. Performance of hands and feet radiographs in differentiation of psoriatic arthritis from rheumatoid arthritis. Int J Rheum Dis. 2012;15:462-7. doi: 10.1111/j.1756-185X.2012.01818.x. PubMed PMID: WOS:000310077300019.
344. Reece R, Canete J, Parsons W, Emery P, Veale D. Distinct vascular patterns of early synovitis in psoriatic, reactive, and rheumatoid arthritis. ARTHRITIS AND RHEUMATISM. 1999;42:1481-4. PubMed PMID: WOS:000081259400023.
345. Cafaro G, McInnes I. Psoriatic arthritis: tissue-directed inflammation? CLINICAL RHEUMATOLOGY. 2018;37:859-68. doi: 10.1007/s10067-018-4012-7. PubMed PMID: WOS:000428989500001.

346. Floudas A, Smith CM, Tynan O, Neto N, Krishna V, Wade SM, et al. Distinct stromal and immune cell interactions shape the pathogenesis of rheumatoid and psoriatic arthritis. Annals of the Rheumatic Diseases. 2022;81(9):1224-42. doi: 10.1136/annrheumdis-2021-221761. PubMed PMID: WOS:000811697900001.
347. Mimpen JY, Paul C, Tendon Seed Network, Cribbs AP, Snelling SJB. Nuclei isolation from snap-frozen tendon tissue for single nucleus RNA Sequencing. protocols.io. 2021; https://doi.org/10.17504/protocols.io.bc6xizfn.
348. Hao YH, Hao S, Andersen-Nissen E, Mauck WM, Zheng SW, Butler A, et al. Integrated analysis of multimodal single-cell data. Cell. 2021;184(13):3573-+. doi: 10.1016/j.cell.2021.04.048. PubMed PMID: WOS:000665547300020.
349. Young MD, Behjati S. SoupX removes ambient RNA contamination from droplet-based single-cell RNA sequencing data. Gigascience. 2020;9(12). doi: 10.1093/gigascience/giaa151. PubMed PMID: WOS:000606077900019.
350. Yang SY, Corbett SE, Koga Y, Wang Z, Johnson WE, Yajima M, et al. Decontamination of ambient RNA in single-cell RNA-seq with DecontX. Genome Biology. 2020;21(1). doi: 10.1186/s13059-020-1950-6. PubMed PMID: WOS:000519049900001.
351. Germain PaL, A and Garcia Meixide, C and Macnair, W and Robinson, MD. Doublet identification in single-cell sequencing data using scDblFinder [version 2; peer review: 2 approved]. F1000Research. 2022;10(979). doi: 10.12688/f1000research.73600.2.
352. Mimpen JY, Ramos-Mucci L, Paul C, Kurjan A, Hulley P, Ikwuanusi C, et al. Single nucleus and spatial transcriptomic profiling of human healthy hamstring tendon. bioRxiv. 2022:2022.12.19.521110. doi: 10.1101/2022.12.19.521110.
353. Edalat SG, Gerber R, Houtman M, Kuret T, Ižanc N, Micheroli R, et al. A reference single-cell map of freshly dissociated human synovium in inflammatory arthritis with an optimized dissociation protocol for prospective synovial biopsy collection. bioRxiv. 2023:2022.06.01.493823. doi: 10.1101/2022.06.01.493823.
354. Alivernini S, MacDonald L, Elmesmari A, Finlay S, Tolusso B, Gigante MR, et al. Distinct synovial tissue macrophage subsets regulate inflammation and remission in rheumatoid arthritis. Nature Medicine. 2020;26(8):1295-+. doi: 10.1038/s41591-020-0939-8. PubMed PMID: WOS:000544159600003.
355. Croft AP, Campos J, Jansen K, Turner JD, Marshall J, Attar M, et al. Distinct fibroblast subsets drive inflammation and damage in arthritis. Nature. 2019;570(7760):246-+. doi: 10.1038/s41586-019-1263-7. PubMed PMID: WOS:000471297600054.
356. Miller SA, Policastro RA, Sriramkumar S, Lai T, Huntington TD, Ladaika CA, et al. LSD1 and Aberrant DNA Methylation Mediate Persistence of Enteroendocrine Progenitors That Support BRAF-Mutant Colorectal Cancer. Cancer Research. 2021;81(14):3791-805. doi: 10.1158/0008-5472.can-20-3562. PubMed PMID: WOS:000674703000006.
357. Jin S, Plikus M, Nie Q. CellChat for systematic analysis of cell-cell communication from single-cell transcriptomics. NATURE PROTOCOLS. 2025;20(1). doi: 10.1038/s41596-024-01045-4. PubMed PMID: WOS:001314820600001.
358. Waltman L, van Eck N. A smart local moving algorithm for large-scale modularity-based community detection. EUROPEAN PHYSICAL JOURNAL B. 2013;86(11). doi: 10.1140/epjb/e2013-40829-0. PubMed PMID: WOS:000326811500007.
359. Edalat S, Gerber R, Houtman M, Lükgen J, Teiseira R, Cisneros M, et al. Molecular maps of synovial cells in inflammatory arthritis using an optimized synovial tissue dissociation protocol. ISCIENCE. 2024;27(6). doi: 10.1016/j.isci.2024.109707. PubMed PMID: WOS:001247122000001.

360. Eberlé D, Hegarty B, Bossard P, Ferré P, Foufelle F. SREBP transcription factors:: master regulators of lipid homeostasis. Biochimie. 2004;86(11):839-48. doi: 10.1016/j.biochi.2004.09.018. PubMed PMID: WOS:000225939400013.
361. Raudvere U, Kolberg L, Kuzmin I, Arak T, Adler P, Peterson H, et al. g:Profiler: a web server for functional enrichment analysis and conversions of gene lists (2019 update). NUCLEIC ACIDS RESEARCH. 2019;47(W1):W191-W8. doi: 10.1093/nar/gkz369. PubMed PMID: WOS:000475901600028.
362. Browaeys R, Saelens W, Saeys Y. NicheNet: modeling intercellular communication by linking ligands to target genes. NATURE METHODS. 2020;17:159-+. doi: 10.1038/s41592-019-0667-5. PubMed PMID: WOS:000613903200001.
363. Heumos L, Schaar AC, Lance C, Litinetskaya A, Drost F, Zappia L, et al. Best practices for single-cell analysis across modalities. Nature Reviews Genetics. 2023;24(8):550-72. doi: 10.1038/s41576-023-00586-w. PubMed PMID: WOS:000961193300001.
364. Baldwin M, Buckley CD, Guilak F, Hulley P, Cribbs AP, Snelling S. A roadmap for delivering a human musculoskeletal cell atlas. Nature Reviews Rheumatology. 2023. doi: 10.1038/s41584-023-01031-2. PubMed PMID: WOS:001076188000001.
365. Eraslan G, Drokhlyansky E, Anand S, Fiskin E, Subramanian A, Slyper M, et al. Single-nucleus cross-tissue molecular reference maps toward understanding disease gene function. Science. 2022;376(6594):712-+. doi: 10.1126/science.abl4290. PubMed PMID: WOS:000798488100037.
366. Gupta A, Weinand K, Nathan A, Sakaue S, Zhang MJ, Donlin L, et al. Dynamic regulatory elements in single-cell multimodal data implicate key immune cell states enriched for autoimmune disease heritability. Nature Genetics. 2023;55(12):2021-2. doi: 10.1038/s41588-023-01577-7. PubMed PMID: WOS:001111853400015.
367. John K, Marino JS, Sanchez ER, Hinds TD. The glucocorticoid receptor: cause of or cure for obesity? Am J Physiol Endocrinol Metab. 2016;310(4):E249-57. Epub 20151229. doi: 10.1152/ajpendo.00478.2015. PubMed PMID: 26714851; PubMed Central PMCID: PMC4838130.
368. Divertie GD, Jensen MD, Miles JM. Stimulation of lipolysis in humans by physiological hypercortisolemia. Diabetes. 1991;40(10):1228-32. doi: 10.2337/diab.40.10.1228. PubMed PMID: 1936585.
369. Xiao X, Li H, Yang J, Qi X, Zu X, Zhong J, et al. Wnt/β-catenin signaling pathway and lipolysis enzymes participate in methylprednisolone induced fat differential distribution between subcutaneous and visceral adipose tissue. Steroids. 2014;84:30-5. Epub 20140320. doi: 10.1016/j.steroids.2014.03.004. PubMed PMID: 24657224.
370. Xu C, He J, Jiang H, Zu L, Zhai W, Pu S, et al. Direct effect of glucocorticoids on lipolysis in adipocytes. Mol Endocrinol. 2009;23(8):1161-70. Epub 20090514. doi: 10.1210/me.2008-0464. PubMed PMID: 19443609; PubMed Central PMCID: PMC5419195.
371. Carmen GY, Víctor SM. Signalling mechanisms regulating lipolysis. Cell Signal. 2006;18(4):401-8. Epub 20050922. doi: 10.1016/j.cellsig.2005.08.009. PubMed PMID: 16182514.
372. Najm A, Costantino F, Alivernini S, Alunno A, Bianchi E, Bignall J, et al. EULAR points to consider for minimal reporting requirements in synovial tissue research in rheumatology. ANNALS OF THE RHEUMATIC DISEASES. 2022;81(12):1640-6. doi: 10.1136/annrheumdis-2021-221875. PubMed PMID: WOS:000765403900001.
373. Dolhain R, Ter Haar N, De Kuiper R, Nieuwenhuis I, Zwinderman A, Breedveld F, et al. Distribution of T cells and signs of T-cell activation in the rheumatoid joint:

Implications for semiquantitative comparative histology. BRITISH JOURNAL OF RHEUMATOLOGY. 1998;37(3):324-30. PubMed PMID: WOS:000072799200015.
374. KENNEDY T, PLATERZYBERK C, PARTRIDGE T, WOODROW D, MAINI R. MORPHOMETRIC COMPARISON OF SYNOVIUM FROM PATIENTS WITH OSTEO-ARTHRITIS AND RHEUMATOID-ARTHRITIS. JOURNAL OF CLINICAL PATHOLOGY. 1988;41(8):847-52. PubMed PMID: WOS:A1988P764000007.
375. Cerwenka A, Lanier L. Natural killer cell memory in infection, inflammation and cancer. NATURE REVIEWS IMMUNOLOGY. 2016;16(2):112-23. doi: 10.1038/nri.2015.9. PubMed PMID: WOS:000369183800014.
376. TAK P, KUMMER J, HACK C, DAHA M, SMEETS T, ERKELENS G, et al. GRANZYME-POSITIVE CYTOTOXIC-CELLS ARE SPECIFICALLY INCREASED IN EARLY RHEUMATOID SYNOVIAL TISSUE. ARTHRITIS AND RHEUMATISM. 1994;37(12):1735-43. PubMed PMID: WOS:A1994PW72800004.
377. Söderström K, Stein E, Colmenero P, Purath U, Müller-Ladner U, de Matos C, et al. Natural killer cells trigger osteoclastogenesis and bone destruction in arthritis. PROCEEDINGS OF THE NATIONAL ACADEMY OF SCIENCES OF THE UNITED STATES OF AMERICA. 2010;107(29):13028-33. doi: 10.1073/pnas.1000546107. PubMed PMID: WOS:000280144500059.
378. Muscari I, Fierabracci A, Adorisio S, Moretti M, Cannarile L, Ayroldi E, et al. Glucocorticoids and natural killer cells: A suppressive relationship. Biochem Pharmacol. 2022;198. doi: 10.1016/j.bcp.2022.114930. PubMed PMID: WOS:000772628100008.
379. Morgan D, Davis D. Distinct effects of Dexamethasone on human natural Killer cell responses Dependent on cytokines. Front Immunol. 2017;8:1-15. doi: 10.3389/fimmu.2017.00432. PubMed PMID: WOS:000399421900001.
380. Perez S, Mahaira L, Demirtzoglou F, Sotiropoulou P, Ioannidis P, Iliopoulou E, et al. A potential role for hydrocortisone in the positive regulation of IL-15-activated NK-cell proliferation and survival. BLOOD. 2005;106(1):158-66. doi: 10.1182/blood-2004-08-3232. PubMed PMID: WOS:000230156500030.
381. Ashwell J, Lu F, Vacchio M. Glucocorticoids in T cell development and function. ANNUAL REVIEW OF IMMUNOLOGY. 2000;18:309-45. PubMed PMID: WOS:000087236500012.
382. Cari L, De Rosa F, Nocentini G, Riccardi C. Context-Dependent Effect of Glucocorticoids on the Proliferation, Differentiation, and Apoptosis of Regulatory T Cells: A Review of the Empirical Evidence and Clinical Applications. INTERNATIONAL JOURNAL OF MOLECULAR SCIENCES. 2019;20(5). doi: 10.3390/ijms20051142. PubMed PMID: WOS:000462542300141.
383. Liu Z, Chen H, Tan C, Zha J, Liu H, Chen G. Activation of CD3+TIM3+T cells contributes to excessive inflammatory response during glucocorticoid treatment. Biochem Pharmacol. 2023;212. doi: 10.1016/j.bcp.2023.115551. PubMed PMID: WOS:000982737100001.
384. Karagiannidis C, Akdis M, Holopainen P, Woolley N, Hense G, Rückert B, et al. Glucocorticoids upregulate FOXP3 expression and regulatory T cells in asthma. JOURNAL OF ALLERGY AND CLINICAL IMMUNOLOGY. 2004;114(6):1425-33. doi: 10.1016/j.jaci.2004.07.014. PubMed PMID: WOS:000225577400027.
385. Sbiera S, Dexneit T, Reichardt S, Michel K, van den Brandt J, Schmull S, et al. Influence of Short-Term Glucocorticoid Therapy on Regulatory T Cells In Vivo. PLOS ONE. 2011;6(9). doi: 10.1371/journal.pone.0024345. PubMed PMID: WOS:000294686100035.
386. Braitch M, Harikrishnan S, Robins R, Nichols C, Fahey A, Showe L, et al. Glucocorticoids increase CD4+CD25high cell percentage and Foxp3 expression in patients

with multiple sclerosis. ACTA NEUROLOGICA SCANDINAVICA. 2009;119(4):239-45. doi: 10.1111/j.1600-0404.2008.01090.x. PubMed PMID: WOS:000263908700004.
387. Chen X, Oppenheim J, Winkler-Pickett R, Ortaldo J, Howard O. Glucocorticoid amplifies IL-2-dependent expansion of functional FoxP3+CD4+CD25+ T regulatory cells in vivo and enhances their capacity to suppress EAE. EUROPEAN JOURNAL OF IMMUNOLOGY. 2006;36(8):2139-49. doi: 10.1002/eji.200635873. PubMed PMID: WOS:000239855900014.
388. Prado C, Gómez J, López P, de Paz B, Gutiérrez C, Suárez A. Dexamethasone upregulates FOXP3 expression without increasing regulatory activity. Immunobiology. 2011;216(3):386-92. doi: 10.1016/j.imbio.2010.06.013. PubMed PMID: WOS:000288722500015.
389. Kang Y, Chen L. Structure and mechanism of NALCN-FAM155A-UNC79-UNC80 channel complex. NATURE COMMUNICATIONS. 2022;13(1). doi: 10.1038/s41467-022-30403-7. PubMed PMID: WOS:000795171100052.
390. Smith M, Gao V, Periyakoil P, Kochen A, DiCarlo E, Goodman S, et al. Drivers of heterogeneity in synovial fibroblasts in rheumatoid arthritis. NATURE IMMUNOLOGY. 2023;24(7):1200-+. doi: 10.1038/s41590-023-01527-9. PubMed PMID: WOS:001000774700001.
391. Ren D. Sodium Leak Channels in Neuronal Excitability and Rhythmic Behaviors. NEURON. 2011;72(6):899-911. doi: 10.1016/j.neuron.2011.12.007. PubMed PMID: WOS:000298771000006.
392. Zhang D, Wei Y. Role of sodium leak channel (NALCN) in sensation and pain: an overview. FRONTIERS IN PHARMACOLOGY. 2024;14. doi: 10.3389/fphar.2023.1349438. PubMed PMID: WOS:001147892900001.
393. Zhang K, Hocker J, Miller M, Hou X, Chiou J, Poirion O, et al. A single-cell atlas of chromatin accessibility in the human genome. CELL. 2021;184(24):5985-+. doi: 10.1016/j.cell.2021.10.024. PubMed PMID: WOS:000722314300003.
394. Zhao N, Bennett D, Baskozos G, Barry A. Predicting 'pain genes': multi-modal data integration using probabilistic classifiers and interaction networks. BIOINFORMATICS ADVANCES. 2024;4(1). doi: 10.1093/bioadv/vbae156. PubMed PMID: WOS:001351156600001.
395. Kumar V, Soni U, Maurya V, Singh K, Jha R. Integrin beta8 (ITGB8) activates VAV-RAC1 signaling via FAK in the acquisition of endometrial epithelial cell receptivity for blastocyst implantation. SCIENTIFIC REPORTS. 2017;7. doi: 10.1038/s41598-017-01764-7. PubMed PMID: WOS:000425899400004.
396. Cambier S, Mu D, O'Connell D, Boylen K, Travis W, Liu W, et al. A role for the integrin αvβ8 in the negative regulation of epithelial cell growth. CANCER RESEARCH. 2000;60(24):7084-93. PubMed PMID: WOS:000166201500054.
397. Reyes S, Narayanan A, Lee H, Tchaicha J, Aldape K, Lang F, et al. αvβ8 integrin interacts with RhoGDI1 to regulate Rac1 and Cdc42 activation and drive glioblastoma cell invasion. Mol Biol Cell. 2013;24(4):474-82. doi: 10.1091/mbc.E12-07-0521. PubMed PMID: WOS:000321117800005.
398. Li C, Zheng Z. Cartilage Targets of Knee Osteoarthritis Shared by Both Genders. INTERNATIONAL JOURNAL OF MOLECULAR SCIENCES. 2021;22(2). doi: 10.3390/ijms22020569. PubMed PMID: WOS:000611289900001.
399. LaPointe V, Verpoorte A, Stevens M. The Changing Integrin Expression and a Role for Integrin β8 in the Chondrogenic Differentiation of Mesenchymal Stem Cells. PLOS ONE. 2013;8(11). doi: 10.1371/journal.pone.0082035. PubMed PMID: WOS:000327652100108.

400. Schoeps B, Frädrich J, Krüger A. Cut loose TIMP-1: an emerging cytokine in inflammation. TRENDS IN CELL BIOLOGY. 2023;33:413-26. doi: 10.1016/j.tcb.2022.08.005. PubMed PMID: WOS:000984598800001.
401. Metzemaekers M, Cambier S, Blanter M, Vandooren J, de Carvalho A, Malengier-Devlies B, et al. Kinetics of peripheral blood neutrophils in severe coronavirus disease 2019. CLINICAL & TRANSLATIONAL IMMUNOLOGY. 2021;10. doi: 10.1002/cti2.1271. PubMed PMID: WOS:000648333400014.
402. Schoeps B, Eckfeld C, Prokopchuk O, Böttcher J, Häussler D, Steiger K, et al. TIMP1 Triggers Neutrophil Extracellular Trap Formation in Pancreatic Cancer. CANCER RESEARCH. 2021;81:3568-79. doi: 10.1158/0008-5472.CAN-20-4125. PubMed PMID: WOS:000670539900013.
403. Barnes B, Adrover J, Baxter-Stoltzfus A, Borczuk A, Cools-Lartigue J, Crawford J, et al. Targeting potential drivers of COVID-19: Neutrophil extracellular traps. JOURNAL OF EXPERIMENTAL MEDICINE. 2020;217. doi: 10.1084/jem.20200652. PubMed PMID: WOS:000538138000018.
404. Horby P, Lim W, Emberson J, Mafham M, Bell J, Linsell L, et al. Dexamethasone in Hospitalized Patients with Covid-19. NEW ENGLAND JOURNAL OF MEDICINE. 2021;384:693-704. doi: 10.1056/NEJMoa2021436. PubMed PMID: WOS:000623807600009.
405. Rivera S, Khrestchatisky M, Kaczmarek L, Rosenberg G, Jaworski D. Metzincin Proteases and Their Inhibitors: Foes or Friends in Nervous System Physiology? JOURNAL OF NEUROSCIENCE. 2010;30:15337-57. doi: 10.1523/JNEUROSCI.3467-10.2010. PubMed PMID: WOS:000284358500001.
406. Thevenard J, Verzeaux L, Devy J, Etique N, Jeanne A, Schneider C, et al. Low-Density Lipoprotein Receptor-Related Protein-1 Mediates Endocytic Clearance of Tissue Inhibitor of Metalloproteinases-1 and Promotes Its Cytokine-Like Activities. PLOS ONE. 2014;9. doi: 10.1371/journal.pone.0103839. PubMed PMID: WOS:000340028800082.
407. Bai ZL, Bartelo N, Aslam M, Murphy EA, Hale CR, Blachere NE, et al. Synovial fibroblast gene expression is associated with sensory nerve growth and pain in rheumatoid arthritis. Science Translational Medicine. 2024;16(742). doi: 10.1126/scitranslmed.adk3506. PubMed PMID: WOS:001200565100006.
408. Uhlen M, Fagerberg L, Hallström BM, Lindskog C, Oksvold P, Mardinoglu A, et al. Tissue-based map of the human proteome. Science. 2015;347(6220). doi: 10.1126/science.1260419. PubMed PMID: WOS:000348225800036.
409. Clanchy F, Borghese F, Bystrom J, Balog A, Penn H, Taylor P, et al. Disease status in human and experimental arthritis, and response to TNF blockade, is associated with MHC class II invariant chain (CD74) isoform expression. JOURNAL OF AUTOIMMUNITY. 2022;128. doi: 10.1016/j.jaut.2022.102810. PubMed PMID: WOS:000788393600001.
410. Su H, Na N, Zhang X, Zhao Y. The biological function and significance of CD74 in immune diseases. INFLAMMATION RESEARCH. 2017;66:209-16. doi: 10.1007/s00011-016-0995-1. PubMed PMID: WOS:000394317000002.
411. Warner R, Najy A, Jung Y, Fridman R, Kim S, Kim H. Establishment of Structure-Function Relationship of Tissue Inhibitor of Metalloproteinase-1 for Its Interaction with CD63: Implication for Cancer Therapy. SCIENTIFIC REPORTS. 2020;10. doi: 10.1038/s41598-020-58964-x. PubMed PMID: WOS:000562828300016.
412. Wallace D, Figueras F, Wegener W, Goldenberg D. Experience with milatuzumab, an anti-CD74 antibody against immunomodulatory macrophage migration inhibitory factor (MIF) receptor, for systemic lupus erythematosus (SLE). ANNALS OF THE

RHEUMATIC DISEASES. 2021;80:954-5. doi: 10.1136/annrheumdis-2020-219803. PubMed PMID: WOS:000667725300036.
413. Fadda A, Syed N, Mackeh R, Papadopoulou A, Suzuki S, Jithesh PV, et al. Genome-wide Regulatory Roles of the C2H2-type Zinc Finger Protein ZNF764 on the Glucocorticoid Receptor. Sci Rep. 2017;7:41598. Epub 20170131. doi: 10.1038/srep41598. PubMed PMID: 28139699; PubMed Central PMCID: PMC5282477.
414. Vitellius G, Fagart J, Delemer B, Amazit L, Ramos N, Bouligand J, et al. Three Novel Heterozygous Point Mutations of NR3C1 Causing Glucocorticoid Resistance. Hum Mutat. 2016;37(8):794-803. Epub 20160511. doi: 10.1002/humu.23008. PubMed PMID: 27120390.
415. Faust H, Cheng T, Korsunsky I, Watts G, Gal-oz S, Trim W, et al. Adipocyte associated glucocorticoid signaling regulates normal fibroblast function which is lost in inflammatory arthritis. NATURE COMMUNICATIONS. 2024;15(1). doi: 10.1038/s41467-024-52586-x. PubMed PMID: WOS:001376484000001.
416. Ayhan E, Kesmezacar H, Akgun I. Intraarticular injections (corticosteroid, hyaluronic acid, platelet rich plasma) for the knee osteoarthritis. World J Orthop. 2014;5(3):351-61. Epub 20140718. doi: 10.5312/wjo.v5.i3.351. PubMed PMID: 25035839; PubMed Central PMCID: PMC4095029.
417. Cushman DM, Kobayashi JK, Wheelwright JC, English J, Monson N, Teramoto M, et al. Prospective Evaluation of Pain Flares and Time Until Pain Relief Following Musculoskeletal Corticosteroid Injections. Sports Health. 2023;15(2):227-33. Epub 20220324. doi: 10.1177/19417381221076470. PubMed PMID: 35331061; PubMed Central PMCID: PMC9950997.
418. CHANDLER GN, WRIGHT V. Deleterious effect of intra-articular hydrocortisone. Lancet. 1958;2(7048):661-3. doi: 10.1016/s0140-6736(58)92262-1. PubMed PMID: 13588963.
419. Stifel U, Wolfschmitt E, Vogt J, Wachter U, Vettorazzi S, Tews D, et al. Glucocorticoids coordinate macrophage metabolism through the regulation of the tricarboxylic acid cycle. MOLECULAR METABOLISM. 2022;57. doi: 10.1016/j.molmet.2021.101424. PubMed PMID: WOS:000747198200001.
420. Lee M, Gong D, Burkey B, Fried S. Pathways regulated by glucocorticoids in omental and subcutaneous human adipose tissues: a microarray study. AMERICAN JOURNAL OF PHYSIOLOGY-ENDOCRINOLOGY AND METABOLISM. 2011;300:E571-E80. doi: 10.1152/ajpendo.00231.2010. PubMed PMID: WOS:000287796200016.
421. Koh JH, Yoon SJ, Kim M, Cho S, Lim J, Park Y, et al. Lipidome profile predictive of disease evolution and activity in rheumatoid arthritis. Experimental and Molecular Medicine. 2022;54(2):143-55. doi: 10.1038/s12276-022-00725-z. PubMed PMID: WOS:000755448200001.
422. Robinson G, Pineda-Torra I, Ciurtin C, Jury EC. Lipid metabolism in autoimmune rheumatic disease: implications for modern and conventional therapies. Journal of Clinical Investigation. 2022;132(2). doi: 10.1172/jci148552. PubMed PMID: WOS:000747836200003.
423. Ananth L, Prete PE, Kashyap ML. Apolipoproteins A-I and B and cholesterol in synovial fluid of patients with rheumatoid arthritis. Metabolism. 1993;42(7):803-6. doi: 10.1016/0026-0495(93)90050-x. PubMed PMID: 8345790.
424. WILLIAMSON M, HUMM G, CRISP A. H-1 NUCLEAR MAGNETIC-RESONANCE INVESTIGATION OF SYNOVIAL-FLUID COMPONENTS IN OSTEO-ARTHRITIS, RHEUMATOID-ARTHRITIS AND TRAUMATIC EFFUSIONS.

BRITISH JOURNAL OF RHEUMATOLOGY. 1989;28:23-7. PubMed PMID: WOS:A1989T401500007.
425. Giera M, Ioan-Facsinay A, Toes R, Gao F, Dalli J, Deelder A, et al. Lipid and lipid mediator profiling of human synovial fluid in rheumatoid arthritis patients by means of LC-MS/MS. BIOCHIMICA ET BIOPHYSICA ACTA-MOLECULAR AND CELL BIOLOGY OF LIPIDS. 2012;1821:1415-24. doi: 10.1016/j.bbalip.2012.07.011. PubMed PMID: WOS:000309312100005.
426. Huh JY, Kim JI, Park YJ, Hwang IJ, Lee YS, Sohn JH, et al. A Novel Function of Adipocytes in Lipid Antigen Presentation to iNKT Cells. Molecular and Cellular Biology. 2013;33(2):328-39. doi: 10.1128/mcb.00552-12. PubMed PMID: WOS:000317186300012.
427. Fasshauer M, Blüher M. Adipokines in health and disease. Trends in Pharmacological Sciences. 2015;36(7):461-70. doi: 10.1016/j.tips.2015.04.014. PubMed PMID: WOS:000358463700005.
428. Deng T, Lyon CJ, Minze LJ, Lin JX, Zou J, Liu JZ, et al. Class II Major Histocompatibility Complex Plays an Essential Role in Obesity-Induced Adipose Inflammation. Cell Metabolism. 2013;17(3):411-22. doi: 10.1016/j.cmet.2013.02.009. PubMed PMID: WOS:000326265400012.
429. Lee YS, Kim JW, Osborne O, Oh DY, Sasik R, Schenk S, et al. Increased Adipocyte O₂ Consumption Triggers HIF-1α, Causing Inflammation and Insulin Resistance in Obesity. Cell. 2014;157(6):1339-52. doi: 10.1016/j.cell.2014.05.012. PubMed PMID: WOS:000340881400011.
430. Li XF, Sun YY, Bao J, Chen X, Li YH, Yang Y, et al. Functional role of PPAR-γ on the proliferation and migration of fibroblast-like synoviocytes in rheumatoid arthritis. Sci Rep. 2017;7(1):12671. Epub 20171004. doi: 10.1038/s41598-017-12570-6. PubMed PMID: 28978936; PubMed Central PMCID: PMC5627284.
431. Poulsen L, Siersbæk M, Mandrup S. PPARs: fatty acid sensors controlling metabolism. Semin Cell Dev Biol. 2012;23(6):631-9. Epub 20120118. doi: 10.1016/j.semcdb.2012.01.003. PubMed PMID: 22273692.
432. Ormseth MJ, Oeser AM, Cunningham A, Bian A, Shintani A, Solus J, et al. Peroxisome proliferator-activated receptor γ agonist effect on rheumatoid arthritis: a randomized controlled trial. Arthritis Res Ther. 2013;15(5):R110. doi: 10.1186/ar4290. PubMed PMID: 24020899; PubMed Central PMCID: PMC3978636.
433. Bongartz T, Coras B, Vogt T, Schölmerich J, Müller-Ladner U. Treatment of active psoriatic arthritis with the PPARgamma ligand pioglitazone: an open-label pilot study. Rheumatology (Oxford). 2005;44(1):126-9. Epub 20041012. doi: 10.1093/rheumatology/keh423. PubMed PMID: 15479756.
434. Rocha B, Ruiz-Romero C, Blanco F. Mass spectrometry imaging: a novel technology in rheumatology. NATURE REVIEWS RHEUMATOLOGY. 2017;13:52-63. doi: 10.1038/nrrheum.2016.184. PubMed PMID: WOS:000391344100008.
435. Rocha B, Cillero-Pastor B, Blanco F, Ruiz-Romero C. MALDI mass spectrometry imaging in rheumatic diseases. BIOCHIMICA ET BIOPHYSICA ACTA-PROTEINS AND PROTEOMICS. 2017;1865:784-94. doi: 10.1016/j.bbapap.2016.10.004. PubMed PMID: WOS:000404825500007.
436. Rocha B, Cillero-Pastor B, Illiano A, Calamia V, Puente P, Lourido L, et al. DIFFERENTIAL MOLECULAR PROFILES IN THE SYNOVIAL TISSUE AND SYNOVIAL FLUID OF PATIENTS WITH RHEUMATOID ARTHRITIS AND PSORIATIC ARTHRITIS. ANNALS OF THE RHEUMATIC DISEASES. 2022;81:486-. doi: 10.1136/annrheumdis-2022-eular.4459. PubMed PMID: WOS:000850279001400.

437. Rocha B, Cillero-Pastor B, Illiano A, Calamia V, Pinto G, Amoresano A, et al. Distinct Lipidomic Signatures in Synovium and Synovial Fluid of Patients with Rheumatoid Arthritis versus Psoriatic Arthritis. ARTHRITIS & RHEUMATOLOGY. 2021;73:1970-2. PubMed PMID: WOS:000744545203201.
438. McDougall A, Fosang A, Faggian J, Wallace M, Crossley K, Cole T, et al. Glucocorticoids influence versican and chondroitin sulphate proteoglycan levels in the fetal sheep lung. RESPIRATORY RESEARCH. 2018;19. doi: 10.1186/s12931-018-0854-4. PubMed PMID: WOS:000442199000001.
439. Short K, Bird A, Seow B, Ng J, McDougall A, Wallace M, et al. Glucocorticoid signalling drives reduced versican levels in the fetal mouse lung. JOURNAL OF MOLECULAR ENDOCRINOLOGY. 2020;64(3):155-64. doi: 10.1530/JME-19-0235. PubMed PMID: WOS:000523308200004.
440. Matsumoto K, Kamiya N, Suwan K, Atsumi F, Shimizu K, Shinomura T, et al. Identification and characterization of versican/PG-M aggregates in cartilage. J Biol Chem. 2006;281(26):18257-63. doi: 10.1074/jbc.M510330200. PubMed PMID: WOS:000238490300078.
441. Wight T, Kang I, Merrilees M. Versican and the control of inflammation. MATRIX BIOLOGY. 2014;35:152-61. doi: 10.1016/j.matbio.2014.01.015. PubMed PMID: WOS:000337556500020.
442. Andersson-Sjöland A, Hallgren O, Rolandsson S, Weitoft M, Tykesson E, Larsson-Callerfelt A, et al. Versican in inflammation and tissue remodeling: The impact on lung disorders. GLYCOBIOLOGY. 2015;25(3):243-51. doi: 10.1093/glycob/cwu120. PubMed PMID: WOS:000350902900001.
443. Pol J, Caudana P, Paillet J, Piaggio E, Kroemer G. Effects of interleukin-2 in immunostimulation and immunosuppression. JOURNAL OF EXPERIMENTAL MEDICINE. 2020;217(1). doi: 10.1084/jem.20191247. PubMed PMID: WOS:000523641000021.
444. Hinks A, Ke X, Barton A, Eyre S, Bowes J, Worthington J, et al. Association of the IL2RA/CD25 Gene With Juvenile Idiopathic Arthritis. ARTHRITIS AND RHEUMATISM. 2009;60(1):251-7. doi: 10.1002/art.24187. PubMed PMID: WOS:000262416600029.
445. van Steenbergen H, van Nies J, Ruyssen-Witrand A, Huizinga T, Cantagrel A, Berenbaum F, et al. IL2RA is associated with persistence of rheumatoid arthritis. ARTHRITIS RESEARCH & THERAPY. 2015;17. doi: 10.1186/s13075-015-0739-6. PubMed PMID: WOS:000360877100001.
446. BATUMAN O, FERRERO A, DIAZ A, BERGER B, POMERANTZ R. GLUCOCORTICOID-MEDIATED INHIBITION OF INTERLEUKIN-2 RECEPTOR-ALPHA AND RECEPTOR-BETA SUBUNIT EXPRESSION BY HUMAN T-CELLS. IMMUNOPHARMACOLOGY. 1994;27(1):43-55. PubMed PMID: WOS:A1994MV72600005.
447. MURAGUCHI A, KEHRL J, LONGO D, VOLKMAN D, SMITH K, FAUCI A. INTERLEUKIN-2 RECEPTORS ON HUMAN B-CELLS - IMPLICATIONS FOR THE ROLE OF INTERLEUKIN-2 IN HUMAN B-CELL FUNCTION. JOURNAL OF EXPERIMENTAL MEDICINE. 1985;161(1):181-97. PubMed PMID: WOS:A1985AAV9200013.
448. Mormile I, Rossi F, Prevete N, Granata F, Pucino V, de Paulis A. The N-Formyl Peptide Receptors and Rheumatoid Arthritis: A Dangerous Liaison or Confusing Relationship? Front Immunol. 2021;12. doi: 10.3389/fimmu.2021.685214. PubMed PMID: WOS:000669028400001.

449. Kim S, Kim J, Jo S, Lee H, Lee S, Shim J, et al. Functional Expression of Formyl Peptide Receptor Family in Human NK Cells. JOURNAL OF IMMUNOLOGY. 2009;183(9):5511-7. doi: 10.4049/jimmunol.0802986. PubMed PMID: WOS:000271488500012.
450. Lawrance W, Banerji S, Day A, Bhattacharjee S, Jackson D. Binding of Hyaluronan to the Native Lymphatic Vessel Endothelial Receptor LYVE-1 Is Critically Dependent on Receptor Clustering and Hyaluronan Organization. J Biol Chem. 2016;291:8014-30. doi: 10.1074/jbc.M115.708305. PubMed PMID: WOS:000374056700022.
451. Niwa Y, Kanda G, Yamada R, Shi S, Sunagawa G, Ukai-Tadenuma M, et al. Muscarinic Acetylcholine Receptors Chrm1 and Chrm3 Are Essential for REM Sleep. CELL REPORTS. 2018;24:2231-+. doi: 10.1016/j.celrep.2018.07.082. PubMed PMID: WOS:000442923900004.
452. Wolman M, Liu Y, Tawarayama H, Shoji W, Halloran M. Repulsion and attraction of axons by Semaphorin3D are mediated by different neuropilins in vivo. JOURNAL OF NEUROSCIENCE. 2004;24:8428-35. doi: 10.1523/JNEUROSCI.2349-04.2004. PubMed PMID: WOS:000224175000007.
453. Hernández-Acosta N, Cabrera-Socorro A, Morlans M, Delgado F, Suárez-Solá M, Sottocornola R, et al. Dynamic expression of the p53 family members p63 and p73 in the mouse and human telencephalon during development and in adulthood. BRAIN RESEARCH. 2011;1372:29-40. doi: 10.1016/j.brainres.2010.11.041. PubMed PMID: WOS:000287293700004.
454. Marro S, Chanda S, Yang N, Janas J, Valperga G, Trotter J, et al. Neuroligin-4 Regulates Excitatory Synaptic Transmission in Human Neurons. NEURON. 2019;103:617-+. doi: 10.1016/j.neuron.2019.05.043. PubMed PMID: WOS:000482179900010.
455. Coba M, Komiyama N, Nithianantharajah J, Kopanitsa M, Indersmitten T, Skene N, et al. TNiK Is Required for Postsynaptic and Nuclear Signaling Pathways and Cognitive Function. JOURNAL OF NEUROSCIENCE. 2012;32:13987-99. doi: 10.1523/JNEUROSCI.2433-12.2012. PubMed PMID: WOS:000309506600031.
456. Renthal W. Localization of migraine susceptibility genes in human brain by single-cell RNA sequencing. CEPHALALGIA. 2018;38:1976-83. doi: 10.1177/0333102418762476. PubMed PMID: WOS:000450358000010.
457. Asgrímsdóttir E, Arenas E. Midbrain Dopaminergic Neuron Development at the Single Cell Level:In vivoand in Stem Cells. FRONTIERS IN CELL AND DEVELOPMENTAL BIOLOGY. 2020;8. doi: 10.3389/fcell.2020.00463. PubMed PMID: WOS:000553962400001.
458. Puvogel S, Alsema A, North H, Webster M, Weickert C, Eggen B. Single-Nucleus RNA-Seq Characterizes the Cell Types Along the Neuronal Lineage in the Adult Human Subependymal Zone and Reveals Reduced Oligodendrocyte Progenitor Abundance with Age. ENEURO. 2024;11. doi: 10.1523/ENEURO.0246-23.2024. PubMed PMID: WOS:001181376400002.
459. Kim J, Yoo I, Lim J, Moon J. Pathological phenotypes of astrocytes in Alzheimer's disease. EXPERIMENTAL AND MOLECULAR MEDICINE. 2024;56:95-9. doi: 10.1038/s12276-023-01148-0. PubMed PMID: WOS:001135877200007.
460. Cheng T, Gong Q. Secreted TARSH regulates olfactory mitral cell dendritic complexity. EUROPEAN JOURNAL OF NEUROSCIENCE. 2009;29:1083-95. doi: 10.1111/j.1460-9568.2009.06660.x. PubMed PMID: WOS:000264065500001.
461. Rutter-Locher Z, Kirkham B, Bannister K, Bennett D, Buckley C, Taams L, et al. An interdisciplinary perspective on peripheral drivers of pain in rheumatoid arthritis.

NATURE REVIEWS RHEUMATOLOGY. 2024. doi: 10.1038/s41584-024-01155-z. PubMed PMID: WOS:001306558600001.
462. Udit S, Blake K, Chiu I. Somatosensory and autonomic neuronal regulation of the immune response. NATURE REVIEWS NEUROSCIENCE. 2022;23:157-71. doi: 10.1038/s41583-021-00555-4. PubMed PMID: WOS:000740181200001.
463. Sunzini F, Schrepf A, Clauw D, Basu N. The Biology of Pain: Through the Rheumatology Lens. ARTHRITIS & RHEUMATOLOGY. 2023;75:650-60. doi: 10.1002/art.42429. PubMed PMID: WOS:000953679800001.
464. Hochberg M, Carrino J, Schnitzer T, Guermazi A, Walsh D, White A, et al. Long-Term Safety and Efficacy of Subcutaneous Tanezumab Versus Nonsteroidal Antiinflammatory Drugs for Hip or Knee Osteoarthritis: A Randomized Trial. ARTHRITIS & RHEUMATOLOGY. 2021;73:1167-77. doi: 10.1002/art.41674. PubMed PMID: WOS:000658263800001.
465. Carrino J, McAlindon T, Schnitzer T, Guermazi A, Hochberg M, Conaghan P, et al. Characterization of adverse joint outcomes in patients with osteoarthritis treated with subcutaneous tanezumab. OSTEOARTHRITIS AND CARTILAGE. 2023;31:1612-26. doi: 10.1016/j.joca.2023.08.010. PubMed PMID: WOS:001122423100001.
466. Zhou R, Fu W, Vasylyev D, Waxman S, Liu C. Ion channels in osteoarthritis: emerging roles and potential targets. NATURE REVIEWS RHEUMATOLOGY. 2024;20:545-64. doi: 10.1038/s41584-024-01146-0. PubMed PMID: WOS:001287443100001.
467. Kasianowicz J. Introduction to Ion Channels and Disease. CHEMICAL REVIEWS. 2012;112:6215-7. doi: 10.1021/cr300444k. PubMed PMID: WOS:000312121900001.
468. Matta C, Takács R, Ducza L, Ebeid RA, Choi H, Mobasheri A. Ion channels involved in inflammation and pain in osteoarthritis and related musculoskeletal disorders. Am J Physiol Cell Physiol. 2023;325(1):C257-C71. Epub 20230612. doi: 10.1152/ajpcell.00040.2023. PubMed PMID: 37306390.
469. Law S, Chan M, Marathe G, Parveen F, Chen C, Ke L. An Updated Review of Lysophosphatidylcholine Metabolism in Human Diseases. INTERNATIONAL JOURNAL OF MOLECULAR SCIENCES. 2019;20. doi: 10.3390/ijms20051149. PubMed PMID: WOS:000462542300148.
470. Jacquot F, Khoury S, Labrum B, Delanoe K, Pidoux L, Barbier J, et al. Lysophosphatidylcholine 16:0 mediates chronic joint pain associated to rheumatic diseases through acid-sensing ion channel 3. PAIN. 2022;163:1999-2013. doi: 10.1097/j.pain.0000000000002596. PubMed PMID: WOS:000854379700016.
471. Khoury S, Colas J, Breuil V, Kosek E, Ahmed A, Svensson C, et al. Identification of Lipid Biomarkers for Chronic Joint Pain Associated with Different Joint Diseases. BIOMOLECULES. 2023;13. doi: 10.3390/biom13020342. PubMed PMID: WOS:000938469500001.
472. Pidoux L, Delanoe K, Barbier J, Marchand F, Lingueglia E, Deval E. Single Subcutaneous Injection of Lysophosphatidyl-Choline Evokes ASIC3-Dependent Increases of Spinal Dorsal Horn Neuron Activity. FRONTIERS IN MOLECULAR NEUROSCIENCE. 2022;15. doi: 10.3389/fnmol.2022.880651. PubMed PMID: WOS:000818581500001.
473. Kraev A, Quednau BD, Leach S, Li XF, Dong H, Winkfein R, et al. Molecular cloning of a third member of the potassium-dependent sodium-calcium exchanger gene family, NCKX3. J Biol Chem. 2001;276(25):23161-72. Epub 20010409. doi: 10.1074/jbc.M102314200. PubMed PMID: 11294880.

474. Torres A, Pedersen B, Guma M. Solute carrier nutrient transporters in rheumatoid arthritis fibroblast-like synoviocytes. Front Immunol. 2022;13:984408. Epub 20221020. doi: 10.3389/fimmu.2022.984408. PubMed PMID: 36341411; PubMed Central PMCID: PMC9632162.
475. Tran D, Go S, Park S, Jung E, Jeung E. Loss of Nckx3 Exacerbates Experimental DSS-Induced Colitis in Mice through p53/NF-κB Pathway. INTERNATIONAL JOURNAL OF MOLECULAR SCIENCES. 2021;22. doi: 10.3390/ijms22052645. PubMed PMID: WOS:000628288400001.
476. Aneiros E, Philipp S, Lis A, Freichel M, Cavalié A. Modulation of Ca²⁺ signaling by Na⁺/Ca²⁺ exchangers in mast cells. JOURNAL OF IMMUNOLOGY. 2005;174:119-30. PubMed PMID: WOS:000225852900016.
477. Rivellese F, Nerviani A, Rossi F, Marone G, Matucci-Cerinic M, de Paulis A, et al. Mast cells in rheumatoid arthritis: friends or foes? AUTOIMMUNITY REVIEWS. 2017;16:557-63. doi: 10.1016/j.autrev.2017.04.001. PubMed PMID: WOS:000400969200001.
478. Bradding P. Mast cell ion channels. Chem Immunol Allergy. 2005;87:163-78. doi: 10.1159/000087643. PubMed PMID: 16107771.
479. Ouyang D, Huang C, Liu H, Xie W, Chen C, Su B, et al. Comprehensive analysis of genetic associations and single-cell expression profiles reveals potential links between migraine and multiple diseases: a phenome-wide association study. FRONTIERS IN NEUROLOGY. 2024;15. doi: 10.3389/fneur.2024.1301208. PubMed PMID: WOS:001164811700001.
480. Qu X, Shi Z, Guo J, Guo C, Qiu J, Hua K. Identification of a novel six-gene signature with potential prognostic and therapeutic value in cervical cancer. CANCER MEDICINE. 2021;10:6881-96. doi: 10.1002/cam4.4054. PubMed PMID: WOS:000693741600001.
481. Zhou S, Jin Q, Yao H, Ying J, Tian L, Jiang X, et al. Pain-Related Gene Solute Carrier Family 24 Member 3 Is a Prognostic Biomarker and Correlated with Immune Infiltrates in Cervical Squamous Cell Carcinoma and Endocervical Adenocarcinoma: A Study via Integrated Bioinformatics Analyses and Experimental Verification. Comput Math Methods Med. 2023;2023:4164232. Epub 20230207. doi: 10.1155/2023/4164232. PubMed PMID: 36798148; PubMed Central PMCID: PMC9928512.
482. Fagerberg L, Hallström BM, Oksvold P, Kampf C, Djureinovic D, Odeberg J, et al. Analysis of the human tissue-specific expression by genome-wide integration of transcriptomics and antibody-based proteomics. Mol Cell Proteomics. 2014;13(2):397-406. Epub 20131205. doi: 10.1074/mcp.M113.035600. PubMed PMID: 24309898; PubMed Central PMCID: PMC3916642.
483. Habuka M, Fagerberg L, Hallström BM, Kampf C, Edlund K, Sivertsson Å, et al. The kidney transcriptome and proteome defined by transcriptomics and antibody-based profiling. PLoS One. 2014;9(12):e116125. Epub 20141231. doi: 10.1371/journal.pone.0116125. PubMed PMID: 25551756; PubMed Central PMCID: PMC4281243.
484. Kornblum H, Zurcher S, Werb Z, Derynck R, Seroogy K. Multiple trophic actions of heparin-binding epidermal growth factor (HB-EGF) in the central nervous system. EUROPEAN JOURNAL OF NEUROSCIENCE. 1999;11:3236-46. PubMed PMID: WOS:000083004800024.
485. Ha S, Lee D, Cho Y, Chung C, Yoo Y, Kim J, et al. Cerebellar Shank2 Regulates Excitatory Synapse Density, Motor Coordination, and Specific Repetitive and Anxiety-

Like Behaviors. JOURNAL OF NEUROSCIENCE. 2016;36:12129-43. doi: 10.1523/JNEUROSCI.1849-16.2016. PubMed PMID: WOS:000391140400007.
486. Galakhova A, Hunt S, Wilbers R, Heyer D, de Kock C, Mansvelder H, et al. Evolution of cortical neurons supporting human cognition. TRENDS IN COGNITIVE SCIENCES. 2022;26:909-22. doi: 10.1016/j.tics.2022.08.012. PubMed PMID: WOS:000875597400004.
487. Zheng C, Chen D, Zhang Y, Bai Y, Huang S, Zheng D, et al. FAM19A1 is a new ligand for GPR1 that modulates neural stem-cell proliferation and differentiation. FASEB JOURNAL. 2018;32:5874-90. doi: 10.1096/fj.201800020RRR. PubMed PMID: WOS:000447172000010.
488. Sasaki T, Sakuma J, Ichikawa T, Matsumoto M, Tiwari P, Young W, et al. Effects of methylprednisolone on axonal depression induced by hypoxia, gamma-aminobutyric acid, and (+/-)-8-hydroxy-dipropylaminotetralin hydrobromide. Neurosurgery. 2002;51(6):1477-83; discussion 83. PubMed PMID: 12445354.
489. Lee M, Sakatani K, Young W. A role of GABAA receptors in hypoxia-induced conduction failure of neonatal rat spinal dorsal column axons. Brain Res. 1993;601(1-2):14-9. doi: 10.1016/0006-8993(93)91690-t. PubMed PMID: 8381697.
490. Norreen-Thorsen M, Struck EC, Oling S, Zwahlen M, Von Feilitzen K, Odeberg J, et al. A human adipose tissue cell-type transcriptome atlas. Cell Reports. 2022;40(2). doi: 10.1016/j.celrep.2022.111046. PubMed PMID: WOS:000827457300006.
491. Baschant U, Frappart L, Rauchhaus U, Bruns L, Reichardt H, Kamradt T, et al. Glucocorticoid therapy of antigen-induced arthritis depends on the dimerized glucocorticoid receptor in T cells. PROCEEDINGS OF THE NATIONAL ACADEMY OF SCIENCES OF THE UNITED STATES OF AMERICA. 2011;108:19317-22. doi: 10.1073/pnas.1105857108. PubMed PMID: WOS:000297463100047.
492. Koenen M, Culemann S, Vettorazzi S, Caratti G, Frappart L, Baum W, et al. Glucocorticoid receptor in stromal cells is essential for glucocorticoid-mediated suppression of inflammation in arthritis. ANNALS OF THE RHEUMATIC DISEASES. 2018;77:1610-8. doi: 10.1136/annrheumdis-2017-212762. PubMed PMID: WOS:000450414300020.
493. Wu F, Gao J, Kang J, Wang X, Niu Q, Liu J, et al. B Cells in Rheumatoid Arthritis:Pathogenic Mechanisms and Treatment Prospects. Front Immunol. 2021;12. doi: 10.3389/fimmu.2021.750753. PubMed PMID: WOS:000706221800001.
494. De Rycke L, Kruithof E, Vandooren B, Tak PP, Baeten D. Pathogenesis of spondyloarthritis: insights from synovial membrane studies. Curr Rheumatol Rep. 2006;8(4):275-82. doi: 10.1007/s11926-006-0008-4. PubMed PMID: 16839506.
495. Baeten D, Demetter P, Cuvelier C, Van Den Bosch F, Kruithof E, Van Damme N, et al. Comparative study of the synovial histology in rheumatoid arthritis, spondyloarthropathy, and osteoarthritis: influence of disease duration and activity. Ann Rheum Dis. 2000;59(12):945-53. doi: 10.1136/ard.59.12.945. PubMed PMID: 11087697; PubMed Central PMCID: PMC1753054.
496. Baeten D, Kruithof E, De Rycke L, Vandooren B, Wyns B, Boullart L, et al. Diagnostic classification of spondylarthropathy and rheumatoid arthritis by synovial histopathology: a prospective study in 154 consecutive patients. Arthritis Rheum. 2004;50(9):2931-41. doi: 10.1002/art.20476. PubMed PMID: 15457462.
497. Wang W, Wang L, Gulko P, Zhu J. Computational deconvolution of synovial tissue cellular composition: presence of adipocytes in synovial tissue decreased during arthritis pathogenesis and progression. PHYSIOLOGICAL GENOMICS. 2019;51:241-53. doi: 10.1152/physiolgenomics.00009.2019. PubMed PMID: WOS:000472621800006.

498. Zawieja D. Lymphatic biology and the microcirculation: Past, present, and future. MICROCIRCULATION. 2005;12:141-50. doi: 10.1080/10739680590900003. PubMed PMID: WOS:000227473300013.
499. Kraus S, Lee E. Engineering approaches to investigate the roles of lymphatics vessels in rheumatoid arthritis. MICROCIRCULATION. 2023;30. doi: 10.1111/micc.12769. PubMed PMID: WOS:000806416200001.
500. Gómez D, Diehl M, Crosby E, Weinkopff T, Debes G. Effector T Cell Egress via Afferent Lymph Modulates Local Tissue Inflammation. JOURNAL OF IMMUNOLOGY. 2015;195:3531-6. doi: 10.4049/jimmunol.1500626. PubMed PMID: WOS:000362968100008.
501. Friedlaender MH, Baer H. Immunologic tolerance: role of the regional lymph node. Science. 1972;176(4032):312-4. doi: 10.1126/science.176.4032.312. PubMed PMID: 5019790.
502. Thomas S, Rutkowski J, Pasquier M, Kuan E, Alitalo K, Randolph G, et al. Impaired Humoral Immunity and Tolerance in K14-VEGFR-3-Ig Mice That Lack Dermal Lymphatic Drainage. JOURNAL OF IMMUNOLOGY. 2012;189:2181-90. doi: 10.4049/jimmunol.1103545. PubMed PMID: WOS:000308083600015.
503. Christiansen A, Dieterich L, Ohs I, Bachmann S, Bianchi R, Proulx S, et al. Lymphatic endothelial cells attenuate inflammation via suppression of dendritic cell maturation. ONCOTARGET. 2016;7:39421-35. doi: 10.18632/oncotarget.9820. PubMed PMID: WOS:000378614700036.
504. Schmaler M, Broggi M, Lagarde N, Stöcklin B, King C, Finke D, et al. IL-7R signaling in regulatory T cells maintains peripheral and allograft tolerance in mice. PROCEEDINGS OF THE NATIONAL ACADEMY OF SCIENCES OF THE UNITED STATES OF AMERICA. 2015;112:13330-5. doi: 10.1073/pnas.1510045112. PubMed PMID: WOS:000363458100062.
505. Steinskog E, Sagstad S, Wagner M, Karlsen T, Yang N, Markhus C, et al. Impaired lymphatic function accelerates cancer growth. ONCOTARGET. 2016;7:45789-802. doi: 10.18632/oncotarget.9953. PubMed PMID: WOS:000385402300074.
506. ROBERTSON M, HART F, WHITE W, NUKI G, BOARDMAN P. RHEUMATOID LYMPHADENOPATHY. ANNALS OF THE RHEUMATIC DISEASES. 1968;27:253-+. PubMed PMID: WOS:A1968B190500008.
507. MULHERIN D, FITZGERALD O, BRESNIHAN B. LYMPHEDEMA OF THE UPPER LIMB IN PATIENTS WITH PSORIATIC-ARTHRITIS. SEMINARS IN ARTHRITIS AND RHEUMATISM. 1993;22:350-6. PubMed PMID: WOS:A1993KX66200006.
508. KIELY P, JOSEPH A, MORTIMER P, BOURKE B. UPPER-LIMB LYMPHEDEMA ASSOCIATED WITH POLYARTHRITIS OF RHEUMATOID TYPE. JOURNAL OF RHEUMATOLOGY. 1994;21:1043-5. PubMed PMID: WOS:A1994NQ33400012.
509. JOOS E, BOURGEOIS P, FAMAEY J. LYMPHATIC DISORDERS IN RHEUMATOID-ARTHRITIS. SEMINARS IN ARTHRITIS AND RHEUMATISM. 1993;22:392-8. PubMed PMID: WOS:A1993LH67900004.
510. Bell R, Rahimi H, Kenney H, Lieberman A, Wood R, Schwarz E, et al. Altered Lymphatic Vessel Anatomy and Markedly Diminished Lymph Clearance in Affected Hands of Patients With Active Rheumatoid Arthritis. ARTHRITIS & RHEUMATOLOGY. 2020;72:1447-55. doi: 10.1002/art.41311. PubMed PMID: WOS:000563216800009.

511. Guo R, Zhou Q, Proulx S, Wood R, Ji R, Ritchlin C, et al. Inhibition of Lymphangiogenesis and Lymphatic Drainage via Vascular Endothelial Growth Factor Receptor 3 Blockade Increases the Severity of Inflammation in a Mouse Model of Chronic Inflammatory Arthritis. ARTHRITIS AND RHEUMATISM. 2009;60:2666-76. doi: 10.1002/art.24764. PubMed PMID: WOS:000270054900016.
512. Zhou Q, Guo R, Wood R, Boyce B, Liang Q, Wang Y, et al. Vascular Endothelial Growth Factor C Attenuates Joint Damage in Chronic Inflammatory Arthritis by Accelerating Local Lymphatic Drainage in Mice. ARTHRITIS AND RHEUMATISM. 2011;63:2318-28. doi: 10.1002/art.30421. PubMed PMID: WOS:000293840200022.
513. Bouta E, Bell R, Rahimi H, Xing L, Wood R, Bingham C, et al. Targeting lymphatic function as a novel therapeutic intervention for rheumatoid arthritis. NATURE REVIEWS RHEUMATOLOGY. 2018;14:94-106. doi: 10.1038/nrrheum.2017.205. PubMed PMID: WOS:000423207700013.
514. Fusaro M, Cianciolo G, Brandi M, Ferrari S, Nickolas T, Tripepi G, et al. Vitamin K and Osteoporosis. NUTRIENTS. 2020;12. doi: 10.3390/nu12123625. PubMed PMID: WOS:000602484700001.
515. Zhang J, Ma Z, Yan K, Wang Y, Yang Y, Wu X. Matrix Gla Protein Promotes the Bone Formation by Up-Regulating Wnt/β-Catenin Signaling Pathway. FRONTIERS IN ENDOCRINOLOGY. 2019;10. doi: 10.3389/fendo.2019.00891. PubMed PMID: WOS:000505481200001.
516. Newman B, Gigout L, Sudre L, Grant M, Wallis G. Coordinated expression of matrix Gla protein is required during endochondral ossification for chondrocyte survival. JOURNAL OF CELL BIOLOGY. 2001;154:659-66. PubMed PMID: WOS:000170377200015.
517. Julien M, Khoshniat S, Lacreusette A, Gatius M, Bozec A, Wagner E, et al. Phosphate-Dependent Regulation of MGP in Osteoblasts: Role of ERK1/2 and Fra-1. JOURNAL OF BONE AND MINERAL RESEARCH. 2009;24:1856-68. doi: 10.1359/JBMR.090508. PubMed PMID: WOS:000271730200011.
518. Tieliwaerdi X, Aripova N, Duryee M, Jiang X, Klassen L, O'Dell J, et al. Matrix Gla Protein (MGP) Modified with Malondialdehyde/Acetaldehyde Is Increased in Rheumatoid Arthritis and Cardiovascular Patients. ARTHRITIS & RHEUMATOLOGY. 2020;72. PubMed PMID: WOS:000587568502027.
519. Schoellnast H, Deutschmann HA, Hermann J, Schaffler GJ, Reittner P, Kammerhuber F, et al. Psoriatic arthritis and rheumatoid arthritis: findings in contrast-enhanced MRI. AJR Am J Roentgenol. 2006;187(2):351-7. doi: 10.2214/AJR.04.1798. PubMed PMID: 16861537.
520. FitzGerald O, Winchester R. Psoriatic arthritis: from pathogenesis to therapy. ARTHRITIS RESEARCH & THERAPY. 2009;11. doi: 10.1186/ar2580. PubMed PMID: WOS:000264563000019.
521. Shiraishi M, Fukuda T, Igarashi T, Tokashiki T, Kayama R, Ojiri H. Differentiating Rheumatoid and Psoriatic Arthritis of the Hand: Multimodality Imaging Characteristics. RADIOGRAPHICS. 2020;40:1339-54. doi: 10.1148/rg.2020200029. PubMed PMID: WOS:000564929900012.
522. Narváez J, Narváez J, de Albert M, Gómez-Vaquero C, Nolla J. Can Magnetic Resonance Imaging of the Hand and Wrist Differentiate Between Rheumatoid Arthritis and Psoriatic Arthritis in the Early Stages of the Disease? SEMINARS IN ARTHRITIS AND RHEUMATISM. 2012;42:234-45. doi: 10.1016/j.semarthrit.2012.03.016. PubMed PMID: WOS:000311664800002.
523. Marzo-Ortega H, Tanner S, Rhodes L, Tan A, Conaghan P, Hensor E, et al. Magnetic resonance imaging in the assessment of metacarpophalangeal joint disease in

early psoriatic and rheumatoid arthritis. SCANDINAVIAN JOURNAL OF RHEUMATOLOGY. 2009;38:79-83. doi: 10.1080/03009740802448833. PubMed PMID: WOS:000263992100001.
524. Tsukamoto K, Orimo H, Hosoi T, Miyao M, Yoshida H, Watanabe S, et al. Association of bone mineral density with polymorphism of the human matrix Gla protein locus in elderly women. JOURNAL OF BONE AND MINERAL METABOLISM. 2000;18:27-30. PubMed PMID: WOS:000084319200006.
525. Hu Q, Zhong X, Tian H, Liao P. The Efficacy of Denosumab in Patients With Rheumatoid Arthritis: A Systematic Review and Pooled Analysis of Randomized or Matched Data. Front Immunol. 2021;12:799575. Epub 20220105. doi: 10.3389/fimmu.2021.799575. PubMed PMID: 35069583; PubMed Central PMCID: PMC8766643.
526. Helbing T, Rothweiler R, Heinke J, Goetz L, Diehl P, Zirlik A, et al. BMPER Is Upregulated by Statins and Modulates Endothelial Inflammation by Intercellular Adhesion Molecule-1. Arteriosclerosis Thrombosis and Vascular Biology. 2010;30(3):554-U405. doi: 10.1161/atvbaha.109.201087. PubMed PMID: WOS:000274658700030.
527. Fromm S, Cunningham CC, Dunne MR, Veale DJ, Fearon U, Wade SM. Enhanced angiogenic function in response to fibroblasts from psoriatic arthritis synovium compared to rheumatoid arthritis. Arthritis Research & Therapy. 2019;21(1):11. doi: 10.1186/s13075-019-2088-3. PubMed PMID: WOS:000503830000001.
528. Garritson J, Zhang J, Achenbach A, Ferhat M, Eich E, Stubben C, et al. BMPER is a marker of adipose progenitors and adipocytes and a positive modulator of adipogenesis. COMMUNICATIONS BIOLOGY. 2023;6. doi: 10.1038/s42003-023-05011-w. PubMed PMID: WOS:001009548800004.
529. Conley C, Silburn R, Singer M, Ralston A, Rohwer-Nutter D, Olson D, et al. Crossveinless 2 contains cysteine-rich domains and is required for high levels of BMP-like activity during the formation of the cross veins in Drosophila. DEVELOPMENT. 2000;127:3947-59. PubMed PMID: WOS:000089846200008.
530. Moser M, Binder O, Wu Y, Aitsebaomo J, Ren R, Bode C, et al. BMPER, a novel endothelial cell precursor-derived protein, antagonizes bone morphogenetic protein signaling and endothelial cell differentiation. MOLECULAR AND CELLULAR BIOLOGY. 2003;23:5664-79. doi: 10.1128/MCB.23.16.5664-5679.2003. PubMed PMID: WOS:000184527100016.
531. Moser M, Yu Q, Bode C, Xiong J, Patterson C. BMPER is a conserved regulator of hematopoietic and vascular development in zebrafish. JOURNAL OF MOLECULAR AND CELLULAR CARDIOLOGY. 2007;43(3):243-53. doi: 10.1016/j.yjmcc.2007.05.008. PubMed PMID: WOS:000249611300002.
532. Moreno-Miralles I, Ren RQ, Moser M, Hartnett ME, Patterson C. Bone Morphogenetic Protein Endothelial Cell Precursor-Derived Regulator Regulates Retinal Angiogenesis In Vivo in a Mouse Model of Oxygen-Induced Retinopathy. Arteriosclerosis Thrombosis and Vascular Biology. 2011;31(10):2216-U166. doi: 10.1161/atvbaha.111.230235. PubMed PMID: WOS:000294843700009.
533. Dyer L, Lockyer P, Wu Y, Saha A, Cyr C, Moser M, et al. BMPER Promotes Epithelial-Mesenchymal Transition in the Developing Cardiac Cushions. PLOS ONE. 2015;10(9). doi: 10.1371/journal.pone.0139209. PubMed PMID: WOS:000362171400064.
534. ten Dijke P, Arthur H. Extracellular control of TGFβ signalling in vascular development and disease. NATURE REVIEWS MOLECULAR CELL BIOLOGY. 2007;8(11):857-69. doi: 10.1038/nrm2262. PubMed PMID: WOS:000250338800011.
535. Heinke J, Wehofsits L, Zhou Q, Zoeller C, Baar KM, Helbing T, et al. BMPER is an endothelial cell regulator and controls bone morphogenetic protein-4-dependent

angiogenesis. Circulation Research. 2008;103(8):804-U65. doi: 10.1161/circresaha.108.178434. PubMed PMID: WOS:000259925900008.
536. Lockyer P, Mao H, Fan Q, Li L, Yu-Lee L, Eissa N, et al. LRP1-Dependent BMPER Signaling Regulates Lipopolysaccharide-Induced Vascular Inflammation. ARTERIOSCLEROSIS THROMBOSIS AND VASCULAR BIOLOGY. 2017;37(8):1524-+. doi: 10.1161/ATVBAHA.117.309521. PubMed PMID: WOS:000406304500015.
537. Kelley R, Ren R, Pi X, Wu Y, Moreno I, Willis M, et al. A concentration-dependent endocytic trap and sink mechanism converts Bmper from an activator to an inhibitor of Bmp signaling. JOURNAL OF CELL BIOLOGY. 2009;184(4):597-609. doi: 10.1083/jcb.200808064. PubMed PMID: WOS:000264016600013.
538. Helbing T, Rothweiler R, Ketterer E, Goetz L, Heinke J, Grundmann S, et al. BMP activity controlled by BMPER regulates the proinflammatory phenotype of endothelium. Blood. 2011;118(18):5040-9. doi: 10.1182/blood-2011-03-339762. PubMed PMID: WOS:000296714500035.
539. Pi X, Lockyer P, Dyer L, Schisler J, Russell B, Carey S, et al. Bmper Inhibits Endothelial Expression of Inflammatory Adhesion Molecules and Protects Against Atherosclerosis. ARTERIOSCLEROSIS THROMBOSIS AND VASCULAR BIOLOGY. 2012;32(9):2214-+. doi: 10.1161/ATVBAHA.112.252015. PubMed PMID: WOS:000307773100024.
540. Yao Y, Bennett B, Wang X, Rosenfeld M, Giachelli C, Lusis A, et al. Inhibition of Bone Morphogenetic Proteins Protects Against Atherosclerosis and Vascular Calcification. CIRCULATION RESEARCH. 2010;107(4):485-U102. doi: 10.1161/CIRCRESAHA.110.219071. PubMed PMID: WOS:000281157800008.
541. Yao Y, Nowak S, Yochelis A, Garfinkel A, Bostroem K. Matrix GLA protein, an inhibitory morphogen in pulmonary vascular development. J Biol Chem. 2007;282(41):30131-42. doi: 10.1074/jbc.M704297200. PubMed PMID: WOS:000249981200043.
542. Thrupp N, Frigerio CS, Wolfs L, Skene NG, Fattorelli N, Poovathingal S, et al. Single-Nucleus RNA-Seq Is Not Suitable for Detection of Microglial Activation Genes in Humans. Cell Reports. 2020;32(13). doi: 10.1016/j.celrep.2020.108189. PubMed PMID: WOS:000573722100004.
543. Liu F, Lu Y, Wang X, Sun S, Pan H, Wang M, et al. Identification of FOXO1 as a geroprotector in human synovium through single-nucleus transcriptomic profiling. PROTEIN & CELL. 2024;15(6):441-59. doi: 10.1093/procel/pwad060. PubMed PMID: WOS:001193099500001.
544. Janssen P, Kliesmete Z, Vieth B, Adiconis X, Simmons S, Marshall J, et al. The effect of background noise and its removal on the analysis of single-cell expression data. Genome Biology. 2023;24(1). doi: 10.1186/s13059-023-02978-x. PubMed PMID: WOS:001015106300003.
545. Zhang YR, Ma YL, Huang YK, Zhang Y, Jiang Q, Zhou M, et al. Benchmarking algorithms for pathway activity transformation of single-cell RNA-seq data. Computational and Structural Biotechnology Journal. 2020;18:2953-61. doi: 10.1016/j.csbj.2020.10.007. PubMed PMID: WOS:000607299700009.
546. Finak G, McDavid A, Yajima M, Deng J, Gersuk V, Shalek A, et al. MAST: a flexible statistical framework for assessing transcriptional changes and characterizing heterogeneity in single-cell RNA sequencing data. GENOME BIOLOGY. 2015;16. doi: 10.1186/s13059-015-0844-5. PubMed PMID: WOS:000366105700002.
547. Thomas T, Friedrich M, Rich-Griffin C, Pohin M, Agarwal D, Pakpoor J, et al. A longitudinal single-cell atlas of anti-tumour necrosis factor treatment in inflammatory

bowel disease. NATURE IMMUNOLOGY. 2024;25(11). doi: 10.1038/s41590-024-01994-8. PubMed PMID: WOS:001338098700001.
548. Luo G, Ducy P, McKee M, Pinero G, Loyer E, Behringer R, et al. Spontaneous calcification of arteries and cartilage in mice lacking matrix GLA protein. NATURE. 1997;386:78-81. PubMed PMID: WOS:A1997WL74600054.
549. Alvarez P, Augustín J, Tamayo E, Iglesias M, Acinas O, Mendiguren M, et al. Therapeutic Effects of Anti-Bone Morphogenetic Protein and Activin Membrane-Bound Inhibitor Treatment in Psoriasis and Arthritis. ARTHRITIS & RHEUMATOLOGY. 2020;72(9):1547-58. doi: 10.1002/art.41272. PubMed PMID: WOS:000553484000001.

7. List of Supplementary Tables

8. List of Supplementary Figures

9. Supplementary Tables

Supplementary Table 1 Cell cluster annotation markers

	Positive cell cluster annotation markers	Negative cell cluster annotation markers
Adipocytes	Perilipin 1 (*PLIN1*), lipoprotein lipase (*LPL*)	
B cells	B lymphocyte kinase proto-oncogene, Src family tyrosine kinase (*BLK*), B cell scaffold protein with ankyrin repeats 1 (*BANK1*), paired box 5 (*PAX5*)	
Dendritic cells	Cell adhesion molecule 1 (*CADM1*), Fms related receptor tyrosine kinase 3 (*FLT3*), WDFY family member 4 (*WDFY4*), interferon regulatory factor 8 (*IRF8*)	
Fast twitch skeletal myocytes	Myosin heavy chain 1 (*MYH1*), nebulin (*NEB*)	Troponin T1, slow skeletal type (*TNNT1*), troponin I1, slow skeletal type (*TNNI1*)
Granulocytes	KIT proto-oncogene, receptor tyrosine kinase (*KIT*), interleukin 18 receptor 1 (*IL18R1*)	
Lining fibroblasts	Fibroblast activation protein alpha (*FAP*), chloride intracellular channel 5 (*CLIC5*), proteoglycan 4 (*PRG4*)	Decorin (*DCN*), Thy-1 cell surface antigen (*THY1*), fibrillin 1 (*FBN1*)
Lymphatic endothelial cells	Prospero Homeobox 1 (*PROX1*), C-C motif chemokine ligand 21 (*CCL21*), lymphatic vessel endothelial hyaluronan receptor 1 (*LYVE1*)	
MERTKhi macrophages	*CD163* , MER proto-oncogene, tyrosine kinase (*MERTK*)	Lysozyme (*LYZ*), cathepsin S (*CTSS*), ficolin 1 (*FCN1*)
MERTKlo macrophages	Lysozyme (*LYZ*), cathepsin S (*CTSS*), ficolin 1 (*FCN1*)	*CD163* , MER proto-oncogene, tyrosine kinase (*MERTK*)
Mural cells	Notch receptor 3 (*NOTCH3*), platelet derived growth factor receptor beta (*PDGFRB*), myosin IB (*MYO1B*)	
NK cells/NKT cells	Granulysin (*GNLY*), *CD247* , killer cell lectin like receptor D1 (*KLRD1*)	
Plasma cells	Interferon regulatory factor 4 (*IRF4*), immunoglobulin lambda constant 2 (*IGLC2*), immunoglobulin heavy constant gamma 1 (*IGHG1*)	
Plasmacytoid dendritic cells	Placenta associated 8 (*PLAC8*), interferon regulatory factor 8 (*IRF8*)	
Proliferating cells	Centromere protein F (*CENPF*), DNA polymerase theta (*POLQ*)	
Ribosomal RNA hi T cells	Interleukin 7 receptor (*IL7R*), lymphoid enhancer binding factor 1 (*LEF1*), ribosomal protein S27 (*RPS27*), ribosomal protein L10 (*RPL10*)	
Ribosomal RNA lo T cells	Interleukin 7 receptor (*IL7R*), lymphoid enhancer binding factor 1 (*LEF1*)	Ribosomal protein S27 (*RPS27*), ribosomal protein L10 (*RPL10*)
Slow twitch skeletal myocytes	Nebulin (*NEB*), troponin T1 slow skeletal type (*TNNT1*), troponin I1, slow skeletal type (*TNNI1*)	Myosin heavy chain 1 (*MYH1*)
Sublining fibroblasts	Fibroblast activation protein alpha (*FAP*), decorin (*DCN*), Thy-1 cell surface antigen (*THY1*), fibrillin 1 (*FBN1*)	Chloride intracellular channel 5 (*CLIC5*), proteoglycan 4 (*PRG4*)
Vascular endothelial cells	Protein tyrosine phosphatase receptor type B (*PTPRB*), Von Willebrand Factor (*VWF*)	

Supplementary Table 2 Number of differentially expressed genes with intra-articular methylprednisolone injection by disease subgroups (NA denotes analysis was not possible as there were not at least 10 cells of that cell type from at least 3 participants)

P values were corrected for multiple testing using the Benjamini and Hochberg method in DESeq2 by default (270, 272).

	RA		PsA	
	Log2FoldChange < -1 and adjusted p value < 0.05 (Downregulated in RA)	Log2FoldChange > 1 and adjusted p value < 0.05 (Upregulated in RA)	Log2FoldChange < -1 and adjusted p value < 0.05 (Downregulated in PsA)	Log2FoldChange > 1 and adjusted p value < 0.05 (Upregulated in PsA)
Adipocytes	0	0	0	2
B cells	0	0	0	0
Dendritic cells	0	0	0	0
Fast twitch skeletal myocytes	0	0	Not applicable	Not applicable
Granulocytes	0	0	0	0
Lining fibroblasts	0	0	14	4
Lymphatic endothelial cells	Not applicable	Not applicable	0	0
MERTKhi macrophages	0	0	0	0
MERTKlo macrophages	0	0	0	0
Mural cells	0	0	0	0
NK cells/NKT cells	0	0	0	0
Plasma cells	0	0	0	1
Plasmacytoid dendritic cells	Not applicable	Not applicable	0	0
Proliferating cells	0	0	0	0
Ribosomal RNA hi T cells	0	0	0	0
Ribosomal RNA lo T cells	1	0	0	0
Slow twitch skeletal myocytes	Not applicable	Not applicable	Not applicable	Not applicable
Sublining fibroblasts	1	0	0	0
Vascular endothelial cells	0	0	0	1

Supplementary Table 3 Differentially expressed genes in PsA compared to RA in pre- and post-treatment synovium (NA denotes analysis was not possible as there were not at least 10 cells of that cell type from at least 3 participants)

P values were corrected for multiple testing using the Benjamini and Hochberg method in DESeq2 by default (270, 272).

	PsA vs RA (pre-treatment)		PsA vs RA (post-treatment)	
	Log2FoldChange < -1 and adjusted p value < 0.05 (Upregulated in RA)	Log2FoldChange > 1 and adjusted p value < 0.05 (Upregulated in PsA)	Log2FoldChange < -1 and adjusted p value < 0.05 (Upregulated in RA)	Log2FoldChange > 1 and adjusted p value < 0.05 (Upregulated in PsA)
Adipocytes	0	0	0	0
B cells	0	0	0	0
Dendritic cells	0	0	0	0
Fast twitch skeletal myocytes	0	0	NA	NA
Granulocytes	0	0	0	0
Lining fibroblasts	26	55	0	1
Lymphatic endothelial cells	NA	NA	NA	NA
MERTKhi macrophages	0	1	1	0
MERTKlo macrophages	0	0	0	0
Mural cells	0	0	0	0
NK cells/NKT cells	0	0	0	0
Plasma cells	0	0	NA	NA
Plasmacytoid dendritic cells	0	0	NA	NA
Proliferating cells	0	0	0	0
Ribosomal RNA hi T cells	0	0	0	0
Ribosomal RNA lo T cells	0	0	0	2
Slow twitch skeletal myocytes	NA	NA	NA	NA
Sublining fibroblasts	0	0	0	1
Vascular endothelial cells	0	0	0	0

10. Supplementary Figures

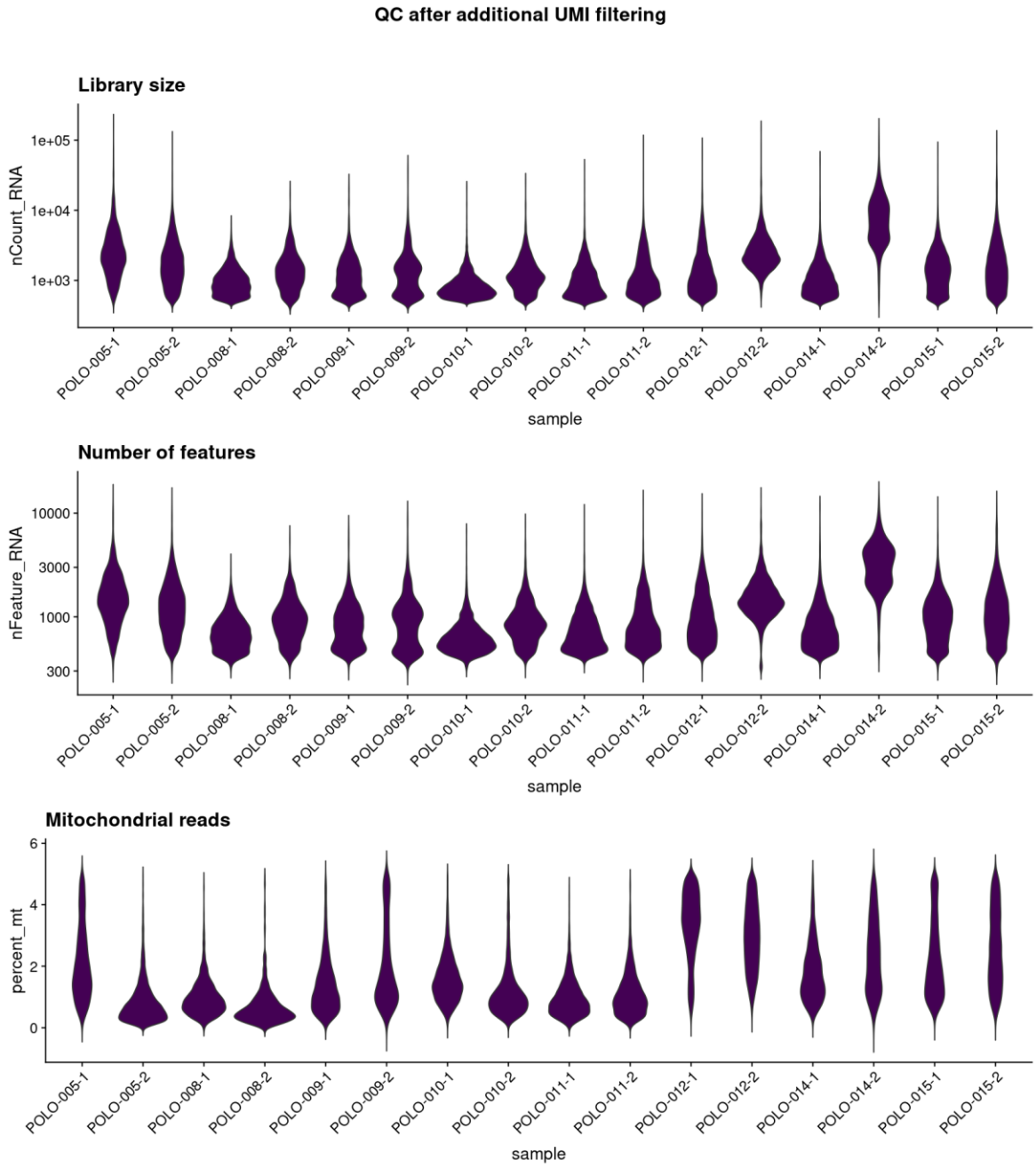

Supplementary Figure 1 *Violin plot of library size, number of features and percentage of mitochondrial reads of each sample after filtering out droplets 3 median absolute deviations from the median, droplets with fewer than 300 unique genes expressed, fewer than 500 UMIs, where more than 5% of reads are mitochondrial genes*

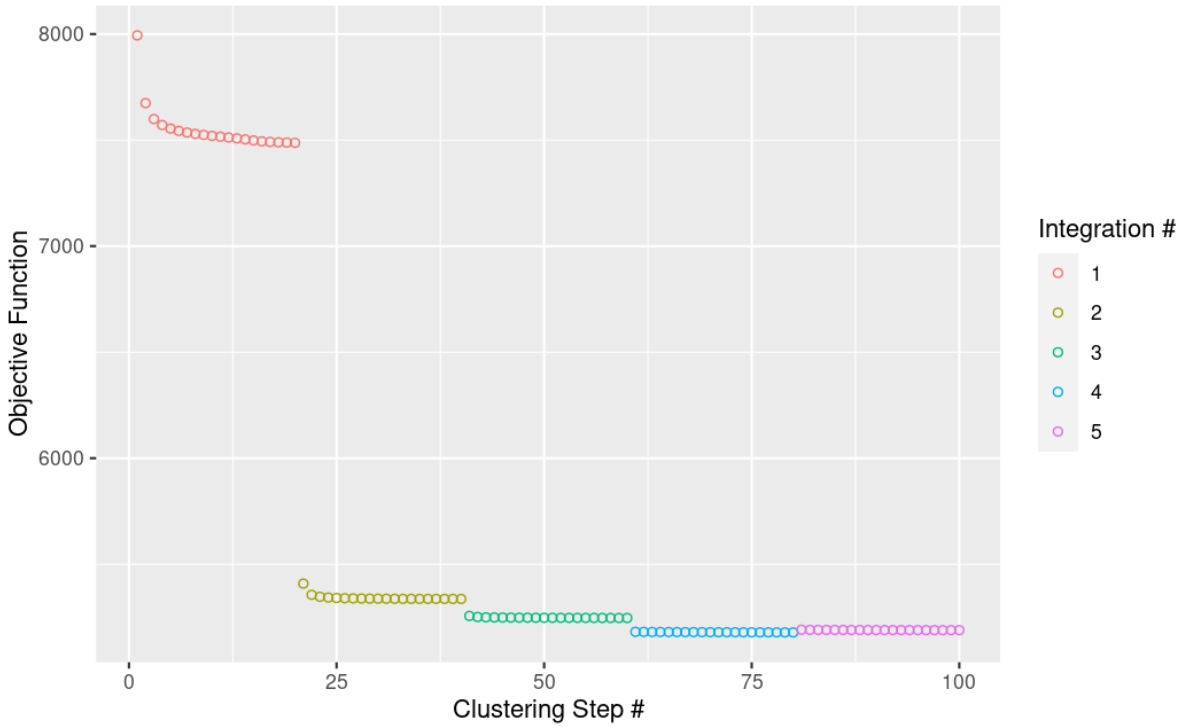

Supplementary Figure 2 Integration of merged object with Harmony (reduction.use = pca_name, group.by.vars = "orig.ident", dims.use = 1:40, kmeans_init_nstart = 20, kmeans_init_inter_max = 100)

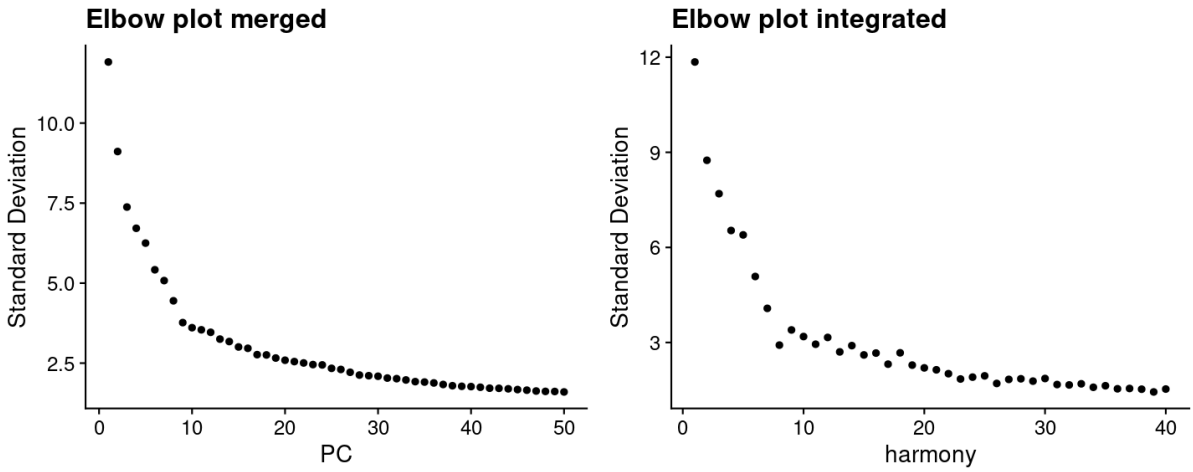

Supplementary Figure 3 Elbow plots to compare merged and integrated object as quality control to assess integration

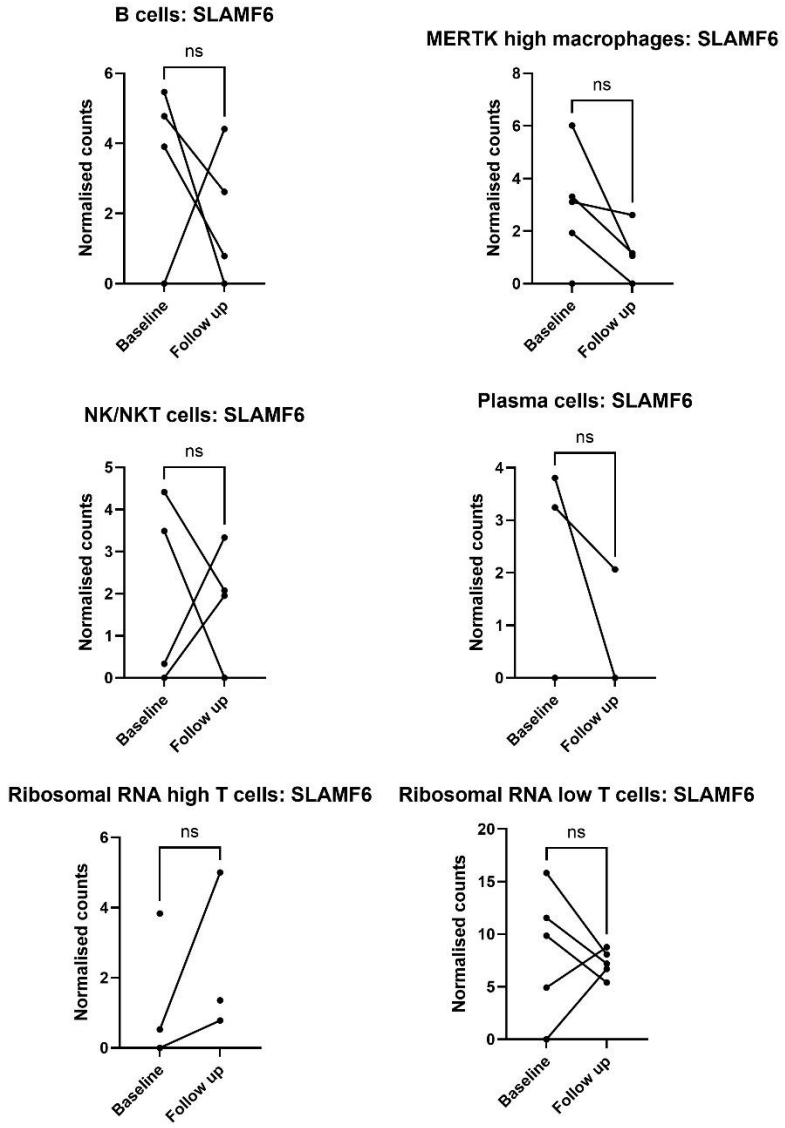

Supplementary Figure 4 SLAMF6 expression in B cells, MERTK high macrophages, NK/NKT cells, plasma cells, ribosomal RNA high T cells and ribosomal RNA low T cells at baseline and follow-up after intra-articular methylprednisolone injection, excluding samples from patients containing skeletal myocytes (N = 5; 2 RA and 3 PsA). Analysis of SLAMF6 expression in other cell types was not possible as there were not at least 10 cells of that cell type from at least 3 participants.

ns denotes padj > 0.05 by DESeq2 analysis of pseudobulked data. P values were corrected for multiple testing using the Benjamini and Hochberg method in DESeq2 by default (270, 272)

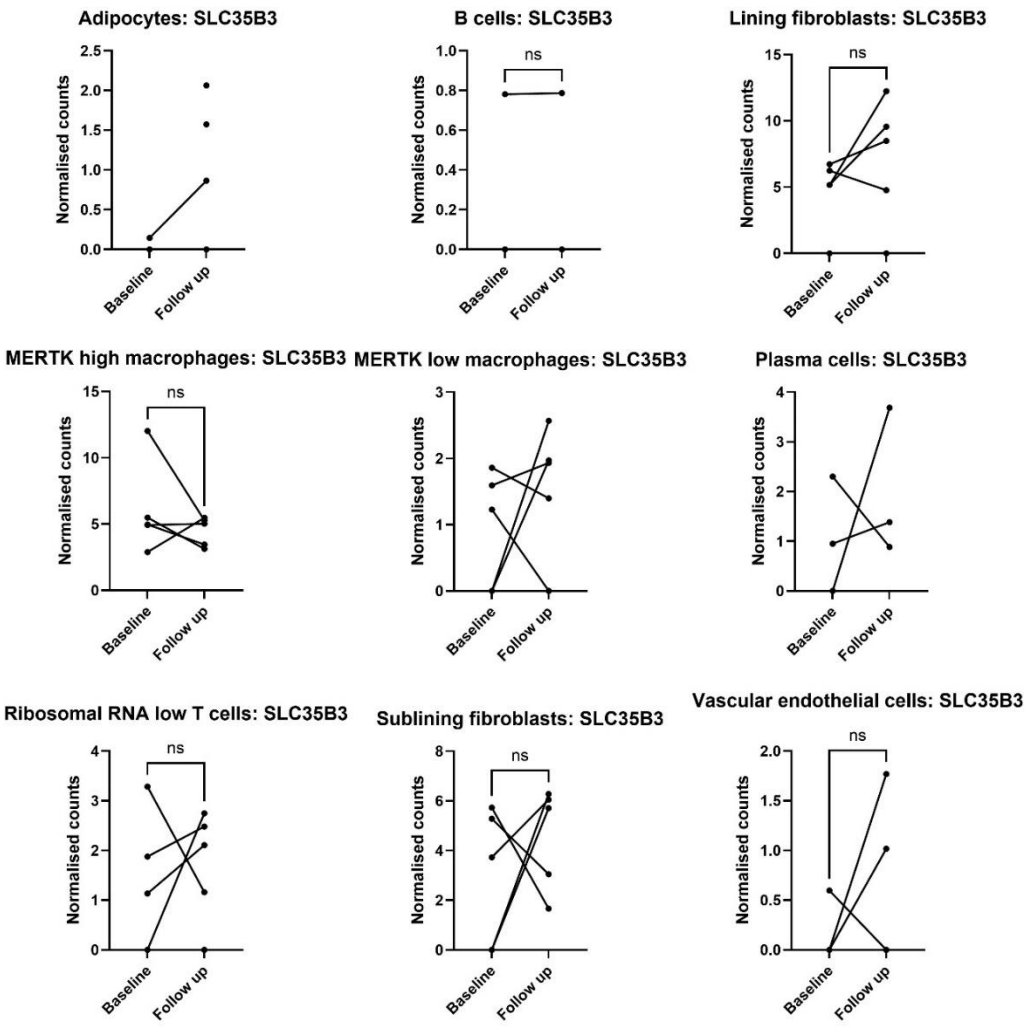

Supplementary Figure 5 SLC35B3 expression in adipocytes, B cells, lining fibroblasts, MERTK high macrophages, MERTK low macrophages, plasma cells, ribosomal RNA low T cells, sublining fibroblasts and vascular endothelial cells at baseline and follow-up after intra-articular methylprednisolone injection, excluding samples from patients containing skeletal myocytes (N = 5; 2 RA and 3 PsA). Analysis of SLC35B3 expression in other cell types was not possible as there were not at least 10 cells of that cell type from at least 3 participants.

ns denotes padj > 0.05 by DESeq2 analysis of pseudobulked data. P values were corrected for multiple testing using the Benjamini and Hochberg method in DESeq2 by default (270, 272)

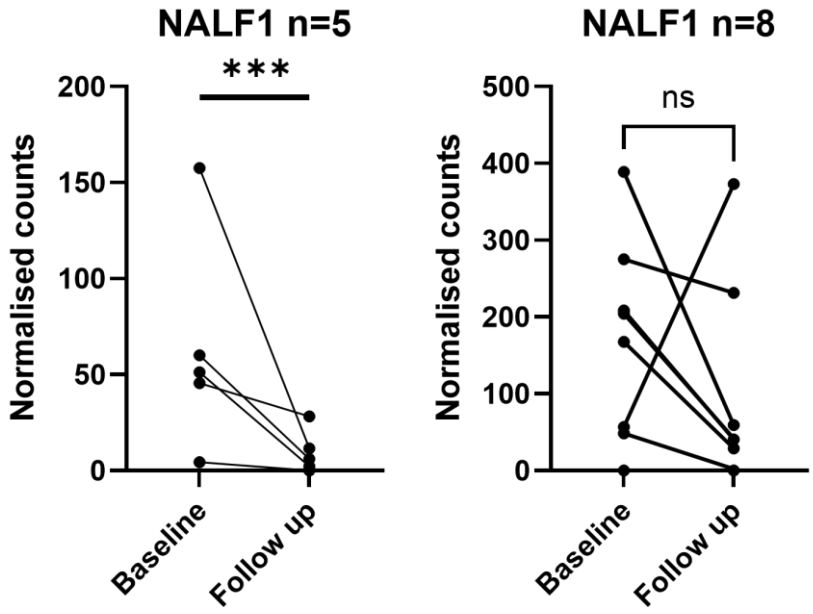

Supplementary Figure 6 NALF1 expression in sublining fibroblasts at baseline and follow-up after intra-articular methylprednisolone injection when (left) excluding samples from patients containing skeletal myocytes (n = 5; 2 RA and 3 PsA), and (right) including samples from patients containing skeletal myocytes (n = 8; 4 RA and 4 PsA)

**** denotes padj < 0.001 and ns denotes padj > 0.05 by DESeq2 analysis of pseudobulked data. P values were corrected for multiple testing using the Benjamini and Hochberg method in DESeq2 by default (270, 272)*

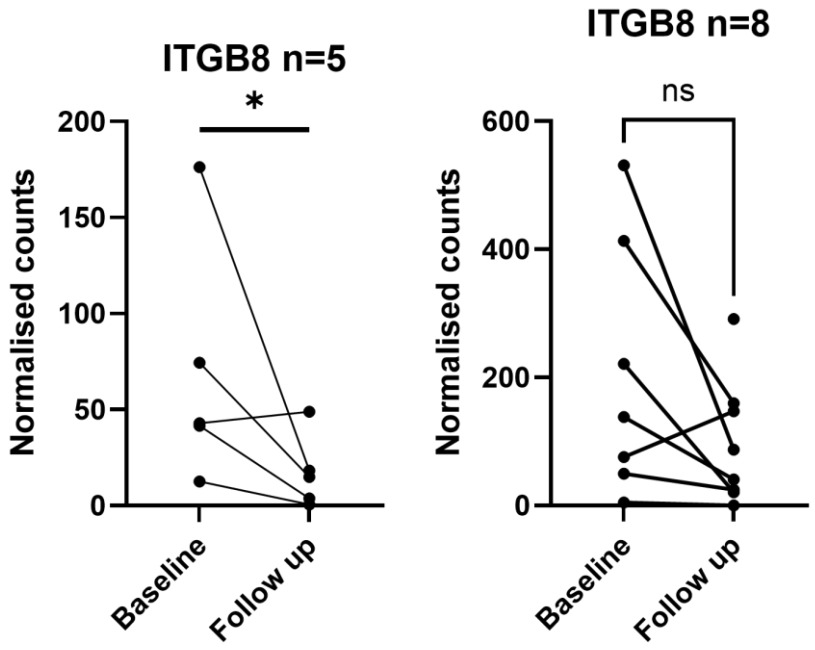

Supplementary Figure 7 ITGB8 expression in sublining fibroblasts at baseline and follow-up after intra-articular methylprednisolone injection when (left) excluding samples from patients containing skeletal myocytes (n = 5; 2 RA and 3 PsA), and (right) including samples from patients containing skeletal myocytes (n = 8; 4 RA and 4 PsA)

** denotes padj < 0.05 and ns denotes padj > 0.05 by DESeq2 analysis of pseudobulked data. P values were corrected for multiple testing using the Benjamini and Hochberg method in DESeq2 by default (270, 272)*

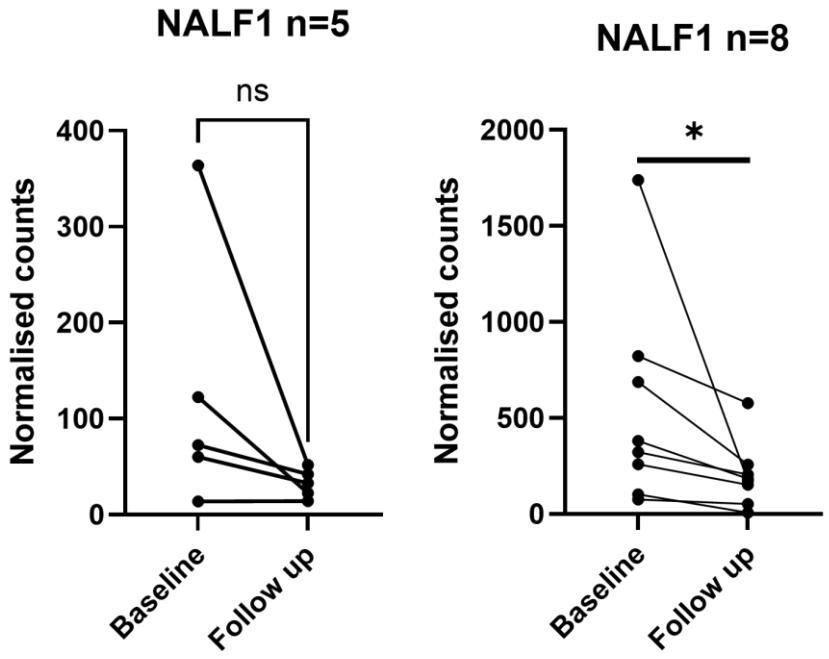

Supplementary Figure 8 NALF1 expression in lining fibroblasts at baseline and follow-up after intra-articular methylprednisolone injection when (left) excluding samples from patients containing skeletal myocytes (n = 5; 2 RA and 3 PsA), and (right) including samples from patients containing skeletal myocytes (n = 8; 4 RA and 4 PsA)

** denotes padj < 0.05 and ns denotes padj > 0.05 by DESeq2 analysis of pseudobulked data. P values were corrected for multiple testing using the Benjamini and Hochberg method in DESeq2 by default (270, 272)*

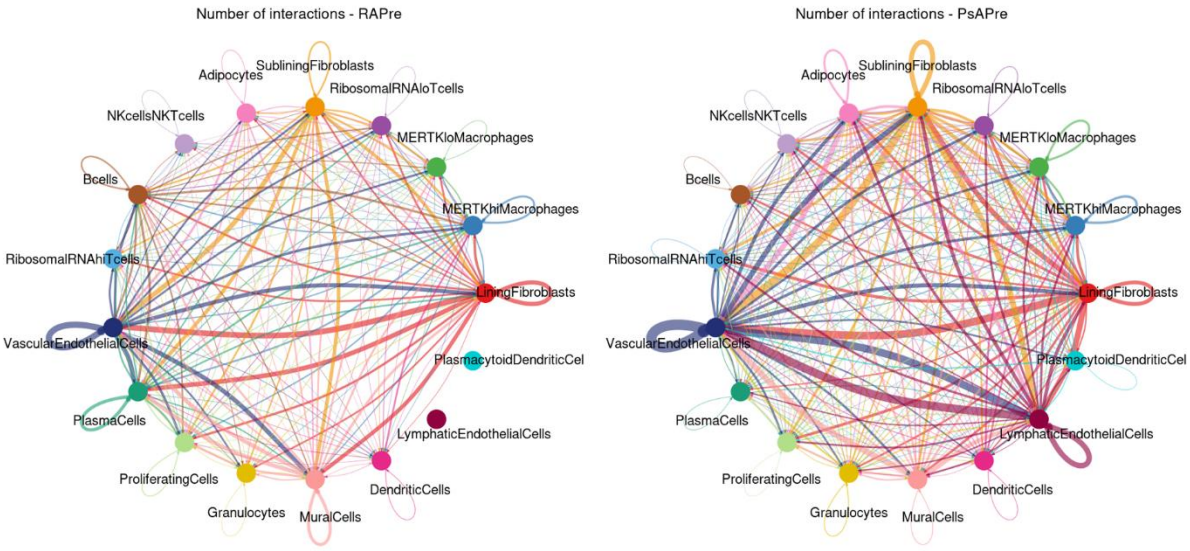

Supplementary Figure 9 Circle plots of interaction numbers in pre-treatment samples in RA and PsA

```
weight.max <- getMaxWeight(object.list, attribute = c("idents","count"))
par(mfrow = c(1,2), xpd=TRUE)
for (i in 1:length(object.list)) {netVisual_circle(object.list[[i]]@net$count, weight.scale = T, label.edge= F, edge.weight.max = weight.max[2], edge.width.max = 12, title.name = paste0("Number of interactions - ", names(object.list)[i]))
```

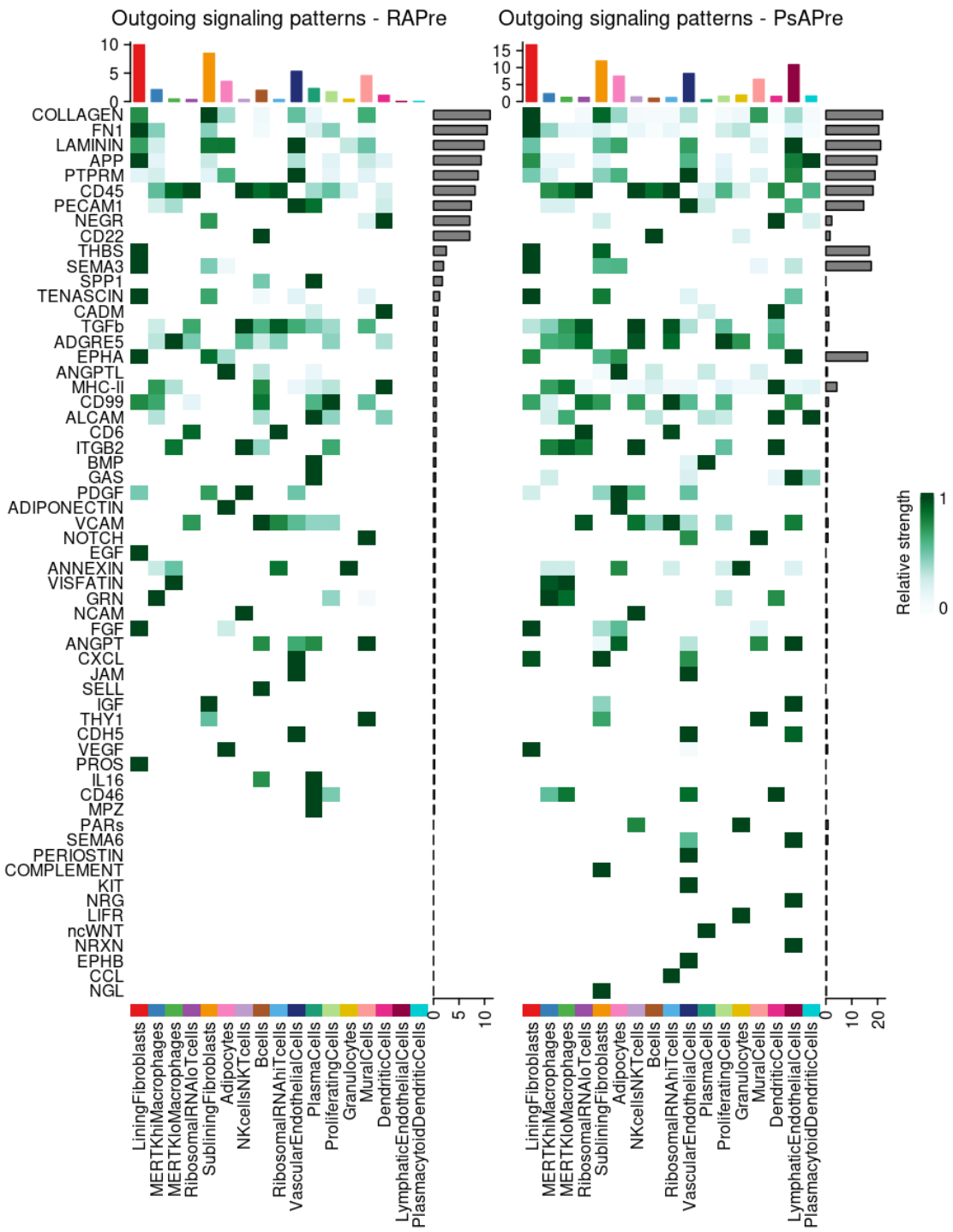

Supplementary Figure 10 Heatmap showing the outgoing signalling patterns in each cell cluster split by disease (pre-treatment)

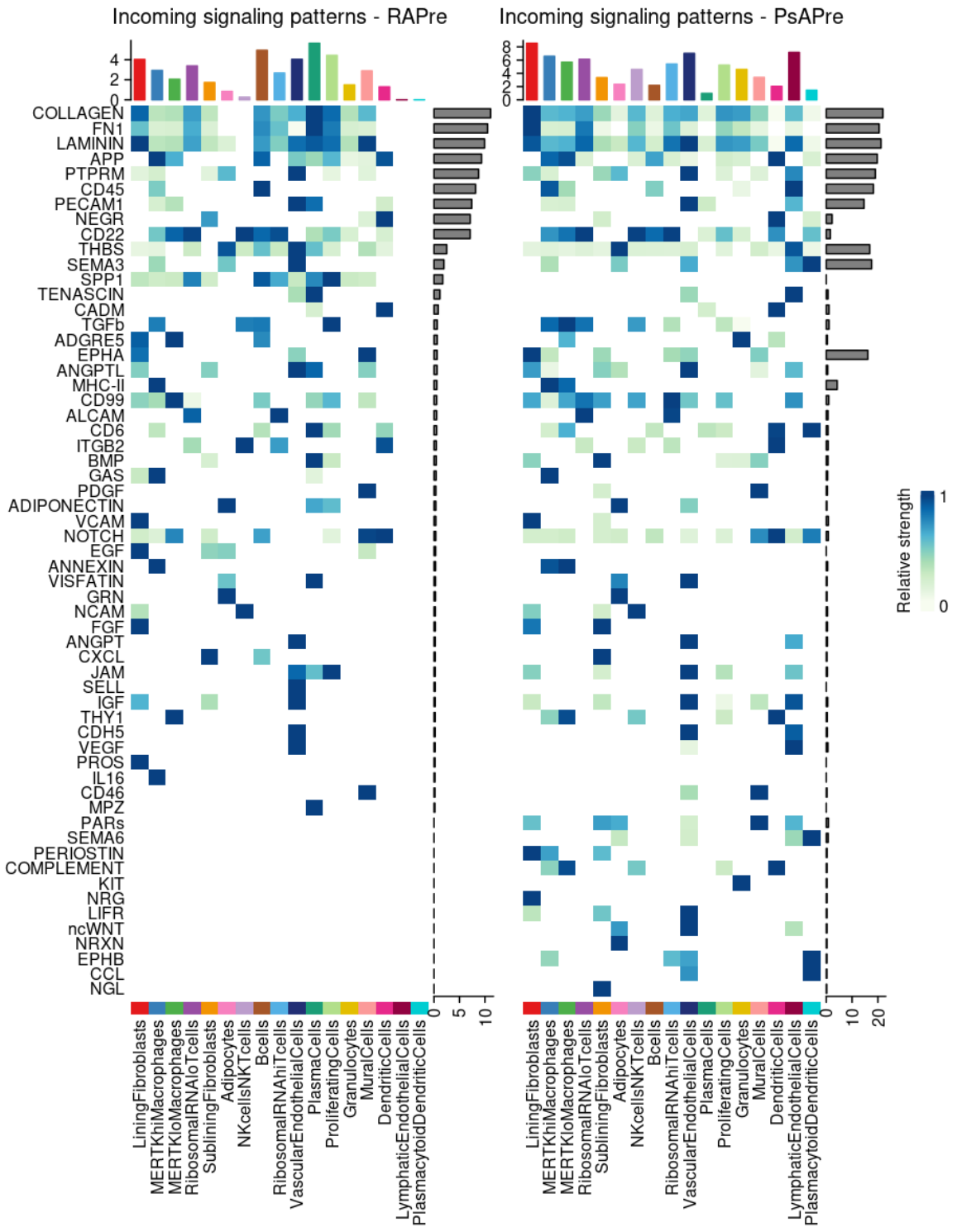

Supplementary Figure 11 Heatmap showing the incoming signalling patterns in each cell cluster split by disease (pre-treatment)

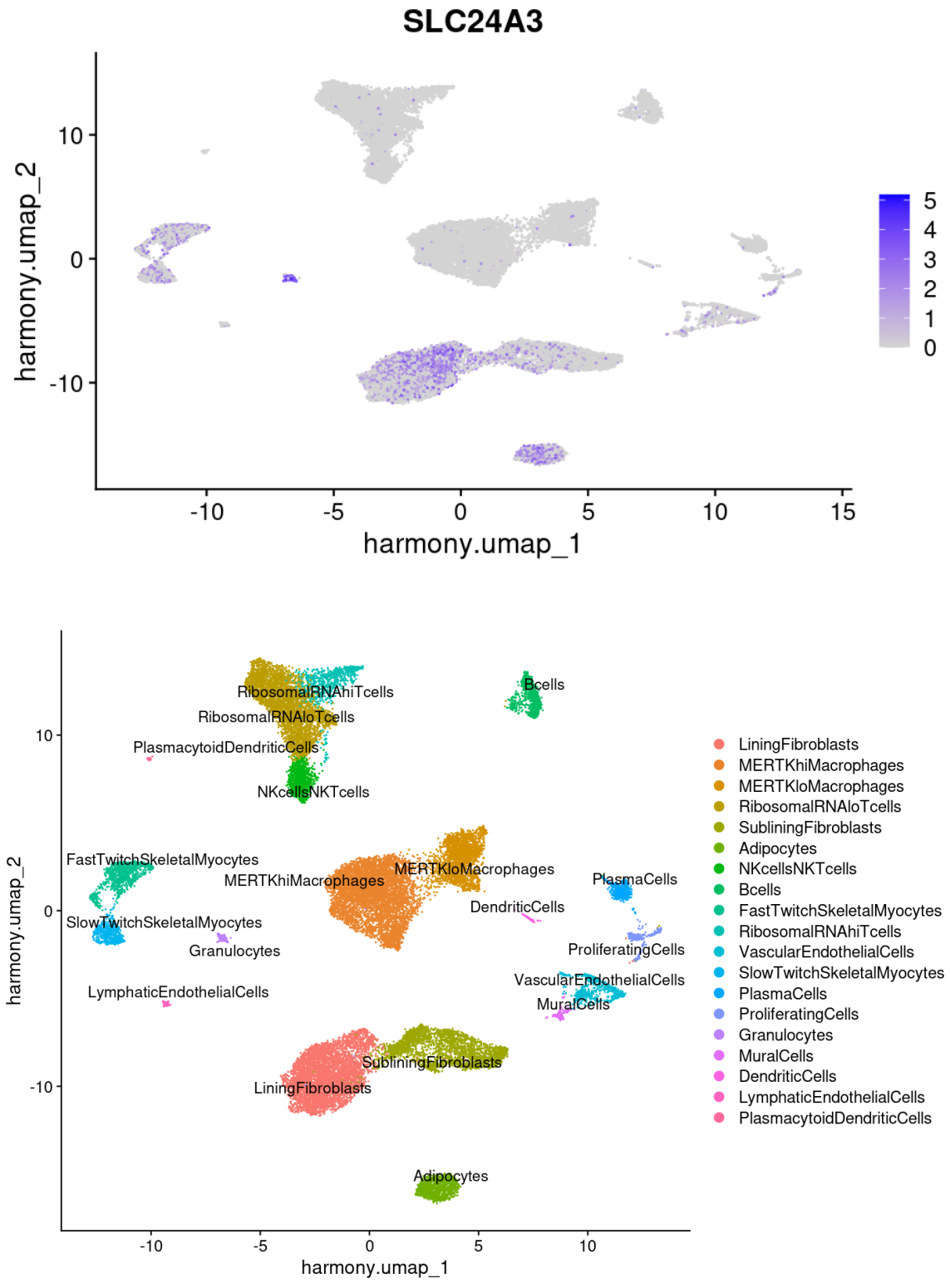

Supplementary Figure 12 UMAP of SLC24A3 expression (top) and cell cluster annotations (bottom) of synovial tissue snRNA-seq

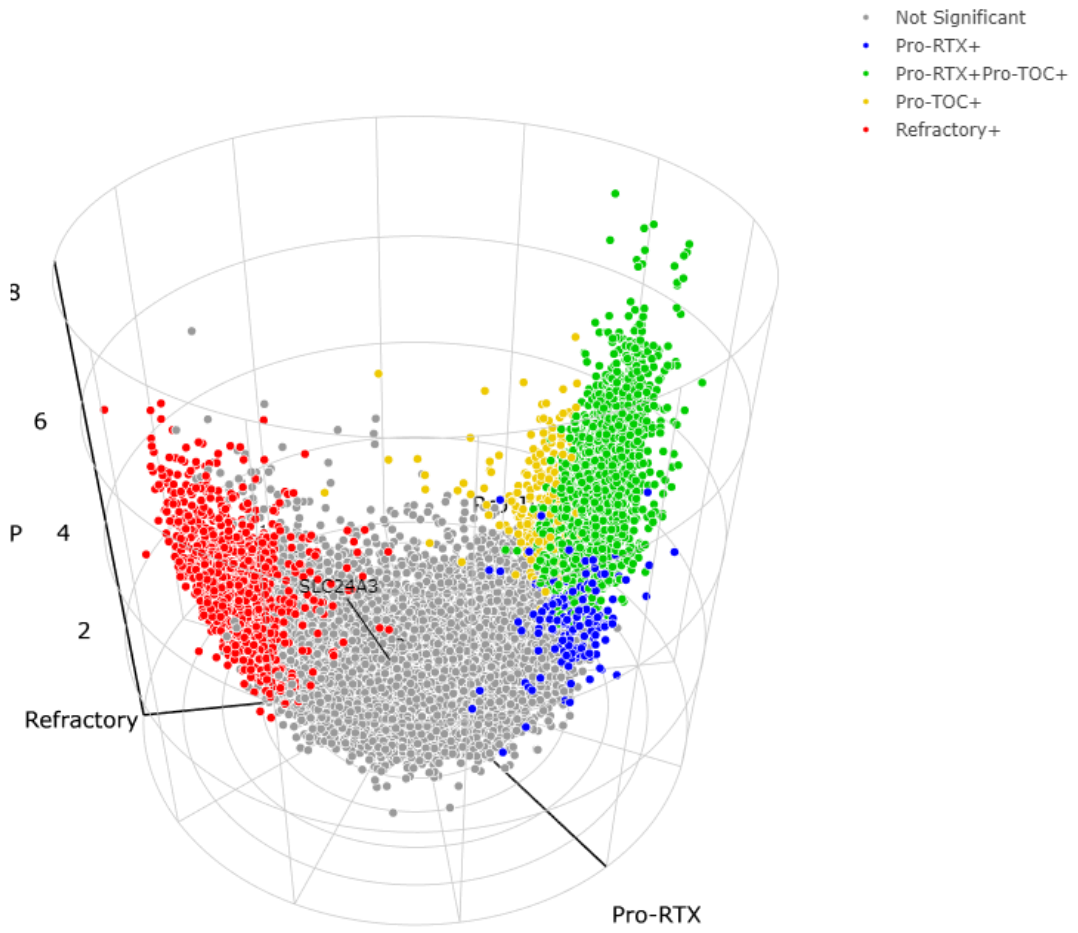

Supplementary Figure 13 Differential gene expression of SLC24A3 in synovial tissues from patients with RA after treatment with response.

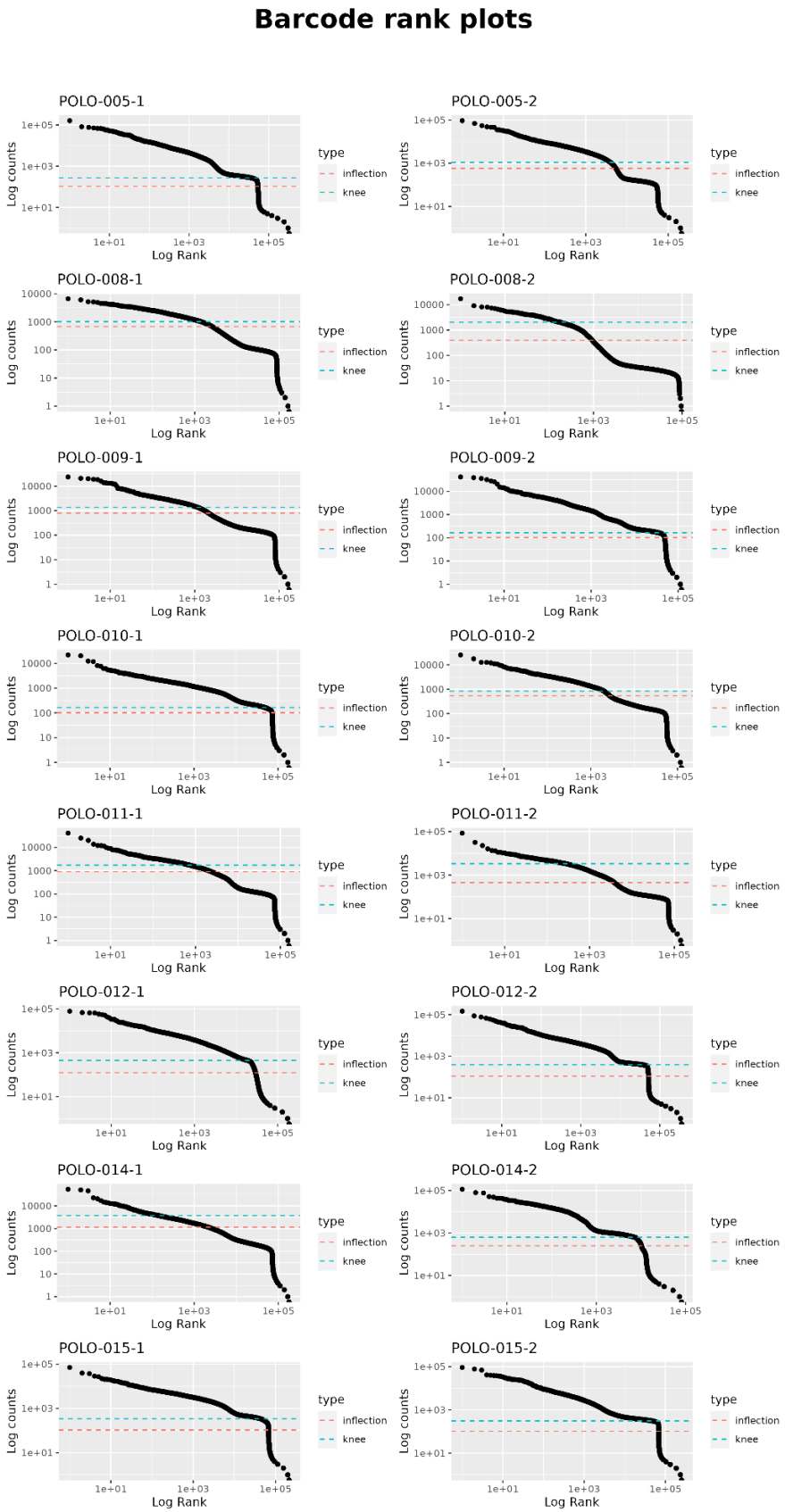

Supplementary Figure 14 Barcode rank plots of synovial tissues snRNA-seq

11. Appendix A: Scoping literature review data processing

Using Endnote 20, a new output style was created. Under bibliography, a new template was created with reference type “Journal Article”. Insert fields Author, Year, Journal Title, Journal, with tab inserted after each field. Author name is shown as full name with order Last Name, First Name. This was saved as Excel output style.

The selected references above were copied to a new library in order to remove carriage returns. Find and Replace function was used to find carriage returns in any fields and replaced with semicolon and space. Selected references were then exported in Excel export style as a text file. Then this text file was opened with Excel with Text Import Wizard. Delimited was selected as File Type, Tab as Delimiter, and General as Column Data Format. All citations were manually reviewed for relevance to hypoxia and oxygen measurements in human joints and entheses. Relevant citations were then reviewed to provide an overview of the patient population studied, sample size, method of pO_2 measurement, and the pO_2 finding in studies.

12. Appendix B: Clinical study to investigate whether nanobubbles improve joint hypoxia

Study design

This was a randomised, double-blind, single-centre, controlled pilot study to investigate the biological effects of nanobubbles on joint hypoxia versus control in 20 patients with RA and PsA. 10 participants would be randomised to study control and 10 participants would be randomised to study intervention (nanobubbles). Participants would be expected to attend at Day 1 (baseline) and at Day 28 (study end). Clinical parameters such as disease activity and biological samples including blood, synovial fluid and synovial tissues were planned to be collected at Day 1 and at Day 28. Further details of the study are described in 12. Appendix B: Clinical study to investigate whether nanobubbles improve joint hypoxia. The standard operating procedure for synovial fluid and tissue collection is described in 13. Appendix C: Ultrasound guided synovial tissue needle biopsy.

This study was registered on clinicaltrials.gov (https://clinicaltrials.gov/study/NCT04844008). University of Oxford acted as the sponsor for this clinical study. This study was generously funded by the Climax Donation at University of Oxford. Professor Duncan Richards and Professor Laura Coates were the Chief Investigator and Principal Investigator, respectively. I was the sub-investigator who wrote the study design in collaboration with the Chief Investigator, Principal Investigator, as well as co-investigators Professor Eleanor Stride, Professor Philippa Hulley and Dr Helen Knowles. As the sub-investigator, I submitted the

Integrated Research Application System (IRAS) for sponsor, REC and HRA approval. The London Riverside REC approved this clinical study of nanobubbles (REC reference: 21/LO/0030). This study was approved by the HRA and OUH.

Eligibility criteria

RA and PsA are common forms of inflammatory arthritis with similar, albeit not identical, disease processes (2). The ACR/EULAR 2010 classification criteria for RA and CASPAR 2006 classification criteria for PsA were selected as inclusion criteria to ensure that only patients with definite RA or PsA were included in the study (Table 14).

The exclusion criteria were designed to avoid confounders that may affect analysis of the effects of nanobubbles, and to limit risk from synovial tissue biopsy (Table 14). Patients on oxygen therapy were excluded from the study as their oxygen therapy may directly impact assessments of nanobubble effects on joint hypoxia. Similarly, patients with unstable treatment regimens such as corticosteroid, NSAIDs, and DMARDs were excluded from the study to avoid confounding effects on analysis of nanobubbles. Ultrasound guided synovial tissue biopsy was planned to study perturbation effects of orally delivered nanobubbles on synovial tissues. Due to the risks of synovial tissue biopsy, patients with history of septic arthritis or haemophilia, or on anticoagulation treatment were excluded from the study (Table 14).

Table 14 Eligibility criteria for nanobubble study

Inclusion criteria
• Participant is willing and able to give informed consent for participation in the study.
• Male or Female, aged 18 years or above.
• Fulfil American College of Rheumatology/European League Against Rheumatism criteria (ACR/EULAR) 2010 Rheumatoid Arthritis Classification Criteria or fulfil Classification Criteria for Psoriatic Arthritis 2006 (CASPAR).
• Selected joint for biopsy must be minimum Grade 2 synovial thickening for large joint (knee) and medium joint (wrist), or minimum Grade 3 synovial thickening for small joint (metacarpophalangeal).
• Women of child bearing potential who are willing to use effective contraception (i.e. barrier, oral contraceptive pill, implanted contraception, or previous hysterectomy, bilateral oophorectomy) for the duration of the study.
Exclusion criteria
• Currently on oxygen therapy.
• Current enrolment in any other clinical study involving an investigational study treatment.
• Pregnant or lactating, or women planning to become pregnant or initiating breastfeeding.
• Intramuscular, intravenous or intra-articular administration of corticosteroid within 4 weeks prior to baseline visit.
• Oral corticosteroid > 10 mg/day prednisolone or equivalent within 4 weeks prior to baseline visit.

• Oral corticosteroid dose not stable for at least 4 weeks prior to baseline visit.
• Oral non-steroidal anti-inflammatory drugs (including aspirin > 75 mg/ day and selective-cyclooxygenase inhibitors) dose not stable for at least 4 weeks prior to baseline visit.
• Disease modifying anti-rheumatic drugs (DMARDs) dose not stable for at least 4 weeks prior to baseline visit.
• History of septic arthritis.
• Participants on warfarin, heparin, low molecular weight heparin, direct oral anticoagulants. Oral anti-platelet agents are permitted.
• History of haemophilia.
• Known hypersensitivity to any of the ingredients of the study treatments.

Interventions

To investigate whether orally delivered nanobubbles relieve joint hypoxia, the clinical study was designed to be a double-blinded single-centre controlled study with participants randomised to drink either Avrox nanobubble drinks or Dioralyte solutions (Table 15, Table 16). Avrox Technologies Ltd. has licensed the patent on nanobubbles to provide commercially available sachets to make up drinks using this patented oxygen delivery system (https://avrox.co.uk/) (Table 15). This beverage is classified as a foodstuff and therefore does not fall into the category of Clinical Trial of an Investigational Medicinal Product as classified by the Medicines and Healthcare products Regulatory Agency. The comparator arm was assigned to drink Dioralyte, a citrus flavoured drink used as an electrolyte replacement solution, which would not be expected to affect joint hypoxia.

Table 15 Composition of 200 mL of Avrox nanobubble drink

Ingredient	**Quantity**
Purified water	Unspecified
Glycerol	0.0125 mL/mL
Citric acid	5 mg/mL
Lecithin	3 mg/mL
Sweetener (Stevia)	Unspecified
Ferrous sulphate	0.014 mg/mL
Vitamin B12	0.003 ug/mL
Potassium sorbate	Unspecified
Glycyrrhizin	0.2 mg/mL

Table 16 Composition of 200 mL of prepared Dioralyte solution

Composition of 200 mL of prepared Dioralyte solution	
Sodium	12 mmol
Potassium	4 mmol
Glucose	18 mmol
Citrate	2 mmol
Chloride	12 mmol

The study was designed for participants to drink 200 mL of the intervention (nanobubble drinks or Dioralyte) twice daily for 28 days. Participants would be instructed to consume study drinks morning and evening at approximately the same time daily and taken without food.

Participants would be provided with drink powder sachets, a drinks bottle with a lid, and an instruction sheet on how to make up study drinks at home. The instructions involve tearing the top of the sachet and pouring contents into the provided drinks bottle containing 200 mL of water. Regardless of whether they would be drinking nanobubbles or citrus flavoured Dioralyte, all participants would be instructed to replace the bottle cap and shake vigorously for 30 seconds (to load nanobubbles with oxygen per manufacturer's instructions) and drink bottle contents immediately.

Outcome measures

The main research question is whether orally delivered nanobubbles altered oxygen tension in arthritic joints of patients with RA and PsA, compared to control (citrus flavoured Dioralyte). The primary outcome therefore was change in synovial fluid pO_2 at baseline and 28 days after consuming study drinks twice daily. The secondary outcome measure was the change in HIF-1α protein levels in synovial tissues at baseline and after 28 days, as this was the main evidence for oral nanobubble effects on tissue hypoxia in the animal study (120).

Recruitment

Recruitment was planned to take place at Nuffield Orthopaedic Centre, OUH. Potentially eligible participants would be provided with an invitation letter and participant information

sheet prior to attending rheumatology clinics. The participant must sign and date the latest approved version of the informed consent form before any study procedures are performed. Written and verbal versions of the participant information sheet and informed consent form would be presented to the participants detailing no less than: the exact nature of the study; the implications and constraints of the protocol; the known side effects and any risks involved in taking part.

Screening and eligibility assessment

After informed consent is given, all screening assessments must be completed within 42 days prior to randomisation. Each participant must satisfy all the approved inclusion and exclusion criteria of the protocol. Re-screening would be permitted.

Randomisation

The randomised study would seek to balance interventional arms diagnosis (RA or PsA) by stratification using a web-based commercially available registration system (Sealed Envelope). Randomisation would be performed at the baseline visit. Allocation code would be held by an unblinded study administrator who will also be notified of new randomisation.

Blinding and code-breaking

This randomised interventional study would be double-blinded, i.e. the participant and the clinical research team would be blinded. Members of the research team who are not patient facing would conceal the interventional allocation from the blinded parties by masking the sachet packaging with concealing sticker. If the clinical condition of a participant necessitates breaking the allocation code, the un-blinded central research team would un-

blind participant allocation. Individual envelopes per participant per period will be supplied so that the allocation code may be broken for a single participant without un-blinding the whole study.

Laboratory manual

Blood:

3 mL of blood in lithium heparin tube would be sent to NHS lab for biochemistry and CRP tests. 4 mL of blood in EDTA tube would be sent to NHS lab for haematology and ESR tests. 10 mL of blood would be drawn into EDTA tubes and 3 mL of blood would be drawn into Blood RNA processing tubes. Sample tubes would be labelled with date and subject code. Samples would be kept in ice and transported to Botnar Research Centre.

Blood RNA processing tubes would be stored at -80ºC for analysis using quantitative RT-PCR. Blood in EDTA tubes would be spun at room temperature at a speed of 1,500 x *g* for 10 minutes in centrifuge. The upper supernatant would be removed with a sterile pipette and then centrifuged at 2,000 x *g* for 15 minutes at 4ºC to remove all remaining cells. Aliquot the plasma supernatant (200 µL) in 1.5 mL cryovials and store at -80ºC. To isolate peripheral blood mononuclear cells, the removed plasma would be replaced with an equal amount of Dulbecco's Phosphate Buffered Saline with 2% Fetal Bovine Serum (PBS + 2% FBS). The blood would then be diluted with an equal amount of PBS + 2% FBS. Blood would be layered on top of Lymphoprep™, being careful to minimize mixing of blood with Lymphoprep™. Centrifuge at 800 x *g* for 20 minutes at room temperature with brake off. Remove and discard upper layer without disturbing the plasma:Lymphoprep™ interface. Remove and retain the mononuclear cell layer at the plasma:Lymphoprep™ interface without disturbing the erythrocyte/granulocyte pellet. Wash mononuclear cells

once with medium. Peripheral blood mononuclear cells would be stored for potential flow cytometry experiments to identify biomarkers of the effects of oxygen nanobubbles if primary and secondary outcomes demonstrate positive signals.

Synovial fluid:

1 mL of synovial fluid in blood gas syringe at room temperature would be tested for pO_2 using blood gas analyser. Remaining synovial fluid would be cooled in ice, spun at 4°C at a speed of 2,000 x g for 10 minutes in centrifuge. Synovial fluid would be aliquoted (200 µL) in 1.5 mL cryovials and stored at -80°C. mRNA and protein would be measured using quantitative RT-PCR, Western blotting and immunoassays. Cells from synovial fluid would be stored for potential flow cytometry experiments to identify biomarkers of the effects of oxygen nanobubbles if primary and secondary outcomes demonstrate positive signals.

Synovial tissue:

Synovial tissue would be snapfrozen in optimal cutting temperature (OCT) compound for immunohistochemistry to examine HIF-1α expression before and after drinking either oxygen nanobubbles or citrus flavoured Dioralyte.

Early Discontinuation/Withdrawal of Participants

During the course of the study, a participant may choose to withdraw early from the study at any time. Data and samples obtained up until the point of withdrawal would be retained for use in the study analysis. No further data or samples would be collected after withdrawal. In addition, the investigator may discontinue a participant from the study at any time if the investigator considers it necessary for any reason. Withdrawn participants

would be replaced. Participants that have withdrawn from the study would be seen by the clinical rheumatology care team without further research follow up. If the participant is withdrawn due to an adverse event, the investigator would arrange for follow up until the adverse event has resolved or stabilised.

Statistical Analysis Plan

This is an exploratory hypothesis generating study of the biological effects of nanobubbles. Descriptive outcomes will be reported using 95% confidence intervals to look for intra-arm (Day 28 versus baseline) and inter-arm (nanobubble drinks versus citrus flavoured Dioralyte drinks) effects. A sample size of 20 (10 in each arm) was selected pragmatically for this pilot study based on clinical prevalence.

All eligible participants (per protocol analysis) would be included in the analyses. Data would be included from participants who have been un-blinded. There would be no interim analysis.

13. Appendix C: Ultrasound guided synovial tissue needle biopsy

Equipment

- Quick-Core biopsy needles (16G)
- 21G / 19G needles
- Sterile drapes
- Sterile Ultrasound sheath
- Sterile gown and gloves
- Procedure pack
- Face mask / hair cover
- Sterile swabs
- Chlorhexidine skin prep applicator
- 10mls / 20mls syringes
- 1 % Lidocaine (max 4.5mg/kg)
- Sterile Dressing
- Sample container for processing

Patient Orientation

The patient was recumbent at 45 degrees with the knee slightly flexed (25-30 degrees) to improve imaging of the supra-patella pouch.

Preparation

- With the patient suitably placed on the bed, suitable absorbent pads were placed under the knee. The skin was prepped with appropriate sterilization. A wide field

was sterilized in excess of the immediate area of interest, approximately mid-thigh to mid-calf both anteriorly and posteriorly.

- Sterile drapes were positioned above, below, medial and lateral to the knee leaving sufficient space for access to the supra-patella pouch and placement of the ultrasound probe for the purposes of imaging.
- The ultrasound probe was placed within the sterile sheath. Ultrasound gel was placed first upon the probes foot-print and slowly lowered into the sheath. The upper end of the sheath was secured with an elastic band provided with the sheath.
- Ultrasound examination of the lateral aspect of the knee was performed to indicate a suitable area for needle insertion distal to the vastus lateralis muscle insertion into the patella.

Biopsy Procedure

- 5-10mls of 1% lidocaine was injected into the subcutaneous and deep tissue at the predetermined point of insertion as identified by the initial ultrasound scan.
- Using a 19G needle and under ultrasound guidance, synovial fluid was aspirated from the suprapatellar pouch. The syringe was disconnected leaving the needle in situ. 20 ml mix of normal saline and lidocaine (10 ml of normal saline and 10 ml of 1% lidocaine) were injected into the suprapatellar pouch to enable a better image to be acquired during the procedure and facilitate clear identification of synovial tissue.
- The quick core biopsy needle was primed before its introduction to the synovial space.
- The biopsy needle was introduced into the suprapatellar pouch under ultrasound guidance.

- The needle was extended and the throw identified on the ultrasound images. The throw of the needle was placed against the surface of the synovium to maximize the opportunity for capturing the lining layer. Gentle pressure was placed on the needle to oppose the throw and synovium. Triggering of the needle mechanism was performed with a small forward movement of the whole needle.
- After synovial tissue biopsy, any remaining fluid suprapatellar pouch was aspirated and a small dressing applied to cover the wound.